TIME RESOLVED ABSORPTION AND FLUORESCENCE STUDIES OF ATOMIC AND MOLECULAR REACTIONS INVOLVING GROUP VI ELEMENTS

BY

MICHAEL CROMBIE ADDISON

A thesis presented for the degree
of Doctor of Philosophy in the
Faculty of Science at the
University of Edinburgh
1980

TO MY PARENTS

ACKNOWLEDGEMENTS

I begin by expressing my thanks to my supervisor, Professor R.J. Donovan. His knowledge of and appetite for the subject of gas kinetics have made the last three years a very informative and stimulating time for me. I have also had the good fortune to work closely with two other excellent scientists, while at A.E.R.E., Harwell, namely Drs. R.A. Cox and J.P. Burrows. To both I extend my thanks, without their considerable assistance Chapter 4 of this thesis would not exist.

The happy working environment established by my numerous colleagues in the research group has been much appreciated. I thank all of them but would particularly like to mention Drs. H. Gillespie, J. McElroy, C. Fotakis and M. Martin and Mr. J. Garraway, all of whom, through numerous discussions, have contributed significantly to my understanding of the experimental and theoretical aspects of gas kinetics.

I have had considerable help from the highly skilled staffs of the electronic, mechanical and glassblowing workshops. I specially mention Mr. J. Broom for his skilful glassblowing - his services were much requested throughout the duration of my Ph.D. and he never failed to give prompt and careful attention to the problems encountered. I should further like to thank him for spending time

in teaching me the fundamentals of glassblowing.

I express my gratitude to Mrs. M. Manson for her excellent typing and presentation of this thesis and also the proof copies of the papers published as a result of this work.

Lastly, I must extend my greatest thanks to my parents. Throughout my education they have shown considerable interest in my studies and have provided a great deal of helpful advice and enthusiastic encouragement. This assistance throughout the years has been greatly appreciated.

ABSTRACT

Kinetic data for the reactions of the ground and first electronically excited states of oxygen and sulphur atoms are presented. Oxygen and sulphur atoms were produced by photolysis of ozone and carbonyl sulphide and carbon disulphide respectively. The atomic species were monitored using time resolved absorption and/or fluorescence techniques.

The reactions of $O(^1D_2)$ with the halogenomethanes CH_3Cl and CCl_4 were studied and the branching ratios into the various product channels measured. Chlorine atom abstraction was found to be a major reaction pathway and the quenching of $O(^1D_2)$ to the ground state appeared significant. The branching ratio for reaction of $O(^1D_2)$ with ozone was also studied. $O(^3P_J)$ growth and yield in the presence of helium and nitrogen buffer gases were monitored and quantum yields for ozone removal measured.

Reaction of $O(^3P_J)$ and $S(^3P_J)$ atoms with the perfluoroalkyl iodides CF_3I and iso C_3F_7I was considered. Rate constants for reaction are given and inferred lower limits to the bond strengths of IO and IS listed.

$S(^1D_2)$ atoms were monitored directly in absorption from photolysis of CS_2 ($\lambda \geqslant 200$ nm) and rate constants for reaction with a considerable number of small molecules were measured under pseudo first order reactions. Rate data for $S(^1D_2)$ atom reactions, with a few notable exceptions, were found to be similar to the analogous reactions of $O(^1D_2)$. Further work, on the

application of the resonance fluorescence technique to the detection of the $S(^1D_2)$ atoms is described. The yield of $S(^1D_2)$ atoms on photolysis of CS_2 at 193 nm (ArF laser) was found to be $\leqslant 30\%$. Rate data for reaction with CH_4, OCS and CS_2 are presented and compared with the analogous absorption data.

In addition to the work on atomic reactions, Chapter 4 discusses work carried out at A.E.R.E., Harwell on the recombination of ClO radicals. Temperature dependent rate data were obtained using the molecular modulation technique with uv absorption spectrophotometric detection of the ClO radicals. From this data and quantum yield measurements information on the reaction mechanism was inferred.

CONTENTS

Page

CHAPTER I: INTRODUCTION

1.1 PROLOGUE 1

1.2 POTENTIAL ENERGY SURFACES 3

A) Ab Initio 6

B) Semi Empirical 6

C) Empirical 9

1.3 CORRELATION DIAGRAMS 11

1.4 COLLISION THEORY 14

(i) Simple Collision Theory 15

(ii) Modified Simple Collision Theory 16

1.5 TRANSITION STATE THEORY 18

1.6 SPECTROSCOPIC CONSIDERATIONS 21

1.7 REFERENCES 26

CHAPTER II: EXPERIMENTAL TECHNIQUES

2.1 INTRODUCTION 28

2.2 FLASH SPECTROSCOPY 29

2.3 ABSORPTION SPECTROPHOTOMETRY 31

2.4 RESONANCE FLUORESCENCE 34

2.5 FLASH PHOTOLYSIS 37

(i) Conventional Discharge Flash Lamp 38

(ii) Pulsed Flash Lamp 39

(iii) Laser Photolysis 40

2.6 DIAGNOSTIC LIGHT SOURCES 41

(i) Spectroflash Lamp 41

(ii) Flow Lamp 42

2.7 SIGNAL DETECTION 53

(i) Photographic Recording 53

(ii) Electronic Recording 55

2.8 GAS HANDLING 60

2.9 MOLECULAR MODULATION SPECTROSCOPY 60

2.10 REFERENCES 67

CHAPTER III: REACTION OF $O(2^1D_2)$ WITH THE HALOGENOMETHANES CCl_4 AND CH_3Cl

3.1 INTRODUCTION 69

3.2 EXPERIMENTAL 70

(1) Flash Spectroscopy 71

(2) OH Absorption Spectrophotometry 72

(3) Atomic Absorption Spectroscopy 72

3.3 RESULTS 73

(1) ClO and Cl Yields 73

(2) OH Yield 81

(3) $O(^3P_J)$ Yield 84

3.4 DISCUSSION 88

3.5 REFERENCES 94

CHAPTER IV: A TEMPERATURE DEPENDENT STUDY OF THE MUTUAL COMBINATION OF ClO RADICALS

4.1 INTRODUCTION 97

4.2 EXPERIMENTAL 99

4.3 DATA ANALYSIS 99

4.4 RESULTS 103

(i) $Cl_2/Cl_2O/O_2$ System 103

(ii) Cl_2/O_2 [Low Pressure] System 116

4.5 DISCUSSION 119

4.6 REFERENCES 123

CHAPTER V: OZONE PHOTOLYSIS - THE REACTION OF $O(^1D_2)$ WITH OZONE

5.1 INTRODUCTION 125

5.2 EXPERIMENTAL 128

5.3 RESULTS AND DISCUSSION 130

5.4 REFERENCES 144

CHAPTER VI: KINETIC STUDY OF THE REACTION OF $O(^3P_J)$ AND $S(^3P_J)$ ATOMS WITH CF_3I AND iso-C_3F_7I

6.1 INTRODUCTION 146

6.2 EXPERIMENTAL 147

(i) $O(^3P_J)$ Production and Detection 147

(ii) $S(^3P_J)$ Production and Detection 148

6.3 DATA ANALYSIS 148

6.4 RESULTS AND DISCUSSION 150

(A) $O(^3P_J)$ + Perfluoroalkyliodides 150

(B) $S(^3P_J)$ + Perfluoroalkyliodides 155

6.5 REFERENCES 164

CHAPTER VII: KINETIC STUDIES OF THE REACTIONS OF $S(3^1D_2)$

7.1 INTRODUCTION 166

7.2 EXPERIMENTAL 167

7.3 DATA ACQUISITION AND ANALYSIS 168

7.4 RESULTS AND DISCUSSION 172

A) $S(3^1D_2)$ Production 172

B) $S(3^1D_2)$ Kinetics 175

(i) CO_2, OCS, CS_2 175

(ii) N_2, O_2, CO, N_2O 180

(iii) The Noble Gases 186

(iv) H_2S and H_2O 192

(v) The Halogens and Halomethanes 195

(vi) The Organic Molecules - CH_4, C_2H_6, C_6H_6, C_6F_6 197

7.5 CONCLUSIONS 202

7.6 REFERENCES 203

CHAPTER VIII: RESONANCE FLUORESCENCE STUDY OF $S(3^1D_2)$ ATOM KINETICS

8.1 INTRODUCTION 206

8.2 EXPERIMENTAL 207

8.3 RESULTS AND DISCUSSION 210

8.4 CONCLUSIONS 221

8.5 REFERENCES 224

APPENDIX 1A 225

APPENDIX 1B 227

APPENDIX II 229

APPENDIX III 230

APPENDIX IV 233

LECTURES ATTENDED 234

CONFERENCES ATTENDED 234

PUBLICATIONS 236

CHAPTER I

INTRODUCTION

1.1 PROLOGUE

Two of the most important questions to be asked of the physical chemist when considering a specific reaction are: 1) what is the position of equilibrium in the system and 2) how long will it take for the equilibrium to be established. The first of these questions is answered by reference to the well characterised subjects of chemical thermodynamics and statistical thermodynamics. The second question concerns the chemical kinetics of the system. At the present time, in contrast to the thermodynamic properties, where kinetic information is desired for a specific system then an experimental study must be undertaken.

Gas kinetics of elementary reactions occupies one area of the field of chemical kinetics. Much of the rate data from gas kinetics is used directly in a variety of applications e.g. combustion, atmospheric chemistry, etc. However, underlying this pragmatic approach it is evident that through these studies the best opportunity is afforded to establish the fundamental principles governing kinetic processes. In rising to this challenge, gas kinetics has evolved, in a series of distinct developments, from examination of the bulk properties of a system to a measurement of the microscopic properties of particular systems. The

major experimental development facilitating the deep probing of the kinetic processes has been the advent of molecular beam and laser monitoring (in particular laser induced fluorescence) techniques. By using molecular beam scattering techniques it is possible to select single quantum states and to explore the dynamics of the molecular collision by examination of the angular and energy dependence of the associated scattering. The increase in the quantity and quality of the detailed information has provided the incentive necessary for the development and evaluation of new theoretical approaches to the problems of chemical kinetics.

In the simplest of terms the rate of any elementary chemical reaction will be dependent on the number of collisions between reactants (proportional to reactant concentration) and a constant reflecting the probability of reaction once collision has occurred. Hence we may write the familiar bulk rate equation for a reaction between two species X and Y.

$$-d[X]/dt = k[X][Y] \qquad 1.a$$

where k was shown by Arrhenius, from empirical data, to obey equation 1.b

$$k = A \exp(-E/RT) \qquad 1.b$$

where A is referred to as the pre-exponential factor and E is the activation energy. Theoretical

derivations of the rate constant (sec. 1.4 and 1.5) have generated the A factor in terms of more fundamental dynamical or statistical propoerties. The prediction of these factors together with the activation energy are extremely difficult problems. Their solution is even more complex than equation 1.b suggests for it must be remembered that the bulk rate constant is a sum over all possible internal quantum states, translational energies and impact parameters of the individual reactants. The main features of the theoretical approaches adopted to elucidate these problems are discussed in the following sections.

The results of such studies have considerable relevance to a full appreciation of the experimental data presented in this work. Experiments have, in the main, been concerned with measurement of rate data and branching ratios for various reactions of oxygen and sulphur atoms in selected electronic states, namely the ground (^3P_J) and first excited ($^1D_2$) states.

1.2 POTENTIAL ENERGY SURFACES

It was first suggested by Marcelin[2] that the course of a chemical reaction could be rationalised in terms of the movement of the constituent atoms over a potential energy surface. The total energy E of a molecule consists of the potential energy and kinetic energies of the nuclei and electrons. The kinetic energy and the coulombic energy of the molecule represent a 'potential energy' under whose influence the nuclei carry out their vibrations. Using the Born Oppenheimer approximation

it is possible to calculate these factors separately and hence map out the potential energy surface for the various internuclear positions. In order to totally define the potential surface for any system 3n-5 (for linear systems 3n-4) dimensions are needed. Due to the difficulty in visualising more than three dimensions it is normal to consider sections through the potential energy surface - obtained by restricting certain parameters to fixed values. Consider reaction (1)

$$A + BC \rightarrow AB + C \qquad 1$$

This may be represented in a three dimensional 'contour map' by considering only linear collisions i.e. $\angle ABC = 180^{\circ}$ (FIG 1.1)

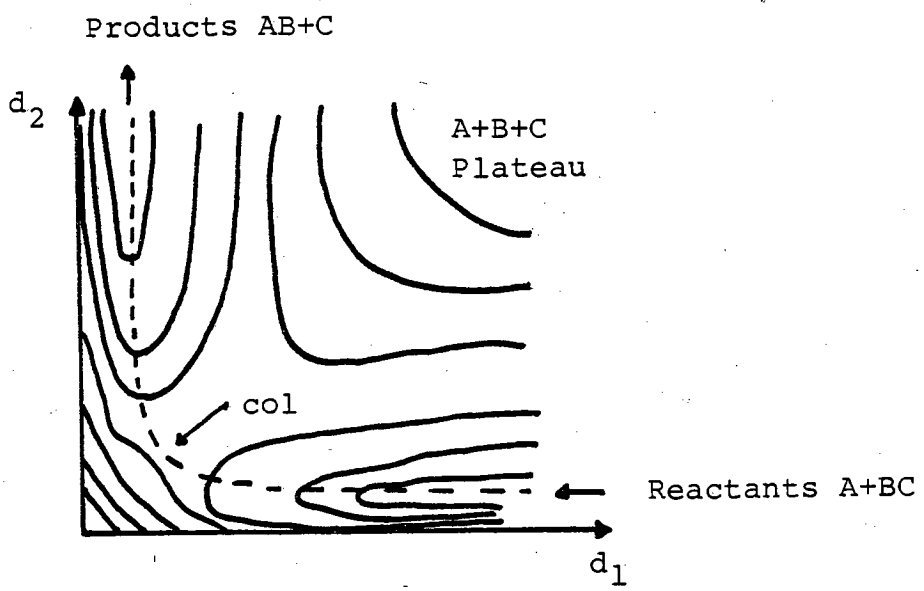

FIG 1.1 A contour map of the potential energy surface for the linear reaction (1).

- - - REACTION COORDINATE

The path of minimum potential energy between the reactant valley (A+BC) and the product valley (AB+C) is indicated in FIG 1.1 by the dotted line. This path is called the reaction coordinate since it is the path of minimum energy and therefore maximum probability (other factors being equal) between reactants and products. FIG 1.2 plots the potential energy as a function of the reaction coordinate.

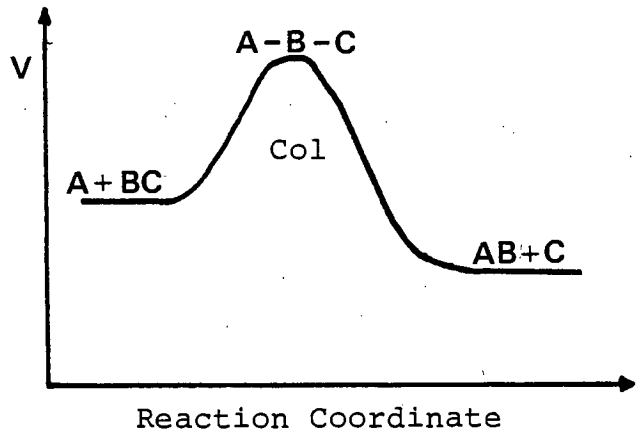

FIG 1.2 The potential energy curve for reaction (1)

Particular significance attaches to the col or saddle point indicated in FIG 1.2. This point although a position of maximum energy with respect to the reaction path is also a position of minimum energy with respect to motions at right angles to the reaction path. The molecular arrangement at this point is known as the activated complex and the energy is closely related to the classical activation energy of the reaction. Hence

calculation of the potential energy surface allows the reaction coordinate to be mapped out and the activation energy measured. Three approaches to this problem have been followed: ab initio, semi-empirical and empirical calculations:

A) Ab initio: It is only very recently that calculation of even the simplest potential energy surfaces by quantum mechanical methods have produced results in good agreement with experimental observations. The problem of accuracy of the calculation arises largely from the nature of the computation. The saddle-point energy is obtained from the difference between two very large values corresponding to total ionisation of the reactants and species at the col. Further, the formidable size and cost of the computer calculations favours the development of more empirical techniques.

B) Semi-empirical treatments: Semi-empirical treatments, although based on quantum mechanical theory, make use of experimental data of the kind they are interpreting to obtain more satisfactory results. An example of this approach is provided by one of the earliest semi-empirical models referred to as London-Eyring-Polanyi (LEP) surfaces[4]. This model begins with the approximation of the Heitler-London and London equations that for a diatomic molecule (B-C) the energy of the ground state (E) is given by the sum of the coulombic (A) and exchange (α) integrals (equation 1.1)

$$E = A + \alpha \qquad 1.1$$

The assumption was then made that the coulombic and exchange energies are constant fractions of the total energy (E) - equation 1.2. A value of 10-15% was obtained for (ρ) using Sugiura's[5] calculations of the coulombic and exchange integrals for the H_2 molecule.

$$\rho = A/(A+\alpha) \qquad 1.2$$

The total energy (E) can be obtained from the spectroscopically monitored dissociation energy (D) and application of the Morse equation (1.3).

$$E = D(\exp(-2\beta(r-r_0)) - 2\exp(-\beta(r-r_0))) \qquad 1.3$$

r_0 = equilibrium internuclear distance

β = constant

For any triatomic configuration it is therefore possible to evaluate, for each pair of atoms, the coulombic and exchange energies. Insertion of these values into the London equation (1.4) provides the required energy of the triatomic species (A--B--C).

$$E = A+B+C \pm \{\tfrac{1}{2}([\alpha-\beta]^2 + [\beta-\gamma]^2 + [\gamma-\alpha]^2)\}^{\frac{1}{2}} \qquad 1.4$$

The notation in the above equation is such that A and α refer to the coulombic and exchange integrals, respectively, for the diatomic B-C with A removed to infinity. Results from this method have not been particularly good in terms of defining the activation energy. Further, certain topological features (e.g. a basin on H_3 surface corresponding to H_3 molecule) obtained from the model appear to have no bearing

on reality. Sato[6,7] improved the topology of the $H+H_2$ surface by including ρ as an adjustable parameter and also modifying the London equation to include the overlap integral. Glasstone et al[8] outline an extension of the procedure to four atom systems and numerous other workers have modified the procedure to increase the accuracy of the results.

An alternative empirical approach is that of the bond-energy bond-order method (BEBO) developed by Johnston et al[9,10]. It was proposed that the potential (E) along the reaction coordinate could be represented by (1.5)

$$E(x) = -E_{AB}(r_{AB}) - E_{BC}(r_{BC}) + E_{REP}(r_{CA}) \qquad 1.5$$

E_{AB} and E_{BC} are the energies associated with the partial bonds between A+B and B+C. $E_{REP}(r_{CA})$ is the repulsive energy between C+A. This latter expression is evaluated from an anti-Morse function of a type used by Sato. In order to obtain the energies of the partial bonds an empirical relationship developed by Pauling (1.6) is united with an equation relating bond strength to bond order (1.7)

$$r = r_s - 0.26 \log_e \eta \qquad 1.6$$

$$V = V_s \eta^P \qquad 1.7$$

where r_s = single bond length for a bond connecting two particular atoms

V = bond energy (subscript refers to single bond)

η = bond order

P = empirical constant.

The total bond order throughout the reaction is considered to be unity. In the original work V and r were substituted by the Lennard Jones parameters ε_{LJ} and r_m for the nearest noble gas pair in the Periodic Table to the bound species of interest in order to evaluate the empirical constant P.

The accuracy of BEBO calculations are very dependent on the value assigned to P. Recently there has been a number of modifications to the method, however the problem of obtaining P would appear to severely limit its applicability as a predictive model.

C) Empirical treatments: A number of empirical relationships have been proposed which relate activation energy to other molecular parameters e.g. heats of reaction, polarisability, etc. In addition a few empirical procedures exist for constructing complete potential energy surfaces. An example of the former is the relationship proposed by Evans and Polanyi[11] (equation 1.8)

$$E_{ACT} = \alpha \Delta H + C \qquad 1.8$$

where $0.0<\alpha<1.0$ and C is an empirical constant. Such an equation is of particular use where the parameters of a reaction are known and one wishes to evaluate new parameters for a change in reactant. Such an approach has been applied to reaction of $O(^3P_J)$ atoms with the halogens[12]. Using an equation of the type presented above (1.8) yields good results with the exception of reaction with fluorine. All results, including fluorine,

were in agreement with a relationship of the form (1.9).

$$E_{ACT} = c/\alpha_{X_2} \qquad 1.9$$

where c = empirical constant

α_{X_2} = mean polarisability of the halogen molecule

Empirical procedures for obtaining the full potential surface make use of modified Morse potentials systematically distorted to produce the familiar features of a potential energy surface.

Kinetic information can be derived directly from potential energy surfaces through study of the three dimensional collision dynamics, by solution of the classical laws of motion. The requirements of such a technique are as follows:

A) An accurate representation of the potential energy surface.

B) A method of selecting the initial positions and momenta of the atoms for computation of each individual trajectory.

C) An averaging technique to convert the raw data into experimentally measurable data.

The first of these requirements has already been considered. The second is solved using the pseudo random 'Monte Carlo' procedure. The purpose of Monte Carlo selection is to ensure that the distribution of each initial parameter within a sample of trajectories approaches the true statistical distribution as the size of the sample increases. The exact form of the pseudo

random procedure used for assigning different variables e.g. orientation, impact parameter, velocity is dependent on the nature of the parameter. Within the limitations imposed by the selection of a potential energy surface and the use of classical rather than quantum dynamics trajectory studies can provide both microscopic and macroscopic information for bimolecular reactions of the general type illustrated by reaction (1).

Trajectory studies have been of paramount importance in ascertaining general conclusions on how the topology of potential energy surfaces affects both the dynamics of and energy partitioning in elementary chemical reactions. These results have been extensively reviewed[13].

1.3 CORRELATION DIAGRAMS

Symmetry considerations can be of great use in determining the reactants and products that are connected by a single hypersurface and those which would necessitate crossing from one potential hypersurface to another to produce certain desired products. In constructing a correlation diagram no information is provided on the topology of the potential surfaces involved. The basis of correlation diagrams is the conservation of certain symmetry elements during the course of a concerted chemical change. The correlation rules for determining the molecular states that arise when two atoms interact were developed many years ago by Wigner and Witmer[14] (see TABLE 1.1). Extension of these rules to rationalise reaction

mechanisms is more recent in origin and have been extensively reviewed elsewhere[15,16,17].

The adiabatic assumption is most accurate when considering light systems where Russell-Saunders coupling implies that the total electronic wavefunction can be written as a product of spin and spatial components i.e. L and S which specify orbital angular momentum and electronic spin may be considered as 'good' quantum numbers. In considering a chemical reaction in a system of three atoms the symmetry of the orbitals are considered under the lowest possible symmetry to be conserved i.e. the C_s point group (one plane of symmetry). As such the molecular wave functions are either symmetric or antisymmetric with respect to reflection in the plane of symmetry (see TABLE 1.1). Of equal importance in characterisation of the reaction is the electron spin which must also be conserved. If the reactants before interaction had spins S_i then after interaction the spin must take up values given by the vector sum $S = \Sigma_i S_i$ (see TABLE 1.2). In constructing the relevant adiabatic correlations two states of different symmetry are allowed to cross, hence the potential energy surface that constitutes the ground state for one set of internuclear co-ordinates may become an excited state for another set of internuclear co-ordinates. From application of perturbation theory it can be illustrated that two states possessing the same symmetry cannot have the same energy for a specific internuclear separation and

TABLE 1.1 CORRELATION TABLE FOR (i) ATOM+ATOM, AND (ii) ATOM+LINEAR MOLECULE

	Sg Su	Pg Pu	Dg Du
(i)			
Sg	Σ^+	Σ^-,Π	Σ^+,Π,Δ
	Σ^-	Σ^+,Π	Σ^-,Π,Δ
Pg	Σ^-,Π	$\Sigma^+(2),\Sigma^-,\Pi(2),\Delta$	$\Sigma^+,\Sigma^-(2),\Pi(3),\Delta(2),$
	Σ^+,Π	$\Sigma^+,\Sigma^-(2),\Pi(2),\Delta$	$\Sigma^+(2),\Sigma^-,\Pi(3),\Delta(2),$
Dg	Σ^+,Π,Δ	$\Sigma^+,\Sigma^-(2),\Pi(3),\Delta(2),$	$\Sigma^+(3),\Sigma^-(2),\Pi(4),\Delta(3),$ (2),
	Σ^-,Π,Δ	$\Sigma^-(2),\Sigma^+,\Pi(3),\Delta(2),$	$\Sigma^-(2),\Sigma^+(3),\Pi(4),\Delta(3),$ (2),
(ii)			
Σ^+	A'	A' + 2A"	3A' + 2A"
	A"	2A' + A"	2A' + 3A"
Σ^-	A"	2A' + A"	2A' + 3A"
	A'	A' + A"	3A' + 2A"
Π,Δ, etc	A' + A"	3A' + 3A"	5A' + 5A"
	A' + A"	3A' + 3A"	5A' + 5A"

TABLE 1.2 CORRELATION OF ATOMIC AND MOLECULAR MULTIPLICITIES

Separated Species	Multiplicities of Resultant Molec.
1 + 1	1
1 + 2	2
1 + 3	3
2 + 2	1,3
2 + 3	2,4
2 + 4	3,5
3 + 3	1,3,5
3 + 4	2,4,6
4 + 4	1,3,5,7

hence may not cross. It should be pointed out that non-adiabatic transitions between electronic states can take place through coupling between electronic and nuclear motions or spin and orbital motions. Exit through one of these channels would be expected to occur with lower probability than the adiabatic channels, providing the latter were free from sizeable activation energies.

The application of these rules to the reactions of atoms and free radicals are illustrated on numerous occasions throughout this work. Consideration of the symmetry of a molecular system is not only of use in systems of a few atoms. The utilisation of frontier orbital theory has greatly aided the rationalisation of products from numerous organic reactions. Such an approach relies on the fact that only a few critical orbitals dominate the predictions of reactive pathways of ground state reagents. It is the local symmetry of these orbitals rather than the apparent non symmetry of the large molecular systems that are of interest. The basis and application of symmetry rules for many such chemical reactions are dealt with in Ref. 18.

1.4 COLLISION THEORY

The recent development of high speed computers has resulted in a more general applicability of 'Monte Carlo' trajectory calculations. Prior to this development the monumentous computational effort

needed to proceed with such calculations necessitated the usage of simpler theories. Today the cost of computer time also makes it desirable to adopt accurate theories which limit the computational effort. Two of the most widely applied theories are: collision theory, described in this section and transition state theory described in the subsequent section.

(i) Simple Collision Theory (SCT): In simple collision theory the colliding species are assumed to be structure-less spheres that only begin to interact at a critical separation (d); at which point the intermolecular potential rises as a step function. It is assumed that reaction will only occur if E_{LC} (the collision energy directed along the line of centres) exceeds a critical value E^{o} (the threshold energy). E_{LC} is related to the total collision energy (E_T) by equation 1.10.

$$E_{LC} = E_T(1-b^2/d^2) \qquad 1.10$$

where b = impact parameter.

The maximum impact parameter at which reaction will occur for a specific collision energy is provided by equation 1.11.

$$b^2_{MAX} = d^2(1-E^{o}/E_T) \qquad 1.11$$

and hence the reaction cross section (S_r) is given by:

$$S_r(E_T) = \Pi b^2_{MAX} = \Pi d^2(1-E_T{}^{o}/E_T) \qquad 1.12$$

The thermal rate constant (k) is related to the reaction cross section by equation 1.13.

$$k(\eta'/\eta;T) = \int v S_r(\eta'/\eta;v) f(v;T) dv \qquad 1.13$$

where η' and η are the final and initial quantum states respectively.

$f(v;T)dv$ is the fraction of collisions which in a thermal distribution of relative velocities defined by the temperature (T) occur with a relative translational velocity between v and v+dv. Combining equations (1.12) and (1.13) results in the expression (1.14)

$$k_{SCT} = \Pi d^2 (8k_B T/\Pi\mu)^{\frac{1}{2}} \exp(-E^o/k_B T)$$

$$= Z(T) \exp(-E^o/k_B T) \qquad 1.14$$

The model adopted for the calculation of SCT is obviously very crude. Its assumption that orientation of collision is unimportant is often corrected for by the insertion in equation 1.14 of a steric factor P.

(ii) Modified Simple Collision Theory (MSCT):

Orientation effects are dealt with more completely in the MSCT. In this model the potential energy at the surface separating reactants from products and defined by r=D is assumed to depend on the angle (ϕ) between the line OP and an axis drawn in the sphere r=D (see FIG 1.3) The following calculation assumes the axis which defines ϕ to be a homonuclear diatomic molecule. Where reaction is only available

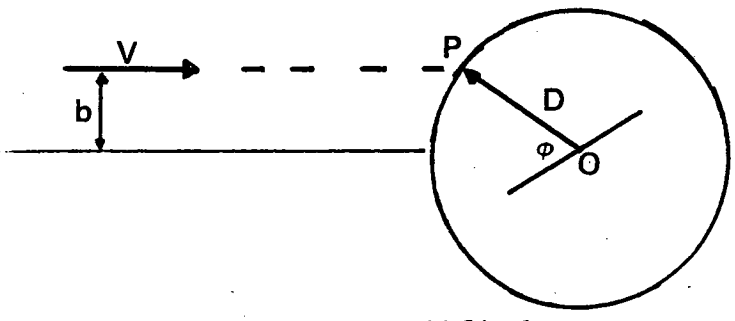

FIG 1.3 Parameters in modified simple collision theory

at one end of the molecule the equations presented should be divided by 2.

$$V(D) = E^{o} + 2E'(1-\cos\phi) \qquad 1.15$$

Hence for reaction:

$$E_{LC} = E_T(1-b^2/D^2) > E^{o} + 2E'(1-\cos\phi) \qquad 1.16$$

and a maximum value of ϕ, if reaction is to occur, is defined (1.17)

$$2(1-\cos\phi_{max}) = \{E_T(1-b^2/D^2) - E^{o}\}/E' \qquad 1.17$$

$P_r(E_T,b)$, the probability of reaction for a specified collision energy and impact parameter is simply the fraction of the surface area of the sphere leading to reaction.

$$P_r(E_T,b) = 0 \quad \text{for } E_T<E^{o} \qquad 1.18$$

$$P_r(E_T,b<b_{max}) = 2\int_{o}^{\phi_{max}} 2\pi D^2 \sin\phi d\phi/4\pi D^2$$

$$= (1-\cos\phi_{max}) = E_T(1-b^2/D^2)-E^{o}\ /2E' \qquad 1.19$$

for $E^{o} < E_T\ (1-b^2/D^2) < E^{o} + 2E'$

$$P_r(E_T, b<b_{max}) = 1 \qquad 1.20$$

for $E_T(1-b^2/D^2) > (2E' + E^o)$

Deriving the rate constant as previously generates equation 1.21

$$k(T) = k_{SCT}(T)(k_BT/2E')(D^2/d^2) \qquad 1.21$$

Although this model represents a considerable improvement over SCT several assumptions and approximations are still inherent in the theory:

1) It uses an oversimplified potential (essentially the interaction switches on at r=D).

2) No allowance is made for the possibility of the mixing of other potential energy hypersurfaces.

3) Once the critical configuration has been reached reaction must occur.

4) Only translational energy is assumed to promote reaction. Vibrational and rotational motions are not considered.

1.5 TRANSITION STATE THEORY (T.S.T.)

Transition state theory focuses attention on the col of the reaction co-ordinate and in particular the rate of passage of reactants through this zone. The transition state is treated as a thermodynamic entity and the rate of reaction is evaluated with regard to the properties of this state.

Considering reaction (1) with the transition state inserted the rate of passage through a transition state

of 'thickness' L is given by 1.22.

$$A + BC \longrightarrow [A\cdots B\cdots C]^{\dagger} \longrightarrow AB + C \qquad 1$$

$$d[C]/dt = [ABC^{\dagger}]\langle \vec{v}_x \rangle /2L \qquad 1.22$$

where $\vec{v}_x$ is the average velocity in the forward (left to right) direction.

It should be noted that in order for T.S.T. to be applicable internal thermodynamic equilibrium must be maintained. Providing the reactants are in internal thermodynamic equilibrium, then the actual rate of reaction in the forward direction is unaffected by the extent to which the reverse reaction is occurring in the system.

$$k(T) = (\langle \vec{v}_x \rangle /2L)([ABC^{\dagger}]/[A][BC]) \qquad 1.23$$

$$= (\langle \vec{v}_x \rangle /2L)K^{\dagger}(T) \qquad 1.24$$

where $K^{\dagger}(T)$ may be evaluated using statistical mechanics[13,19] (Equ. 1.25)

$$K^{\dagger}(T) = [(Q^{\dagger}/V)/\prod_i (Q_i/V)]\exp(-\Delta E_o/k_B T) \qquad 1.25$$

where $Q^{\dagger}$ = total partition function for the activated complexes

ΔE_o = difference between zero point energy of activated complex and that of the separated reactants.

If motion along the reaction co-ordinate (x) is considered separable from the other motions of the

activated complex and adopting suitable expressions for $Q^{\dagger}_{x}$ and v_x transforms 1.25 into 1.26.

$$k(T) = (k_B T/h)[(Q^{\ddagger}/V)/\Pi(Q_i/V)]\exp(-\Delta E_o/k_B T) \qquad 1.26$$

In order to calculate the individual partition functions one needs to know moments of inertia, vibrational frequencies and electronic states. For the reactants this presents few problems, most of the data being available for spectroscopic observations. For the activated complex the calculation of the partition function is much more difficult, providing both conceptual and computational problems. The choice of suitable geometrical parameters and vibrational frequencies are generally obtained from analogy with stable molecules, although such an approach does present further problems[20]. As a rough guide to the magnitude of the 'steric factors' that result naturally from application of T.S.T. (cf. S.C.T.) see TABLE 1.3

TABLE 1.3: STERIC FACTORS FOR BIMOLECULAR REACTIONS (REPRINTED FROM REF. 3)

REACTANTS	COMPLEX	STERIC FACTOR (P)	VALUE OF STERIC FACTOR	η
A+A	L	1	1	$+\frac{1}{2}$
A+L	L	$(q_v/q_r)^2$	10^{-2}	$-\frac{1}{2}$
A+L	N	(q_v/q_r)	10^{-1}	0
A+N	N	$(q_v/q_r)^2$	10^{-2}	$-\frac{1}{2}$
L+L	L	$(q_v/q_r)^4$	10^{-4}	$-\frac{3}{2}$
L+L	N	$(q_v/q_r)^3$	10^{-3}	-1
L+N	N	$(q_v/q_r)^4$	10^{-4}	$-\frac{3}{2}$
N+N	N	$(q_v/q_r)^5$	10^{-5}	-2

A=atom; L=linear molecule; N=non-linear molecule.
η=exponent of temperature in the pre-exponential factor.

Steric factors in TABLE 1.3 have been evaluated assuming the partition functions per degree of translational, rotational and vibrational freedom are the same for all species with values of 10^8-10^9 cm^{-1}, 10-10^2 cm^{-1} and 1-10 cm^{-1} respectively. The exponent in the pre-exponential term (η) arises from the temperature dependence of the partition functions.

The preceding sections have dealt briefly with the major developments in chemical kinetic theory over the last 50years. It provides the language for the rationalisation of much of the kinetic data presented in subsequent chapters.

1.6 SPECTROSCOPIC CONSIDERATIONS

The importance of spectroscopic data for use in theoretical models has already been mentioned. Throughout this work the absorption and emission properties, of the Group VI atoms in particular, have been utilised for detection of the atomic reactants and measurements of kinetic data.

The interaction of electromagnetic radiation with atomic systems is coupled most strongly through the electric dipole moment (M). The probability of a transition between two states 'n' and 'm' is proportional to the square of the magnitude of the 'transition moment' (R_{nm}) (Equ. 1.27)

$$R_{nm} = \int \phi_n^* \, M \, \phi_m \, d\tau \qquad 1.27$$

If this integral is finite then the transition is said to be allowed, if zero the transition is forbidden. Transitions may be induced by coupling of the magnetic

dipole or quadrapole moment, however these effects are considerably weaker (10^{-5} and 10^{-8} of the electric dipole transition probabilities, respectively). See TABLE 1.4 for the selection rules for atomic transitions.

TABLE 1.4 SELECTION RULES FOR ATOMIC TRANSITIONS (REPRINTED FROM REF 24)

ELECTRIC DIPOLE	MAGNETIC DIPOLE	ELECTRIC QUADRAPOLE
$\Delta J=0,\pm1$	$\Delta J=0,\pm1$	$\Delta J=0,\pm1,\pm2$
$(0\leftarrow/\rightarrow0)$	$(0\leftarrow/\rightarrow0)$	$(0\leftarrow/\rightarrow0,\frac{1}{2}\leftarrow/\rightarrow\frac{1}{2},0\leftarrow/\rightarrow1)$
$\Delta M=0,\pm1$	$\Delta M=0,\pm1$	$\Delta M=0,\pm1,\pm2$
PARITY CHANGE	NO PARITY CHANGE	NO PARITY CHANGE
ONE ELECTRON JUMP	NO ELECTRON JUMP	ONE OR NO ELECTRON JUMP
$\Delta l=\pm1$	$\Delta l=0,\Delta n=0$	$\Delta l=0,\pm2$
$\Delta S=0$	$\Delta S=0$	$\Delta S=0$
$\Delta L=0,\pm1$	$\Delta L=0$	$\Delta L=0,\pm1,\pm2$
$(0\leftarrow/\rightarrow0)$		$(0\leftarrow/\rightarrow0,0\leftarrow/\rightarrow1)$

The relationship between emission and absorption of spectral lines by atomic species and the transition moments were established by Einstein and are stated below.

$$I^{nm}_{emiss} = N_n \, h \, cv_{nm} \, A_{nm} \qquad 1.28$$

$$A_{nm} = \frac{64\Pi^4 v_{nm}^{\ 3}}{3h} \, | \, R_{nm} \, |^2 \qquad 1.29$$

$$I^{nm}_{abs} = I^{nm}_{o} \; N_m \, B_{mn} \, hv_{nm} . \Delta x \qquad 1.30$$

$$B_{mn} = \frac{8\Pi^3}{3h^2 c} \, | \, R_{nm} \, |^2 \qquad 1.31$$

where n and m refer to the upper and lower states respectively

v = wave number

c = velocity of light

A_{nm} = Einstein transition probability of spontaneous emission

B_{mn} = Einstein transition probability of absorption.

The relationship between emission/absorption intensity and frequency should be noted.

The Group VI elements possess a s^2,p^4 electronic configuration in the valence shell which generates a ^3P_J ground state and $^1D_2$ first excited state. (The energy levels of these states and the $^1S_0$ state are illustrated for oxygen and sulphur in FIG 1.4). Reference to TABLE 1.4 explains the metastable nature of the first excited state with radiative lifetimes of 128 s and 28 s for oxygen and sulphur, respectively.

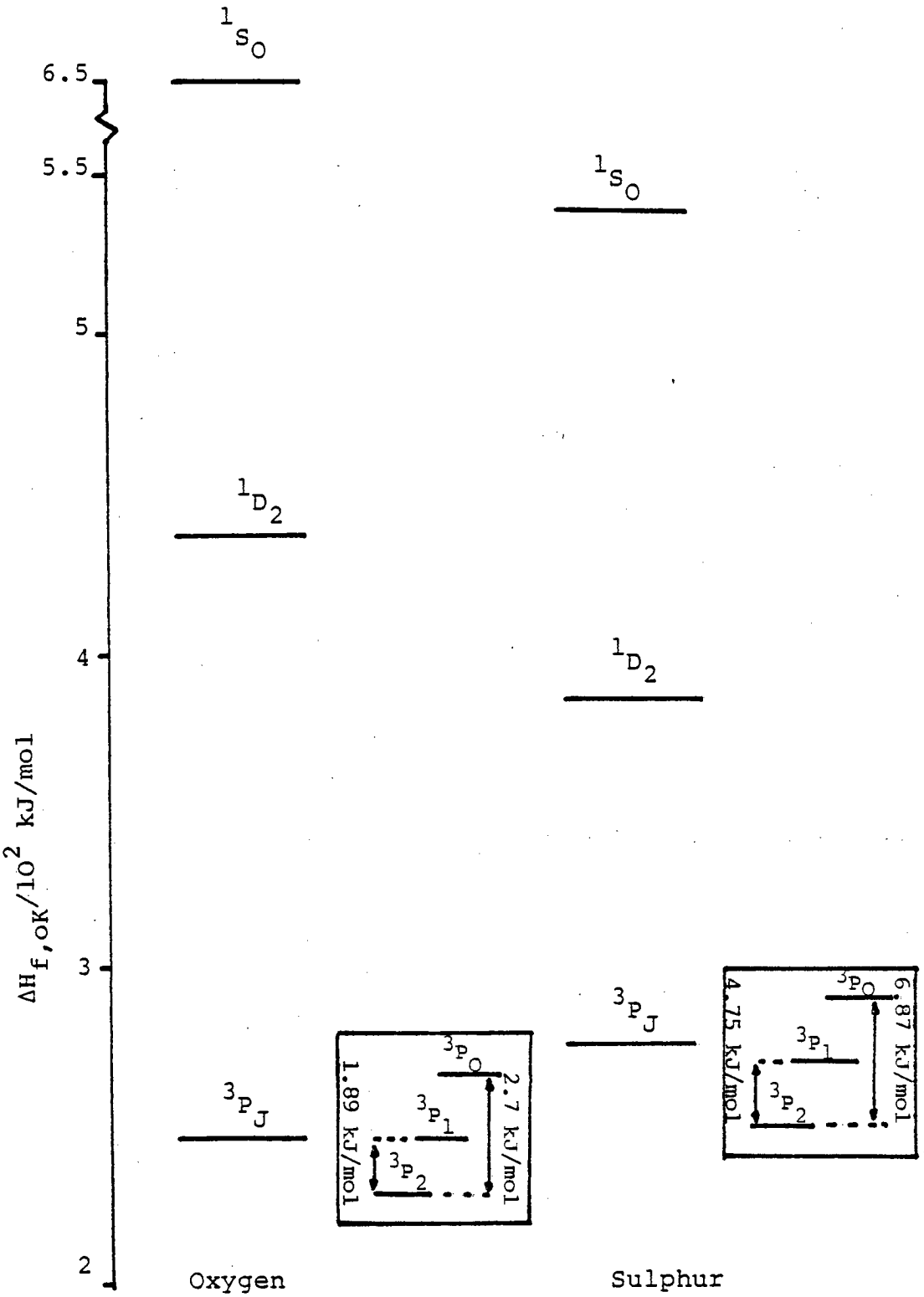

FIG 1.4 Energies of the ground and first two excited states of atomic Oxygen and Sulphur

The long radiative lifetimes result in removal of these species through chemical reaction or quenching to the ground state. The reactivity of the ($^1D_2$) state compared to the (^3P_J) ground state is in general very different. In many instances this may be attributed to thermodynamic constraints, in others where both have exothermic reaction channels available the use of correlation diagrams has aided the rationalisation of the kinetic data[16].

Oxygen atom chemistry has been extensively studied and has been well reviewed[21,22]. Sulphur atom chemistry has received much less attention although it was the subject of early work on excited state chemistry[23]. The work presented in this thesis advances the knowledge of both these elements, the S($^1D_2$) work being facilitated by development of the first direct observation techniques for this species.

1.7 REFERENCES

1. K.J. Laidler, Theories of Chemical Reaction Rates, Publ. McGraw-Hill Book Co. (1969).
2. A. Marcelin, Ann. Phys. 3, (1915), 158.
3. G.L. Pratt, Gas Kinetics, Publ. John Wiley & Sons Ltd. (1969).
4. H. Eyring and M. Polanyi, Z. Physik. Chem. (Leipzig), B12, (1931), 279.
5. Y. Sugiura, Z. Physik 45, (1927), 484.
6. S. Sato, Bull. Chem. Soc. Japan 28, (1955), 450.
7. S. Sato, J. Chem. Phys. 23, (1955), 592.
8. S. Glasstone, K.J. Laidler and H. Eyring, The Theory of Rate Processes, Publ. McGraw Hill Book Co. (1941).
9. H.S. Johnston, Advan. Chem. Phys. 3, (1960), 131.
10. H.S. Johnston and C. Parr, J. Am. Chem. Soc., 85, 2544, (1963).
11. M.G. Evans and M. Polanyi, Trans. Faraday Soc. 34, (1938), 11.
12. R.H. Krech, G.J. Diebold and D.L. McFadden, J. Amer. Chem. Soc. 99, (1977), 4605.
13. I.W.M. Smith, Kinetics and Dynamics of Elementary Gas Reactions, Publ. Butterworths (1980).
14. E. Wigner and E.E. Witmer, Z. Physik 51, (1928), 859.
15. K.E. Shuler, J. Chem. Phys. 21, (1953), 624.
16. R.J. Donovan and D. Husain, Chem. Rev. 70, (1970), 489.
17. B.H. Mahan, Acc. Chem. Research 8, (1975), 55.
18. R.G. Pearson, Symmetry Rules for Chemical Reactions, Publ. Wiley Interscience, (1976).

19. J.H. Knox, Molecular Thermodynamics, Publ. Wiley-Interscience (1971).

20. H.S. Johnston, Gas Phase Reaction Rate Theory, Publ. Ronald, New York (1966).

21. R.J. Donovan, D. Husain and L.J. Kirsch, Ann. Rep. Chem. Soc. 69, (1972), 19.

22. M.C. Lin, 'Dynamics of Oxygen Atom Reactions' in Potential Energy Surfaces (Ed.) K.P. Lawley; Advances in Chemical Physics XLII; Publ. Wiley Interscience.

23. O.P. Strausz and H.E. Gunning, Adv. Photochem., 4, (1966), 143.

24. R.J. Donovan, Prog. in Reaction Kinetics 10, (1979).

CHAPTER II

EXPERIMENTAL TECHNIQUES

2.1 INTRODUCTION

Physical chemistry is concerned with the measurement of fundamental properties of chemical systems. As such the success or failure of any experiment is very dependent on the careful design and construction of apparatus that will allow these objectives to be reached. In the study of gas kinetics of atomic and molecular reactions the continuing growth in knowledge owes much to a concomitant advance in the fields of electronics, optics and instrument design[1,2].

The atomic and free radical species studied in this work, whether in the ground or electronically excited states, are of a reactive nature - existing for only ca 1 to 10,000 collisions. As at atmospheric pressure there are 10^9 collisions s^{-1} it is quickly appreciated that in order to follow a reaction (even at greatly reduced pressures) rapid production and mixing of the specified reactants and fast detection techniques are necessary. The first of these requirements has been fulfilled exclusively, in this work, by the technique of flash photolysis. The second has been achieved through the construction and modification of various systems - all utilising the u.v. absorption spectra of the reactants and products of interest. The principle feature of any detection system, providing data acquisition is of the required speed, is its sensitivity

and selectivity for a specific species. The development of techniques both in this work and in the field in general has been reflected by improved performance in each of these areas.

The pages following present a brief outline of the experimental systems used throughout this work. This is followed by a more detailed discussion of the component parts of each system. Finally the technique of molecular modulation spectroscopy is discussed.

2.2 FLASH SPECTROSCOPY (F.S.)

The technique of flash spectroscopy coupled to flash photolysis was developed by Porter and Norrish[3], and provided the first direct observational technique for many short lived radicals. The system used in this work was designed and built by D. Little (FIG 2.1). Reactant species were generated by flash photolysis (E≈1000 J). The quartz reaction vessel of 1 m length lay parallel to the flash lamp. At a pre-arranged delay time (10 μs - 1 s) following the firing of the photolysis lamp a spectroflash lamp (E≈75 J) placed at one end of the reaction vessel was fired. The white light from this source was focussed through the reaction vessel and onto the entrance slit of a spectrograph to be dispersed and recorded on a photographic plate. Any species generated in the reaction vessel possessing an absorption spectrum in the wavelength region from 200-650 nm will be recorded on the photographic plate. The evolution of the species with time may be

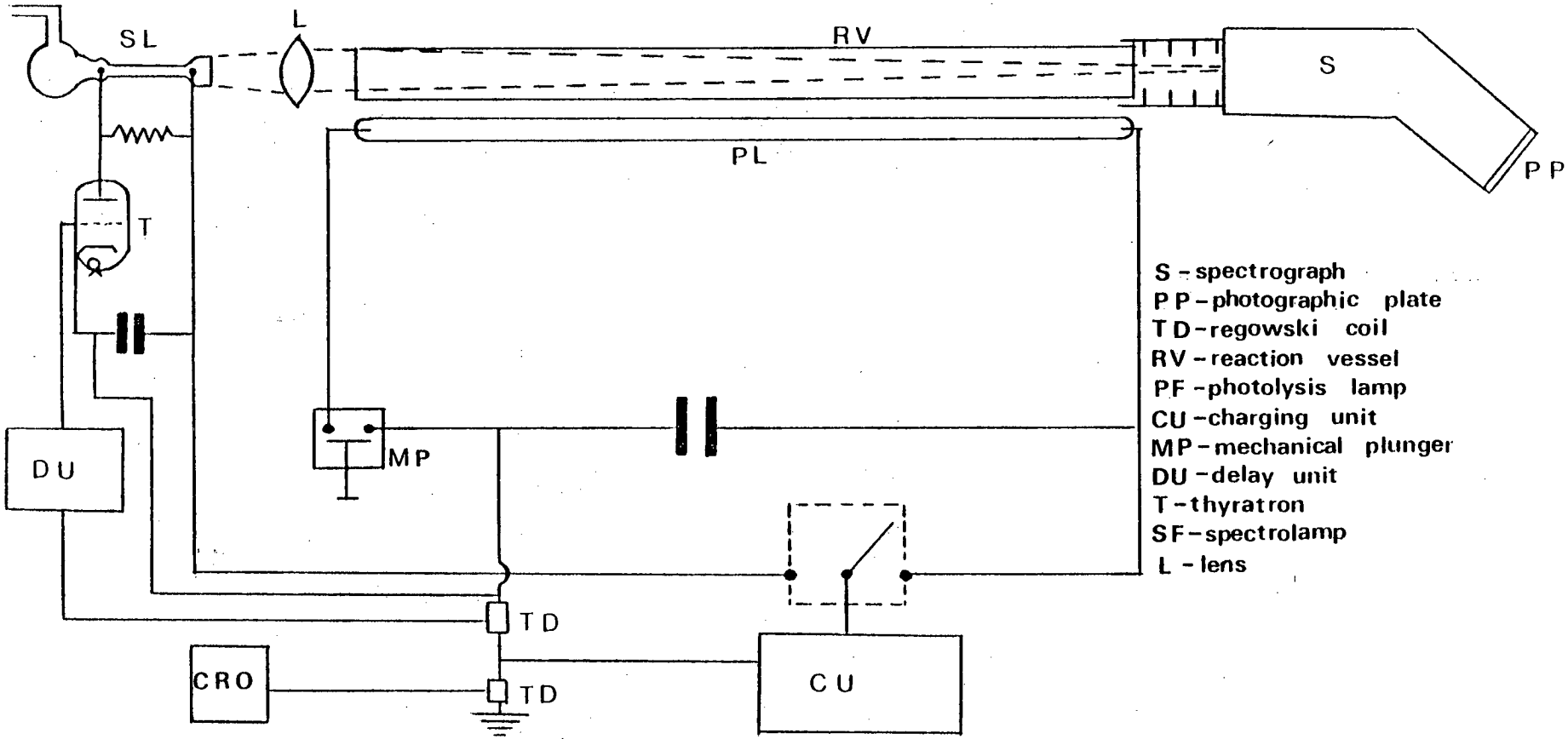

FIG 2.1 FLASH SPECTROSCOPY SYSTEM

monitored by recording the spectrum at various delays following the firing of the photolysis lamp. This technique is invaluable in the characterisation of new chemical systems, allowing the instantaneous recording of all absorbers in the system at any time throughout the reaction. In obtaining kinetic information, however, it suffers from the disadvantage that many experiments must be performed under constant conditions. This coupled with inherent signal to noise problems, through the use of photographic plates, can lead to relatively large errors on final results.

2.3 ABSORPTION SPECTROPHOTOMETRY (A.S.)

The technique of atomic absorption spectroscopy has wide use as an analytical tool. Its application to gas kinetics and expansion to cover absorption by molecular species has been reviewed in detail by Porter and West[4]. In this work a versatile system enabling vacuum u.v. detection of atomic species was employed (FIG 2.2). Further a system was developed in collaboration with J. Garraway to observe the hydroxyl radical in the near u.v. (FIG 2.3). This apparatus followed a design by Morley and Smith[5].

As previously, reactant species were generated by flash photolysis of suitable molecules. The atomic or radical concentration produced on photolysis was then monitored by photoelectric observation of the attenuation of a constant light source emitting at a wavelength known to be absorbed by the species of interest. In all cases

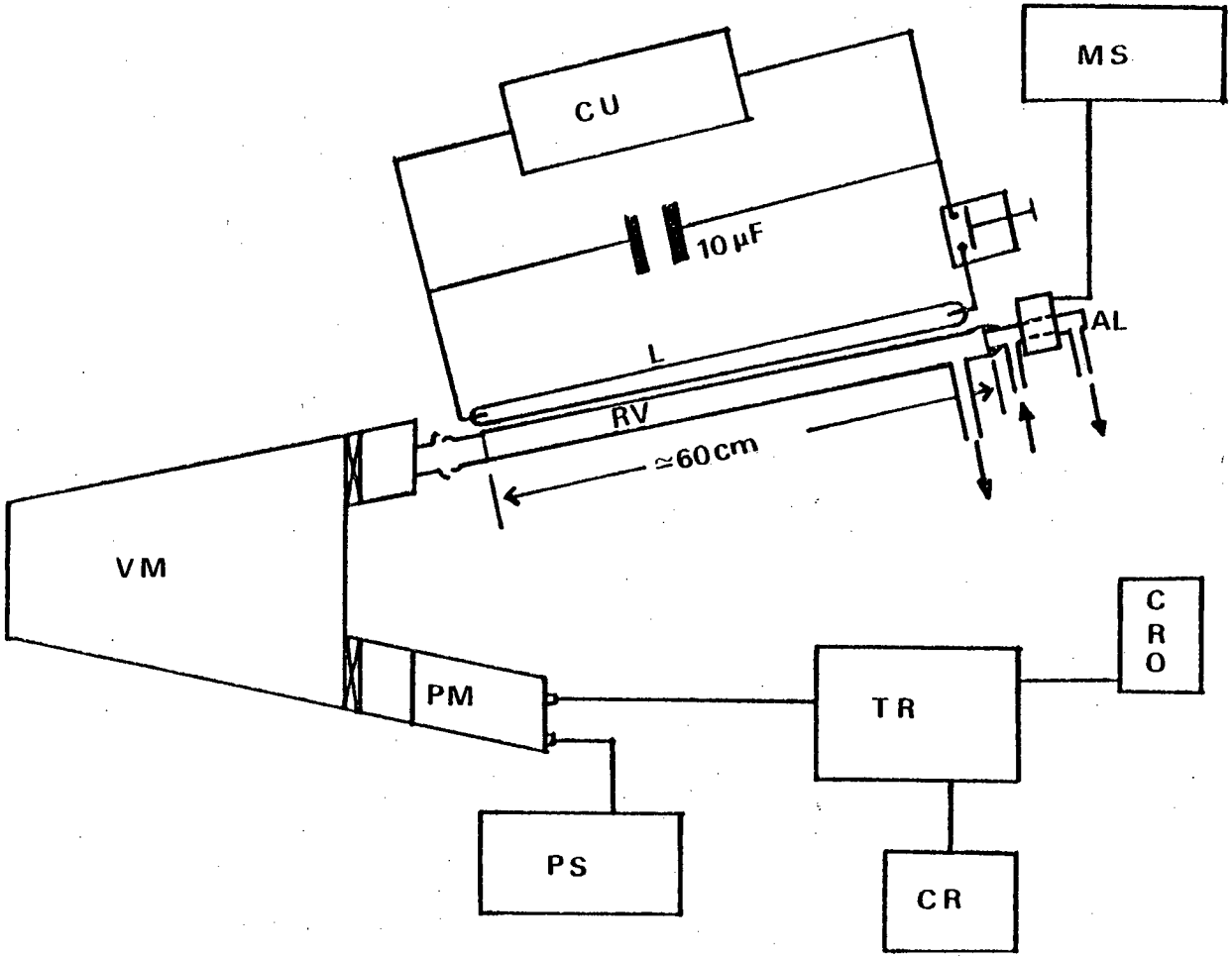

MS - Microwave power supply
CU - Charging unit
L - Photolysis lamp
AL - Atomic lamp
RV - Reaction vessel
VM - Vacuum monochromator
PM - Photomultiplier
PS - Power supply
TR - Transient recorder
CR - Chart recorder

FIG 2.2: Atomic Absorption Spectrophotometer

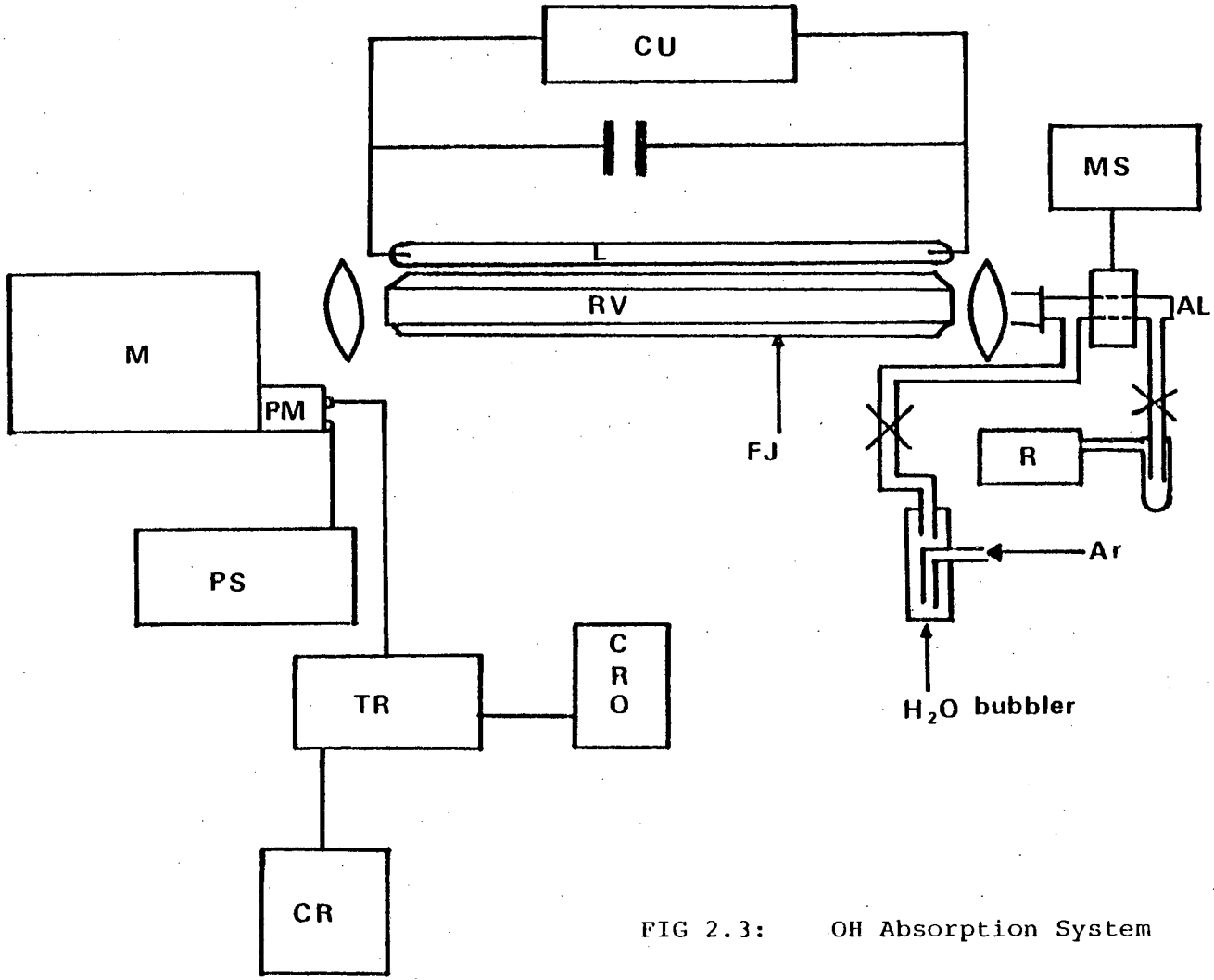

MS - Microwave power supply
CU - Charging unit
R - Rotary pump
L - Photolysis lamp
RV - Reaction vessel
FJ - Filter jacket
M - Monochromator
PM - Photomultiplier
PS - Power supply
TR - Transient recorder
CR - Chart recorder
AL - Atomic lamp

FIG 2.3: OH Absorption System

the monitoring light beam was generated using a microwave powered flow lamp. The selected wavelength was isolated by use of a monochromator. The photoelectric detection system comprised a suitable photomultiplier coupled to a fast transient recorder. Absorption spectrophotometry provides an excellent means of monitoring rapid growth or removal processes directly. If a good light source is available concentrations of $\gtrsim 10^{10}$ molecules cm^{-3}, for atoms with large oscillator strengths, may be monitored. The disadvantage of the technique lies in the often observed non linear relationship between the absorbance and concentration. This must be corrected for in the kinetic analysis. Further, observation of weakly absorbing species invariably results in poor signal to noise ratios unless signal averaging techniques are employed.

2.4 RESONANCE FLUORESCENCE (R.F.)

The resonance fluorescence technique, at the present time, represents one of the most sensitive detection systems available to the gas kineticist. Two systems were employed in this work. The first was designed and constructed by H.M. Gillespie to observe the kinetics of $I(5^2P_{1/2})$, this was the first use of the technique to monitor excited, as opposed to ground state, species[6]. For the present work the detection system was altered to allow observation of $O(2^3P_{2,1,0})$ atoms. See FIG 2.4. The second system (FIG 2.5) was developed for use with an excimer laser photolysis source.

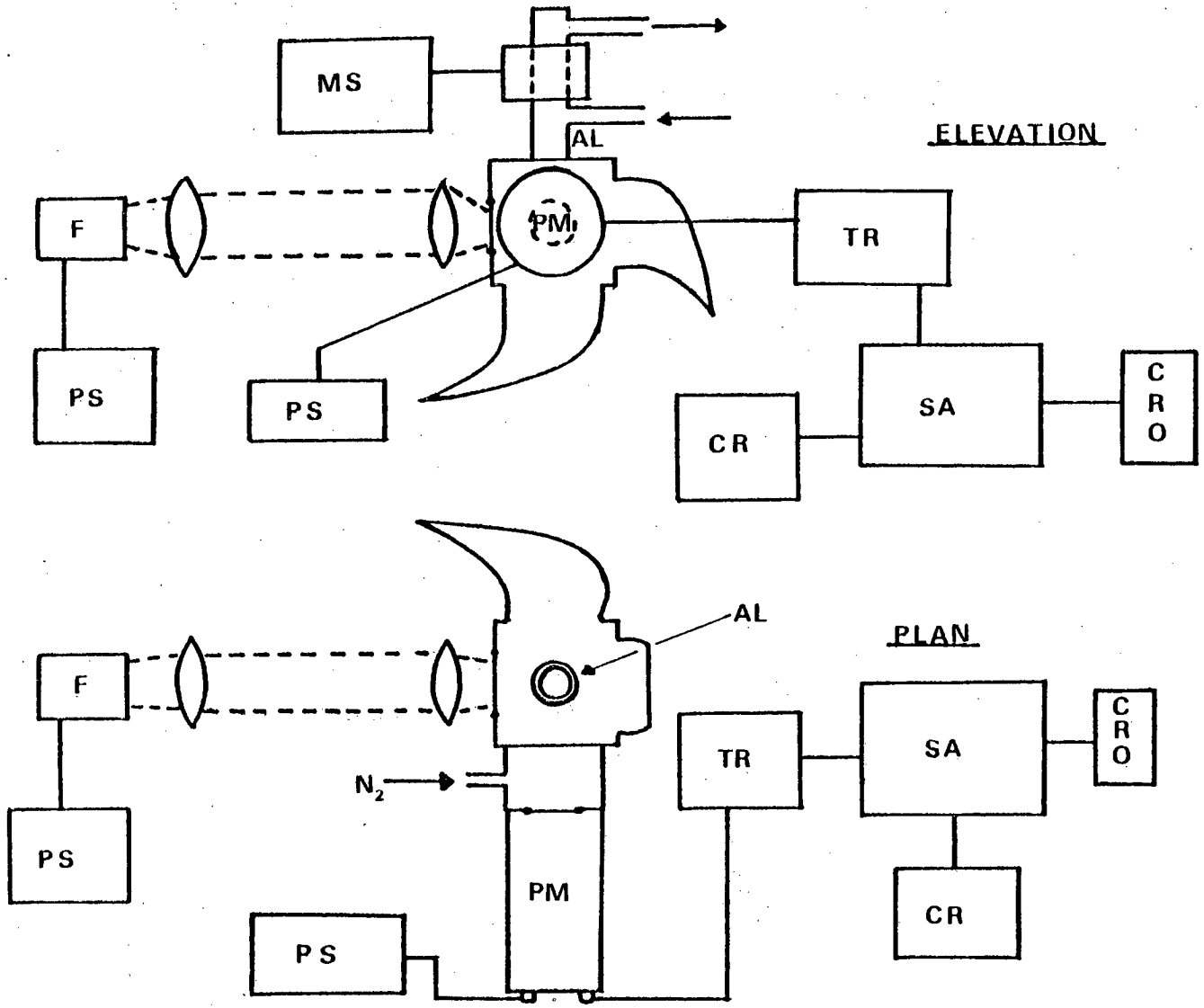

AL - Atomic lamp
F - Photolysis lamp
PM - Photomultiplier
MS - Microwave power supply
TR - Transient recorder
SA - Signal averager
CR - Chart recorder
PS - Photomultiplier power supply

FIG 2.4: Resonance fluorescence system

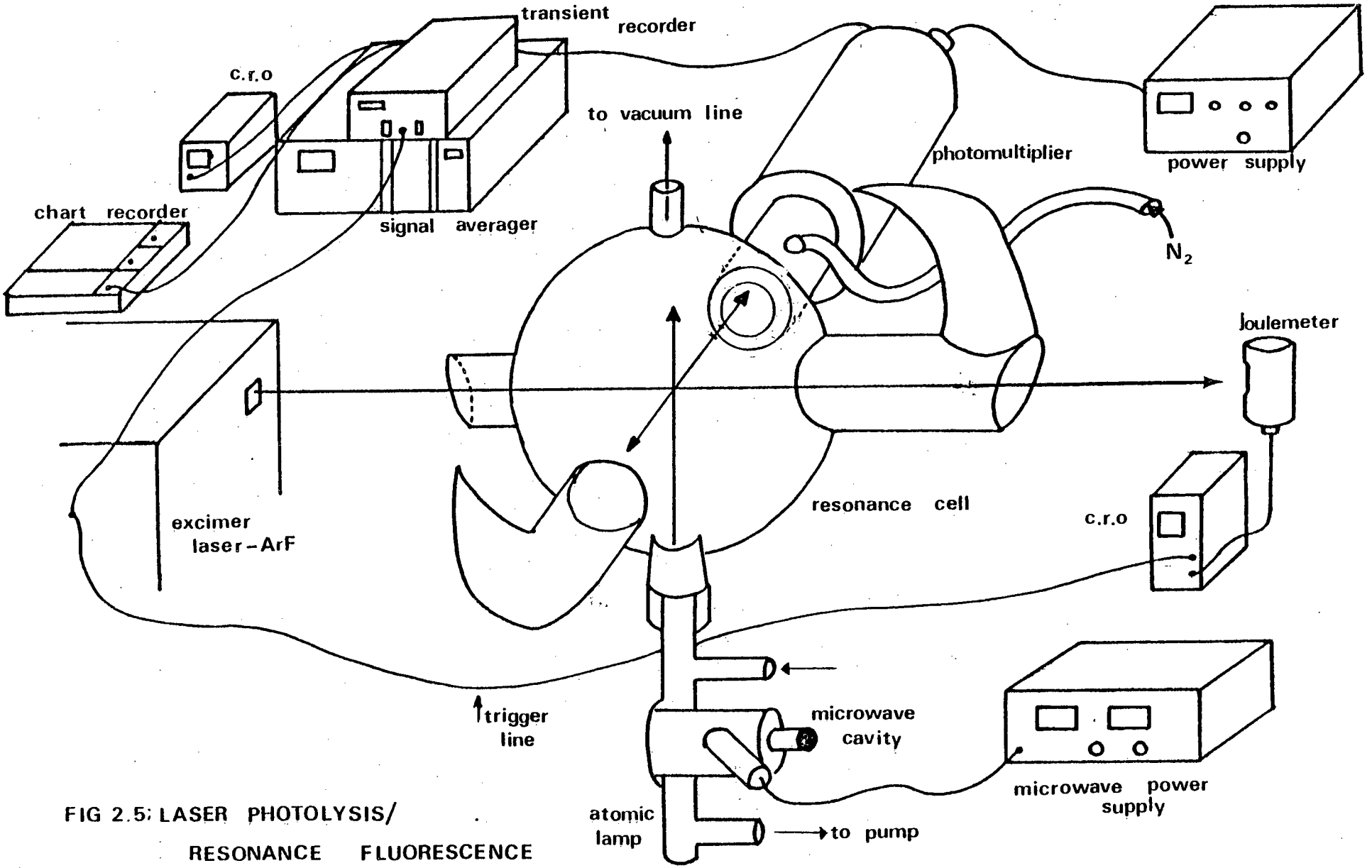

FIG 2.5: LASER PHOTOLYSIS/ RESONANCE FLUORESCENCE SYSTEM

The principles of operation of each system are the same. Orthogonal to, and intersecting, the photolysing light one positions a light source emitting wavelengths which are absorbed by the species to be observed. Rather than observing the attenuation of this light source a photomultiplier set orthogonal to both photolytic and probing light sources captures the reemission from the now 'excited' molecule or atom of interest. This technique is potentially more sensitive than the absorption technique since it detects only the fluorescence signal. In absorption one observes small attenuations of a relatively large continuous light level. This increased sensitivity allows operation at low radical concentrations, in the region where fluorescence intensity is directly proportional to the concentration of the emitting species. Further, low detectable concentrations enables low energy photolysis sources and short pathlengths to be used, when coupled to signal averaging for the improvement of signal to noise ratios. This has even facilitated the use of resonance fluorescence techniques on balloon and rocket experiments sampling the Earth's atmosphere[7,8].

2.5 FLASH PHOTOLYSIS

The requirements of any flashlamp employed for the purpose of initiating a chemical reaction through dissociation of a parent molecule are three fold: the flash duration must be short in comparison to the time scale of the reaction; the energy dissipated and time characteristics must be reproducible over a large number

of experiments; the emission from the lamp should match the absorption spectrum of the parent molecule.

In achieving these requirements three types of flash lamp have been employed.

(i) CONVENTIONAL DISCHARGE FLASH LAMP This type of flash lamp was used in conjunction with the flash spectroscopy and absorption spectrophotometry detection systems. The design of the lamp and firing circuit is discussed fully elsewhere[9]. Briefly the lamps of 15 mm internal diameter, ranged from 1 m to 0.5 m in length. The machined mild steel or tungsten electrodes were secured to either end of the quartz lamp by means of Picein wax. Each lamp was filled with krypton to a pressure of 650-1000 Nm^{-2} and was found to have a working life of >200 flashes per gas filling. Across the electrodes a capacitor was connected which could be charged, by means of a high voltage supply - Hivotronic Ltd. 50-20-1 (F.S., FIG 2.1), Hipotronics 820-20 (A.A.S.) and Applied Photophysics (OH, A.S.) - to deliver a maximum flash energy of 980 J (F.S.) and 320 J (A.S.). In all cases the capacitors were discharged through the depression of a mechanical plunger. In the flash photolysis/A.A.S. system the charging circuit was designed to be self screening (in terms of electrical noise) by running the earth line through the earth connection of the coaxial cable carrying the live (centre core) connection from the capacitor to the flash lamp. Whether this made a large improvement is difficult to judge, although noise from this source was rarely a problem. The spectral output from this

type of lamp under the conditions used has been shown to provide an essentially continuous white light source. Where problems were envisaged by unwanted photolysis of some reactant, filter jackets fitted around the reaction vessel, lying between it and the parallel mounted flash lamp, when filled with the correct filter solution eradicated the problem. The pulse duration displayed by these lamps was approximately 15 μs. Good optical coupling of the flash lamp and reaction vessel were achieved through use of a 'wrap around' aluminium foil reflector.

(ii) PULSED FLASH LAMP Basically the principles of operation of this commercially available flash lamp (Oriel Pulsed Xenon Light Source/Supply 3021) are the same as that described above. Due to the cut off of the glass used in the lamp construction (3025 Xenon lamp), the spectral output of the lamp maximised at 250 nm and was negligible below 205 nm. Two energy settings were available, low (0.03 J, pulse duration = 2.5 μs) and high (0.25 J, pulse duration = 6.5 μs). The lamp was used only in the resonance fluorescence (FIG 2.4) system where it was run exclusively on the high energy setting and at repetition rates of approximately 1 Hz. In this system lenses were used to collect and focus the light into the resonance cell. The repetitive pulse operation of the lamp made it ideal for use with signal averaging techniques.

The theoretical constraints to be considered in the design of discharge flash lamps is reviewed in depth by Porter and West[4]. The main results are summarised in appendix 2.

(iii) LASER PHOTOLYSIS The laser presents an ideal light source for many photochemical applications. Its special properties of monochromaticity, temporal and spatial coherence and high power make it exceedingly versatile. Further the advent of a range of dye lasers possessing tunability over the range from 300 to 750 nm and the introduction of frequency doubling and quadrupling devices has greatly extended the laser's sphere of influence.

In using a laser as a photolysis source one exploits the short pulse duration and spatial coherence of the beam. The former ensures fast reactions may be monitored in the absence of complications from a convoluted flash profile. In the detection systems employed in this work however, scattered light saturating the photomultipler was the limiting process in obtaining kinetic data at short times (e.g. <200 μs) after initiation. The spacial coherence of the laser reduces the problem when compared to conventional flash lamps of similar energies. In this work laser photolysis was used exclusively for the production of $S(3^1D_2)$ atoms from CS_2. The $S(3^1D_2)$ atom concentration was monitored through the use of a resonance fluorescence detection system (FIG 2.5). The laser used was a Lambda Physik Excimer EMG500 Multigas laser. In all experiments the lasing medium used was argon fluoride. The gas mixture in the laser cavity was renewed whenever output energies, after passage through the resonance cell, had fallen below 0.8 mJ per shot. The laser was filled with high purity gases to the following pressures: F_2/He (5% F_2) = 16 kNm^{-2}, Ar = 53.2 kNm^{-2},

He (buffer gas) = 130.3 kNm^{-2}. Output from the laser was at 193±1 nm and of 14 ns pulse width. The beam dimensions were 5 mm (horiz.) x 22 mm (vert.). Experiments were conducted at laser energies, after reflection from two mirrors and passage through a path length in the atmosphere of approximately 1.5 m and the resonance cell (0.15 m), of between 2 and 0.8 mJ per shot. Preioniser and main discharge settings were 22 kV and 25-27 kV respectively. Laser energy was monitored by means of a Gen-Tec Model ED-200 fast response joulemeter coupled to a C.R.O. (Telequipment DM64). When several shots were required the laser was fired at repetition rates of approximately 0.75 Hz. The theory behind laser action[10,11] in general and excimer laser operation[12] in particular have been covered extensively elsewhere. A summary of the basic principles involved appears in Appendix 3.

2.6 DIAGNOSTIC LIGHT SOURCES

(i) SPECTROFLASH LAMP The spectroflash lamp provides the monitoring light beam in the flash spectroscopy system (FIG 2.1). Ideally this source should produce white light. This was indeed the case with the lamp used although some superposed atomic lines were observed. The lamp was a conventional quartz capillary lamp (I.D. = 2 mm), the design having been discussed elsewhere[9]. The lamp was filled to a pressure of approximately 500 Nm^{-2} with krypton and had a working life per filling of several hundred flashes. When the capacitor supplying the lamp is charged (10 kV) - a 165 MΩ resistor placed across the tungsten electrodes maintains each at high voltage - the

lamp may be fired either manually or automatically, at some pre-set delay after the firing of the photolysis lamp. The firing of the photolysis lamp is sensed by pick-up from a Regowski induction coil connected across the common earth line. This in turn triggers a delay unit (Hivotronic Ltd.) which at the preset delay produces a 100 V spike across the grid of a hydrogen thyratron. The circuit is completed by the potential now developed across the thyratron and the capacitor discharges to earth, firing the lamp. The delay between photoflash and spectroflash was monitored by a further Regowski coil connected to a Tektronix Type 549 Storage Oscilloscope.

(ii) FLOW LAMP The term flow lamp is used throughout to signify a lamp in which light emanates from a microwave generated plasma in a flowing gas mixture. Generally these lamps are used as atomic line sources (TABLE 2.1) and occasionally for detection of specific radicals through generation of their band spectra e.g. $OH(X^2\Pi)$. The design of the lamps used both for absorption and fluorescence work were basically the same with only minor alterations in dimensions. The design largely follows that of Davis and Braun[13]. The lamp was made from pyrex, the optical window being fixed to the lamp body by Picein wax or epoxy resin such that in no circumstances would the plasma come into contact with the seal (FIG 2.6). The choice of window was governed by the emitted wavelength of interest. In all atomic absorption and resonance fluorescence experiments MgF_2 windows were preferred (22 mm diameter, 2 mm thick, cut-off $\sim$ 115 nm). They

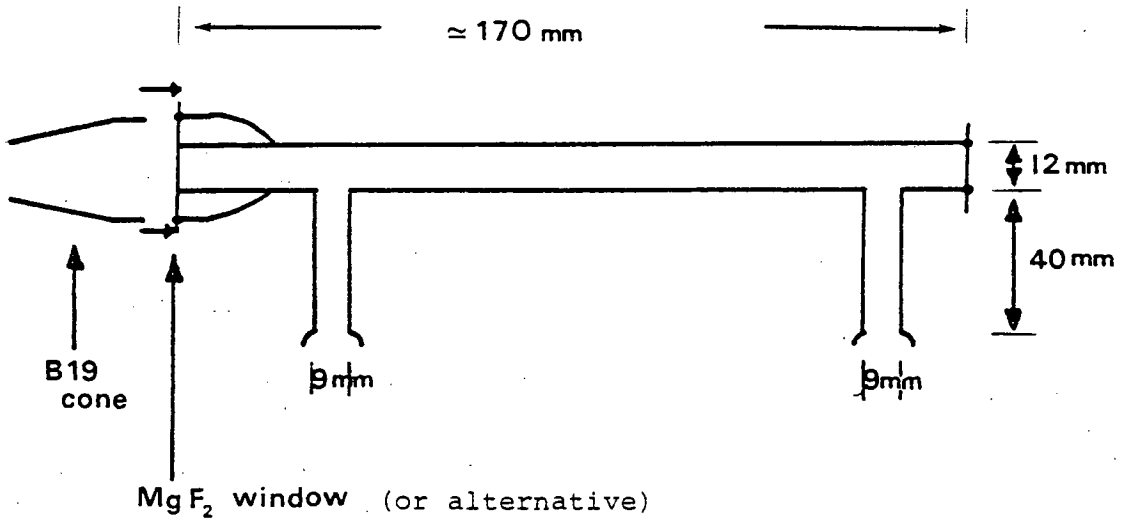

FIG 2.6: Typical Flow Lamp Design

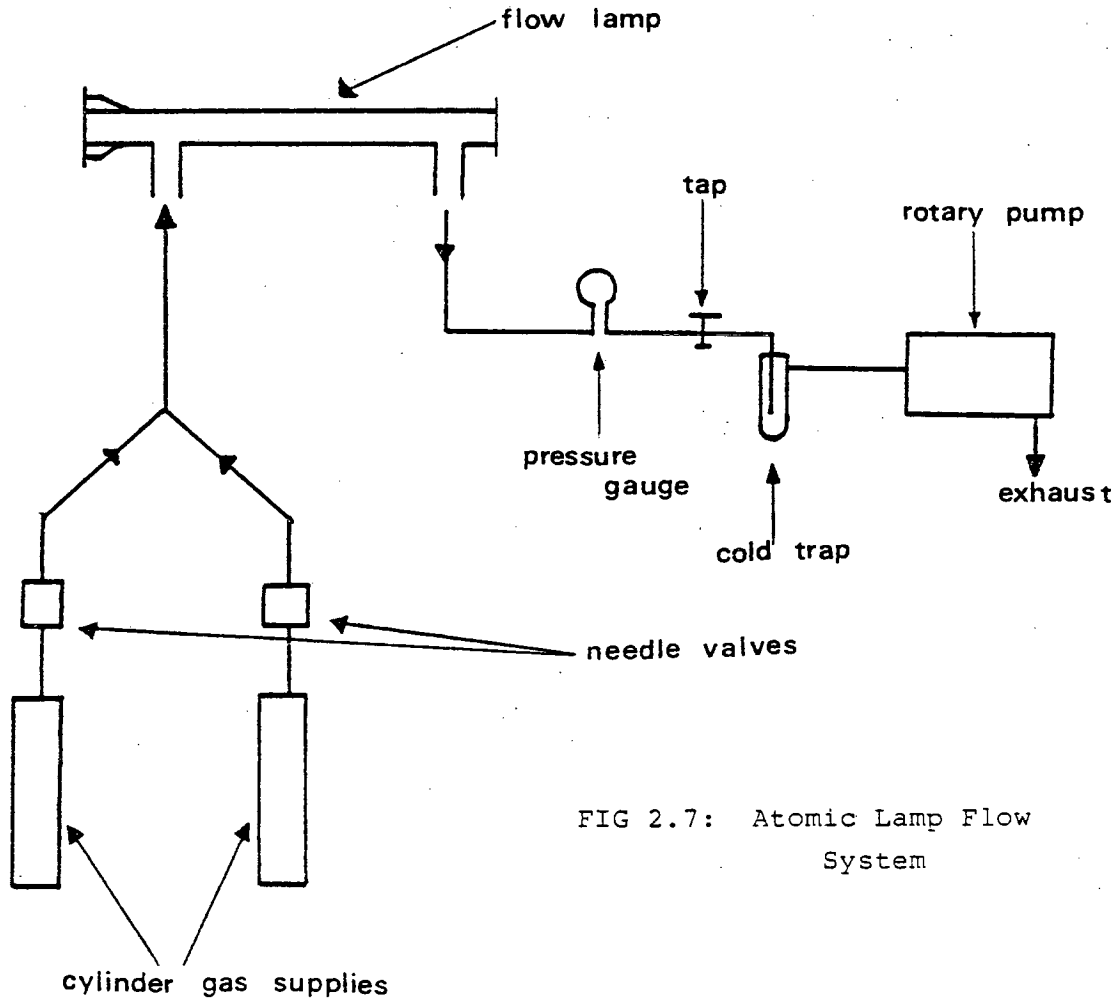

FIG 2.7: Atomic Lamp Flow System

TABLE 2.1: ATOMIC LINE SOURCES (REPRINTED IN PART FROM REF 13)

Atomic Species	Source Molecule	Emission Line/nm	Transition
H	H_2	121.57	$(2p)\,^2P_{1/2} \rightarrow (1s)\,^2S_{1/2}$
Xe	Xe	146.96	$(5p^5 6s)\,^2P_{3/2} \rightarrow (5p^6)\,^1S_O$
Kr	Kr	123.58	$(4p^5 5s)\,^2P_{3/2} \rightarrow (4p^6)\,^1S_O$
		116.49	$P_{1/2} \rightarrow S_O$
O	O_2	130.22	$(2p^3 3s)\,^3S_1^O \rightarrow (2p^4)\,^3P_2$
		130.49	$^3S_1^O \rightarrow {}^3P_1$
		130.60	$^3S_1^O \rightarrow {}^3P_O$
		115.2	$^1D_2^O \rightarrow {}^1D_2$
N	N_2	174.52 }	$(2p^2 3s)\,^2P \rightarrow (2p^3)\,^2P_O$
		174.27 }	
		149.47 }	$^2P \rightarrow {}^2D_O$
		149.26 }	
		141.19	$^2D \rightarrow {}^2P_O$

TABLE 2.1 continued

Atomic Species	Source Molecule	Emission Line/nm	Transition
Cl	Cl_2	139.65	$(3p^4 4s)\,^4P_{3/2} \rightarrow (3p^5)\,^2P^O_{1/2}$
		138.99	$^4P_{1/2} \rightarrow {}^2P^O_{1/2}$
		137.96	$^4P_{3/2} \rightarrow {}^2P^O_{3/2}$
		136.35	$^2P_{3/2} \rightarrow {}^2P^O_{1/2}$
		135.17	$^2P_{1/2} \rightarrow {}^2P^O_{1/2}$
		134.73	$^2P_{3/2} \rightarrow {}^2P^O_{3/2}$
Br	Br_2	163.36	$(4p^4 5s)\,^4P_{3/2} \rightarrow (4p^5)\,^2P^O_{1/2}$
		158.24	$^4P_{1/2} \rightarrow {}^2P^O_{1/2}$
		157.65	$^4P_{3/2} \rightarrow {}^2P^O_{3/2}$
		154.08	$^4P_{3/2} \rightarrow {}^2P^O_{3/2}$
		157.50	$^2P_{3/2} \rightarrow {}^2P^O_{3/2}$
		153.19	$^2P_{1/2} \rightarrow {}^2P^O_{1/2}$
		148.86	$^2P_{3/2} \rightarrow {}^2P^O_{1/2}$
		144.99	$^2P_{1/2} \rightarrow {}^2P^O_{3/2}$
		138.46	$^4P_{1/2} \rightarrow {}^2P^O_{1/2}$

TABLE 2.1 continued

Atomic Species	Source Molecule	Emission Line/nm	Transition
C	CH_4	193.09	$(2s^2 2p^3 s)\,{}^1P^O_1 \rightarrow (2s^2 2p^2)\,{}^1D_2$
		165.81	
		165.70	${}^3P^O \rightarrow {}^3P$
		165.63	
		156.03	
		156.07	${}^3D_O \rightarrow {}^3P$
		156.14	
S	H_2S	191.49	$(3p^3 4s)\,{}^5S^O_2 \rightarrow (^3p^4)\,{}^3P_1$
		190.03	${}^5S^O_2 \rightarrow {}^3P_2$
		182.63	${}^3S^O_1 \rightarrow {}^3P_O$
		182.04	${}^3S^O_1 \rightarrow {}^3P_1$
		180.73	${}^3S^O_1 \rightarrow {}^3P_2$
		166.7	${}^1D^O_2 \rightarrow {}^1D_2$

proved considerably tougher, of better optical quality and more resistant to radiation damage than the corresponding LiF windows available. For OH absorption spectroscopy good quality spectrosil windows (cut-off λ 165 nm) were used. In the apparatus illustrated in FIG 2.2 (A.A.S.) and FIG 2.5 (R.F.) the total number of windows in the system were reduced by the use of a B19 cone connection on the flow lamp (attached to the window by epoxy resin) which matched with the corresponding socket on the reaction vessel.

The basic flow system used is shown in FIG 2.7. This system was designed to allow the continuous flow of two gases from high pressure reservoirs. Unfortunately the poor quality of needle valves did not produce the reproducibility of conditions that was often desired. Hence the system was frequently operated using a 2 litre bulb of premixed gases to provide the flow mixture. This was easily interchangeable with the system illustrated by isolation of one of the gas feed lines and connection of the bulb in place of the cylinder on the other feed line. In the OH flow lamp the argon flow gas was passed through a water bubbler. The saturated argon produced sufficiently intense OH emission bands. Pressures were monitored either with an oil (n-butyl pthalate) manometer or a low pressure Bourdon gauge. Typical standing pressures in the lamp were of the order of 0.2 - 0.5 kNm^{-2} although in certain experiments pressures used were as high as 1.9 kNm^{-2}. A liquid nitrogen trap between pump and lamp prevented back diffusion of oil onto the windows. Another precaution against window contamination was to ensure the gas flow was away from the window. The microwave cavity was of the

Evenson-Broida design and was powered from a microwave power supply operating at 2450 MHz (EMS Microtron 200). Incident powers used ranged from 30-75 W, with the cavity tuned to produce a stable, non fluctuating plasma at low reflected powers.

Lamp performance and spectral characteristics In employing a flow lamp as an atomic or radical detector, either through use in an absorption or fluorescence system, the parameters of greatest importance are overall intensity and the self absorption (or reversal) of the light source. The interaction of these two parameters and their subsequent effect on the monitored absorbance or fluorescence for a given reactant concentration is a complex problem which has been the subject of much theoretical[14,15] and experimental[16,17] work in recent years. In an absorption experiment one is interested in the ratio of I_O/I_{TR} where I_{TR} and I_O are the light intensities falling on the detector in the presence and absence of absorbers, respectively. In a fluorescence experiment fluorescent emission is maximised by increasing the absolute rate of absorption of energy.

Within any lamp emitters and absorbers will be present at finite concentrations. In the type of lamp exploited in this work the gradient of absorber concentration toward the wall will be largely determined by the diffusion rate and the efficiency of removal of absorbers at the wall. If this removal is inefficient, the ratio of the excited to 'ground state' atom concentration will become small toward the wall and this will constitute a reversing layer. The action of the reversing layer may be understood

with reference to FIG 2.8. The linewidth of any atomic line emitted by the lamp is governed almost entirely by Doppler broadening which is in turn related to the temperature of the plasma. Hence the emission from the centre of the plasma will be broader than that of the absorption structure at the cooler extremities of the lamp. The resultant line shape is shown in FIG 2.8B. This pictorial representation illustrates that while the overall intensity of the lamp may well increase the absorbance or absolute energy absorbed may both decrease. The theoretical computation of this problem is by no means an easy one. The simplest approach follows that of Braun and Carrington[14] in which a three layer model is used (see FIG 2.9). Where the atomic structure is of a well resolved multiplet arising from emission from a common upper state to a 'split level' ground state, application of this model results in a variation of the ratio of the multiplet intensities with the optical depth of the reversing layer. Hence in such systems one has a simple diagnostic test as to the reversal in the lamp. However, for quantitative kinetic studies, the relationship between the various lamp parameters e.g. incident power, flow rates and constitution, and the functional dependence of absorbance or fluorescence on atomic concentration is of prime importance. Much experimental work was undertaken to optimise absorption and fluorescence signals. A detailed study, illustrating the very sensitive nature of the absorption measurements with respect to flow lamp conditions was undertaken on the sulphur atom transitions

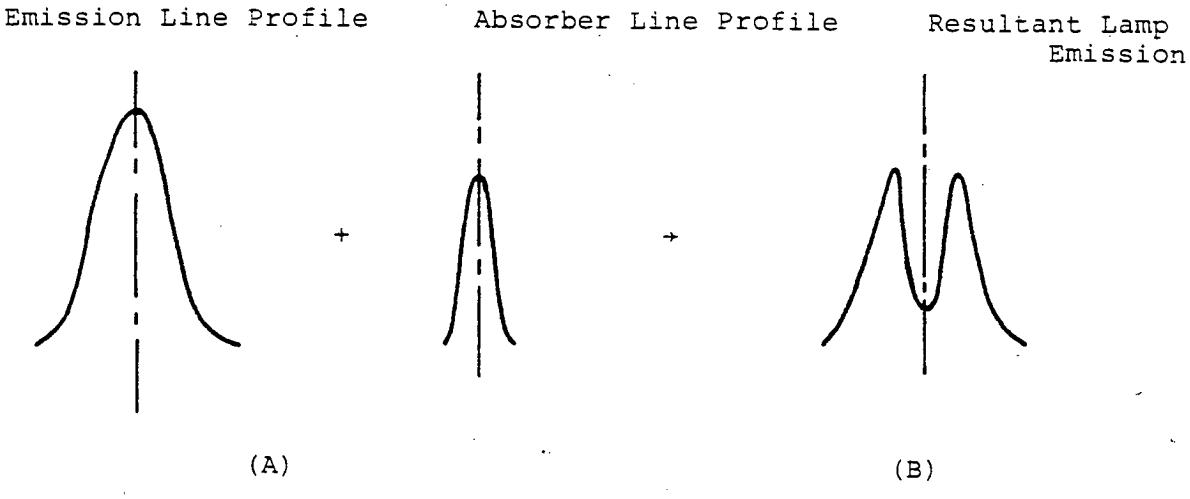

FIG 2.8: Pictorial Representation of Atomic Line Reversal

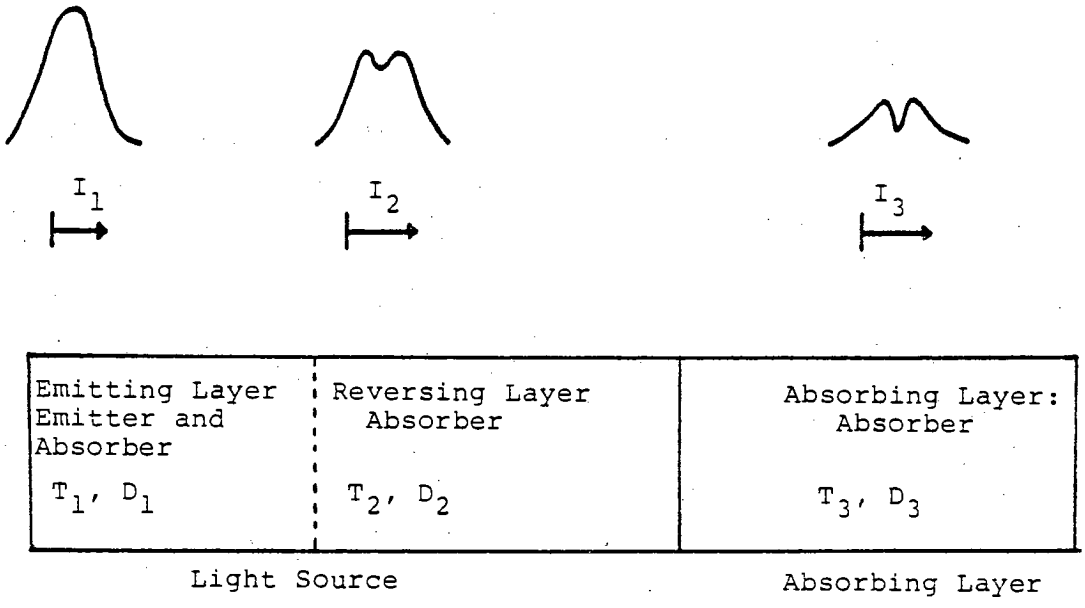

FIG 2.9: Three Layer Model for Light Source and Absorber. T, D and I are Doppler Temperature, Optical Depth at Centre of Line, and Outgoing Intensity.

$[(3p^3 4s)\,^3S_1^o \rightarrow (3p^4)\,^3P_J]$. The relatively large splitting of the J levels allows resolution, with good signal to noise ratios, of the individual triplet lines - see FIG 2.10. For an optically thin system an unreversed lamp would produce absorption signals governed by the Beer Lambert Law (equation 2.1):

$$I_{TR} = I_o \exp(-\varepsilon c l) \qquad 2.1$$

where c = absorber concentration

l = path length

ε = extinction coefficient (see Appendix 4).

In experiments where a reversed light source is used a plot of $\log_e I_o/I_{TR}$ against c is invariably found to be curved. In order to correct for this deviation a modified Beer Lambert equation is employed, of form (2.2)

$$I_{TR} = I_o \exp(-\varepsilon c l)^{\gamma} \qquad 2.2$$

where the γ coefficient may be experimentally determined by a straight line plot of $\ln(\ln I_o/I_{TR})_{t=0}$ against ln c. In flash photolysis work c is rarely determined absolutely. However, for optically thin systems c is directly proportional to the concentration of the parent molecule provided the flash energy remains constant. It should be noted that there is no theoretical justification for the introduction of the gamma coefficient, however, over limited absorber concentration ranges the linearity of the $\ln(\ln I_o/I_{TR})_{t=0}$ against ln c plot in numerous experimental instances justifies its use.

In radical absorption work the major source of deviation from the Beer Lambert law is through the

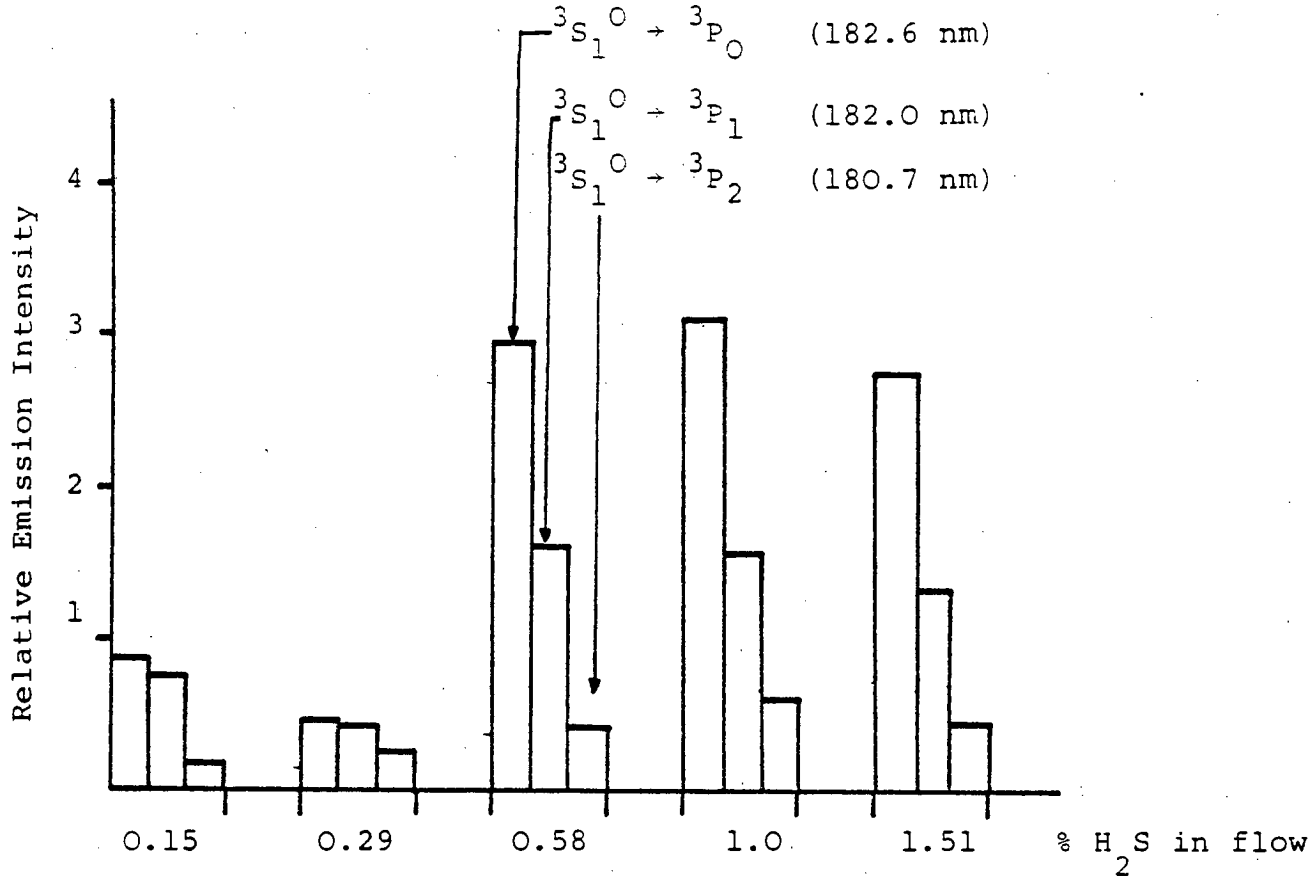

Incident Power = 50 W Spectral Bandwidth = 0.14 nm

Standing Pressure = 400±100 Nm^{-2}

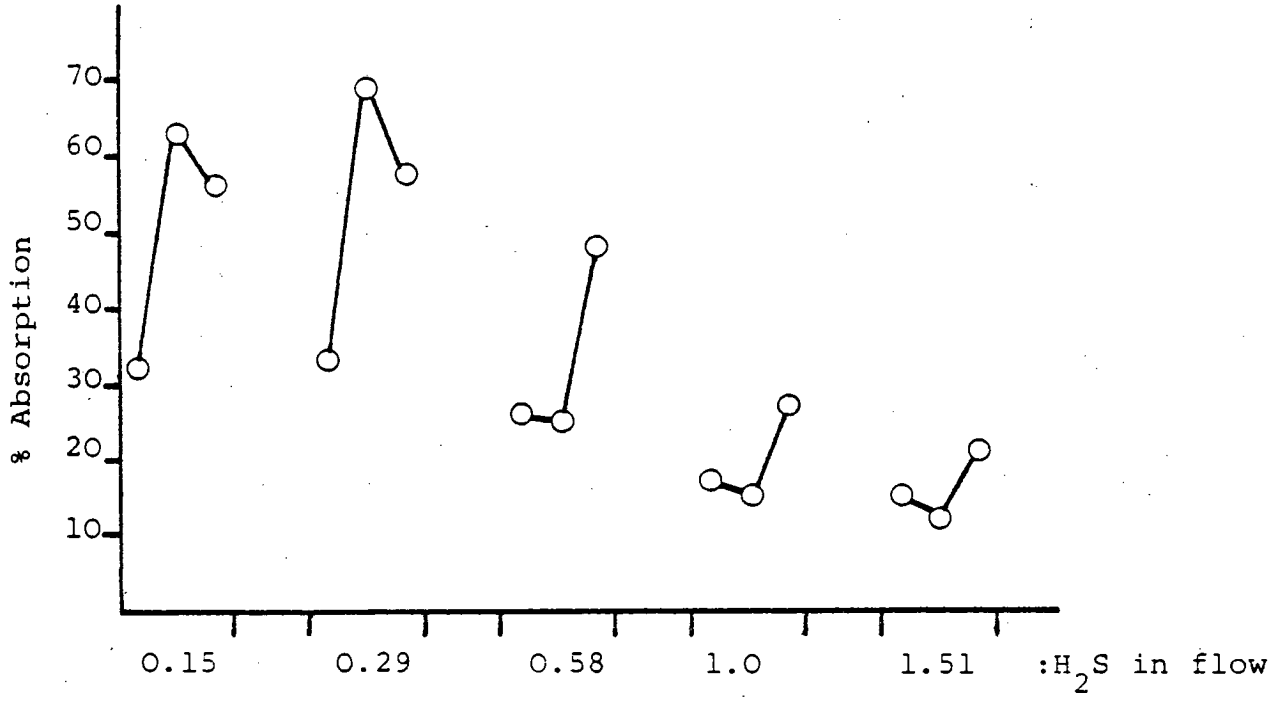

[OCS] = 13±2 Nm^{-2}, Flash Energy = 245 J

FIG 2.10: Flow Lamp Performance (S^3P_J)

non-matching of the rotational temperatures of absorber and emitter in an isolated vibrational band. Any problem over the linearity may generally be resolved by use of the modified Beer Lambert law as with atomic absorption spectrophotometry.

In resonance fluorescence work, experiments are normally conducted in a region where the fluorescence intensity (I_f) is directly proportional to absorber concentration.

2.7 SIGNAL DETECTION EQUIPMENT

In monitoring any region of the electromagnetic spectrum sensitivity, resolution and accurate recording of the optical data are of prime importance. Essentially only two forms of detection equipment have been employed in this work - photographic and electronic. In the latter many devices are available both for signal collection and recording. This work has relied exclusively on the photomultiplier/transient recorder combination as the basic unit of the system.

(i) PHOTOGRAPHIC RECORDING This method was employed with the flash spectroscopy arrangement. Light from the spectroflash lamp was focussed through the reaction cell onto the entrance slits of a Hilger Watts medium quartz spectrograph to be dispersed onto a photographic plate. Kodak Panchro Royal film had been shown previously[9] to possess a sufficient compromise between contrast, plate resolution and film speed for the work undertaken and was used throughout. While silver halides are sensitive

to u.v. light the absorption of gelatin restricts the use of untreated film to above 250 nm. Below 250 nm films can be coated with sodium salicylate (0.5 M solution in methanol) which through its fluorescence at 420 nm enables recording in the u.v. and vacuum u.v. regions of the spectrum. Plates were developed with Ilford Contrast FF Developer (1 part developer + 3 parts water) for 5 min at 20°C. Quantitative optical density measurements were recorded with a Joyce Loebl double beam recording microdensitometer.

For any photographic emulsion a D - log E curve relates film speed, contrast and exposure. Over a specific exposure range such a plot is linear and equation 2.3 may be written:

$$D_O - D_t = \gamma \log {}^{E_O}/_{E_t} = \gamma \log {}^{I_O}/_{I_t} \qquad 2.3$$

where $D_{O,t}$ = plate density at t=0 (no absorbers present) and t (absorbers present) after the flash

$E_{O,t}$ = exposure

$I_{O,t}$ = intensity

γ = constant (gradient of D - log E plot)

If the Beer Lambert law (2.1) is obeyed then the optical densities are directly proportional to absorber concentration i.e.

$$D_O - D_t = \gamma \varepsilon c l \qquad 2.4$$

The symbols have there usual meanings. It should be noted that in order to obtain absolute concentrations ε must be known and γ measured under the conditions used.

(ii) ELECTRONIC RECORDING Electronic signal recording offers many obvious advantages over photographic recording and was used in the majority of the work. The light intensity of the monitored beam is measured by means of a photomultiplier (set at the exit slit of a monochromator if wavelength resolution is desired) which converts the light to electrical current. The analogue electrical signal is then digitised for rapid recording and storage by a fast transient recorder (Datalab DL905). In certain experiments a capacitor was connected across the input to earth, hence providing a high frequency noise filter. Care must be taken in the utilisation of such a device to ensure that the time constant (τ) developed in such an electrical circuit (τ = RC where R = resistance and C = capacitance) is not of sufficient duration to interfere with 'true' signal recording. If single shot recording gave a sufficiently good signal to noise ratio (e.g. A.S. experiments) as viewed on a C.R.O. (Telequipment DM64) then the data was recorded in analogue fashion with a fast response, flat-bed chart recorder (Bryans XY Recorder, 26000 A4). In the resonance fluorescence experiments signal averaging was needed to improve signal to noise ratios and was achieved through the interface of a signal averager (Datalab DL400) to the transient recorder. To ensure the traces were free from earth ripple it was found necessary to ensure that all equipment involved in signal detection was earthed at one point (generally through the photomultiplier power supply).

Monochromators In the resonance fluorescence experiments the introduction of a monochromator was unnecessary. In the absorption work however, monochromators were essential for isolation of the wavelength of interest. Two types of monochromator were employed. In the atomic absorption spectrophotometry system a Hilger Watts E766 one metre normal incidence vacuum monochromator was used. Pressures within the monochromator were maintained below 10^{-4} Nm^{-2} (as measured on a Penning gauge) by means of an Edwards oil vapour diffusion pump (model E04) backed by a rotary pump (ES200). The diffraction grating of 1200 lines/mm and blazed at 120 nm gave the system a linear dispersion of 0.42 nm/mm. Slit widths used ranged from 25 μm to 1200 μm.

In the OH absorption spectrophotometry work a McKee Pedersen monochromator, model MP-1018B was employed. The diffraction grating had 1180 lines/mm and allowed wavelengths to be monitored in the region from 200 to 1000 nm. The linear dispersion at the exit slit is 1.75 nm/mm in the first order. Slit widths of approximately 250 μm were used such that good signal to noise ratios on single shot recording were employed.

Photomultipliers The performance of any photomultiplier may be judged by reference to four important parameters[18]: quantum efficiency, gain, dark current and noise. The coupling of quantum efficiency, at any particular wavelength, and the gain of the photomultiplier tube determines the output currents one may expect with any particular photo-detector. The gain of a photomultiplier may be represented by equation 2.5:

$$GAIN = f(g\delta)^n \qquad 2.5$$

f = collection efficiency

g = transfer efficiency between dynodes

δ = average secondary emission coefficient

$\delta \propto V_s^x$ where $x < 1$

V_s = interdynode voltage

n = number of dynodes.

It should be noted that gain is extremely sensitive to the number of dynodes between photocathode and anode.

In fast kinetic spectrophotometric applications shot noise is the principle limitation to sensitivity as defined by equation 2.6.

$$S/N = \sqrt{I_c/2\Delta f e} \qquad 2.6$$

S/N = signal to noise ratio

Δf = bandwidth of measuring circuit

I_c = photocathode current.

A detailed description of the relevance of equation 2.6 to photomultiplier design is given by Porter and West[4].

The photomultipliers used throughout this work were selected to optimise performance with respect to the limitations briefly outlined above.

For the $O(^3P)$ and $S(^1D)$ atomic absorption and $S(^1D)$ resonance fluorescence work an EMR Model 542 photomultiplier was used. The photomultiplier was of the extreme solar blind variety and employed an 18 stage, end on, lithium fluoride window tube with a 28 mm diameter

semitransparent cesium iodide photocathode. The tube was generally run at 3000 V from a Fluke Model 408B High Voltage Power Supply. The circuit and specification of this tube are shown in FIG. 2.11 and FIG. 2.12, respectively. A further extreme solar blind photomultiplier employed (for $O(^3P)$ resonance fluorescence work) was an EMI Gencom Model G26E315. In this device the tube was again of the end on variety but employed a MgF_2 end window. The CsI photocathode was coupled to a 15 dynode chain and had a gain of 10^6 at 3830 V. The tube was run at from 2600-3000 V, using the same power supply as above. The sensitivity of this photomultiplier appeared considerably greater than the EMR model, however, this sensitivity extended to higher wavelengths than the EMR version hence limiting its use, in fast response applications, where the 'dead time' resulting from scattered photolysis light proved too great. For the $S(^3P)$ atomic absorption work an EMI 9616QB photomultiplier was used employing a thirteen dynode chain. This photomultiplier was run at 1000 V from a Brandenburg Photomultiplier Power Supply Model 472R. All the tubes fore-mentioned were enclosed in a sturdy mu-metal shield to prolong working life and limit noise. Where work was conducted in the vacuum u.v., without the presence of a monochromator, the photomultiplier was set against a collimating tube, the other end of which contacted the reaction vessel. The intervening region was then flushed continuously with nitrogen ensuring good through put of radiation.

In the OH absorption work an EMI 9661B tube was used operating at 870 V from a Brandenburg Power Supply[19].

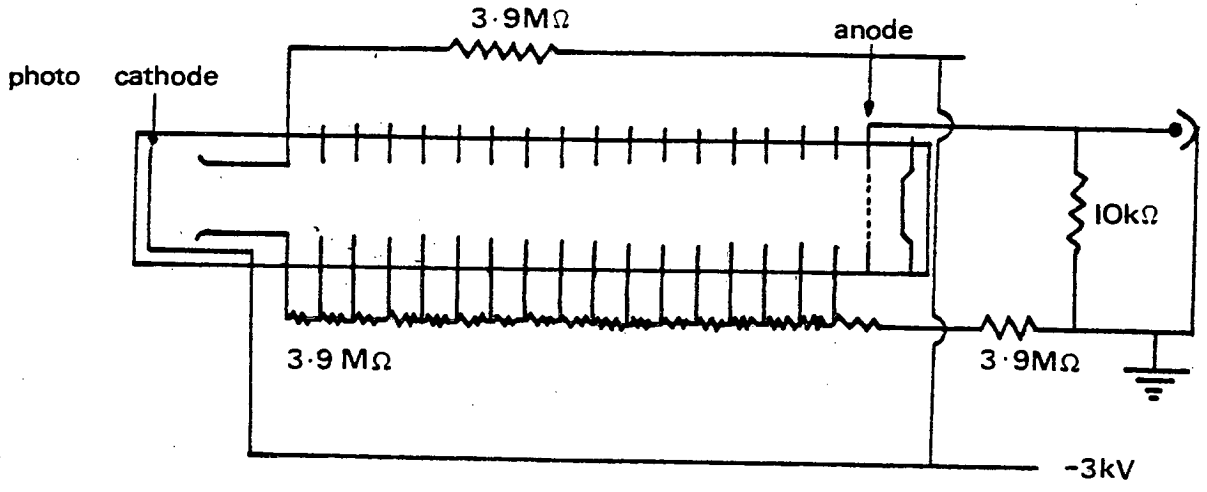

FIG 2.11: EMR (Solar Blind) Photomultiplier - Circuit Design

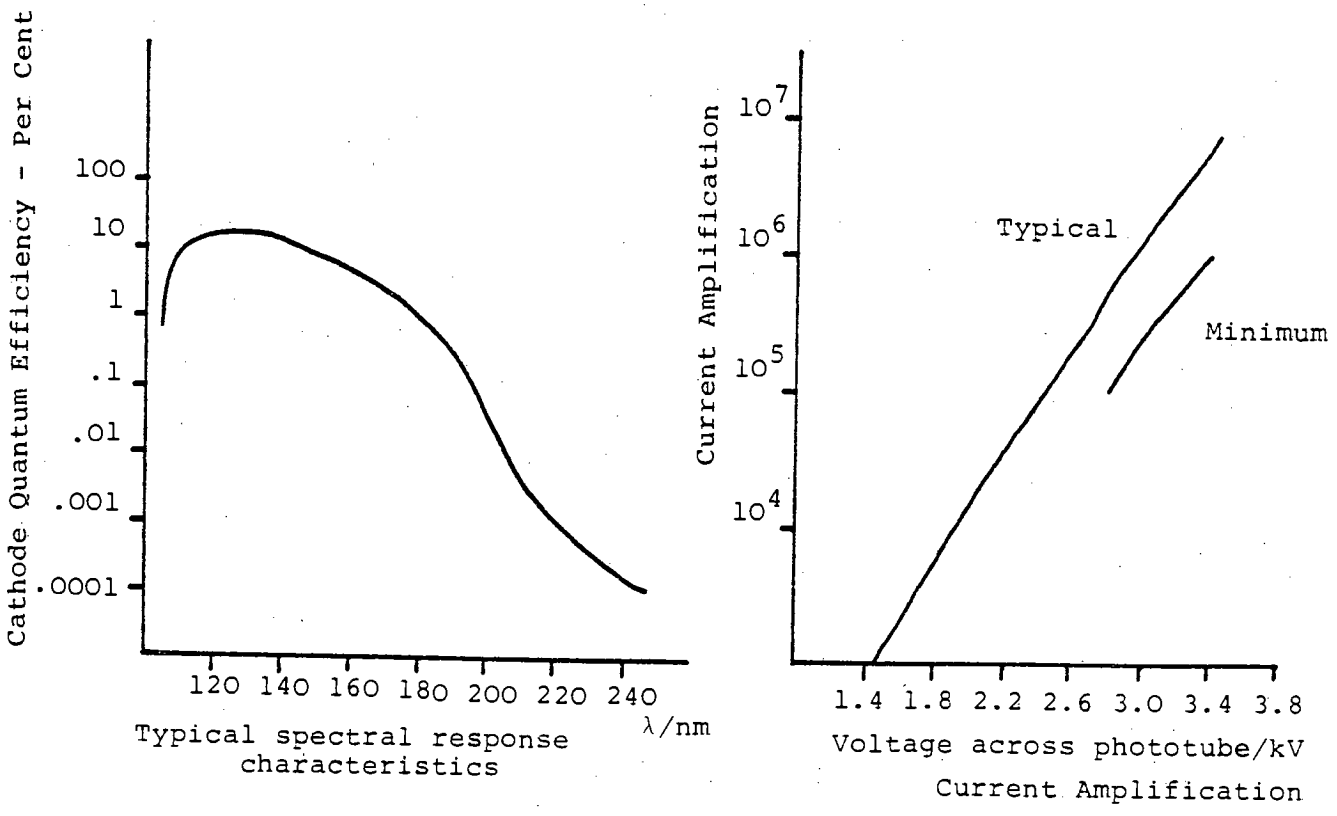

FIG 2.12: EMR Photomultiplier Performance Curves

2.8 GAS HANDLING

Four vacuum lines were employed in the various sections of this work. All were constructed of pyrex with, in the working part of the line at least, greaseless glass or teflon taps. The vacuum was maintained in all cases by either a mercury or oil diffusion pump backed by a rotary pump. Gases sensitive to light were stored in blackened bulbs. All gases, where suitable, were freeze-pump-thawed prior to use. Many gases were vacuum distilled on introduction to the line (see Appendix 1 for sources and purities of gases used). Gas mixtures were prepared in a mixing bulb which was thoroughly agitated for approximately two minutes by a glass paddle mixer driven by electric motor. The dead volume in the mixer was pumped out prior to use. Good vacuum techniques were employed throughout. Pressures for all work with the exception of that employing the flash spectroscopy technique were monitored by two MKS Baratron pressure gauges with working ranges of 0-1330 Nm^{-2} with three decimal places and 0-133 kNm^{-2} with one decimal place. Both gauges were accurate to $\pm$2%. In the vacuum line coupled to the flash spectroscopy system pressures from 0-13.3 kNm^{-2} were measured with an oil backed spiral gauge (accurate to $\pm$10%). Higher pressures were monitored with a conventional mercury manometer.

2.9 MOLECULAR MODULATION SPECTROSCOPY

The allocation of this technique to a sub-section in isolation to the preceding presentation is due to geographical rather than scientific reasons. The

molecular modulation spectrometer used in Chapter 4 was constructed by Dr. R.A. Cox[10] at A.E.R.E., Harwell, Oxfordshire. While the operational principles involved in this technique are quite different to those previously described the fundamental science involved is very similar. The basic aim of the molecular modulation spectrometer used was to monitor the attenuation of a constant light source by photolytically produced absorbers in order to ascertain the kinetics of their removal from the system. Rather than making a single kinetic measurement, however, as would be the case with the atomic absorption experiment a type of signal averaging is attained through modulation of the photolysis source and collection of the subsequently modulated attenuated absorption signal. The relationship between the absorption signal in phase and in quadrature (90^{o} out of phase) with the photolysis modulation may be related to the kinetics of the radical or atom observed. The experimental system is shown schematically in FIG. 2.13 and is described in detail below.

The jacketed reaction vessel used throughout this work was made of borosilicate glass with plane silica end windows and had dimensions 1200 mm long x 26 mm I.D. Temperature control of the vessel was ensured by use of a thermostatted water circulator system (Churchill). The modulated photolysis light was provided by six radially mounted photolysis lights (Phillips L40/08 fluorescent black lights) operating on a 250 V D.C. rectified 3 phase supply. Modulation was achieved using a special control circuit, similar in design to that described by Pinto[21],

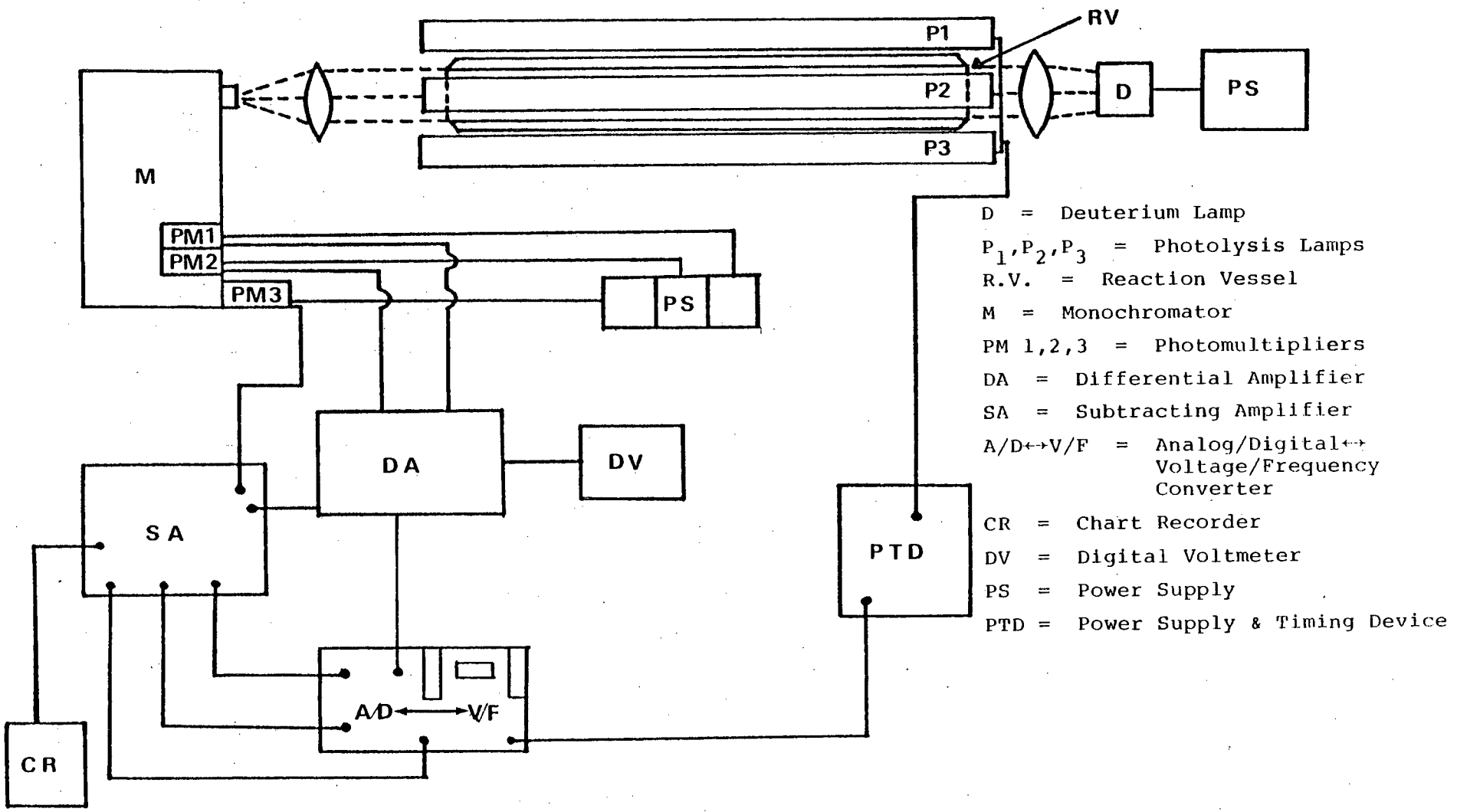

FIG 2.13: Molecular modulation spectrometer

which activated the lamps by switching the D.C. supply on and off through a pair of power transistors, in response to a timing pulse derived from a crystal controlled clock pulse generator. An operational amplifier was incorporated to control the lamp current. In order to ensure instantaneous firing the lamps were preionised by a PTFE insulted wire held at a potential of 1 kV, strapped to the external wall of the fluorescent tubes. Observation of the photolysis light scattered into the spectrometer showed it to be a true square wave, free from distortion up to 50 Hz ($310 \text{ nm} \leqslant \lambda \leqslant 410 \text{ nm}$). Radical species generated on photolysis were detected by absorption measurements made continuously using varying modulated photolysis periods. The monitoring beam was provided by a deuterium lamp (Point Source) operating at 180-350 nm. On passing through the reaction vessel the beam was focussed onto the entrance slit of a 0.75 m grating spectrometer (Spex Model 1700). Detection of the incident light intensity was made by one of two methods. The first involved direct measurement via an EMI 9526A photomultiplier set at the exit slits. The second method was one of differential detection incorporating the placement of a pair of 0.3 mm slits, 0.8 mm apart in the spectrometer, which were monitored independently and simultaneously by two additional photomultipliers of the same design. The output from them was fed to a bridge circuit and the off-balance signal, caused by the changes in the light transmitted in the optical path at one wavelength relative to the other, was measured on a

fast differential Electrometer Amplifier (Kiethley Model 604). Such a system allows unambiguous detection of species possessing banded absorption profiles in the presence of continuum absorbers. For calibration the difference signal was recorded relative to a fixed reference voltage when known amounts of ClO were present (measured via the direct mode using $\sigma = 7.26 \times 10^{-18}$ cm^2 molecule^{-1})[22]. ClO was monitored using the 11-0 band of the A-X system at 277.2 nm. Kinetic data were recorded in the main, through monitoring the relationship between absorption signal both in phase and 90^{o} out of phase with the modulated photolysis light at varying photolysis periods. This was achieved in the following manner. If the direct signal is considered then it is evident that the photomultiplier outputs a large D.C. signal on which is superimposed a small A.C. component. The separation of the A.C. component from the D.C. was achieved by using a differencing amplifier of the same specification as that used by Parkes et al[23]. When monitoring on the differential mode the differencing amplifier was bypassed and the phase relationship of the off balance signal measured directly. The modulation amplitude and the phase relationship between the A.C. absorption signal and the photolytic illumination was measured using a digital lock in system which followed the design originally developed by Morris[24] and subsequently used by Wu and Johnston[25]. The signal now containing the amplified A.C. component was fed to a voltage-to-

frequency converter and the digital output was accumulated in two reversible counters. The operation of these counters was controlled by timing pulses from the master timing circuits which also controls the photolysis lamps. One counter counted up when the photolysis lamps were on and down during the dark period and the other counted up from midway through the on period to midway through the dark period and down during the remaining half cycle. See FIG 2.14. From FIG 2.14 it is seen that if the radical half life is $t_{\frac{1}{2}}$ then for τ (the photolysis period) >> $t_{\frac{1}{2}}$ the in phase count (P) maximises while the in-quadrature count (Q) tends to zero i.e. the radical follows the flash profile. For τ << $t_{\frac{1}{2}}$, P tends to zero and Q tends to zero i.e. the absorption is little changed whether the lights are on or off. The data obtained in the counters is easily converted to concentration proportional quantities by use of the Beer Lambert law. The basic data was then plotted in terms of the in phase/in quadrature absorption against the photolysis period (see Chapter 4). In certain experiments further rate data was obtained by direct absorption experiments conducted at long photolysis periods ($\approx$40 s) and invoking steady state conditions in order to allow kinetic analysis of the resulting data.

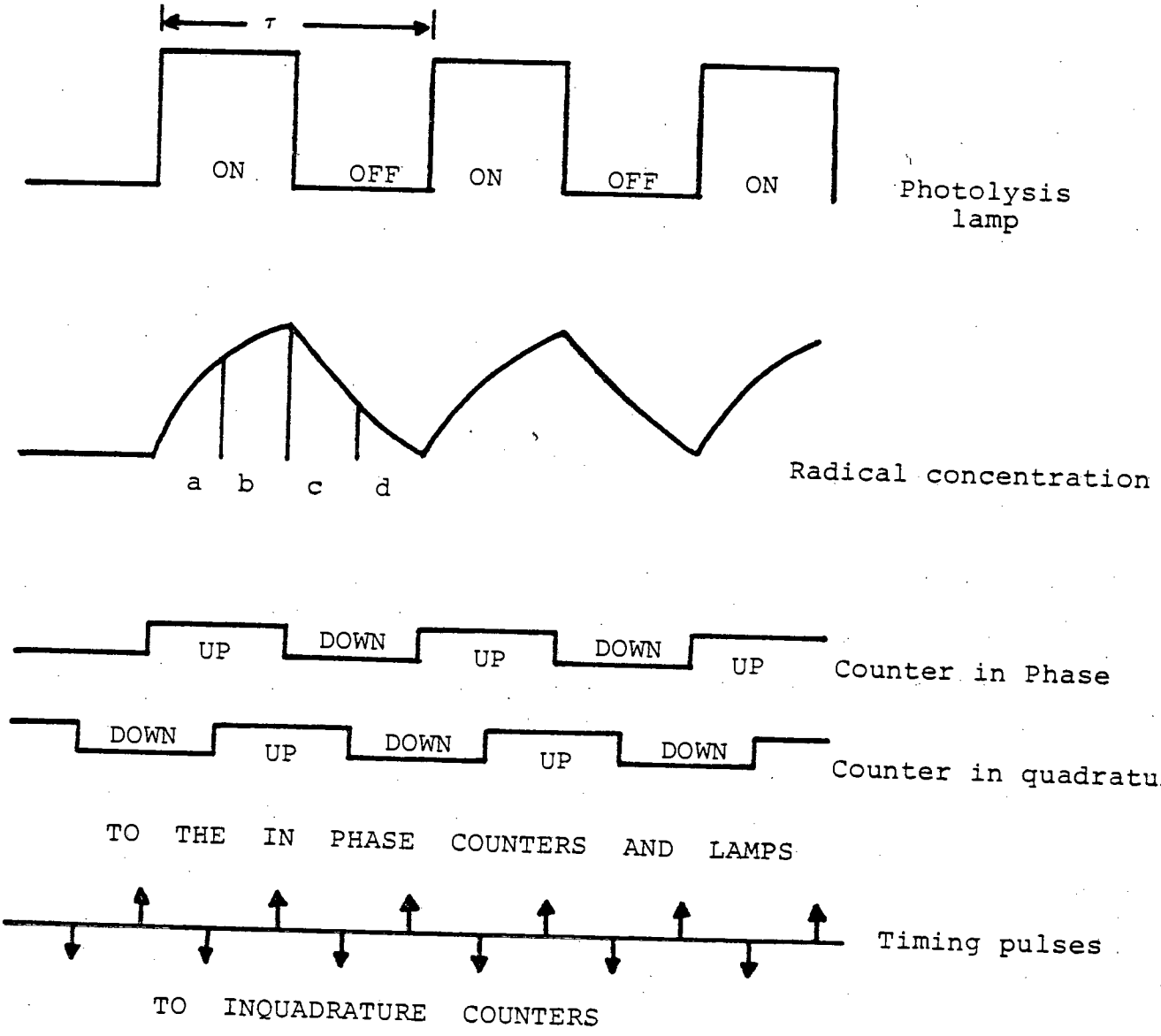

In phase signal = $N[(a+b) - (c+d)]$

In quadrature = $N[(b+c) - (a+d)]$

FIG 2.14: Molecular Modulation Phase Relationships

2.10 REFERENCES

1. M.A. West in Chem. Soc. Specialist Periodical Reports, Photochemistry 10, 3, (1979).
2. ibid, 8, 3, (1977).
3. R.G.W. Norrish and G. Porter, Nature 164, (1949), 658.
4. G. Porter and M.A. West in 'Investigation of rates and mechanisms of reactions' (2nd Ed.) Part 2, Edited by G.G. Hammes (Wiley Interscience).
5. C. Morley and I.W.M. Smith, J. Chem. Soc. Faraday II 68, (1972), 1016.
6. R.J. Donovan, H.M. Gillespie and R.H. Strain, J.C.S. Faraday II 73, (1977), 1553.
7. E.L. Baardsen and R.W. Terhune, Appl. Phys. Lett. 21, (1972), 209.
8. J.G. Anderson, Geophys. Res. Lett. 2, (1975), 231.
9. D.J. Little, Ph.D. Thesis, University of Edinburgh (1974).
10. An introduction to lasers and their applications, D.C. O'Shea, W.R. Callen and W.T. Rhodes, Publ. Addison-Wesley, (1977).
11. Lasers (2nd Edn.), B.A. Lengyel, Publ. Wiley Interscience, (1971).
12. High frequency uv lasers, J.J. Ewing and C.A. Brau in Tunable Lasers and Applications, Ed. A. Mooradian, T. Jaeger and P. Stokseth, Berlin, (1976).
13. D. Davis and W. Braun, App. Optics 7, (1968), 2071.

14. W. Braun and T. Carrington, J. Quant. Spectrosc. Radiat. Transfer 9, (1969), 1133.

15. R.D. Cowan and G.H. Dieke, Rev. Mod. Phys. 20, (1948), 418.

16. P.P. Bemand and M.A.A. Clyne, J. Chem. Soc. Faraday Trans. II 69, (1973), 1643.

17. P.J. Cross and D. Husain, J. of Photochem. 10, (1979), 251.

18. EMI Publication, Photomultiplier Tubes.

19. J. Garraway, Ph.D. Thesis, University of Edinburgh to be published.

20. R.A. Cox, R.G. Derwent, A.E.J. Eggleton and H.J. Reid, J. Chem. Soc. Faraday I, in press.

21. J. Pinto, J. Opt. Soc. Amer. 60, (1970), 870.

22. M.A.A. Clyne and J.A. Coxon, Proc. Roy. Soc. A, 303, (1968), 207.

23. D.A. Parkes, D.H. Paul and C.P. Quinn, J. Chem. Soc. Faraday I 72, (1976), 1935.

24. E.D. Morris Jr., Ph.D. Dissertation, University of California, Berkeley (1969).

25. C.F. Wu and H. Johnston, Bull. Belg. Chem. Soc. 81, (1972), 135.

CHAPTER III

REACTION OF $O(2^1D_2)$ WITH THE HALOGENOMETHANES CCl_4 AND CH_3Cl

3.1 INTRODUCTION

The hypothesis proposed by Molina and Rowland[1] in 1974 that chlorofluorocarbons (in particular $CFCl_3$ and CF_2Cl_2 - the major propellants used in aerosol spray cans) posed a threat to the ozone layer has led to considerable work on the formation and destruction of the chlorine oxide intermediates involved. In the model developed by Rowland and Molina it was suggested that the major fate of the chlorofluorocarbons was through photolysis in the stratosphere to yield chlorine atoms (1). The chlorine atoms then participate in the removal of ozone through a catalytic chain reaction (2-3).

$$CF_xCl_y + h\nu \ (\lambda<200 \text{ nm}) \rightarrow CF_xCl_{y-1} + Cl \qquad 1$$

$$Cl + O_3 \rightarrow ClO + O_2 \qquad 2$$

$$O + ClO \rightarrow O_2 + Cl \qquad 3$$

$(k_2 = 1.2\times10^{-11} \text{ cm}^3 \text{ molecule}^{-1} \text{ s}^{-1})$[2,3]

$(k_3 = 5.3\times10^{-11} \text{ cm}^3 \text{ molecule}^{-1} \text{ s}^{-1})$[4].

There seems little doubt that if the chlorofluorocarbons do indeed reach the stratosphere (no major sink in the troposphere has yet been found) then

photolysis by solar u.v. radiation will be the major removal pathway[5]. A minor removal pathway in the stratosphere also leading to ClO production is through reaction with the first excited state of atomic oxygen ($O(^1D_2)$). The work presented in this chapter considers the detailed mechanism of the $O(^1D_2)$ reaction with CCl_4 and the major naturally occurring source of chlorine in the atmosphere - CH_3Cl. This study in which product branching ratios into the various reactive and non-reactive channels are monitored follows the initial work of H.M. Gillespie and J. Garraway on the reaction of $O(^1D_2)$ with the chlorofluorocarbons[6,7].

The analogous reactions of $O(^1D_2)$ with alkanes have been extensively studied[8,9,10] and hence offer an interesting comparison between the behaviour of the C-H and C-Cl bonds under $O(^1D_2)$ attack.

3.2 EXPERIMENTAL

Three experimental systems have been used in this study to monitor the various products of reaction. The flash spectroscopy arrangement (FIG 2.1) was used for detection of ClO and Cl intermediates (the latter in an indirect manner). Atomic absorption spectroscopy (FIG 2.2) was used to monitor $O(^1D_2)$ quenching through detection of $O(^3P_J)$ atom concentrations. This type of experiment was only pursued for the molecules CF_3Cl and CF_2HCl, however the results are of relevance to the

carbon tetrachloride and methyl chloride systems. OH absorption spectroscopy (FIG 2.3) was used to obtain the branching ratio into OH production from the reaction of $O(^1D_2)$ with methyl chloride.

1. Flash Spectroscopy: The apparatus for flash spectroscopy was discussed in detail in Chapter 2. $O(2^1D_2)$ atoms were generated by photolysis of ozone in the Hartley Bands (200 nm $\leqslant \lambda \leqslant$ 320 nm). Throughout, the photolysis lamp was charged to 12 kV and dissipated an energy of 720 J. In order to prevent sizeable photolysis of CCl_4 or CH_3Cl (the former in particular absorbs strongly below 230 nm) a jacketed quartz reaction cell was employed. The outer jacket was filled with a 3.6×10^{-4} M potassium iodide filter solution to remove wavelengths $\leqslant$240 nm. Ozone was prepared by the method of Clough and Thrush[11] (see APPENDIX 1B) and was stored in dilute form with helium in a blackened bulb. Its purity was determined daily by u.v. spectrophotometry at λ = 257 nm using a Perkin Elmer Model 402 spectrophotometer. Having prepared a mixture the desired pressure was admitted to the reaction vessel. ClO produced on photolysis was monitored in absorption by flash spectroscopy (see Ref. 7). Optical density traces were obtained using a Joyce-Loebl microdensitometer. The concentration of ClO was determined from the optical density in the (5,0) band of the $A^2\Pi_{3/2} \rightarrow X^2\Pi_{3/2}$ system. An extinction coefficient of $\varepsilon(5,0) = 1.43 \times 10^{-18}$ cm^2 molecule^{-1} was employed[7]. The contrast at this wavelength was determined for each plate by the method described by

Basco[12] i.e. optical density as a function of the entrance slit width to the spectrometer was recorded using constant spectroflash energy . A plot of optical density against log exposure (directly proportional to slit width) yielded a straight line, the slope of which is equivalent to the contrast.

2. OH Absorption Spectrophotometry: The intense OH emission produced by a microwave discharge through a flowing mixture of water vapour in argon carrier gas (standing pressure $\sim$200 Nm^{-2}) was focussed through the reaction vessel and onto the slit of a monochromator which selected the $Q_1 3$ and $P_1 1$ lines at 308.15 nm. The incident power supplied to the lamp was 75 W. The output from the photomultiplier was fed directly to a transient recorder for signal recording and storage. A chlorine gas filter, approximately 80 kNm^{-2} in pressure, surrounded the reaction vessel in order to reduce scattered light reaching the photomultiplier. See FIG 2.3.

3. Atomic Absorption Spectroscopy: The atomic absorption system (FIG 2.2) was used to monitor $O(^3P_J)$ atom concentrations. The flow lamp operated from a helium cylinder supply, enough oxygen impurity being present to generate sufficiently intense oxygen atomic lines at 130 nm. The standing pressure and incident power supplied to the lamp were 400 Nm^{-2} and 50 W respectively. The slit widths entering (750 μm) and exiting (750 μm) from the monochromator were such that the atomic triplet at 130 nm was unresolved. This radiation was incident on an EMR solar blind photomultiplier interfaced with a transient recorder. No external amplifier or signal averager was used.

3.3 RESULTS

1. ClO and Cl Yields: In calculating the branching ratio into the various channels it was necessary to make a direct measurement of the $O(^1D_2)$ concentration produced on photolysis. If ozone (26.7 Nm^{-2}) is photolysed in the presence of a large excess of CO_2 (2.5 kNm^{-2}) the following (4-6) represents the fast reactions occurring in the system. The subsequent reactions of $O_2(^1\Delta_g)$ and $O(^3P_J)$ are slow on the time scale used and need not be considered.

$$O_3 + h\nu \rightarrow O(^1D_2) + O_2(^1\Delta_g) \quad 4$$

$$\rightarrow O(^3P_J) + O_2 \quad 5$$

$$O(^1D) + CO_2 \rightarrow O(^3P_J) + CO_2^{\ddagger} \quad 6$$

$$(k_6 = 1.2\times10^{-10}\ cm^3\ molecule^{-1}\ s^{-1})^{13}$$

The quantum yield for $O(^3P_J)$ production (5) has been shown to be minor ($\approx$10%) and hence to a good approximation the amount of ozone removed at short times after photolysis (approx. 80 μs) will be equivalent to the $O(^1D_2)$ primary yield. Ozone concentrations measured before and after photolysis by microdensitometry and using the absorption coefficients of Griggs[14] yielded 13$\pm$4% ozone removal by the flash.

Considering reaction of $O(^1D_2)$ with CCl_4 the following pathways are all highly exothermic.

$$O(^1D_2) + CCl_4 \rightarrow ClO + CCl_3 \quad 7$$

$$\rightarrow Cl + CCl_3O \quad 8$$

$$\rightarrow O(^3P_J) + CCl_4 \quad 9$$

$$\rightarrow CCl_2O + 2Cl \quad 10$$

$$\rightarrow CCl_2O + Cl_2 \quad 11$$

($k_{O(^1D) + CCl_4} = 3.1 \times 10^{-10}$ cm^3 molecule^{-1} s^{-1})[15].

Reaction (7) leads to ClO directly whereas reactions (8) and (10) also produce ClO through secondary reaction of chlorine atoms with ozone (2). This reaction may be suppressed by the addition of a suitable concentration of ethane ($[O_3]$ = 27 Nm^{-2}, $[CCl_4]$ = 533 Nm^{-2} and $[C_2H_6]$ = 67 Nm^{-2}) to scavenge the chlorine atoms via reaction (12)

$$C_2H_6 + Cl \rightarrow HCl + C_2H_5 \quad 12$$

($k_{12} = 6.7 \times 10^{-11}$ cm^3 molecule^{-1} s^{-1})[16].

It was therefore possible to distinguish between ClO formed by direct abstraction and that formed by chlorine atom reaction with ozone. FIG 3.1 illustrates a typical microdensitometer trace for such an experiment with FIG 3.2 showing the measured ClO concentrations, both in the presence and absence of ethane, as a function of time after the photolysis flash. The errors shown in FIG 3.2 correspond to the errors inherent in the microdensitometry of the plates (each error bar representing the extremes of low and high noise traces obtained using different optical wedges). Any scatter in the points outwith the error bars may be attributed, in the main, to the

$A^2\Pi_{3/2} \leftrightarrow X^2\Pi_{3/2}$

System

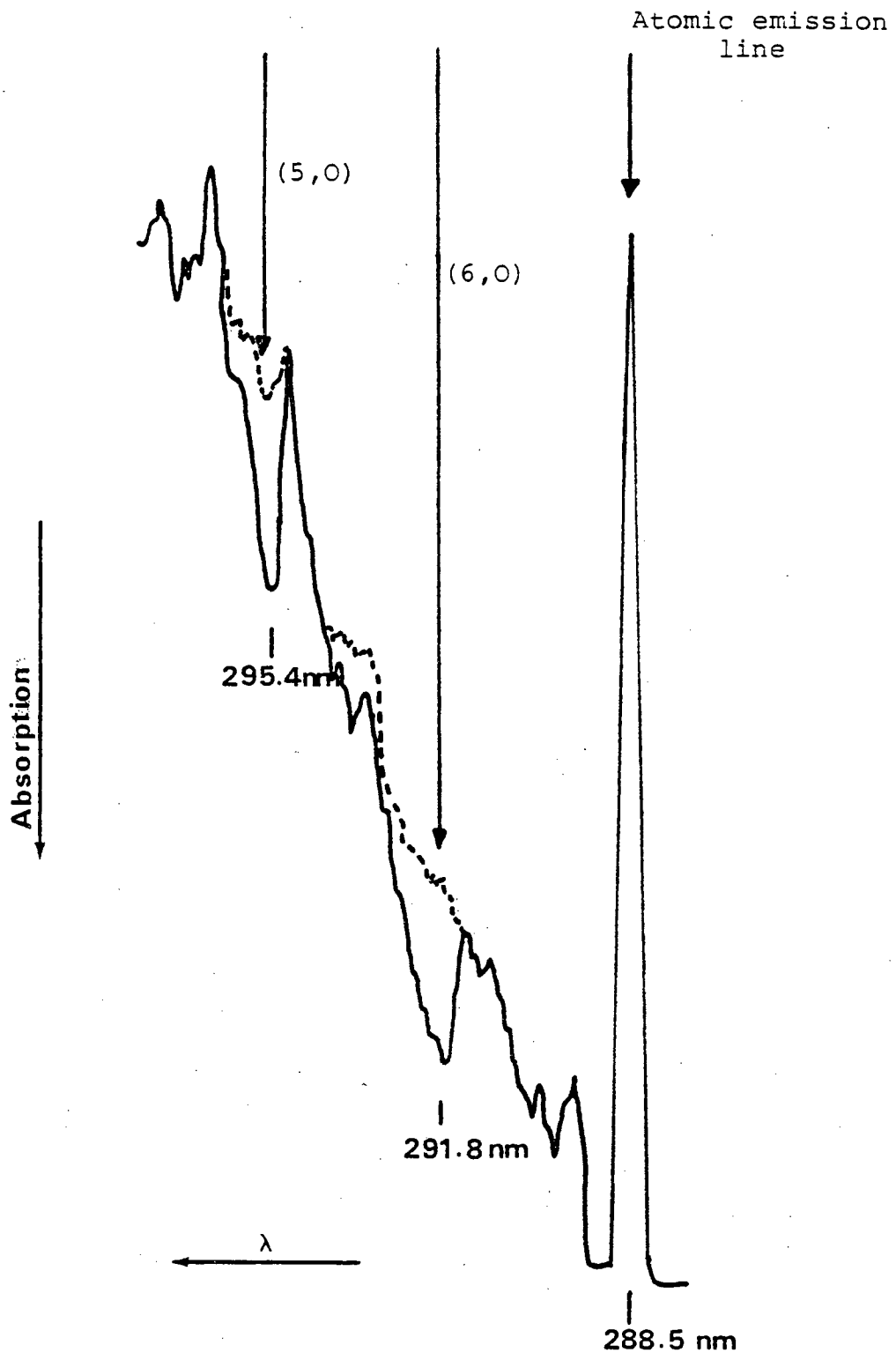

FIG 3.1 Typical microdensitometry trace illustrating ClO band structure. Conditions: Time = 76 μs [ClO] = 4.9×10^{14} molecules cm^{-3}.

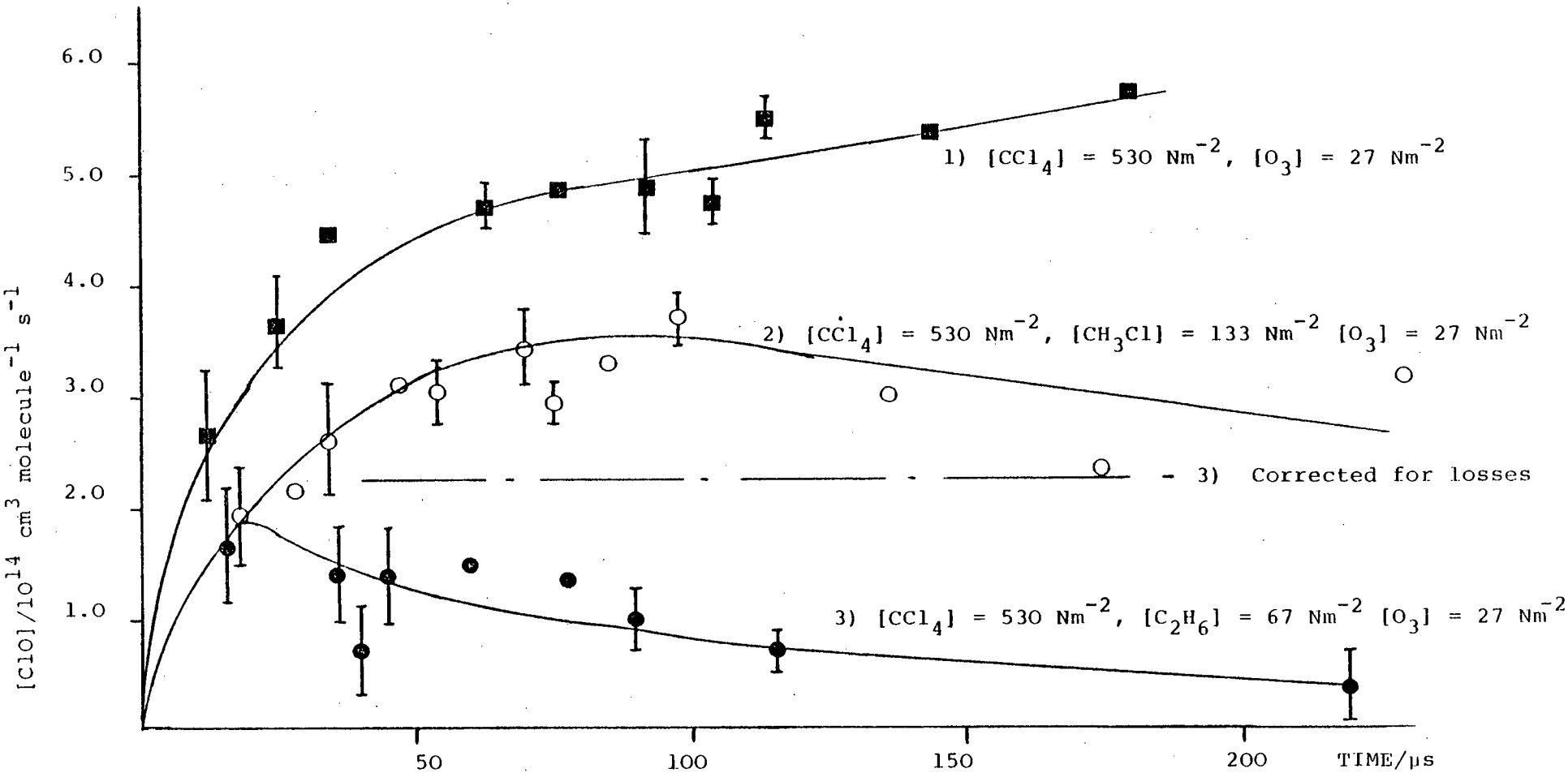

FIG 3.2: [ClO] vs TIME; $O(^1D_2)$ + CCl_4 SYSTEM

sensitivity of the spiral gauge used in monitoring mixture pressures. Errors recorded in the subsequent calculations are stated considering these two main error sources. The data obtained in the ethane experiment were corrected for any ClO loss in the time required to reach maximum concentration using the following procedure. Tangents to the decay curves were drawn and the d[ClO]/dt data so obtained plotted against time and extrapolated back to the origin. Summing the area under this curve provides a method for correcting for the loss processes occurring at short times.

From (FIG 3.2) the corrected ethane experiment provides the ClO yield formed by direct abstraction (2.25×10^{14} molecules cm^{-3}). At the ethane pressure employed 7% of the chlorine atoms generated in the system react with ozone. The chlorine atom concentration may be estimated at short times (15 μs) from the difference between the ethane and non ethane experiments. Employing this correction term lowers the ClO formed by direct abstraction to $2.2 \pm 0.3 \times 10^{14}$ molecules cm^{-3}. Comparison of this value with the $O(^1D_2)$ reacting with CCl_4 yields a branching ratio into direct abstraction of $30\ ^{+20\%}_{-10\%}$. In calculating the fraction of $O(^1D_2)$ reacting with CCl_4 (86.2% in ethane experiment, 96.3% in non ethane experiment) the following rate data were employed.

$$k_{O(^1D) + O_3} = 2.4 \times 10^{-10}\ cm^3\ molecule^{-1}\ s^{-1} \quad [13]$$

$$k_{O(^1D) + C_2H_6} = 3.0 \times 10^{-10}\ cm^3\ molecule^{-1}\ s^{-1} \quad [17]$$

Due to the secondary formation of ClO by radical/ozone reactions it is not possible to obtain a branching ratio into reactions (8) and (10) directly. However by considering the concentration profiles both in the presence and in the absence of ethane at short time ca 15 μs it is possible to give an upper limit into chlorine atom production by all channels of 38%.

In the absence of ethane any decay in the ClO concentration is masked by the secondary growth processes. Where ethane is added, however, secondary production of ClO through reaction (2) is halted and the decay processes are clearly seen. The initial decay process is rapid ($\tau_{\frac{1}{2}} \approx$ 70 μs) being too fast to be accounted for by ClO disproportionation. More likely is reaction (13):

$$O(^3P) + ClO \rightarrow Cl + O_2 \qquad 13$$

($k_{13} = 5.3 \times 10^{-11}$ cm^3 molecule^{-1} s^{-1})[18]

or possibly reaction with radicals produced in the primary reaction of $O(^1D_2)$ atoms with CCl_4.

Reaction of $O(^1D_2)$ with methyl chloride may proceed by attack at C-Cl or C-H bonds (14-16).

$$O(^1D_2) + CH_3Cl \rightarrow CH_3 + ClO \qquad 14$$

$$\rightarrow Cl + CH_3O \qquad 15$$

$$\rightarrow Cl + H + CH_2O \qquad 16$$

($k_{O(^1D) + CH_3Cl} = 1.7 \times 10^{-10}$ cm^3 molecule^{-1} s^{-1})
[evaluated][15].

In this system due to the absence of secondary reactions producing ClO it is in theory possible to calculate directly a branching ratio into direct chlorine abstraction (14) and chlorine atom displacement reactions (15,16). FIG 3.3 illustrates the results obtained from two different pressures of CH_3Cl [133 Nm^{-2} and 532 Nm^{-2}, O_3 = 26 Nm^{-2}]. It is readily seen that the signals obtained were small and subsequently were subject to a large percentage error. Addition of ethane to the system or raising the CH_3Cl concentration to ca 2.5 kNm^{-2} had the effect of reducing the observable ClO concentration beyond the reliable detection limits of the system. The effect of increasing methyl chloride concentrations is due to the reaction of chlorine atoms with the methyl chloride substrate (17):

$$CH_3Cl + Cl \rightarrow CH_2Cl + HCl \qquad 17$$

(k_{17} = 5 x 10^{-13} cm^3 $molecule^{-1}$ s^{-1} (at 300 K))[19*]

The total ClO production may be measured from FIG 2.3 and, after normalisation for 100% reaction of $O(^1D)$ with CH_3Cl, is represented mathematically by equation 3.1:

$$[ClO]_{TOTAL} = [ClO]_{DIRECT} + x[Cl] \qquad 3.1$$

where x = fraction of chlorine atoms reacting with O_3.

x may be easily evaluated for the two pressures of CH_3Cl used and two simultaneous equations of the form of 3.1 are obtained allowing calculation of the branching ratios into Cl and ClO production. Application of this procedure, due

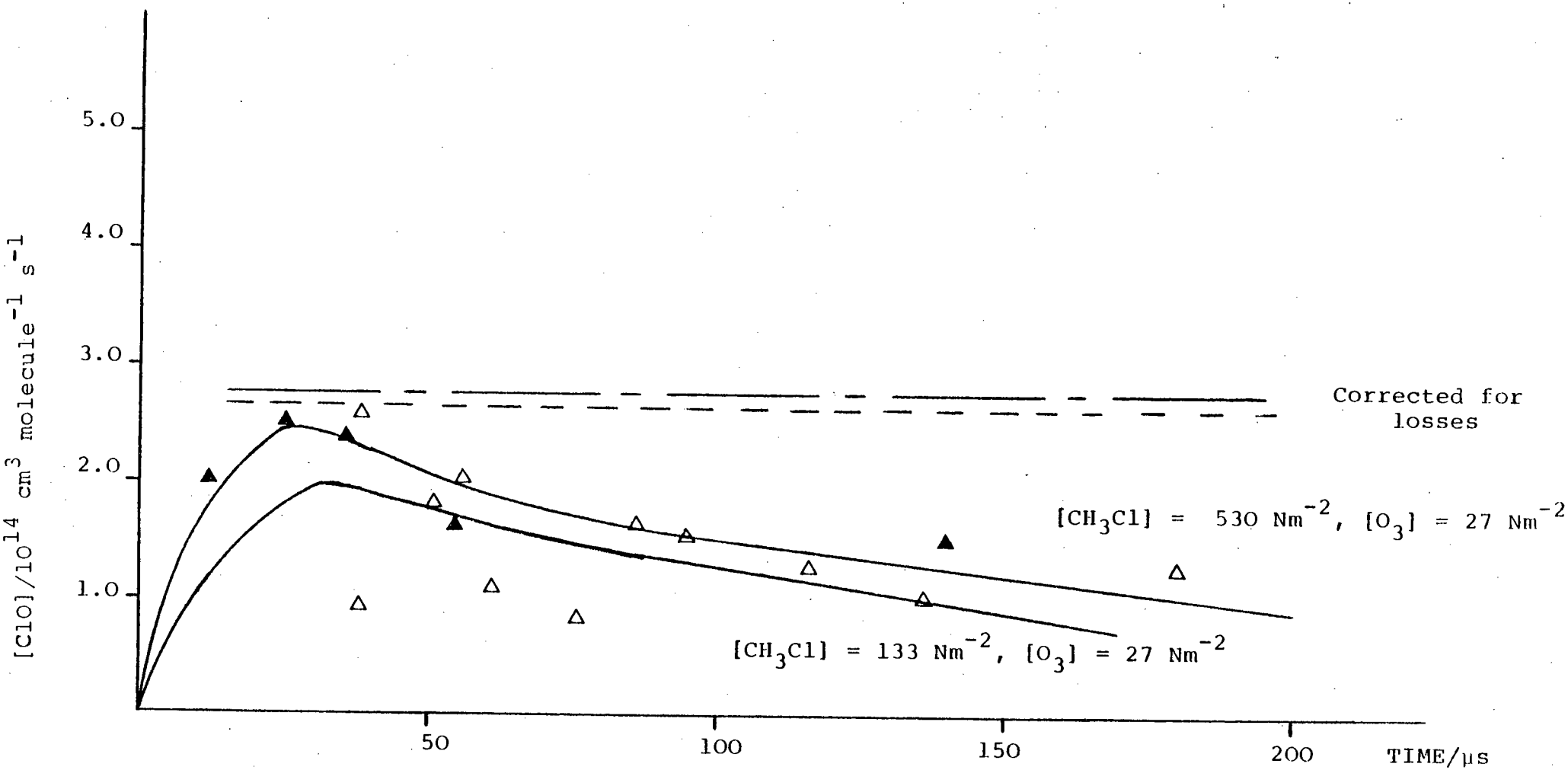

FIG 3.3: [ClO] vs TIME; $O(^1D_2)$ + CH_3Cl SYSTEM

to the nature of the calculations and the large error limits on the input data resulted in meaningful individual branching ratios being unattainable. The most reliable information to be deduced from this approach is that the branching ratio for the combined Cl atom abstraction and displacement reactions lies between the values of 23% and 76%.

* An attempt was made to measure k_{17} in this system by comparing the yields of ClO generated from reaction of $O(^1D)$ with CCl_4 both in the presence and absence of CH_3Cl. The chlorine atom concentration was evaluated at 50 μs from the $[ClO]_{CCl_4/CH_3Cl} - [ClO]_{C_2H_6}$ (see FIG 3.2) after all points had been normalised to equivalent $O(^1D)$ reaction with CCl_4.

  Using these data and equation 3.2 to relate the fraction of chlorine atoms reacting with O_3 (f_{O_3}) to the relevant rate data a lower limit to $k_{17} \geqslant 5 \times 10^{-13}$ was established.

$$f_{O_3} = k_2[O_3]/k_2[O_3] + k_{17}[CH_3Cl] \qquad 3.2$$

2. OH Yield: The formation of OH radicals was not observed using plate photometry. Using the more sensitive technique of time resolved spectrophotometry at 308 nm, formation of OH from $O(^1D_2)$ reaction with methyl chloride was detected (18,19).

$$O(^1D) + CH_3Cl \rightarrow CH_2ClOH^{\ddagger} \quad 18$$

$$\rightarrow CH_2Cl + OH \quad 19$$

$$\rightarrow CHOCl + H_2 \quad 20$$

$$\rightarrow CH_2O + HCl \quad 21$$

Initially a careful calibration of the system was undertaken, utilising reaction (22) as a source of OH radicals.

$$O(^1D) + H_2O \rightarrow 2OH \quad 22$$

$(k_{22} = 2.3 \times 10^{-10}\ cm^3\ molecule^{-1}\ s^{-1})$ [13]

Varying OH concentrations were generated by photolysis of ozone (2-6 Nm^{-2}) in the presence of excess H_2O (530 Nm^{-2}) and a curve of growth constructed (FIG 3.4). The absolute hydroxyl radical concentration may be inferred from the measured ozone concentration knowing the fractional photolysis per flash equals 7.3% [7] and assuming each $O(^1D_2)$ generates two OH radicals i.e. $[OH] = 0.15\ [O_3]$.

OH yields from $O(^1D)$ attack on CH_3Cl were investigated by flash photolysis of various ozone/methyl chloride mixtures [O_3 = 14-22 Nm^{-2}, CH_3Cl = 130-200 Nm^{-2}]. Comparison of OH yields with the $O(^1D_2)$ concentration reacting with methyl chloride yielded a branching ratio into reaction (19) of 35±6%. The error limit refers to one standard deviation on four separate experimental results. The decay kinetics of OH in the presence of CH_3Cl were consistent with reaction 23. (see FIG 3.5)

$$OH + CH_3Cl \rightarrow CH_2Cl + H_2O \quad 23$$

$(k_{23} = 4.9 \times 10^{-14}\ cm^3\ molecule^{-1}\ s^{-1})$ [20]

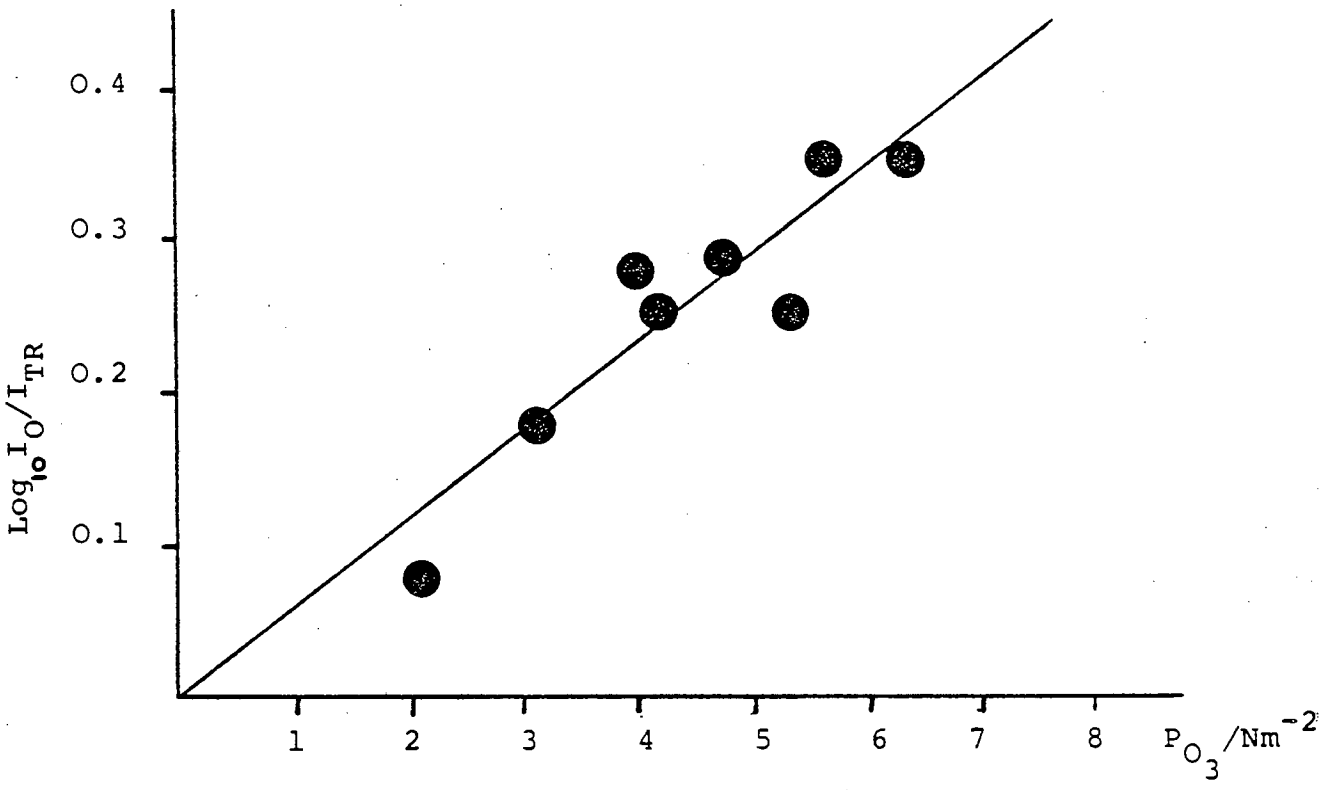

FIG 3.4: Curve of growth (OH radical)

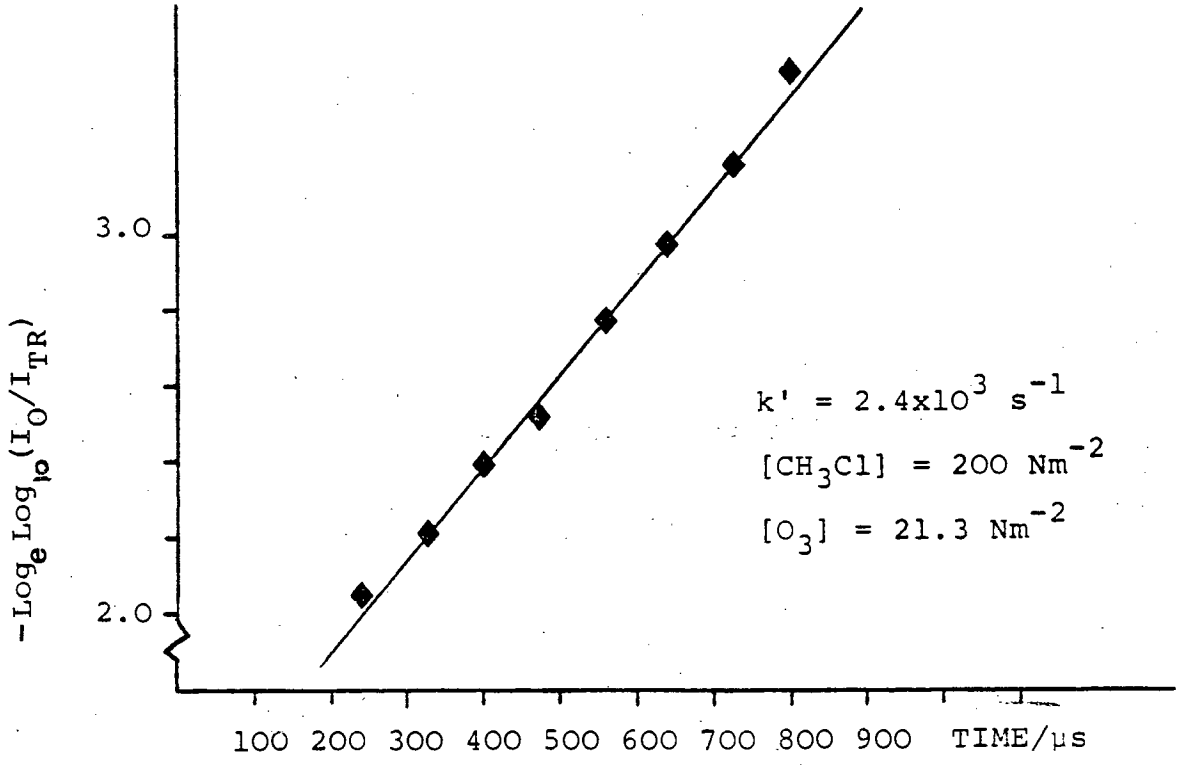

FIG 3.5: Pseudo first order plot (OH + CH_3Cl)

A calculated value from the present system (FIG 3.5) of $k_{23} = 3.5 \times 10^{-14}$ must be considered fortuitously accurate as a number of interfering reactions will occur in the O_3/CH_3Cl system (24, 25)

$$OH + ClO \rightarrow PRODUCTS \quad 24$$

$$O(^3P) + CH_3 \rightarrow CH_2 + OH \quad 25$$

Removal of OH in the pure ozone environment had been measured previously in this system ($k_{OH+O_3} = 1.2 \times 10^{-13}$ cm^3 $molecule^{-1}$ s^{-1})[7]. This value is twice the recognised value for OH removal by ozone alone and was rationalised by the following reaction scheme (26, 27)

$$OH + O_3 \rightarrow HO_2 + O_2 \quad 26$$

$$HO_2 + OH \rightarrow H_2O + O_2 \quad 27$$

These removal processes were allowed for in the calculation of k_{23}.

3. <u>$O(^3P_J)$ Yields</u>: Essentially the same experiment was planned to monitor $O(^3P)$ yields as that described for the OH measurements. $O(^1D_2)$ was quenched with excess nitrogen and a curve of growth constructed relating absorbance to ground state oxygen atom concentration. The experiment was then repeated with the chloro-fluorocarbon replacing the nitrogen. $O(^3P_J)$ yields at t=0 may then by correlated to the branching ratio into $O(^1D_2)$ quenching. The strong absorption of the chlorofluorocarbons used (CF_2HCl and CF_3Cl) produced two major problems (1) the low light transmittance

resulted in poor signal to noise ratios; (2) it was observed that the addition of a strong absorber resulted in a variation in the curve of growth (see FIG 3.6). This latter difficulty was overcome by constructing the relevant curves of growth in large excess of nitrogen but with the chlorofluorocarbon present at the concentration used in the quenching experiments.

Due to the difficulties involved with the absorption technique an attempt was made to make the same measurements using the resonance fluorescence technique to monitor $O(^3P_J)$ atom concentration. However, the necessary pressures of chlorofluorocarbon were such that the fluorescence signal was reduced below easily processable levels hence giving no improvement in data accuracy as compared to the absorption technique.

Results (see TABLE 3.1) were obtained under the following experimental conditions: $[O_3] = 0.5\ Nm^{-2}$, $[O_2] = 0.7\ Nm^{-2}$, $[C.F.M] = 4\ Nm^{-2}$. Under these conditions it was assumed that each $O(^1D_2)$ reacting with ozone (see Chapter 5) or oxygen was stochiometrically converted to $O(^3P_J)$. In the reaction of $O(^1D_2)$ with O_2 in the presence of ozone, reactions (28) and (29) represent the primary and secondary processes.

$$O(^1D_2) + O_2 \rightarrow O(^3P) + O_2(^1\Sigma_g^+) \qquad 28$$

$$O_2(^1\Sigma_g^+) + O_3 \rightarrow 2O_2 + O(^3P) \qquad 29$$

The fate of the $O_2(^1\Sigma_g^+)$ in the experimental system with relatively large chlorofluorocarbon concentrations is

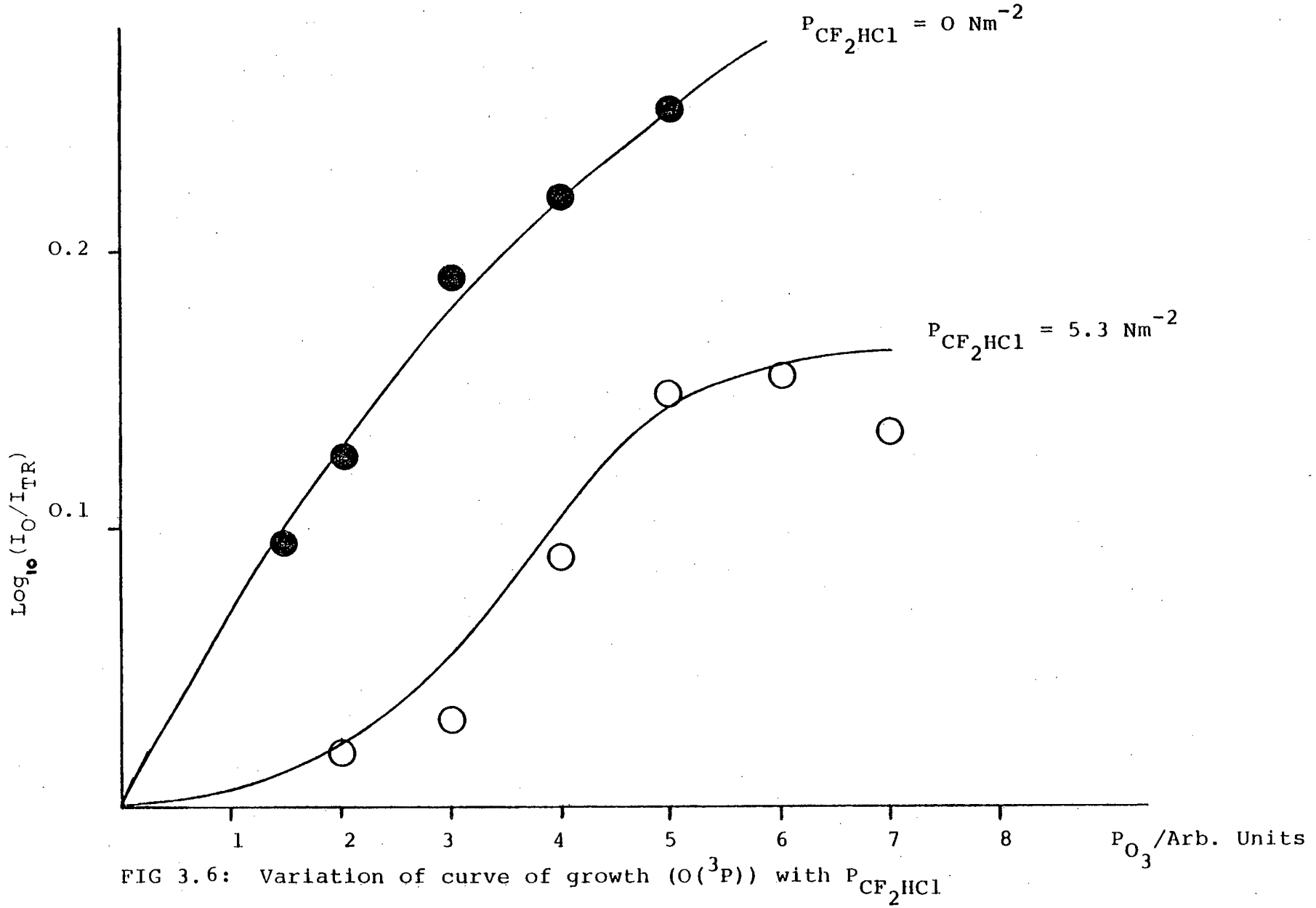

FIG 3.6: Variation of curve of growth ($O(^3P)$) with P_{CF_2HCl}

TABLE 3.1 QUENCHING OF $O(^1D_2)$ BY CHLOROFLUOROCARBONS:-

EXPERIMENTAL DATA

Quenching Molecule	Total $O(^3P)$ Yield†	$O(^3P)$ Prod. From Reaction		$O(^3P)$ From Reaction with CFM†	% Of $O(^1D)$ Encounters Leading to Quenching
		With O_3†	With O_2†		
CH_2HCl	2.3	0.96	0.19	1.15	40
CF_3Cl	2.3	0.92	0.19	1.19	40
CH_4	1.6	0.72	0.15	0.73	23

† Figures refer to relative $O(^3P)$ yields $O(^3P)$ yield in excess N_2 (under otherwise identical conditions)]=4.0.

uncertain, however, if reaction (30) predominates then on the time scale of the experiment each $O(^1D)$ reacting with O_2 will yield two $O(^3P)$ atoms. Further, experiments designed to monitor $O(^3P)$ production immediately following photolysis in the Hartley bands failed to detect any production in the initial photochemical act. Recent studies have however suggested that the primary quantum yield of $O(^3P_J)$ atoms following photolysis below 300 nm is of the order of 10%.[21-23] Strong interference from either of these channels will tend to lower the branching ratios listed in TABLE 3.1. As a form of calibration, quenching by methane was investigated in an analogous manner.

3.4 DISCUSSION

It is evident that while most of the measurements described in the preceding pages are subject to relatively large error limits certain trends are readily apparent.

Reaction of $O(^1D_2)$ with CCl_4 follows the trend shown with other chlorofluorocarbons in that a major reaction pathway leads to the formation of ClO. Two mechanisms can be devised which lead to the primary production of ClO. The most direct route is via an abstraction reaction in which it may be envisaged that electron donation from chlorine to the empty p-orbital of the $O(^1D_2)$ atom facilitates the exchange of the chlorine atom. Another possible explanation

involves an insertion reaction into the C-Cl bond to form a vibrationally excited hypochlorite molecule, $CCl_3OCl^{\ddagger}$. However from thermodynamic considerations the preferred decomposition of the hypochlorite should involve the scission of the CCl_3O-Cl bond to form free chlorine atoms as opposed to scission of the CCl_3-OCl bond, hence suggesting that direct abstraction accounts for the branching ratio into ClO production ($30^{+20\%}_{-10\%}$). The insertion reaction may account for the observed chlorine atom production ($\leqslant 38\%$). This behaviour may be contrasted with the reaction of $O(^1D_2)$ with hydrocarbons which were found to proceed in the main through insertion into the C-H bonds. Recent data suggests, however, that direct abstraction increases in importance as the size of the alkane increases[24]. Confusion also exists on the relative importance of the quenching reaction of $O(^1D_2)$ with hydrocarbons. A recent paper by Aminoto et al[25] suggested a value of $12\pm4\%$ of the total reaction cross section. This figure, which is in broad agreement with the value presented here ($13\pm7\%$) may however be an upper limit due to the undetected initial $O(^3P_J)$ quantum yield from ozone photolysis. (The final data presented in this work has been corrected for a 10% initial $O(^3P_J)$ quantum yield). Earlier work suggested the quenching channel for $O(^1D_2)$ attack on alkanes to be negligible. From the present work with CF_3Cl and CF_2HCl it appears that the fraction of collisions leading to quenching ($30\pm^{10\%}_{15\%}$)

is increased with the chlorofluoromethanes as compared to the alkanes. The quenching process is indicative of accessible crossing points between singlet and triplet potential surfaces. It may be that the chlorofluoromethane surface crossings occur at lower energies than with the analogous alkane surfaces, facilitated perhaps by the involvement of a mimimum in the singlet surface corresponding to a $CF_xCl_{3-x}ClO$ intermediate. Certainly the spin orbit coupling between the surfaces would be expected to increase for the heavier chlorofluoromethanes as compared to the lighter alkanes.

Two other studies on the reaction of $O(^1D_2)$ with CCl_4 have been carried out. In neither system was ClO produced from $O(^1D_2)$ reaction, through the abstraction mechanism, viewed directly. Heicklen et al[26] suggested from work employing quantum yield measurements that reaction of $O(^1D_2)$ with CCl_4 goes almost exclusively via direct abstraction. This result was obtained by rationalising the quantum yields of phosgene and chlorine and measured ozone depletion levels, to the following reaction scheme:

$O(^1D) + CCl_4$	→	$ClO + CCl_3$	7
	→	$CCl_2O + Cl_2$	11
	→	$O(^3P) + CCl_4$	9
$CCl_3 + O_3$	→	$CCl_3O + O_2$	30
CCl_3O	→	$CCl_2O + Cl$	31
$Cl + O_3$	→	$ClO + O_2$	2
$2ClO$	→	$Cl_2 + O_2$	32
	→	$2Cl + O_2$	33

From this reaction scheme

$$\Phi(COCl_2) = \Phi(Cl_2) = \phi(30) + \phi(11)$$

From experimental results $\Phi(Cl_2) = \Phi(COCl_2) = 1.0 \pm 0.2$ suggesting $\phi(9) \lesssim 0.20$. - $\Phi(O_3)$ was measured as >6 suggesting channel (7) to be dominant. Consistent with these measurements are the inclusion of the following reaction pathways (8,10).

$O(^1D) + CCl_4$	→	$CCl_3O + Cl$	8
	→	$CCl_2O + 2Cl$	10

If reactions (8) and (10) were important the above data could not be used to distinguish between them and reaction (7). Similarly in view of the uncertainty in the relative contributions of reactions (32) and (33) - see Chapter 4 - it would be extremely difficult to judge the importance

of channel (11) from quantum yields alone.

The work of Meaburn et al[27] uses the technique of pulsed radiolysis of CO_2, N_2O and CO as a source of oxygen atoms. On radiolysis of a CO_2-O_2-CCl_4 mixture the ClO spectrum was detected in absorption. However this system gives no way of differentiating between the various channels which may lead to its production.

The reaction of $O(^1D_2)$ with methyl chloride proved difficult to monitor through ClO detection. The branching ratio into OH production - 35±6% - is of considerable interest. This result may be evaluated with consideration of the expected yield if bond additivity rules governing the reaction kinetics of $O(^1D)$ with the halomethanes, as suggested by Davidson et al[15], were applicable to product branching ratios also. From bond additivity rules the fraction of oxygen atoms attacking the C-H bonds corresponds to 56.5% of the total reaction cross section. Of this, it is expected that 85-95% should lead to hydroxyl radical formation directly under the conditions of the experiment. The present result together with previous work on CF_2HCl[28] indicates that less OH radicals are produced than may be expected from the additivity rules. It seems unlikely that the presence of adjacent halogen atoms as opposed to hydrogen atoms greatly affects product formation (with the possible exception of the quenching process) once the $O(^1D_2)$ has been 'captured' by a specific bond. A more likely explanation of the breakdown of bond additivity rules in predicting

reaction products concerns the range of interaction of the various substituents attached to the carbon. Considering the relative sizes of the hydrogen and chlorine atoms it is suggested that the range of the interaction potential between the oxygen and chlorine confers a directing effect to the chlorine atom - reaction at this bond presenting the first opportunity for oxygen atom attack. Reaction with hydrogen occurs at shorter range and necessitates the close approach of the oxygen atom, having evaded capture by the chlorine atom.

The methylene radical is isoelectronic with the oxygen atom. The reactivity of the singlet states with halomethanes has been compared previously[28]. Work by Setser et al[29] estimated that in the reaction of singlet methylene with CH_3Cl approximately 20-30% of reactive collisions resulted in hydrogen abstraction. Again, a strong similarity between the chemistry of these two species is demonstrated.

3.5 REFERENCES

1. F.S. Rowland and M.J. Molina, Nature 249, (1974), 810.
2. M.J. Kurylo and W. Braun, Chem. Phys. Lett. 37, (1976), 232.
3. M.S. Zahniser, F. Kaufmann and J.G. Anderson, Chem. Phys. Lett. 37, (1976), 226.
4. P. Bemand, M.A.A. Clyne and R.T. Watson, J. Chem. Soc. Faraday Trans. 69, (1973), 1356.
5. F.S. Rowland and M.J. Molina, Rev. Geophys. Space Phys. 13, (1975), 1.
6. H.M. Gillespie, J. Garraway and R.J. Donovan, J. of Photochem. 7, (1977), 29.
7. J. Garraway, Ph.D. Thesis, University of Edinburgh, to be published.
8. H. Yamazaki and R.J. Cvetanovic, J. Chem. Phys. 41, (1964), 3703.
9. A.J. Colussi and R.J. Cvetanovic, J. Phys. Chem. 79, (1975), 1891.
10. P. Michaud, G. Paraskevopoulos and R.J. Cvetanovic, J. Phys. Chem. 78, (1974), 1457.
11. P.N. Clough and B.A. Thrush, Chem. and Ind. 1971, (1966).
12. N. Basco, D.G.L. James and R.D. Suart, Int. J. Chem. Kinetics 2, (1970), 215.
13. G.E. Streit, C.J. Howard, A.L. Schmeltekopf, J.A. Davidson and H.I. Schiff, J. Chem. Phys. 65, (1976), 4761.

14. M. Griggs, J. Chem. Phys. 49, (1968), 857.

15. J.A. Davidson, H.I. Schiff, T.J. Brown and C.J. Howard, J. Chem. Phys. 69, (1978), 4277.

16. R.G. Manning and M.J. Kurylo, J. Phys. Chem. 81, (1977), 291.

17. R.F. Hampson Jr. and D. Garvin (Eds), NBS Special Publication 513, (1977).

18. M.A.A. Clyne and W.S. Nip, J. Chem. Soc. Faraday Trans. II 72, (1976), 838.

19. M.A.A. Clyne and R.F. Walker, J. Chem. Soc. Faraday I 69, (1973), 1547.

20. R.D. Hudson, Ed., NASA Reference Publ. 1010, August (1977).

21. R.K. Sparks, L.R. Carlson, K. Shobatake, M.L. Kowalczyk and Y.T. Lee, J. Chem. Phys. 72, (1980), 1401.

22. C.E. Fairchild, E.J. Stone and G.M. Lawrence, J. Chem. Phys. 69, (1978), 3632.

23. J.C. Brock and R.T. Watson, 14th Informal Conf. on Photochemistry, Newport Beach, California, March/April, 1980.

24. A.C. Luntz, 14th Informal Conf. on Photochemistry, Newport Beach, California, March/April 1980.

25. S.T. Amimoto, A.P. Force, R.G. Gulotty Jr. and J.R. Wiesenfeld, J. Chem. Phys. 71, (1979), 3640.

26. R.K.M. Jayanty, R. Simonaitis and J. Heicklen, J. Photochem. 4, (1975), 203.

27. G.M. Meaburn, D. Perner, J. Lecalve and M. Bourene, J. of Phys. Chem. 72, (1968), 3920.

28. M.C. Addison, R.J. Donovan and J. Garraway, Faraday Disc. 67, (1979), 286.

29. D.W. Setser, R. Littrell and J.C. Hassler, J. Amer. Chem. Soc. 87, (1965), 2062.

CHAPTER IV

A TEMPERATURE DEPENDENT STUDY OF THE MUTUAL COMBINATION OF ClO RADICALS

4.1 INTRODUCTION

The recombination reaction of chlorine monoxide (ClO) radicals has received much attention since the introduction of flash photolysis techniques.

Porter and Wright[1] working with the Cl_2/O_2 system using flash photolysis and plate photometric detection observed ClO production and loss. The loss process was observed to be second order with respect to ClO and was independent of total pressure. Studies of the effect of temperature at $4x10^4$ Nm^{-2} total pressure showed little dependence. Removal of ClO was explained using the following reaction scheme:

$$ClO + ClO \rightarrow Cl_2O_2 \quad \text{(press. independent)}$$

$$Cl_2O_2 \rightarrow Cl_2 + O_2$$

Johnston, Morris and Van den Bogaerde[2] using the technique of molecular modulation spectroscopy with u.v. absorption observed ClOO and ClO radicals from photolysis of Cl_2/O_2 mixtures. Their results provide strong evidence for the involvement of a third order removal mechanism for ClO. Clyne and various co-workers[3,4], using a discharge flow system, have made numerous detailed kinetic studies of ClO kinetics and have come to the conclusion that any three body

removal mechanisms for ClO play a very minor role in the kinetics of ClO disproportionation at low pressure. Observation of chlorine atom production has led to the following reaction being postulated as the main removal channel for chlorine monoxide:

$$ClO + ClO \rightarrow Cl + ClOO$$

Temperature dependent kinetic studies have been carried out at low pressure and an Arrhenius expression for the rate constant of the overall reaction obtained.[18] Wu and Johnston[5] using molecular modulation spectroscopy coupled to mass spectrometric detection of the Cl_2/O_2 system at low pressures observed a pressure dependence to the ClO removal rate. Discrepancies between their work and other researchers, however, led the authors to conclude that the reaction mechanism used did not describe all observations. Very recently Cox and Derwent[6,7] and Basco and Hunt[8] using different techniques (M.M.S. in the former, flash photolysis with kinetic absorption spectroscopy in the latter) seem to have provided unequivocal evidence for the existence of a third order reaction leading to generation of an intermediate $(ClO)_2$ dimer.

This work continues that of Cox and Derwent - the MMS technique being used in various systems (previously used for the generation and observation of ClO) to observe the temperature dependence of ClO disproportionation kinetics.

4.2 EXPERIMENTAL

Two systems were used for the production of ClO, namely: (i) $Cl_2/Cl_2O/O_2$ and (ii) Cl_2/O_2 (low pressure $\approx$6.5 kNm^{-2}). All kinetic data were obtained using the molecular modulation spectrometer described fully in section 2.9. With the $Cl_2/Cl_2O/O_2$ system experiments were carried out in the stopped flow regime. Flow rates were set prior to experimentation and admission of gases to and from the reaction vessel were controlled by electrically operated solenoid valves. In the Cl_2/O_2 system the reaction vessel was filled to the desired pressure, all experiments then being conducted on that one mixture.

Cl_2, N_2 (high purity) and O_2 (breathing grade) were used directly from cylinders. Cl_2O was prepared by diverting part of the chlorine flow through a 20 cm mercuric oxide [HgO]/glass bead support column. Good conversion of Cl_2 to Cl_2O was observed. Concentrations of reactants, intermediates and products were measured by absorption spectroscopy. Concentrations of species were monitored at the following wavelengths: Cl_2(350 nm); Cl_2O(261.2 nm); ClO(277.3 nm) and OClO(351.4 nm). Absorption cross sections used are recorded in TABLE 4.1

4.3 DATA ANALYSIS

As radical absorptions in this system are always small the approximate form of the Beer-Lambert law, relating concentration to absorption can be used i.e.

TABLE 4.1 ABSORPTION CROSS SECTIONS/cm^2

Molecule λ/nm	Cl_2 [9]	Cl_2O [10]	ClO [3]	OClO [3]
350	1.89×10^{-19}	2×10^{-20}		
261.2	2.3×10^{-21}	1.83×10^{-18}		
277.25	2.2×10^{-20}	1.27×10^{-18}	7.26×10^{-18}	
			3.2×10^{-18} †	
351.4	1.83×10^{-19}	2×10^{-20}		1.14×10^{-17}

† Differential absorption cross section

$$I_{abs} = \sigma l [R](t) \qquad 4.1$$

where σ = absorption cross section

l = path length

$[R](t)$ = absorber concentration at time t.

Using the above nomenclature and with reference to FIG 2.14 the molecular modulation counters will accumulate signals due to radical absorption both in phase (P) and in quadrature (Q) with the photolysis lamps governed by equations 4.2 and 4.3 respectively.

$$P = \frac{1}{\tau}(a+b-c-d)$$

$$= c\sigma l\left[\int_{o}^{\tau/2}[R](t)\,dt - \int_{\tau/2}^{\tau}[R](t)\,dt\right] \qquad 4.2$$

$$Q = \frac{1}{\tau}(b+c-d-a)$$

$$= c\sigma l\left[\int_{\tau/4}^{3\tau/4}[R](t)\,dt - \int_{3\tau/4}^{5\tau/4}[R](t)\,dt\right] \qquad 4.3$$

where a, b, c, d are illustrated in FIG 2.14

c = calibration factor relating count rate and absorption.

The form of the experimental results given by equations 4.2 and 4.3 can be calculated by substitution of the appropriate functions for the variation with time of the radical concentrations. The analytical treatment for radicals following first order, second order and mixed first and second order kinetics has been described in detail by Parkes et al[11]. The differential equations for a radical removed by a second order reaction are as follows:

IN THE LIGHT $$\frac{d[R]}{dt} = 2B - 2k[R]^2 \qquad 4.4$$

IN THE DARK $$\frac{d[R]}{dt} = -2k[R]^2 \qquad 4.5$$

2B = rate of production of radicals by photolysis

2k = overall second order decay coefficient.

At long photolysis periods the radicals follow closely the square-wave form of the photolytic intensity. The limiting value of the in-phase count rate is given by one half the steady state solution of equation 4.4 with the corresponding absorption given by equation 4.6.

$$A_{ss} = \frac{\sigma l}{2} \left(\frac{B}{k}\right)^{\frac{1}{2}} \qquad 4.6$$

As the photolysis period decreases the radical lifetime becomes significant and the in phase signal falls as the in quadrature signal rises. The in quadrature signal maximises when the counting rates P and Q are equal and the solution of the relevant equations renders:

$$\tau_o = 2.2/[Bk]^{\frac{1}{2}} \qquad 4.7$$

where τ_o is the period at which the in phase count rate equals the in quadrature count rate.

For a second order reaction

$$A_o = 0.285\ A_{ss}$$

Equations 4.6 and 4.7 illustrate that for second order kinetics, both the steady state concentration of the radical and its 'lifetime' are dependent on the square root of the production rate. In order to incorporate all second order data into one data set it is necessary to divide the absorption measurements and multiply the photolysis period by $B^{\frac{1}{2}}$. See FIG 4.2 for such a plot. In all experiments chlorine was used as the photolytic source of the ClO radicals. Its photodissociation rate was determined from the initial rate of decay of Cl_2 in

the presence of excess H_2 ($3kNm^{-2}$) and O_2 ($98kNm^{-2}$). Under such conditions the following reaction scheme would be followed (1-4):

$$Cl_2 + h\nu \ [310\text{-}410 \text{ nm}] \rightarrow 2Cl \qquad 1$$

$$Cl + H_2 \rightarrow HCl + H \qquad 2$$

$$H + O_2 + M \rightarrow HO_2 \qquad 3$$

$$HO_2 + HO_2 \rightarrow H_2O_2 + O_2 \qquad 4$$

The rate of photolysis was determined as 0.89×10^{-3} s^{-1} per lamp.

4.4 RESULTS

(i) $Cl_2/Cl_2O/O_2$ System

Such a system provides a relatively clean source of ClO radicals through reactions (1) and (5). Due to the assumed slow nature of reaction (6) the disproportionation of ClO (7) is the predominant removal mechanism for ClO radicals in this system.

$$Cl_2 + h\nu \rightarrow 2Cl \qquad 1$$

$$Cl + Cl_2O \rightarrow Cl_2 + ClO \qquad 5$$

$$ClO + Cl_2O \rightarrow \text{PRODUCTS} \qquad 6$$

$$ClO + ClO \ (+M) \rightarrow \text{PRODUCTS} \qquad 7$$

From a steady state analysis of the Cl atom concentration in the system it is readily appreciated that the fast nature of reaction (5) [$k_5 \simeq 1 \times 10^{-10}$ cm^3 $molecule^{-1}$ s^{-1}][12]

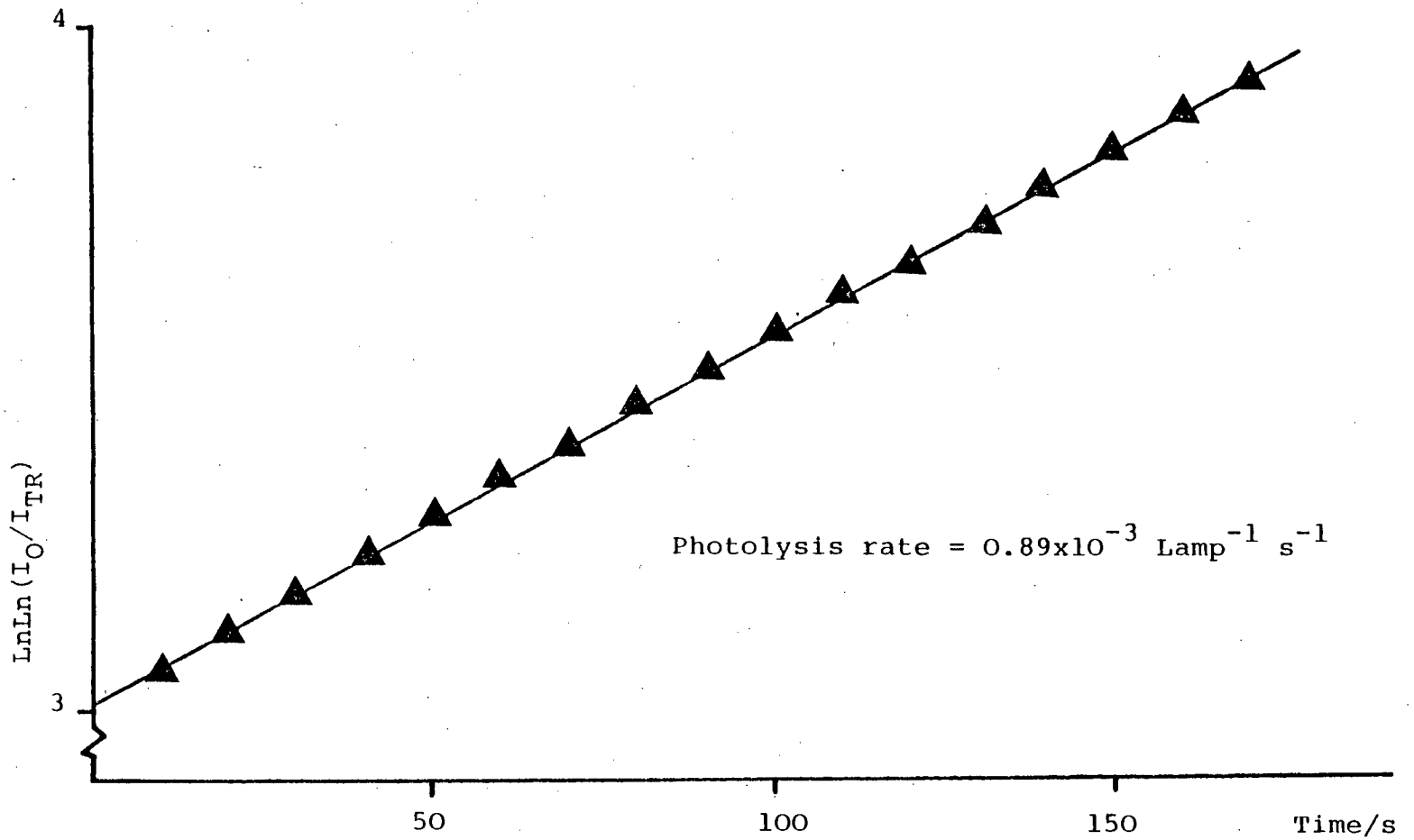

FIG 4.1 First order plot of Cl_2 loss with time (no. of photolysis lamps used = 6).

and conditions used $[Cl_2O] \simeq 2x10^{15}$ molecule cm^{-3}, $[Cl_2] \simeq 2x10^{15}$ molecules cm^{-3} and $[O_2] \simeq 2x10^{19}$ molecules cm^{-3} results in a very low [Cl] atom concentration of approximately 10^7 molecules cm^{-3} during photolysis.

A study was made of the variation of rate constant and quantum yield for removal of Cl_2O over the temperature range 278-346 K. Rate data were obtained using the relationship established in section 4.3, having monitored ClO at 277.25 nm in differential mode (see sec. 2.9). Quantum yield measurements were made by comparing the rate of loss of Cl_2O with the rate of production of Cl atoms in the system (equation 4.8)

$$\Phi = \frac{[Cl_2O]_{LOSS\ RATE} - 0.1\ k_1[Cl_2O]}{*\frac{1}{2}\ k_1[2[Cl_2] + 0.2\ Cl_2O]]} \qquad 4.8$$

$$k_1 = 0.89x10^{-3}\ s^{-1} \text{ per lamp}$$

If Cl atoms were solely produced through photolysis then Φ would equal unity. A value greater than 1 is indicative of Cl atom regeneration through channel (7). The temperature dependence of the Cl_2O decay quantum yield is shown in TABLE 4.2 together with the calculated value α, where α is the fraction of ClO radicals which regenerate Cl atoms. It is easily shown that:

*$\frac{1}{2}$ appears in the denominator due to the lights only being on for half the time.

$$\Phi = \sum_{n=0}^{\infty} \alpha^n \rightarrow \Phi = 1/1-\alpha \qquad 4.9$$

For the following reaction scheme for ClO disproportionation (8-12), α may be represented by equation 4.10.

$$\alpha = k_8 + \beta k_9/k_8 + k_9 + k_{10} \qquad 4.10$$

Where $0.5 \leqslant \beta \leqslant 1$ depending on the percentage of OClO photolysed during the monitoring time.

$ClO + ClO \rightarrow Cl + ClOO$		(8)
$ClO + ClO \rightleftharpoons Cl + OClO$		(9),(-9)
$ClO + ClO \rightarrow Cl_2 + O_2$		(10)
$ClO + ClO + M \rightleftharpoons Cl_2O_2 + M$		(11),(-11)
$ClOO \rightleftharpoons Cl + O_2$		(12),(-12)
$Cl + Cl_2O \rightarrow ClO + Cl_2$		(5)

Reaction (-9) is minor in systems of very low [Cl] atom concentrations. The major fate of the OClO so produced being reaction through channels (13-14)

$OClO + h\nu \rightarrow O + ClO$	(13)
$O + O_2 + M \rightarrow O_3$	(14)

From TABLE 4.2 it is seen that α increases with temperature i.e. $k_8 + \beta k_9$ (the 'branching' reactions) are increasing more rapidly than the total removal rate of ClO. If α is rewritten in terms of k_{BR} and k_{TER} the temperature dependence may be represented by an Arrhenius expression (equation 4.14), then a plot of

TABLE 4.2 TEMPERATURE DEPENDENCE OF THE Cl_2O DECAY QUANTUM YIELD

Temp/K	$(\frac{1}{T}/K^{-1}) \times 10^3$	† Φ ($-Cl_2O$)	α	k_{BR}/k_{TER}
278	3.60	1.56	0.359	0.560
285	3.51	1.91	0.476	0.908
299	3.34	1.97	0.492	0.969
314	3.19	2.29	0.563	1.288
334	2.99	2.5	0.600	1.500

† These values have been corrected for the ozone produced in the system which also absorbs at the monitoring wavelength of 261.2 nm.
(These values are in excellent agreement with early work by Finkelenburg et al[13]).

$\ln(k_{BR}/k_{TER})$ against $\frac{1}{T}$ yields the following relationship between the activation energies into the branching (E_{BR}) and termination steps (E_{TER}).

$$E_{TER} + 13 \text{ kJ mol}^{-1} = E_{BR}$$

This result is obtained from the following analysis*:

$$\alpha = k_8 + \beta k_9/k_8 + \beta k_9 + (1-\beta)k_9 + k_7 \qquad 4.11$$

where $k_8 + \beta k_9 = k_{BRANCHING}$ (k_{BR})

$$k_{10} + (1-\beta)k_9 = k_{TERMINATION} \ (k_{TER})$$

$$\alpha = k_{BR}/k_{BR} + k_{TER} \qquad 4.12$$

$$k_{BR}/k_{TER} = (\alpha^{-1} - 1)^{-1} \qquad 4.13$$

*This analysis is far from rigorous suffering from two sources of error: i) the β used for the evaluation of α and k_{TER}, k_{BR} are slightly different. In the strictest sense β must include provision for all the chlorine dioxide (OClO) molecules photolysed since each leads to ClO production when evaluating k_{TER} and k_{BR}. However, the β used in the expression for α will account only for the ClO radicals so produced which result in Cl atom formation. ii) In using an Arrhenius expression to express k_{BR}/k_{TER} as a sum of activation energies it must be remembered that these rate constants themselves comprise of more than one rate process, each governed by an Arrhenius expression. Hence the linear behaviour of the experimental data is rather surprising and probably a function of the low temperature range covered. The correlation of the resulting 'activation' energy to the individual reactions (8), (9) and (10) is not possible. However the magnitude of this activation energy is indicative of considerable activation energies in the branching reactions as compared to the termination reactions.

Hence using the Arrhenius expression:

$$\log_e[k_{BR}/k_{TER}] = \log_e A_{BR} - \log_e A_{TER} + (E_{TER}-E_{BR})/RT \qquad 4.14$$

Rate data, reduced by $B^{\frac{1}{2}}$, at first inspection are in moderate agreement indicating 2nd order ClO kinetics (see FIG 4.2). The calculated rate constants (using the absorption coefficients (σ) given in TABLE 4.1) from both τ_o and A_o values are plotted in Arrhenius form in FIG 4.3. From FIG 4.3 it is readily seen that on moving to lower temperatures the A_o and τ_o values diverge suggesting some gross deviation from second order behaviour. The A_o values as expected were found to agree with steady state rate constants measured from the ClO steady state concentrations as recorded directly by means of a photomultiplier coupled directly through an amplifier to a chart recorder.

Evaluation of the rate data obtained from the A^o measurements may be represented by the following Arrhenius expression:

$$k = 2.0\times10^{-11} \exp [-19.7 \text{ kJ mol}^{-1}/RT]$$

A similar analysis of the τ_o values (in agreement with the decay from steady state rate data measured directly and illustrated in FIG 4.4) in the temperature range 298-346 K are shown to be meaningless by the magnitude of the calculated A value - 1000x gas kinetic. It is obvious that some other temperature dependent factor is influencing the radical decay time. It must be stressed that any reaction leading to the regeneration

FIG 4.2 Reduced absorbance vs reduced period

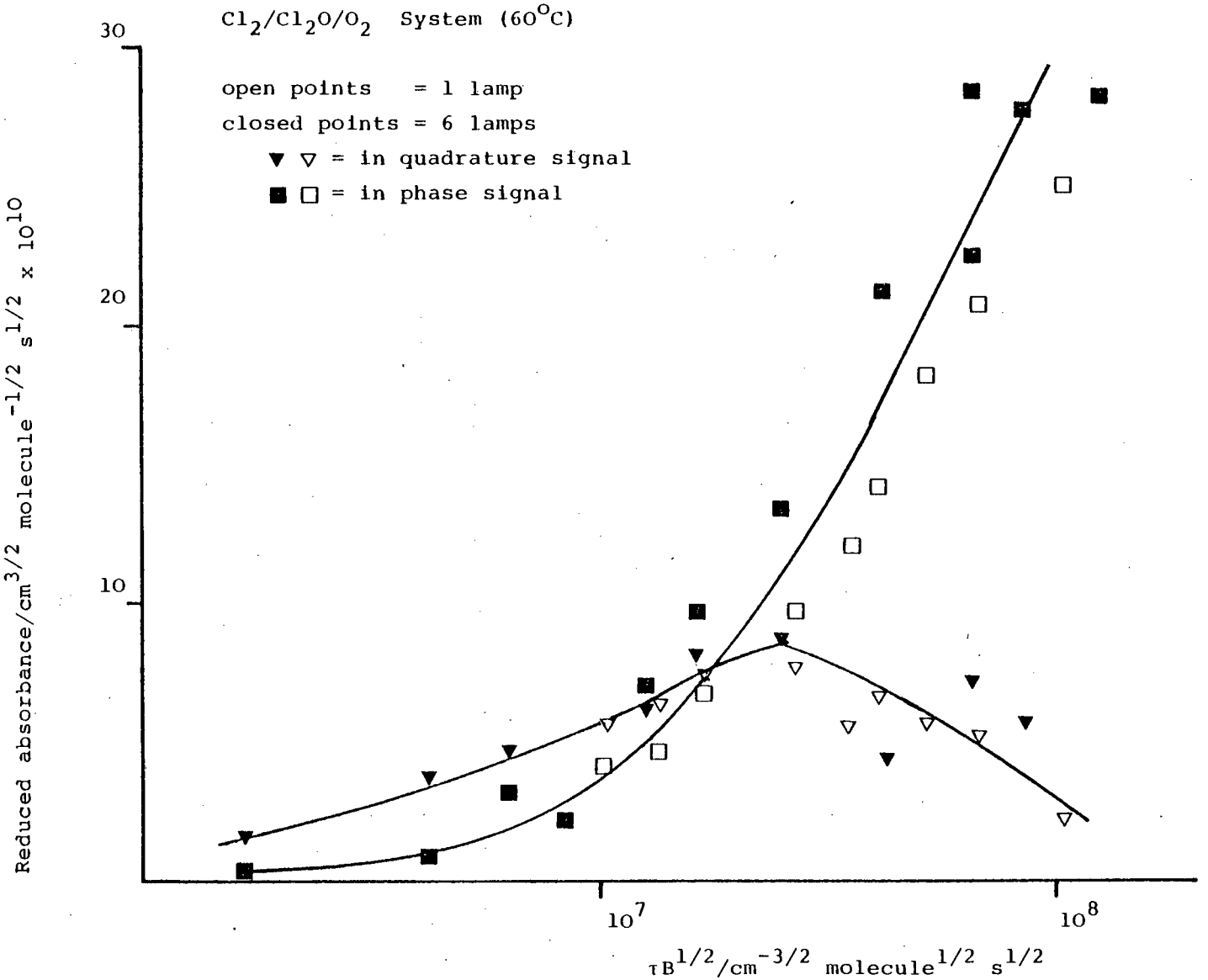

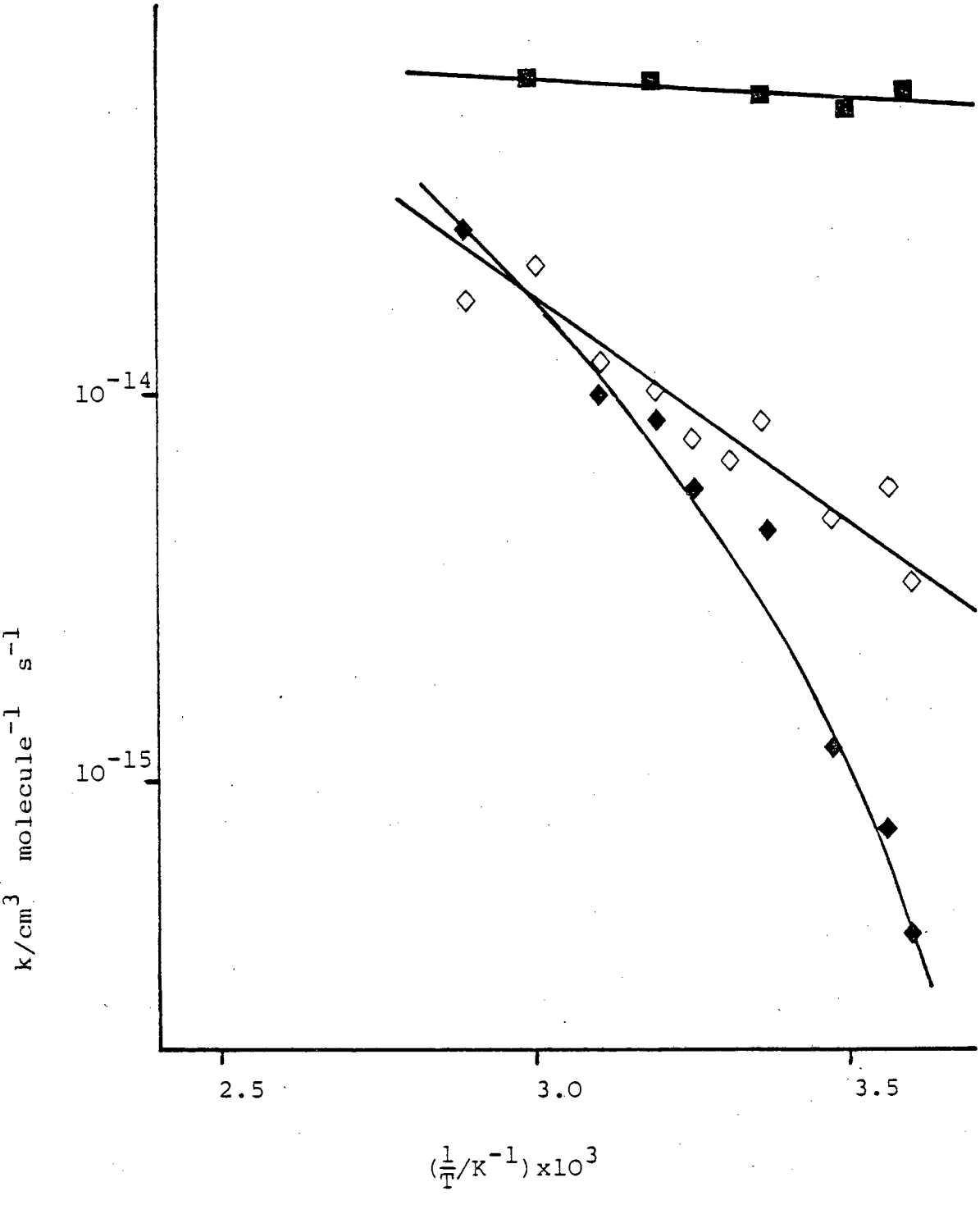

FIG 4.3 Log $k_{ClO+ClO}$ vs $\frac{1}{T}$

■ Cl_2/O_2 (Low Pressure) system from τ_o and A_o values combined

◇ From A^o values)
◆ From τ_o values) $Cl_2/Cl_2O/O_2$ system

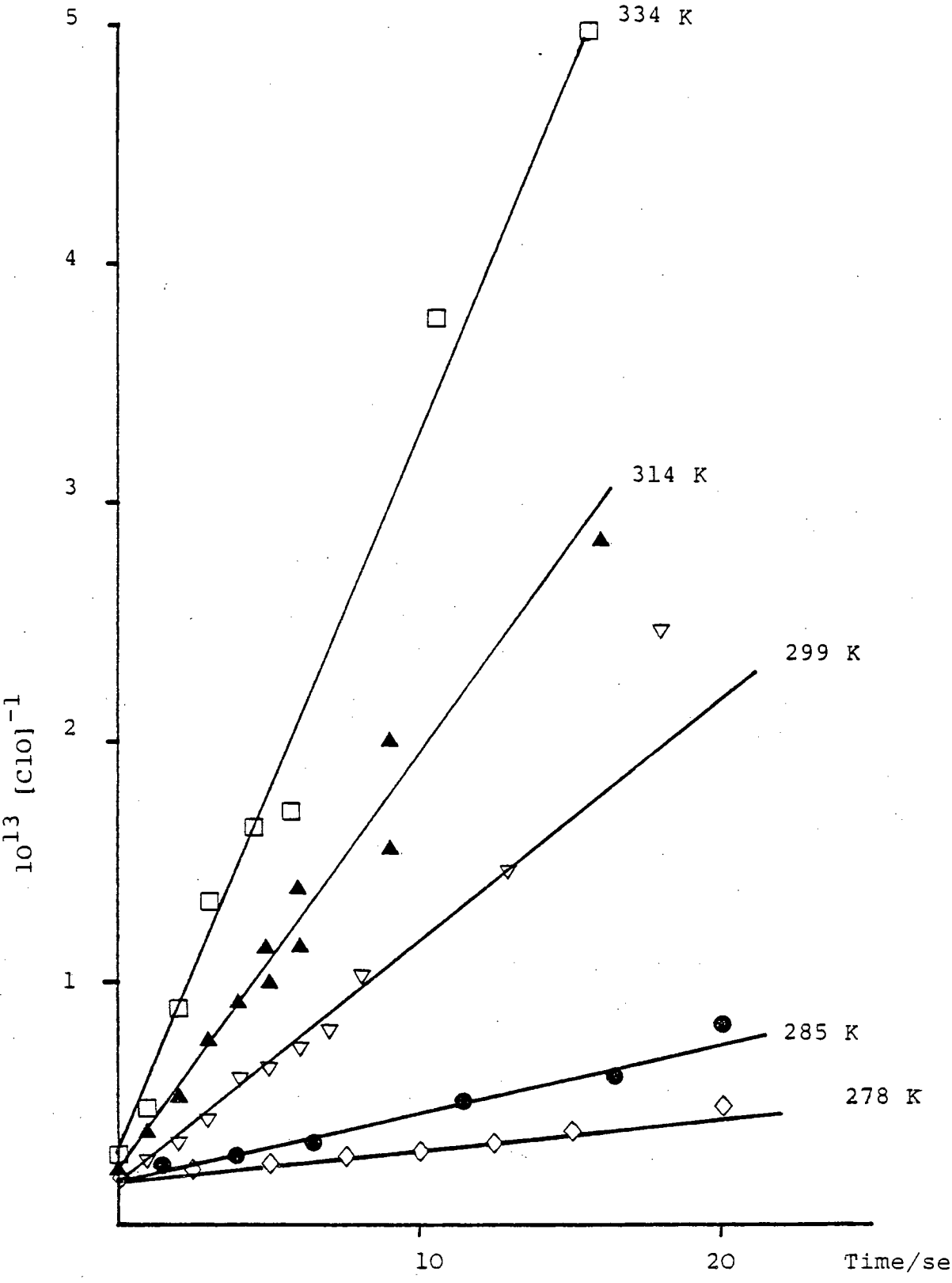

FIG 4.4 Second order plots ($[ClO]^{-1}$ vs time) from observations of ClO decay from steady state in $Cl_2/Cl_2O/O_2$ system.

of ClO i.e. ((8) followed by (12)) and (9) followed by (5) will not be observed in this system in terms of altering the kinetics observed by MMS analysis. Therefore the temperature dependence inferred from the τ_o and A_o values refers only to the termination steps (9) and (10). Coupling then this rate data with the quantum yield measurements we may make the following qualitative statements:

(1) In order for Φ to increase k_8+k_9 must have a positive temperature dependence relative to k_{10}.

(2) In order for k_{TER} to increase k_9+k_{10} must have a positive temperature dependence, if indeed k_9 and k_{10} are the only termination steps.

Evidence for the involvement of reaction (9) and its temperature dependence is two fold: (1) measurement of OClO at 351.4 nm indicated an increase in yield with increasing temperature over the range 278-335 K (see TABLE 4.3) and FIG 4.5 for the growth of OClO as a function of time. (2) in later work by Burrows and Cox[14] ozone produced from the photolysis of OClO in the system (reactions (13) and (14)) was monitored on exit from the reaction vessel using fluorescence detection from the reaction of ozone with C_2H_4. After careful calibration of the system ozone concentrations were recorded at various temperatures. Ozone production was found to be directly proportional to the square of the ClO concentration and to increase with temperature. From a steady state analysis such a dependence on ClO concentration was shown to be justified and the rate of OClO production at 298 K calculated as $5\pm2\times10^{-15}$ cm^3

TABLE 4.3 OClO PRODUCTION AS A FUNCTION OF TEMPERATURE

Temp/K	$[Cl_2O]_{t=0}$ molecules cm^{-3}	$[Cl_2]_{t=0}$ molecules cm^{-3}	$[OClO]_{t=20s}$	$\frac{[OClO]_{t=20s}}{\Sigma [Cl]_{t=0}^{PROD.}}$
278	2.05×10^{15}	3×10^{15}	4.3×10^{13}	0.131
303	2.45×10^{15}	3×10^{15}	6.4×10^{13}	0.216
333	2.45×10^{15}	2.7×10^{15}	7.0×10^{13}	0.228

TABLE 4.4 Cl_2/O_2 SYSTEM:- KINETIC DATA

T/K	No of Lamps Used	τ_o/s	$kf/10^{15}$	$A_o/10^{-4}$	$k/f10^{-12}$	$f/10^{-2}$	$k/10^{-14}$ cm^3 $molec^{-1}$ s^{-1}
279	1	6.2	1.26	6.4	2.89	2.1	6.0
	6	2.1	1.84	20	1.78	3.2	5.7
286	1	5.7	1.49	8.3	1.72	2.9	5.1
	6	2.1	1.93	21.5	1.54	3.5	5.5
298	1	5.0	1.93	7.0	2.42	2.8	6.8
	6	2.2	1.75	22.3	1.43	3.5	5.0
314	1	5.6	1.55	7.0	2.42	2.5	6.1
	6	2.1	1.93	19.0	1.97	3.1	6.2
334	1	5.4	1.67	5.9	3.4	2.2	7.5
	6	2.4	1.41	18.0	2.2	2.5	5.6

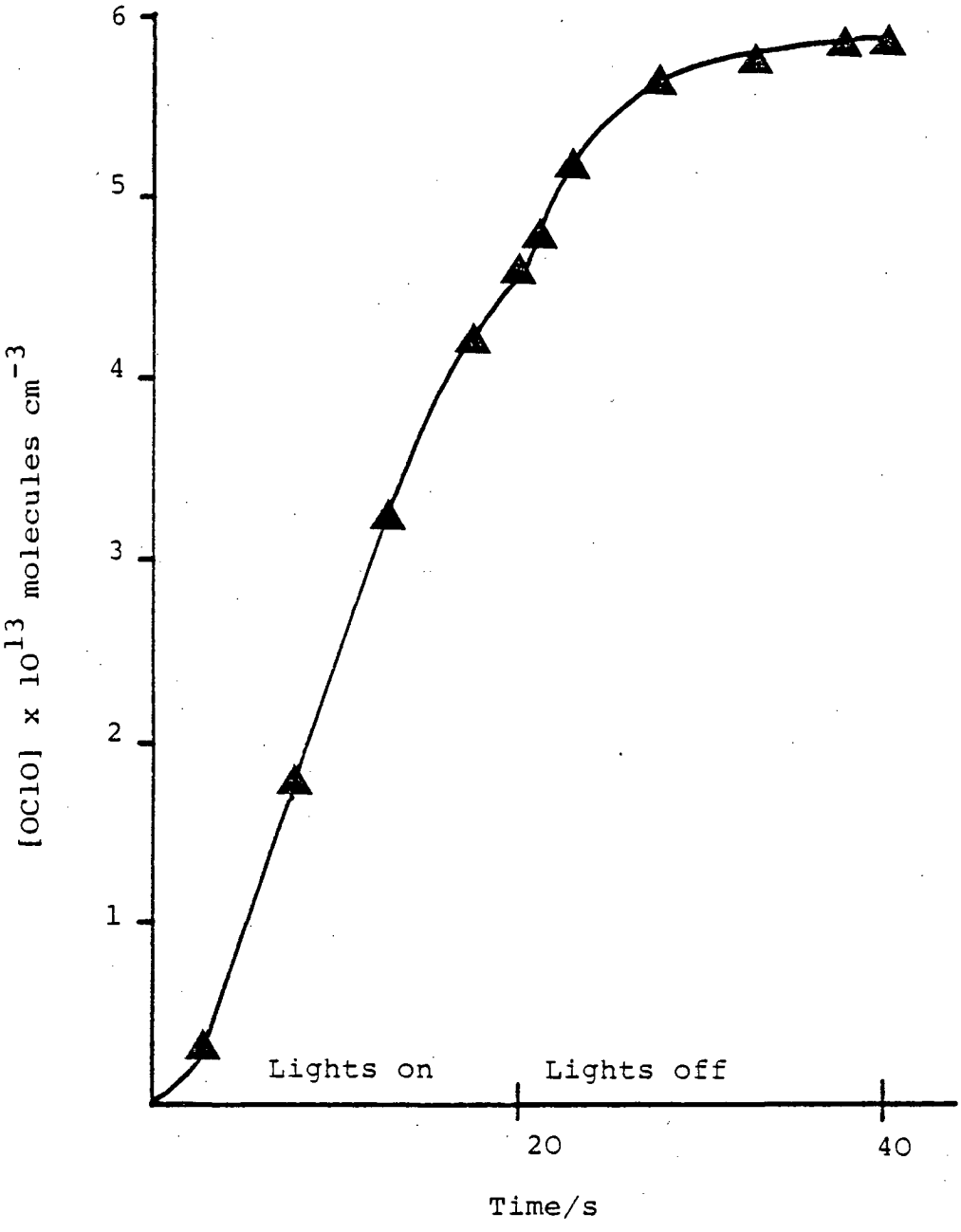

FIG 4.5 Formation of OClO during low frequency photolysis of $Cl_2/Cl_2O/O_2$ mixtures (T = 299 K).

molecule^{-1} s^{-1}. This rate constant is considerably larger than that inferred from the discharge flow studies at low pressure of Clyne et al[4].

Of further interest is the slow growth of OClO after photolysis is over. This together with the large temperature dependence exhibited by the τ_o values supports the conclusion that the involvement of reactions (11) and (-11) provides a temporary store for ClO. Indeed further tentative evidence supporting the participation of a relatively long lived Cl_2O_2 complex was the observation of a transient absorption signal at 225 nm. This absorption we assume to be Cl_2O_2.* This assignment is supported by recent work of Basco and Hunt[8] in which a continuum transient absorption is seen to increase with a concomitant decrease in ClO concentration in a flash photolysis study of the ClO disproportionation reaction.

(ii) <u>Cl_2/O_2 [Low Pressure] System</u>

Concentrations of $Cl_2 \simeq 460$ Nm^{-2} and $O_2 = 6$ kNm^{-2} were used ensuring that the following reaction scheme (1, 15-16) describes ClO production[6]:

*OClO was discounted as the source of the absorption due to its small cross section of $\simeq 10^{-20}$ cm^2 (as measured in this work). Ozone absorbs at 225 nm but was seen as a stable product of reaction quite distinct from the behaviour of the transient absorber.

$$Cl_2 + h\nu \rightarrow 2Cl \qquad 1$$

$$Cl + O_2 + M \rightleftharpoons ClOO \qquad 15$$

$$Cl + ClOO \rightarrow 2ClO \qquad 16a$$

$$\rightarrow Cl_2 + O_2 \qquad 16b$$

If the Cl and ClOO molecules are in steady state then the chlorine atom concentration may be expressed by equation 4.15

$$[Cl]^2 = k_1[Cl_2]/(k_{16a}+k_{16b})xK[O_2] \qquad 4.15$$

Using K (the equilibrium constant for (12), (-12) = 5.4×10^{-21} molecules^{-1} cm^{3} ^{6} renders a [Cl] concentration $\simeq 1 \times 10^{13}$ [No. of LAMPS]$^{\frac{1}{2}}$ molecules cm^{-3} i.e. 10^6 times higher than in the previous system. As in the previous system kinetic data were obtained by steady state analysis and application of MMS analysis over the temperature range 278-335 K. In order to obtain the rate constant from the absorption measurements it is necessary to evaluate the ClO production which in this sytem may be represented by equation 4.16.

$$\frac{d[ClO]}{dt} = 2k_{16a}\,[Cl]\,[ClOO] \qquad 4.16$$

Applying the steady state approximation to Cl and ClOO , equation 4.16 may be shown to be equivalent to equation 4.17

$$\frac{d[ClO]}{dt} = \frac{2k_{16a}}{k_{16a}+k_{16b}}\; k_1[Cl_2] \qquad 4.17$$

where $\frac{2k_{16a}}{k_{16a}+k_{16b}}$ will subsequently be referred to as f.

From the τ_o and A_o values it is possible to calculate kf and k/f (k referes to the rate of removal of ClO from the system). If second order kinetics hold then the two rate constants should be equal and combination of k/f and kf values renders k and f. The experimental data is shown in TABLE 4.4. The temperature dependence in the system is small reflecting a slight activation energy.

$$k = (1.4\pm0.5)\times10^{-13} \exp\left(\frac{-251\pm150}{T}\right)$$

The absolute value of the rate constant at 298 K is in agreement with a previous pressure dependent study by Cox et al[6] and is approximately eight times faster than that observed in the previous system. The enhanced rate of removal of ClO is consistent with the previously proposed[6] removal via channel (11) followed by reaction (17)

$$Cl + Cl_2O_2 \rightarrow \text{PRODUCTS} \qquad 17$$

If [Cl] is high then $k_{17}[Cl] >> k_{-11}$ and k_{11} will determine the rate of removal of ClO. Reaction (11) would be expected to have little barrier to reaction as is observed experimentally.

Three possible product channels may be envisaged to result from reaction (17) namely:

	$\Delta H_f(Cl_2O_2)$/kJ mol^{-1}
$Cl + Cl_2O_2 \rightarrow ClO + Cl_2O$	$\geqslant$-61.5
$Cl + Cl_2O \rightarrow Cl_2 + ClOO$	$\geqslant$-26.8
$Cl + Cl_2O \rightarrow Cl_2 + OClO$	$\geqslant$-18.8

4.5 DISCUSSION

The type of reaction scheme imagined to be involved in the disproportionation of ClO is shown below.

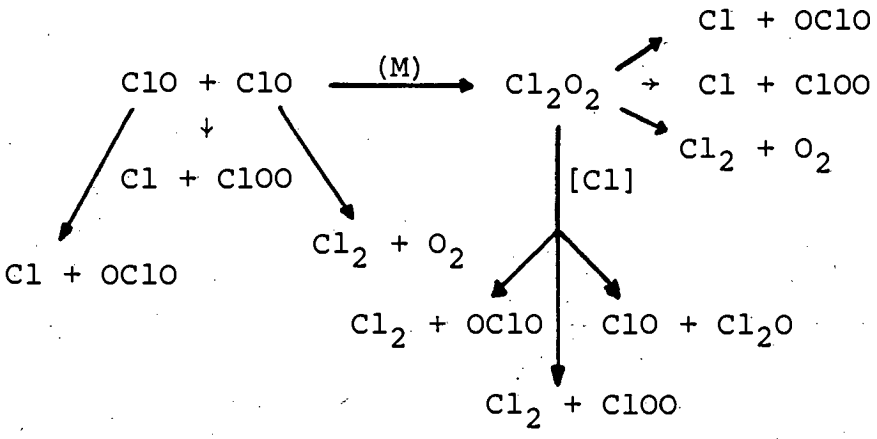

There seems little doubt from previous work by Cox and Derwent[6,7] and Basco and Hunt[8] together with the observations made in this work with the Cl_2/O_2 system that a termolecular pathway exists for the removal of ClO leading to a Cl_2O_2 intermediate. It is proposed that in conditions of high chlorine atom concentration the dominant fate of Cl_2O_2 is through bimolecular reaction with chlorine atoms (reaction 17). The products from such reaction will be largely dependent on the structure and thermochemistry of the Cl_2O_2 molecule. The only evidence for the dimer structure comes from the matrix isolation studies of Pimental

et al[15,16]. In the first of two studies it was suggested that the ClO dimer is bonded not like O_2F_2 or H_2O_2 but rather as in $(NO)_2$ and as such has the following possible structures.

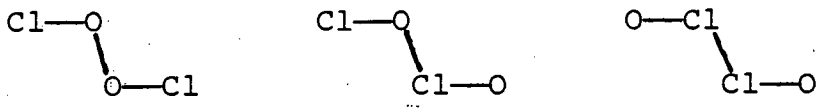

Ia Ib Ic

Further evidence suggested that a structure with two unequivalent oxygens must exist hence providing evidence for structure Ib. In the later work it was stated that the I.R. spectra contained evidence for more than one structure implying little energy discrimination among the possible dimer structures. The previous studies by both Cox and Derwent and Basco and Hunt have postulated a $\Delta H^{o}_{f,298K}$ (Cl_2O_2) ≈ 130 kJ mol^{-1}, hence providing no thermodynamic constraints on the products from chlorine atom reaction with Cl_2O_2. Under high chlorine atom concentrations it should be remembered that production of OClO will not be terminating due to the dominant nature of reaction (-9) whereas ClOO production will result in termination due to reaction (16b)

$$Cl + ClOO \rightarrow Cl_2 + O_2 \qquad 16b$$

In systems of low [Cl] atom concentration the reaction mechanism suggested is not consistent with the

experimental results*. The differences between the A^{o} and τ^{o} values are indicative of gross deviations from second order kinetics. The major problem, however, which appears unresolvable with the reaction mechanism postulated is that the large activation energy from the MMS analysis ($\approx$20 kJ mol^{-1}) relates only to the disproportionation reactions of ClO leading to termination. However the observed increase in quantum yield removal of Cl_2O with increasing temperature demands that the ClO disproportionation reactions leading to chlorine atom production possess an even greater activation energy. As such the participation of the branching steps would be too slow to be of any

*Cox and Burrows[14] have attempted to computer model the $Cl_2/Cl_2O/O_2$ system using the Harwell, FACSIMILE[17] program. Inputing the monitored ClO decay, OClO growth and Cl_2O initial and final yields, the reactions (8), (9), (10) and (-11) were floated to achieve the best fit to the experimental data. As a further check on the system the ozone production calculated from the computer program was compared with that measured experimentally. Under no circumstances did all the floated rate constants show reasonable temperature dependence. The best results which also duplicated the O_3 production rates left reaction (-11) ill defined and assigned activation energies of approximately 20 kJ mol^{-1} and 15 kJ mol^{-1} to reactions (9) and (10) respectively. The same results predicted a more dominant role for reaction (9) than that found in the study of Clyne et al[3,4,18]. From the computer studies k_8/k_9 ranges from 2 to 4 with decreasing temperature from 333 K to 278 K.

significance in the overall removal of ClO which is inconsistent with the observed $\Phi\{-Cl_2O\}$ value of greater than unity and the bimolecular temperature dependent studies of Clyne et al.[18] Clearly important reactions have been omitted in our analysis. The problems inherent in the $Cl_2O/Cl_2/O_2$ system do not however appear to be unique to this system.

De More et al[19] in a recent study of the quantum yield for ozone removal as a function of temperature in the Cl_2/O_3 system buffered both by N_2 and O_2 has also found a very large temperature dependence (in the range 253-298 K). The increase in quantum yield removal in the presence of N_2 ($\Phi\{-O_3\}_{298K} \simeq 3$) is also consistently greater than that in the O_2 system ($\Phi\{-O_3\}_{298K} = 1.6$). These results, like those presented in this work remain irreconcilable with the reactions generally accepted as important in describing the disproportionation of ClO. Clearly after 20 years of intermittant work on these systems the complete description of ClO kinetics has still to be achieved.

4.6 REFERENCES

1. G. Porter and F.J. Wright, Disc. Faraday Soc. 14, (1953), 23.
2. H.S. Johnston, E.D. Morris, Jr. and J. Van Den Bogaerde, J. Amer. Chem. Soc. 91, (1969), 7712.
3. M.A.A. Clyne and J.A. Coxon, Proc. Roy. Soc. A, 303, (1968), 207.
4. M.A.A. Clyne, D.J. McKenney and R.T. Watson, Faraday Trans. I, 71, (1975), 322.
5. C.F. Wu and H.S. Johnston, Bull. Belg. Chem. Soc. 81, (1972), 135.
6. R.A. Cox, R.G. Derwent, A.E.J. Eggleton and H.J. Reid, Faraday Trans I 75, (1979), 1648.
7. R.A. Cox and R.G. Derwent, Faraday Trans. I 75, (1979), 1635.
8. N. Basco and J.E. Hunt, Int. J. Chem. Kinetics, XI, (1979), 649.
9. NBSIR 74-516 Chemical Kinetics Data Survey VIII, Reactions of ClO_x Species of Atmospheric Interest, R.T. Watson, Nat. Bur. Standards, Washington DC 20234 (1974, June).
10. C.F. Goodeve and J.I. Wallace, Trans Faraday Soc. 26, (1930), 254.
11. D.A. Parkes, D.H. Paul and C.P. Quinn, J. Chem. Soc. Faraday I 72, (1976), 1935.
12. J.P. Burrows and R.A. Cox, to be published.

13. W. Finkelnburg, H.J. Schumacher and G. Stieger, Z. Phys. Chem. B15, (1931), 127.

14. J.P. Burrows and R.A. Cox, Private communication.

15. M.M. Rochkind and G.C. Pimental, J. Chem. Phys. 46, (1967), 4481.

16. W.G. Alcock and G.C. Pimental, J. Chem. Phys. 48, (1968), 2373.

17. E.M. Chance, A.R. Curtis, I.P. Jones and C.R. Kirby, FACSIMILE: A Computer Program For Flow and Chemistry Simulation and General Initial Value Problems, A.E.R.E. Report, R8775 (H.M.S.O., London, 1977).

18. M.A.A. Clyne and R.T. Watson, J. Chem. Soc. Faraday I 73, (1977), 1169.

19. W.B. DeMore, private communication.

CHAPTER V

OZONE PHOTOLYSIS - THE REACTION OF $O(^1D_2)$ WITH OZONE

5.1 INTRODUCTION

The importance of ozone to life on Earth, as we know it, is crucial.[1] The greatest ozone concentrations occur at approximately 30 km altitude in the region of the atmosphere known as the stratosphere. The lifetime of any ozone molecule in the stratosphere is very dependent on altitude, a steady state concentration being maintained by rapid formation and destruction processes. The temporal and spacial ozone distribution throughout the stratosphere varies depending on solar intensity, altitude, meterological and other factors, resulting in considerable natural variation in the total column of ozone above any particular place on the Earth's surface. The importance of the 'ozone layer' is due to its action as an optical filter screening out much of the harmful ultraviolet radiation from the Sun. The absorption spectrum of ozone (together with that of oxygen) is illustrated in FIG 5.1. Ozone absorbs in three distinct regions of the spectrum: the Hartley bands (200-300 nm), the Huggins bands (300-360 nm) and the weaker Chappius bands (440-850 nm). The importance of ozone in atmospheric chemistry and its utility as a photolytic source of oxygen has resulted in a wide study of its photochemistry at several wavelengths.

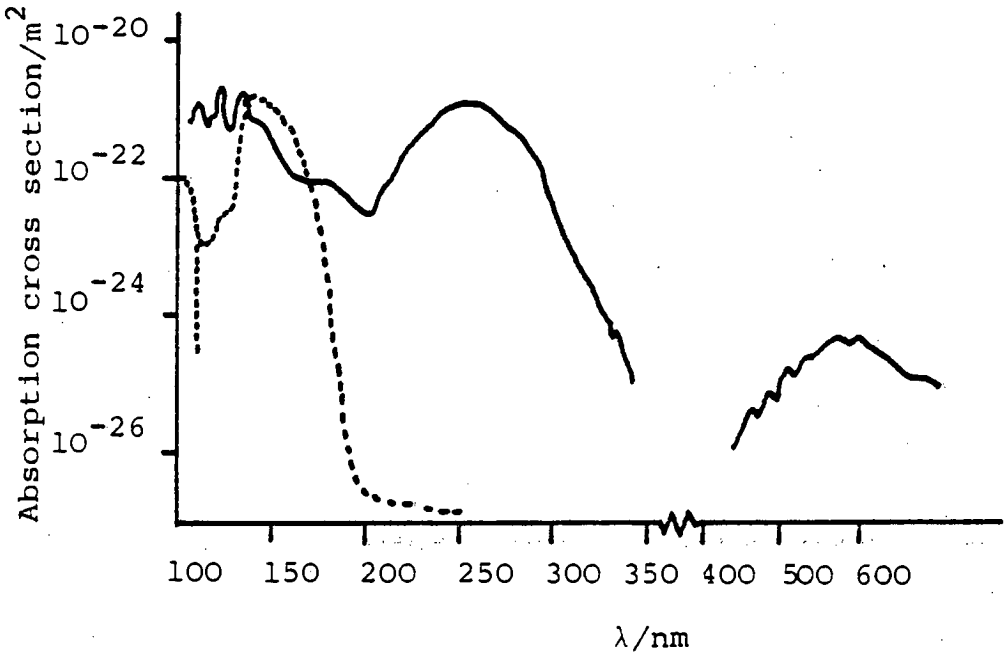

FIG 5.1 The variations with wavelength of the absorption cross sections of molecular oxygen (dashed line) and ozone (solid line).

Photodissociation in the Chappius bands[2] is explained using the following reaction scheme (1-2)

$$O_3 + h\nu \rightarrow O(^3P_J) + O_2(X^3\Sigma_g) \quad 1$$

$$O(^3P) + O_3 \rightarrow 2O_2 \quad 2$$

$$(k_2 = 1.9\times10^{-11} \exp(-2300/T))^3$$

$O_2(^1\Delta_g)$ production is thermodynamically possible below 611 nm but there is no evidence for its formation. Above 320 nm photodissociation in the Huggins bands[4,5] is thought to progress through the following reaction mechanism (2-4)

$$O_3 + h\nu \rightarrow O(^3P) + O_2(^1\Sigma \text{ or } ^1\Delta) \quad 3$$

$$O(^3P) + O_3 \rightarrow 2O_2 \quad 2$$

$$O_2(^1\Sigma \text{ or } ^1\Delta) + O_3 \rightarrow 2O_2 + O(^3P) \quad 4$$

Below 320 nm (5) becomes important

$$O_3 + h\nu \rightarrow O(^1D_2) + O_2(^1\Delta_g) \quad 5$$

Photolysis below 320 nm is the area of strongest absorption by ozone, it is this region of the spectrum that is responsible for the shielding of the Earth's surface from UV-B radiation (280-320 nm). The photochemistry of ozone in this region while receiving considerable attention[6-11] still poses many unresolved problems. This study was instigated to answer one such problem, namely the branching ratio of the reaction of $O(^1D_2)$ with the ozone molecule (6,7)

$$O(^1D) + O_3 \rightarrow 2O_2 \qquad 6$$

$$\rightarrow O_2 + 2O(^3P_J) \qquad 7$$

The precise measurement of the products from this reaction is crucial to an understanding of ozone photochemistry, being necessary for the rationalisation of the much studied quantum yields for ozone removal in various systems.

5.2 EXPERIMENTAL

The main part of this work used the atomic absorption spectrometer in two distinct studies. The first involved monitoring $O(^3P_J)$ growth from the reaction of $O(^1D_2)$ with ozone (7). Due to the fast nature of this reaction the use of an EMR 542 advanced solar blind photomultiplier, to eliminate detection of scattered light, was of considerable importance. The flow lamp was operated on a pure helium supply ($P \approx 500\ Nm^{-2}$) and run at low incident powers of 30 W. $O(^3P_2)$ concentrations were monitored by attenuation of the 130.6 nm radiation isolated by the vacuum monochromator. Flash energies of 180 J were used throughout these experiments. Final $O(^3P_2)$ concentrations at $t \approx 2$ ms were compared from experiments conducted both in the presence and absence of nitrogen.

In the second series of experiments the atomic absorption spectrometer was used essentially as a UV

spectrophotometer in order to monitor ozone concentrations before and after (30 s) the photolysis flash. The ozone concentration was monitored through attenuation of the unresolved oxygen triplet line at 130 nm. Flow lamp mixtures ranged from cylinder helium to 1% oxygen in helium ($P \approx 400\ Nm^{-2}$). The incident power supplied to the lamp was 50 W. Varying degrees of photolysis by the atomic lamp were observed and evaluated over the time scale of the experiment. The photolysis lamp dissipated 245 J per flash. It is to be emphasised that the conditions in the former experiment were such that baseline fluctuations due to ozone photolysis on the time scale of the experiments were not observed and hence did not interfere with the kinetic information gained from these experiments. Such fluctuations were maximised in the second series of experiments.

Preliminary work on the long time ($\approx$0.2 s) behaviour of $O(^3P_J)$ atoms in the ozone system, following photolysis in the Hartley bands, was begun using the resonance fluorescence technique illustrated in FIG 2.4. Input radiation was provided by an oxygen flow lamp. The best signal to noise ratios were observed using a cylinder helium supply with the lamp operating at high flow pressures ($1.9\ kNm^{-2}$) and incident power (75 W). Fluorescence signals were monitored on an EMI Gencom solar blind photomultiplier coupled to a transient recorder, signal averager combination. Most experiments employed averaging over 256 flashes (flash energy = 0.25 J).

5.3 RESULTS AND DISCUSSION

The branching ratio into reaction (7) was easily obtained from a study of $O(^3P_J)$ evolution with time following photolysis in the Hartley bands. In the presence of pure helium the growth of $O(^3P_J)$ immediately following the photolysis flash was monitored. Comparison between final $O(^3P_J)$ yields in the presence of helium and nitrogen (quenches all the $O(^1D_2)$ to $O(^3P_J)$ under the conditions adopted) then yields the branching ratios into channels (6) and (7). FIG 5.2 illustrates the atomic absorption signals obtained in such an experiment (O_3 = 0.25 Nm^{-2}, O_2 = 0.25 Nm^{-2} and He or N_2 = 800 Nm^{-2}). In order to overcome the difficulties involved in the relationship of absorbance to $O(^3P_J)$ concentration a suitable calibration curve relating absorbance ($O(^3P_J)$) to ozone concentration was constructed (FIG 5.3) and values read directly from it. From the helium experiment the growth of $O(^3P_J)$ is clearly seen and offers a method of measuring the rate of reaction of $O(^1D_2)$ with ozone.

In considering a parallel reaction scheme (6,7) the following kinetic equation may be derived (5.1):

$$O(^1D) + O_3 \xrightarrow{k_6} 2O_2 \qquad 6$$

$$\xrightarrow{k_7} O_2 + 2O(^3P) \qquad 7$$

$$[O(^3P)]_t = \frac{2k_7'}{k_6'+k_7'} [O(^1D)]_{t=0} \left(1 - e^{-(k_7'+k_6')t}\right) \qquad 5.1$$

(The superscript to the rate constants indicates their pseudo first order nature i.e. $k_6' = k_6[O_3]$).

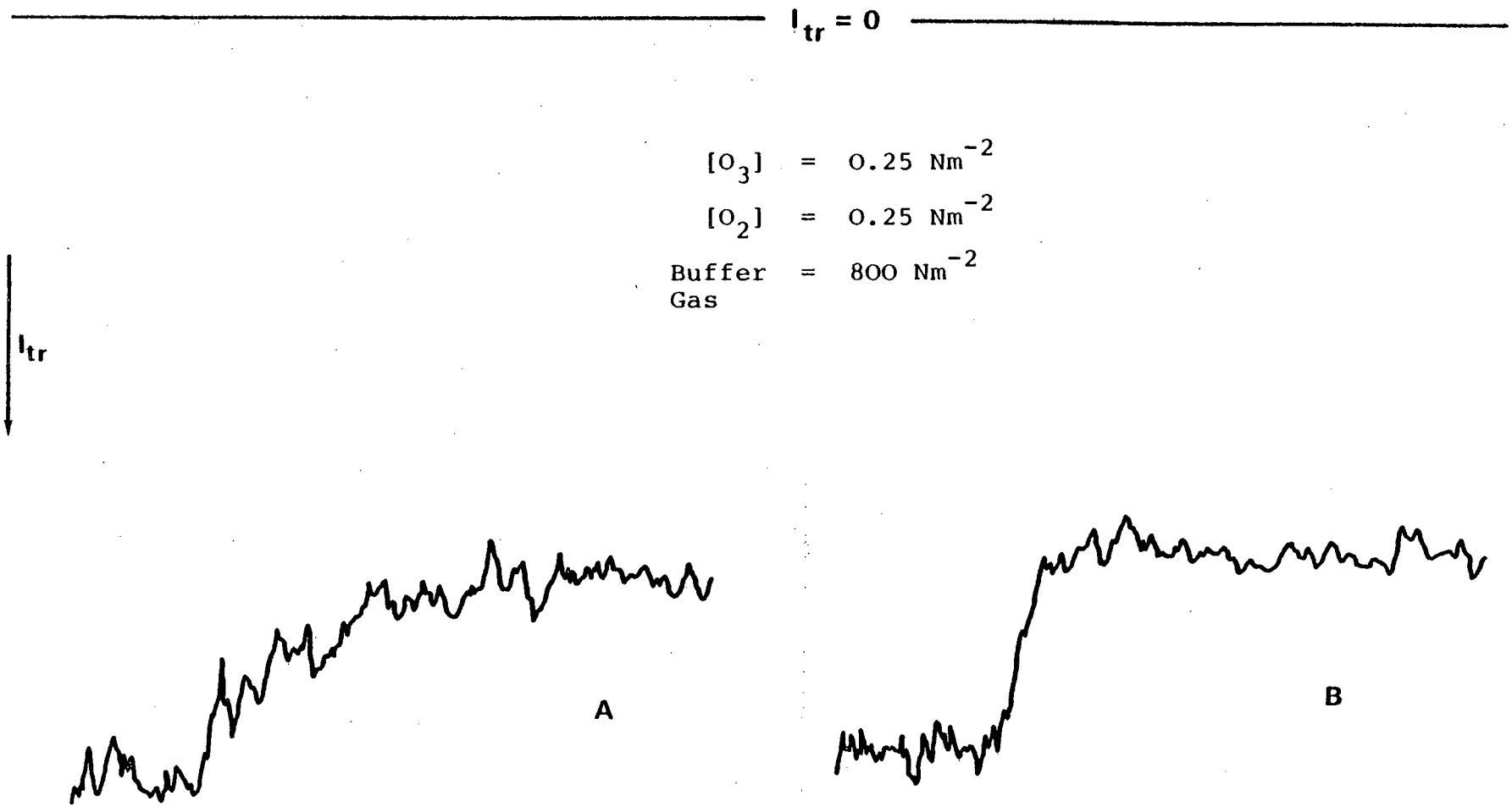

FIG 5.2 $O(^3P)$ growth in the presence of A) Helium, B) Nitrogen buffer gas.

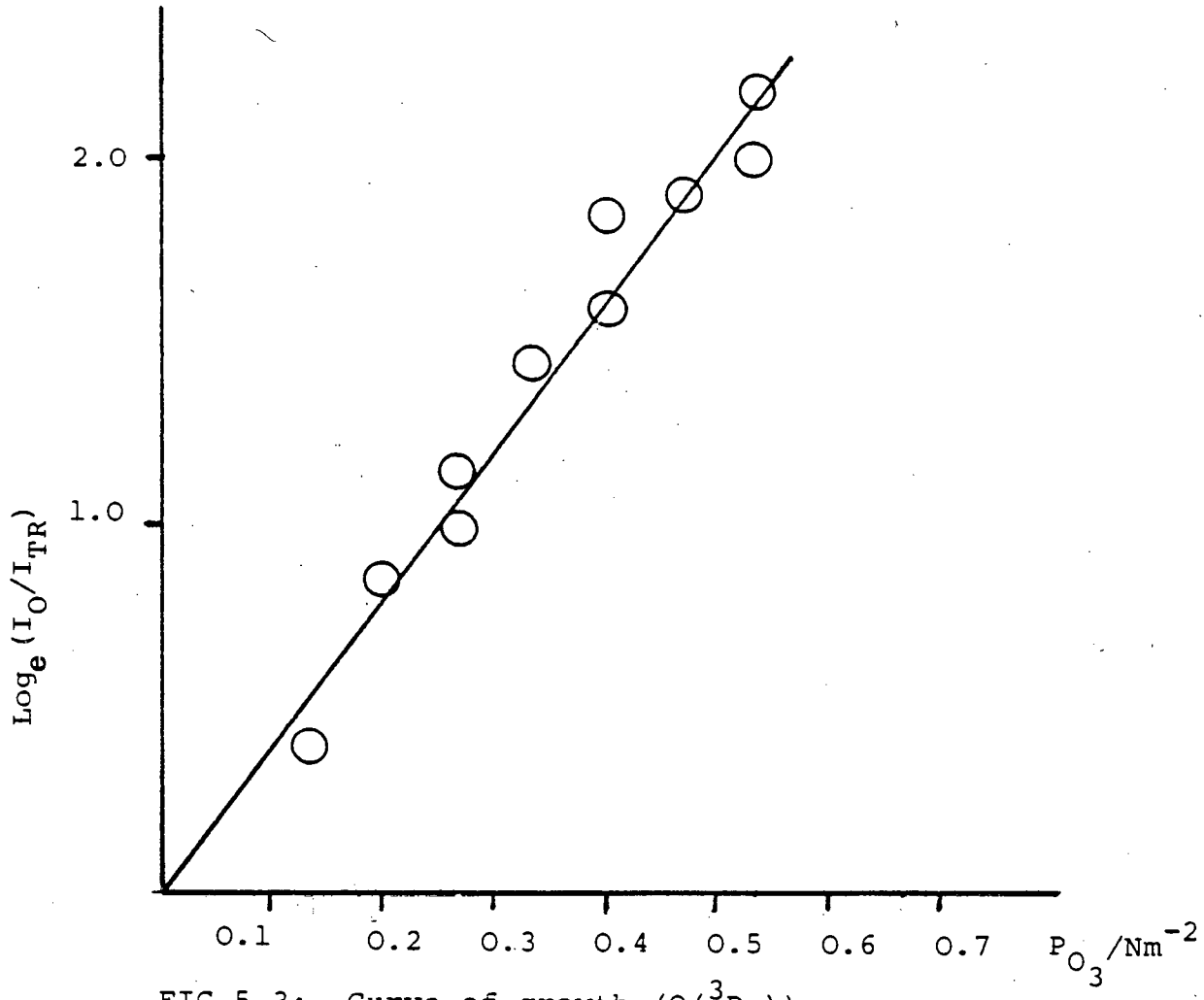

FIG 5.3: Curve of growth $(O(^3P_J))$

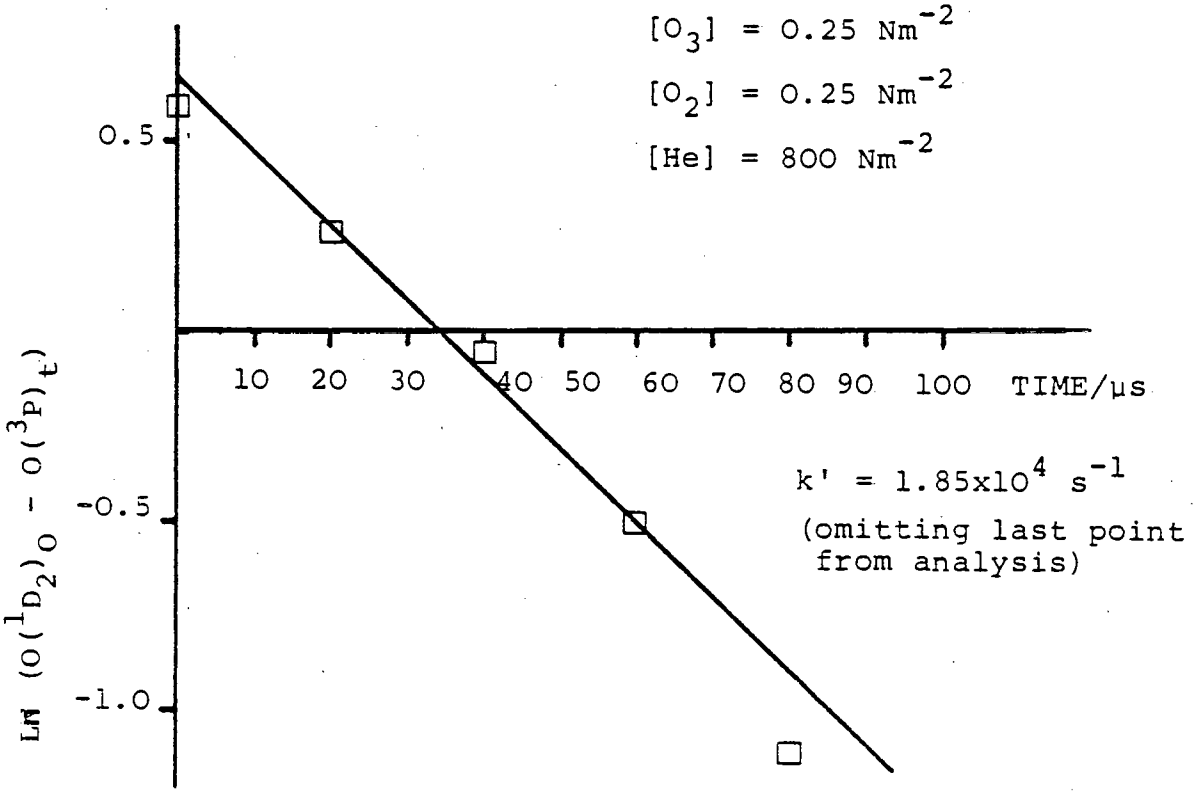

FIG 5.4: Pseudo first order plot $(O(^1D)+O_3)$

If the system is further complicated by an alternative removal process, as is the case in this experiment through reaction (8), the above expression must be modified (equation 5.2).

$$O(^1D_2) + O_2 \xrightarrow{k_8} O(^3P) + O_2(^1\Sigma_g^+) \qquad 8$$

$$[O(^3P)]_t = \frac{2k_7'}{k_6'+k_7'}[O(^1D)]_{t=0}\left(1 - e^{-(k_6'+k_7')t}\right) + [O(^1D)]_{t=0}\left(1 - e^{-k_8't}\right) \qquad 5.2$$

If the ratio $2k_6'/k_7'+k_6' = 1$* equation 5.2 reduces to that of the sum of two first order reactions. As such FIG 5.4 illustrates a plot of $\ln(O(^1D)_0 - O(^3P)_t)$ against time and yields a gradient equal to the pseudo first order rate constant of the growth of $O(^3P_J)$ in the system; $k' = 1.9\pm0.3\times10^4\ s^{-1}$. Correcting this value for production of $O(^3P_J)$ from the primary reaction of $O(^1D_2)$ with oxygen, yields a pseudo first order rate constant of $k_{6+7}' = 1.6\pm0.3 \times 10^4\ s^{-1}$. In making this correction a value of $k_8 = 3.6 \times 10^{-11}\ cm^3\ molecule^{-1}\ s^{-1}$ has been employed and secondary production of $O(^3P_J)$ from reaction (9) has been neglected. Less than 4% of $O(^1D_2)$ reacting with O_2 on the time scale of the experiment (<100 μs) yields an $O(^3P)$ through reaction (9)

$$O_2(^1\Sigma_g^+) + O_3 \rightarrow 2O_2 + O(^3P) \qquad 9$$

Converting the pseudo first order rate constant to the corresponding bimolecular rate constant yields $\underline{k_{6+7} = 2.5 \pm 0.5 \times 10^{-10} \text{ cm}^3 \text{ molecule}^{-1} \text{ s}^{-1}}$. This value is in excellent agreement with two previous studies[12,13] employing direct monitoring of the $O(^1D_2)$ reactant and provides indirect evidence as to the validity of the ratio $2k_7'/k_6'+k_7' = 1$ used. Alternatively using the rate data previously recorded for k_{6+7} and k_8 in equation 5.2 allows determination of $2k_7'/k_6'+k_7'$ directly from a plot of $(O(^3P)_t/O(^1D)_0 - (1 - e^{-k_8't}))$ against $1 - e^{-(k_6'+k_7')t}$ (FIG 5.5) and yielded $k_7/k_6+k_7 = 0.45$.

* From $O(^3P_J)$ absorption traces with and without the presence of excess nitrogen it was seen (FIG 5.2) that within experimental error the yields of $O(^3P_J)$ are the same. As ≈20% of $O(^1D_2)$ in the helium system reacts with oxygen to produce $O(^3P_J)$ and considering the kinetic data it is concluded that <u>the branching ratio into reaction (7) is 50±10%</u>. A large study (≈40 individual measurements) employing varying flow lamp conditions and running concurrently with the quantum yield studies produced results consistent with the above figure.

It should be noted that this experiment suggested essentially no production of $O(^3P_J)$ in the primary photolytic act occurs. Recent evidence employing more accurate detection systems supports a value of approximately 10% production of $O(^3P_J)$[14-16] on ozone photolysis at wavelengths less than 300 nm in the Hartley bands.

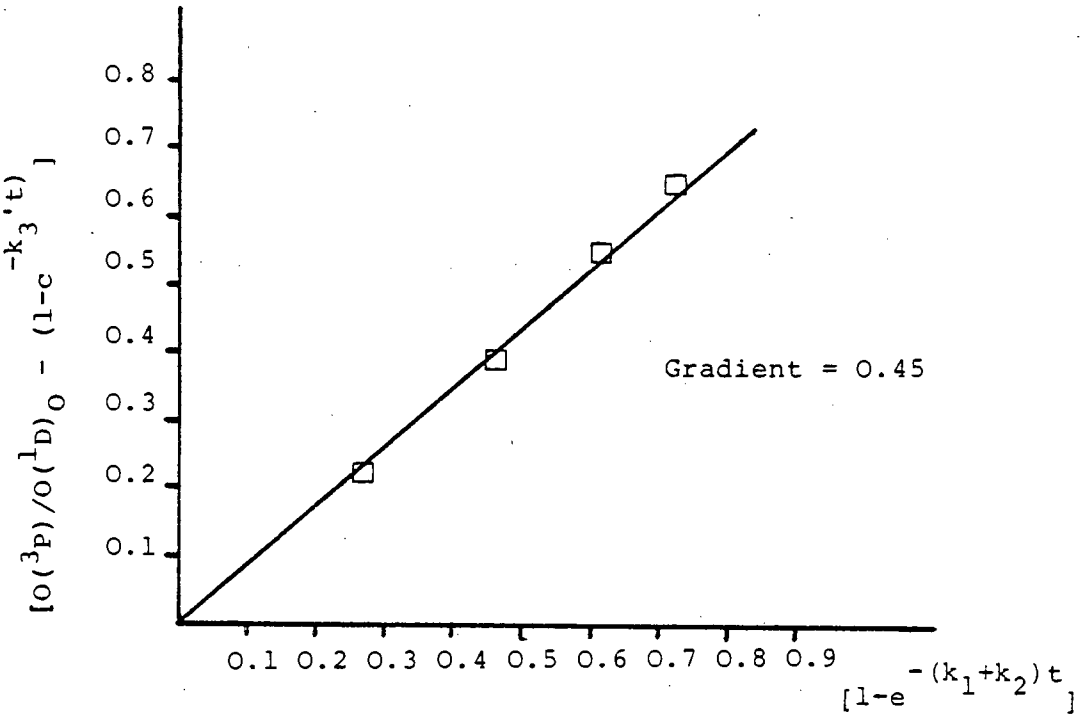

FIG 5.5: Determination of k_7/k_6+k_7

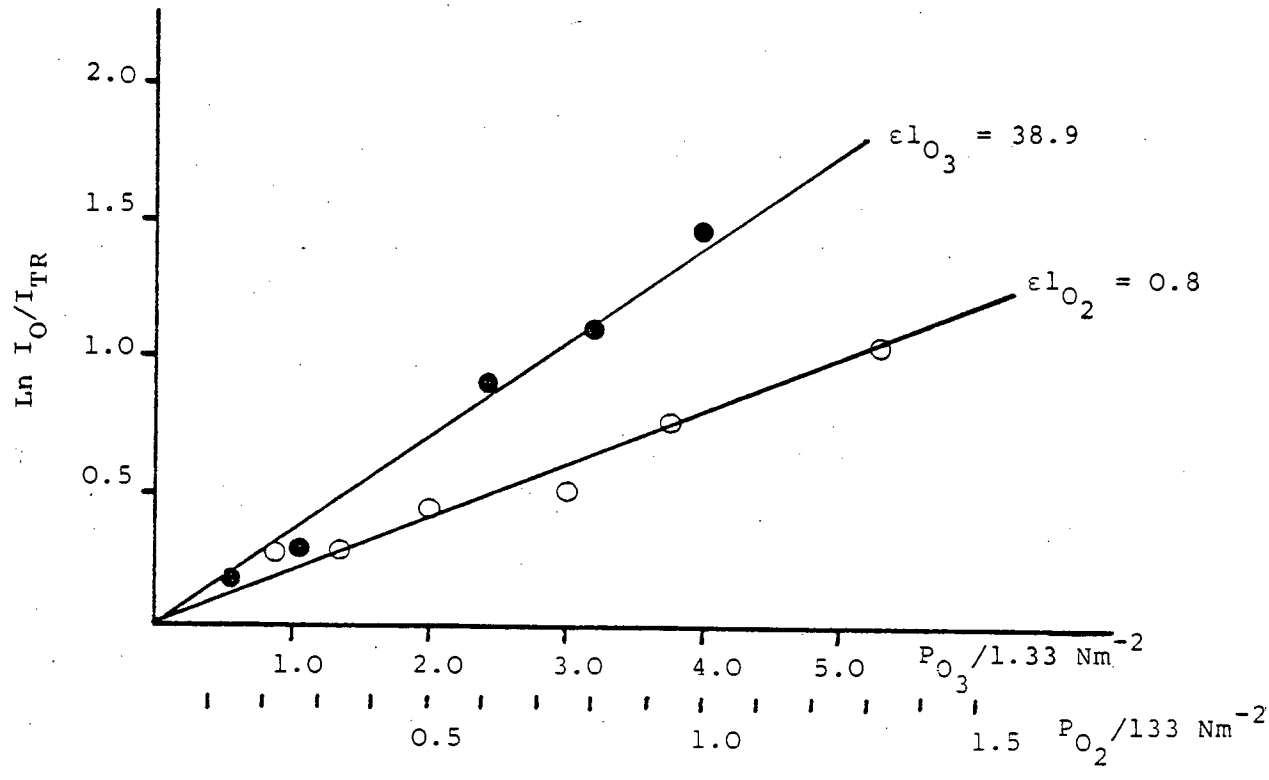

FIG 5.6: Determination of ε_{O_3} and ε_{O_2} at 130 nm

A very similar study to this work and running concurrently with it, employing laser photolysis, was carried out by Amimoto et al[17]. Their basic experimental results duplicated our own data, however their conclusions on the fate of the $O(^1D_2)$, reacting with ozone, were different. They postulated reaction (10) to account for the 1:1 ratio of $O(^1D_2)$ loss and $O(^3P_J)$ production suggesting such a result would be too fortuitous to be explained by reactions (6) and (7).

$$O(^1D_2) + O_3 \rightarrow O(^3P_J) + O_3^* \qquad 10$$

No experimental evidence for the presence of the excited ozone intermediate was presented. In response to this new proposal a study of the ozone removal quantum yields, both in the presence of nitrogen and helium, was carried out. This experiment basically repeated numerous other studies[6-11] of the same system. These studies are summarised in TABLE 5.1 and have been reviewed in more detail recently[18]. The great variety of results is apparent. This study it was hoped would produce a more conclusive result.

Two methods of photolysis were used in these experiments: 1) photolysis by the oxygen flow lamp and 2) flash photolysis. In monitoring ozone concentrations by absorption measurements at 130 nm before and after (30 s) photolysis, it was initially established that absorption by oxygen (the final product from reaction) would not interfere (see FIG 5.6). The ratio of extinction coefficients - $\varepsilon_{O_3}(130\text{ nm})/\varepsilon_{O_2}(130\text{ nm})$ was determined to equal 49 under the conditions used.

TABLE 5.1 QUANTUM YIELDS FOR OZONE REMOVAL AS MONITORED BY SEVERAL WORKERS (REPRINTED FROM REF. 18)

Author	$P_{O_3/kNm^{-2}}$	$-\Phi(O_3)$	System Studied	Comments	Ref.
McGrath and Norrish	0.27-6.7	16.7	O_3/He	Chain mechanism postulated to account for $-\Phi(O_3)$ at high pressures of O_3	9
Norrish and Wayne	0 0.27	4.0 2.0	O_3/He O_3/N_2	Extrapolation to $[O_3]=0$ yields $-\Phi(O_3)=4$. $-\Phi(O_3)=2$ in the presence of N_2	7
Jones and Wayne	0.005-0.27 0.013	4.0 4.5±0.3	O_3/O_2 O_3/He	O_2 added in partial pressures from 10-90%. $-\Phi(O_3)$ remained constant	4
Schumacher et al	1.3-13	6.0	O_3/He	$-\Phi(O_3)$ remained constant over a wide range of O_3 pressures	8
Lissi and Heicklen	0.013-0.36	5.5±0.5 4.2±0.4	O_3/He O_3/N_2	O_2† postulated to account for $-\Phi(O_3)$ in pure ozone	6
Webster and Bair	0.027		O_3/He O_3/N_2	$-\Phi(O_3)_{He}$ (initial) = $-2\Phi(O_3)_{N_2}$ (initial)	10
Giachardi and Wayne	6.7-67 Nm^{-2}		O_3/He	$-\Phi(O_3)_{N_2}$(initial) incorrectly calculated	11

Photolysis by the atomic lamp was monitored using various lamp intensities (varied by altering flow composition) as a function of time and was treated using a first order kinetic analysis - see FIG 5.7. Results from the flash photolysis study are shown in TABLE 5.2.

From the flash photolysis experiments:

$$-\Phi(O_3)_{N_2}/-\Phi(O_3)He = 0.78\pm0.04$$

whereas the static flow experiment yielded a ratio of 0.75.

It is generally accepted that photolysis of ozone in the presence of nitrogen may be represented by:

$$O_3 + h\nu \rightarrow O(^1D) + O_2(^1\Delta_g) \quad 5$$

$$O(^1D) + N_2 \rightarrow O(^3P) + N_2^{\ddagger} \quad 11$$

$$O(^3P) + O_3 \rightarrow 2O_2 \quad 2$$

$$O_2(^1\Delta) + O_3 \rightarrow 2O_2 + O(^3P) \quad 12$$

and hence yields $-\Phi(O_3)_{N_2} = 4$. Therefore in the presence of helium it may be deduced that $-\Phi(O_3)_{He} = 5.3\pm0.3$. This value must be corrected slightly for ≈15% reaction of $O(^1D_2)$ with O_2 in the present system. Assuming $-\Phi(O_3)_{O_2} = 5$ yields a final value of:

$$-\Phi(O_3)_{He} = 5.2\pm0.3$$

Correction for the recombination reaction (13) was considered but was found to be negligible under the conditions used.

$$O(^3P) + O_2 + M \rightarrow O_3 + M \quad 13$$

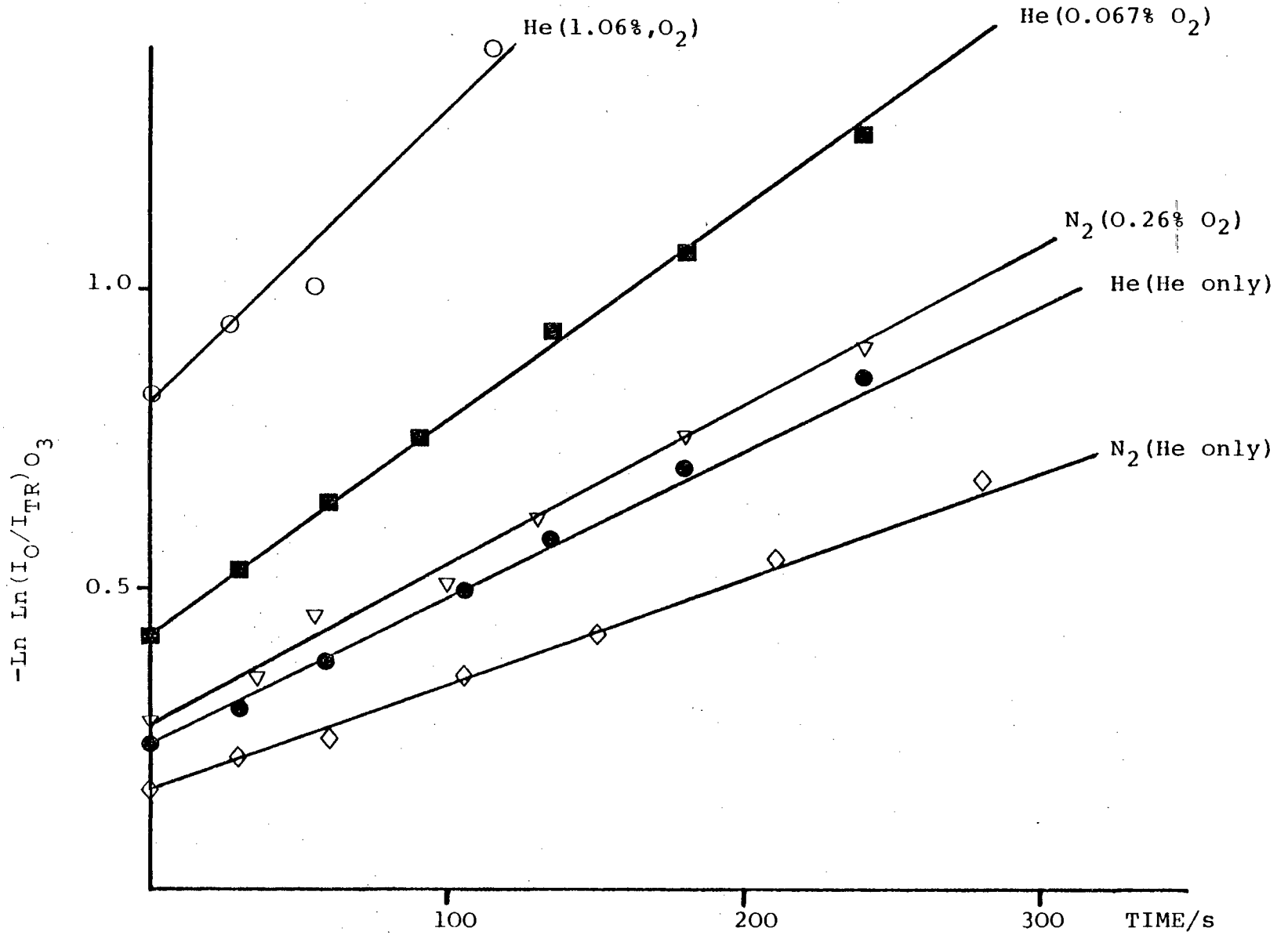

FIG 5.7: Determination of ozone photolysis by atomic lamp using different flow compositions( ), in helium and nitrogen buffer gases.

FIG 5.2 OZONE REMOVAL BY FLASH PHOTOLYSIS - EXPERIMENTAL DATA

% O_2 in Flow Lamp	% Ozone Removed in 30 s						$f = \frac{\Phi(O_3)_{N_2}}{\Phi(O_3)_{He}}$
	N_2	Fraction Removed By Atomic Lamp	N_2 Corrected	He	Fraction Removed By Atomic Lamp	He Corrected	
Pure He	31.8	5.6	26.2	41.9	7.5	34.4	0.76
0.067	35.0	(7.6)	27.4	46.1	10.0	36.1	0.76
0.26	33.7	7.5	26.2	41.6	(10.1)	31.5	0.83
0.06	32.8	(10.5)	22.3	43.9	14.0	29.9	0.75

( ) - Evaluated from measured $-\Phi\{O_3\}_{N_2} / -\Phi\{O_3\}_{He} = 0.75$

Ozone concentrations in experiments ranged from 0.7 - 4 Nm^{-2}.

This result is in good agreement with work of Lissi and Heicklen[6]. This quantum yield is in agreement with the following reaction scheme for ozone photolysis in helium.

$O_3 + h\nu$	→	$O_2(^1\Delta) + O(^1D)$		5
$O(^1D) + O_3$	→	$O_2^{\ddagger} + O_2$	50%	6
	→	$O_2 + 2O(^3P)$	50%	7
$O(^3P) + O_3$	→	$O_2^{\ddagger} + O_2$		2
$O_2(^1\Delta) + O_3$	→	$2O_2 + O(^3P)$		12
$O_2^{\ddagger} + O_3$	→	$2O_2 + O(^3P)$		14
$O_2^{\ddagger} + X$	→	$O_2 + X$		15

$$-\Phi(O_3) = 5 + 2f_{14} \text{ where } 0<f_{14}<0.3$$

No evidence exists for reaction (14) in this system. If $5.2 < -\Phi(He) \leqslant 5.6$ then (14) must be included to account for the observed quantum yield. The error limits for the branching ratio into channel (7) accounts for $5.0 \leqslant -\Phi(He) \leqslant 5.2$.

If reaction schemes involving reaction (10) are considered it is difficult to envisage a dominant one channel fate to O_3^* leading to the experimentally observed quantum yield.

$O_3^* + M$	→	$O_3 + M$	$\{-\Phi(O_3) = 4\}$	16
O_3^*	→	$O_2 + O(^3P)$	$\{-\Phi(O_3) = 6\}$	17
$O_3^* + O_3$	→	$2O_2 + 2O(^3P)$	$\{-\Phi(O_3) = 7\}$	18

If channel (17) or (18) were important a long term growth in $O(^3P_J)$ should be evident. This was never observed in the atomic absorption experiments ($\lesssim$50 ms). Using a more sensitive resonance fluorescence system $O(^3P)$ concentration profiles both in the presence of helium and nitrogen were monitored ($\lesssim$0.2 s). No variation in the $O(^3P)$ kinetics was observed between the helium and nitrogen systems although decay kinetics were more rapid than that suggested from a model employing reactions (12) and (2) to account for ozone production and loss after photolytic initiation (FIG 5.8). Calculation suggests this to be the result of diffusion out of the viewing zone, although if this is indeed the cause of the more rapid decay the lack of variation of helium and nitrogen traces remains puzzling and merits further work.

We conclude that reaction of $O(^1D_2)$ with ozone is best represented by reactions (6) and (7) in which the branching ratio into each channel is 50$\pm$10%. This claim we believe to be supported, over the postulated mechanism of Aminoto et al[17], by the measured quantum yield for ozone removal in a pure helium system namely $-\Phi(O_3)_{He} = 5.2\pm0.3$ providing $-\Phi(O_3)_{N_2} = 4$.

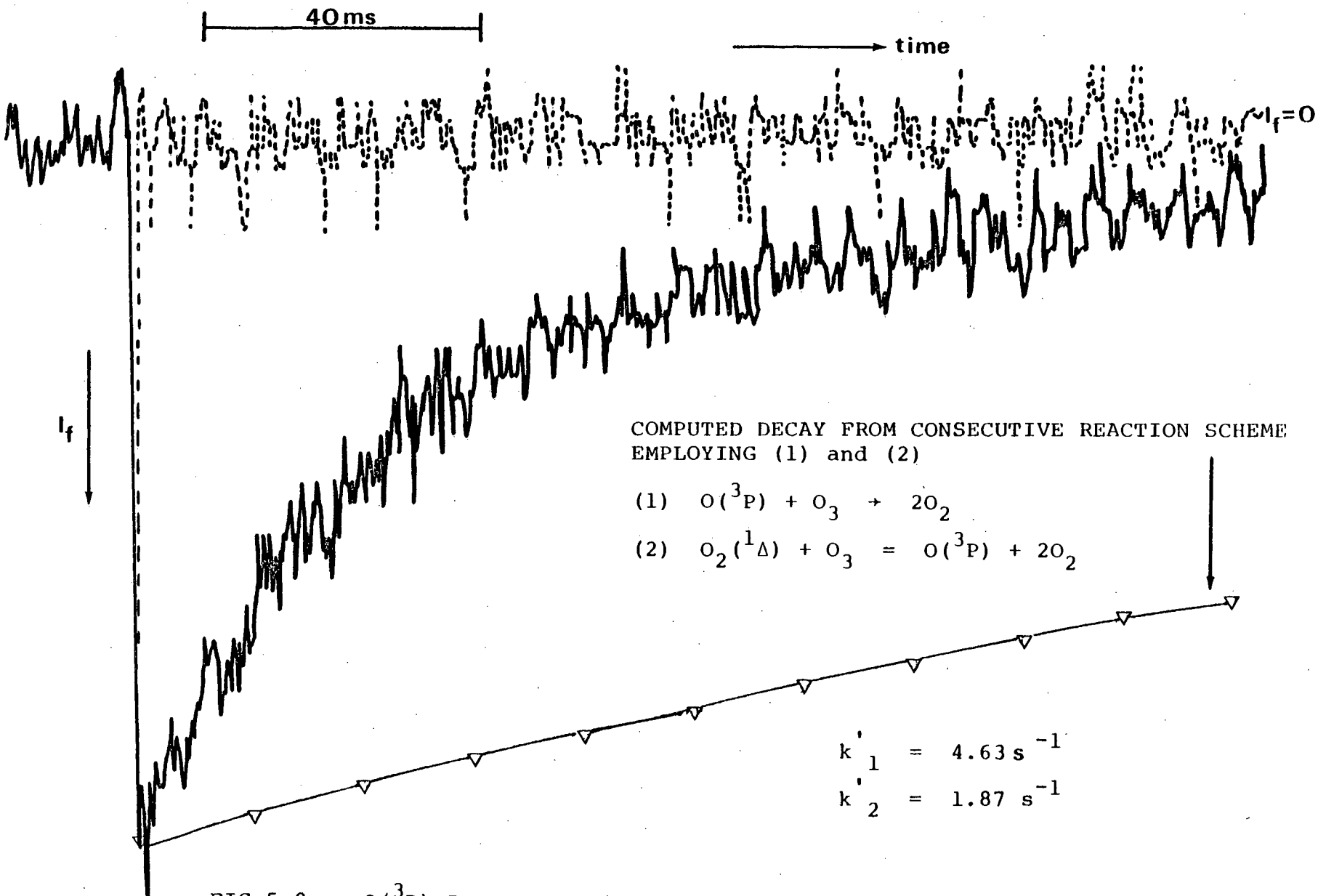

FIG 5.8 $O(^3P)$ Resonance Fluorescence Trace. Flash Energy = 0.25 J, Signal Averaged Over 256 Flashes. $[O_3] = 1.42\ Nm^{-2}$, $[N_2] = 1.33\ kNm^{-2}$.

5.4 REFERENCES

1. Pollution Paper No. 5, Dept. of the Environment (1976).
2. E. Castellano and H.J. Schumacher, J. Chem. Phys. 36, (1962), 2238.
3. R.F. Hampson (Editor), J. Phys. Chem. Ref. Data 2, (1973), 267.
4. I.T.N. Jones and R.P. Wayne, Proc. Roy. Soc. A 319, (1970), 273.
5. O. Kajimoto and R.J. Cvetanovic, Chem. Phys. Lett. 37, (1976), 533.
6. E. Lissi and J. Heicklen, J. Photochem. 1, (1970), 39.
7. R.G.W. Norrish and R.P. Wayne, Proc. Roy. Soc. A 288, (1965), 200.
8. G. Von Ellenreider, E. Castellano and H.J. Schumacher, Chem. Phys. Lett. 9, (1971), 152.
9. W.D. McGrath and R.G.W. Norrish, Proc. Roy. Soc. A 242, (1957), 265.
10. H. Webster and E.J. Bair, J. Chem. Phys. 53, (1970), 4532.
11. D.J. Giachardi and R.P. Wayne, Proc. Roy. Soc. A 330, (1971), 131.
12. G.E. Streit, C.J. Howard, A.L. Schmeltekopf, J.A. Davidson and H.I. Schiff, J. Chem. Phys. 65, (1976), 4761.
13. R.F. Heidner, D. Husain and J.R. Wiesenfeld, J. Chem. Soc., Faraday Trans. II 69, (1973), 927.

14. R.K. Sparks, L.R. Carlson, K. Shobatake, M.L. Kowalczyk and Y.T. Lee, J. Chem. Phys., 72, (1980), 1401.

15. C.E. Fairchild, E.J. Stone and G.M. Lawrence, J. Chem. Phys. 69, (1978), 3632.

16. J.C. Brock and R.T. Watson, Chem. Phys. Lett. 71, (1980), 371.

17. S.T. Amimoto, A.P. Force and J.R. Wiesenfeld, Chem. Phys. Lett. 60, (1978), 40.

18. W.J. McElroy, Ph.D. Thesis, University of Edinburgh.

CHAPTER VI

KINETIC STUDY OF THE REACTION OF $O(^3P_J)$ AND $S(^3P_J)$ ATOMS WITH CF_3I AND iso C_3F_7I.

6.1 INTRODUCTION

A considerable amount of data now exists on the reactions of $O(^3P_J)$ and to a much lesser extent $S(^3P_J)$. Reaction of oxygen and sulphur atoms leading to halogen atom abstraction has been studied for a series of reactants. Clyne and Townsend[1] made the first absolute measurements of the halogen atom abstraction reactions of $S(^3P_J)$ atoms with the halogen molecules F_2, Cl_2 and Br_2. Reaction of the $S(^3P_J)$ species was found to be fast in comparison with the analogous $O(^3P_J)$ reaction. The slow rates of the oxygen atom reactions reflect sizeable activation energies to reaction although the abstraction reactions are exothermic. Halogen atom abstraction from CF_3X where X = Cl or Br by $O(^3P)$ atoms is endothermic. Recent work[2] on the analogous reactions of $S(^3P_J)$ atoms suggests that for X = Br reaction is relatively rapid ($k = 1.1\pm0.3\times10^{-13}$ cm^3 $molecule^{-1}$ s^{-1}).

Prior to this work no rate data for the reaction of $O(^3P_J)$ with the perfluoroalkyl iodides had been presented. The reaction of $O(^3P_J)$ with CF_3I had been shown to yield IO as a reaction product[3]. A later detailed study using molecular beam techniques[4] gave information on the dynamics of reaction but no measurement of the bulk rate constant was presented. Reaction of $O(^3P_J)$ atoms with CH_3I [5] proceeds rapidly at room temperature suggesting an iodine abstraction mechanism

is involved (H atom abstraction reactions by $O(^3P_J)$ atoms generally have appreciable activation energies).

This chapter presents the first rate data for the reaction of $O(^3P)$ and $S(^3P)$ with the perfluoroalkyl iodides CF_3I and iso-C_3F_7I. The results are used to derive lower limits to the bond strengths of the product IO and IS radicals.

6.2 EXPERIMENTAL

All kinetic data were obtained using the technique of time resolved atomic absorption spectrophotometry (FIG 2.2).

(i) $O(^3P_J)$ production and detection. $O(^3P_J)$ atoms were produced by the photolysis (flash energy = 180-320 J) of ozone (P_{O_3} = 1.33 Nm^{-2}) in the presence of excess N_2 (P_{N_2} = 800 Nm^{-2}). Nitrogen pressures were such to ensure that essentially all $O(^1D_2)$ produced from the photolysis of O_3 was quenched to the ground state. $O(^3P_J)$ concentrations were monitored by their attenuation of 130 nm radiation. The resonance radiation at 130 nm was produced from a conventional flow lamp operating on an O_2/He ($\leqslant$0.1%) supply. The pressure and microwave power supplied to the lamp were 250 Nm^{-2} and 30 W. respectively. The unresolved triplet at 130 nm was isolated using a vacuum monochromator (entrance and exit slits = 800 μm) and detected by an EMR 542 solar blind photomultiplier coupled to a Datalab (DL905) transient recorder.

(ii) $S(^3P_J)$ production and detection. $S(^3P_J)$ atoms were generated by the photolysis (flash energy = 320 J) of OCS (P_{OCS} = 23 Nm^{-2}) in large excess of N_2 (P_{N_2} = 1.33 kNm^{-2}). $S(^3P_2)$ atoms were monitored by their absorption at 182.63 nm. The atomic line was produced by a conventional microwave powered flow lamp, incident power = 50 W. The flow lamp was found to produce adequate intensity with a pure helium flow (P_{He} = 520 Nm^{-2}). The sulphur atom concentration in the lamp being maintained from a coating of sulphur on the lamp walls (produced after lamp operation on a $\geq$1% H_2S in He mixture). The 182.63 nm radiation was isolated by passage through a vacuum monochromator (entrance and exit slits = 150 μm) and was monitored by an EMI 9616 QB experimental photomultiplier (operating at 1000 V) coupled to a Datalab (DL905) transient recorder.

6.3 DATA ANALYSIS

When ozone or OCS was photolysed in the presence of nitrogen only, the decay of the ground state oxygen or sulphur atoms was observed to be very slow. Addition of small partial pressures of the perfluoroalkyl iodides (0.13-1.0 Nm^{-2}) resulted in a marked increase in the rate of decay. By measuring the pseudo first-order rate coefficients for removal of $O(^3P_J)/S(^3P_J)$ over a range of perfluoroalkyl iodide pressures the second order rate constant was determined. Such an approach is consistent with reactions of type (1) in parallel with reaction (2).

$$A + B \xrightarrow{k_1} \text{PRODUCTS} \qquad 1$$

$$A \xrightarrow{k_2} \text{PRODUCTS}' \qquad 2$$

$$\frac{-d[A]}{dt} = k_1 [A] [B] + k_2 [A] \qquad 6.1$$

If [B] is in large excess then the kinetics are simply pseudo first order and as such the differential rate expression (6.1) may be integrated to yield (6.2)

$$\log_e\left[\frac{[A]_{t=0}}{[A]_t}\right] = (k_1' + k_2)t \qquad 6.2$$

where $k_1' = k_1[B]$.

In all experiments absorbance was used to monitor atomic concentrations ([A]), the modified Beer Lambert law (6.3) is used to relate intensity measurements to concentration.

$$\log_e I_O/I_{TR} = (\varepsilon [A] \ell)^{\gamma} \qquad 6.3$$

Hence

$$\log_e [A]_t = \frac{1}{\gamma} \log_e \log_e (I_O/I_{TR}) - \gamma \log_e \varepsilon - \gamma \log_e \ell$$

where the symbols have their usual meaning (see 2.6). Substituting the expression for $\log_e (A)_t$ into equation 6.2 yields 6.4

$$\frac{1}{\gamma} \log_e \log_e (I_O/I_{TR}) = k_1' t + k_2 t - \log_e [A]_{t=0} + \gamma \log_e \varepsilon + \gamma \log_e \ell \qquad 6.4$$

Hence plotting $\log_e \log_e (I_O/I_{TR})$ against time (t) yields

a straight line of gradient $\gamma(k_1' + k_2)$. A plot of $\gamma(k_1' + k_2)$ against [B] is again linear and yields a gradient of γk_1. Therefore if γ is known k_1 the bimolecular rate constant is easily found. The unimolecular removal process (k_2) has as its main component diffusion out of the viewing zone and is given as the intercept of the second order plot. Gradients of first and second order plots were calculated by computer using least squares analysis programs EXPGRAPH and LMS, respectively as developed by R.H. Strain[6].

6.4 RESULTS AND DISCUSSION

A) $O(^3P_J)$ + PERFLUOROALKYLIODIDES

The system was initially tested by measurement of the well characterised rate of removal of $O(^3P_J)$ atoms by NO_2. In these experiments $O(^3P_J)$ atoms were formed by photolysis, in the visible and near u.v., of NO_2. The kinetic analysis of the resultant data followed that described in section 6.3 and $k_{O(^3P)+NO_2} = 1.1\pm0.3\times10^{-11}$ cm^3 molecule^{-1} s^{-1} was determined. This result is in excellent agreement with the accepted result obtained by resonance fluorescence ($k = 9.12\pm0.44\times10^{-12}$ cm^3 molecule^{-1} s^{-1} at 295 K)[7].

$O(^3P_J)$ decays were recorded for various pressures of CF_3I[†] and iso C_3F_7I. From the resultant second order plots (FIG 6.1) the bimolecular rate constants were evaluated.

$$k_{O(^3P_J)+CF_3I} = 1.1\pm0.3\times10^{-11} \text{ cm}^3 \text{ molecule}^{-1} \text{ s}^{-1}$$

$$k_{O(^3P_J)+\text{iso } C_3F_7I} = 2.3\pm0.6\times10^{-11} \text{ cm}^3 \text{ molecule}^{-1} \text{ s}^{-1}$$

The above rate data have been calculated using a γ factor = 0.76 - based on the data presented in FIG 6.2. The errors assigned to the above rate constants represent 95% confidence limits. Ozone absorption measurements before and after the flash indicated 3% photolysis of ozone was occurring at a flash energy of 180 J. A comparison of the integrated extinction coefficients over the absorption bands of ozone and CF_3I suggests CF_3I photolysis to be very much less than 3%. In order to ensure that photolysis of the perfluoroalkyl iodide did not interfere with the determined $O(^3P_J)$ removal rate constants the reaction with CF_3I was studied at various flash energies (180-320 J). No significant difference in the decay rate for $O(^3P_J)$ could be detected and it was concluded that radical-radical reactions did not influence the $O(^3P_J)$ decay kinetics.

The bond strength of IO is not well characterised. Early work yielded two different values of the bond

[†]Reaction of ozone and the perfluoroalkyliodides was studied under second order conditions. The ozone concentration was measured (using u.v. spectrophotometry at 257 nm) as a function of time. Under the conditions of the experiment reaction between ozone and the perfluoroalkyl-iodides was found to be unimportant.

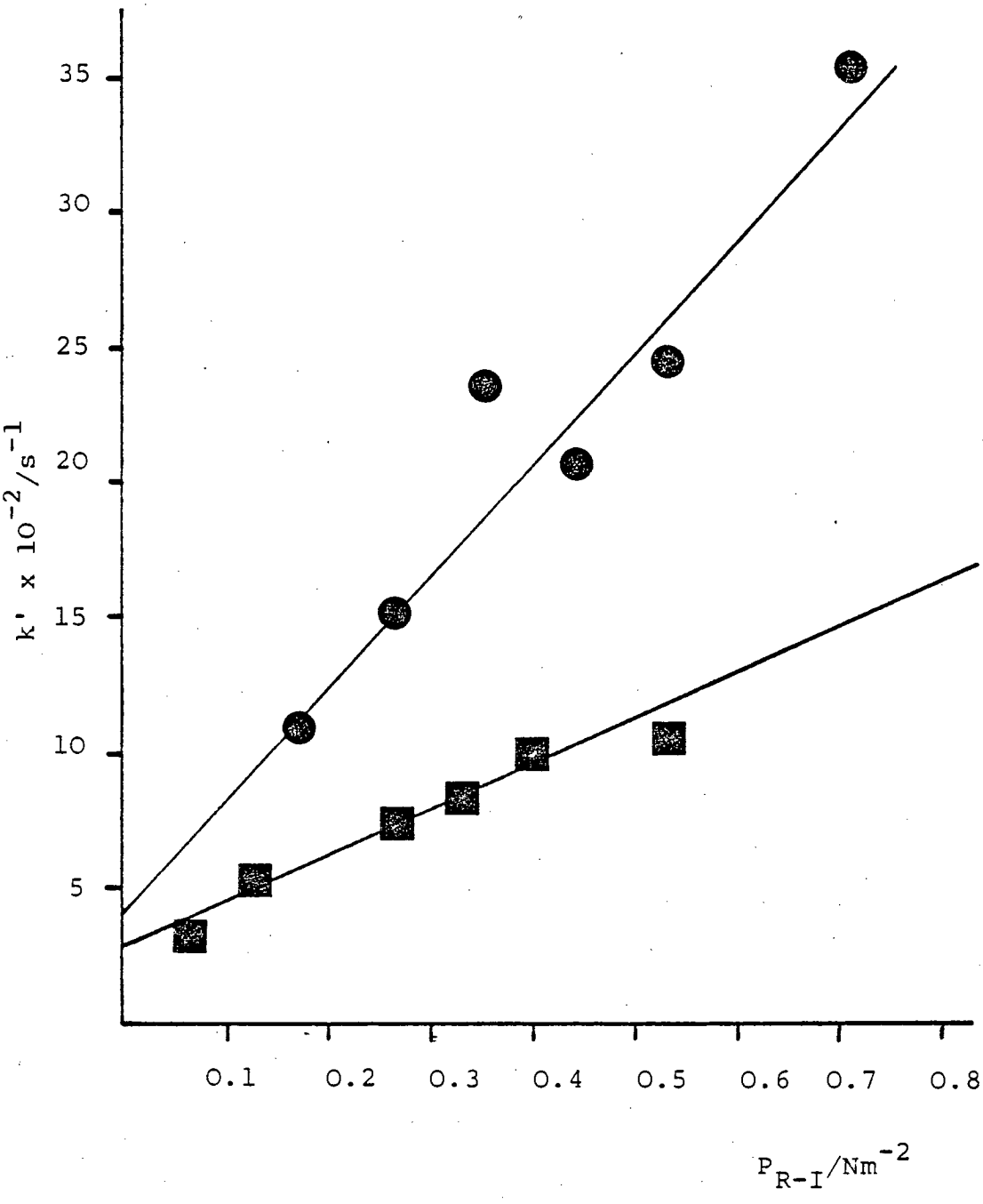

FIG 6.1: Pseudo First Order Rate Constants vs Perfluoroalkyl iodide pressure

(● iso C_3F_7I

■ CF_3I).

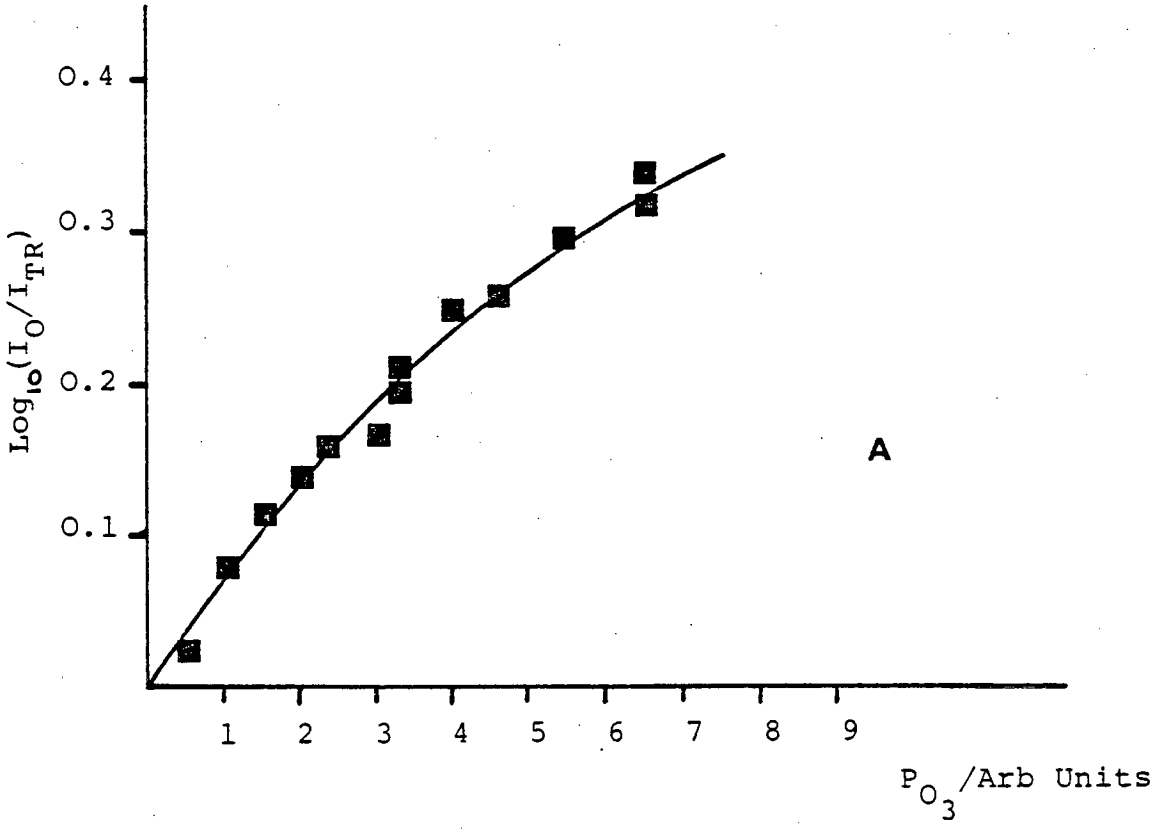

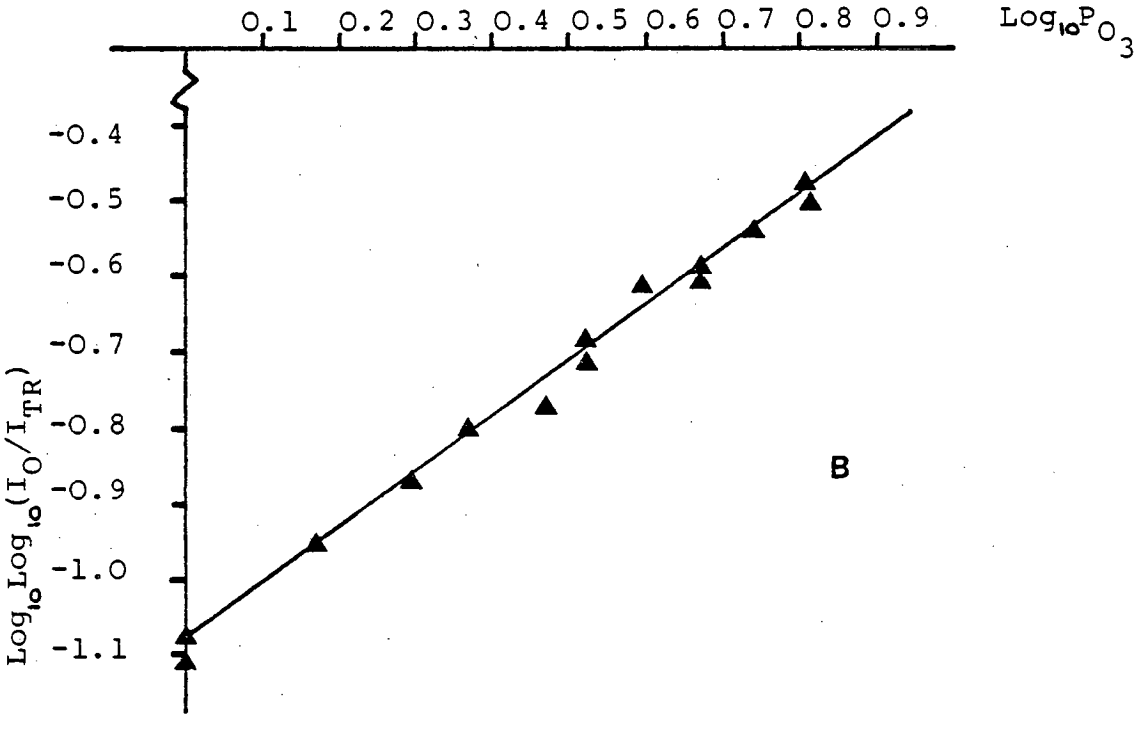

FIG 6.2: A) Curve of Growth for $O(^3P_J)$

B) Linear Plot from (A).

strength, 174±19 kJ mol^{-1} [8] and 238±24 kJ mol^{-1} [9]. More recent work by Radlein et al[10] has supported the latter value with a measured D(IO) = 222±13 kJ mol^{-1}. Using the rate constants obtained above it is possible to calculate a maximum activation energy for reaction (1), by assuming the steric factor (P) to be unity. Then providing the CF_3-I bond strength is known the bond strength of the product IO may be ascertained.

$$O(^3P_J) + CF_3I \rightarrow CF_3 + IO \qquad 1$$

From simple collision theory (section 1.3) the rate constant (k) is represented by the following expression (6.5):

$$k = PZ^o_{AB} [\exp (-E_o/kT)] \qquad 6.5$$

where

$$Z^o_{AB} = \pi D_{AB}^2 (8kT/\pi\mu)^{\frac{1}{2}} \qquad 6.6$$

D_{AB} is the mean collision diameter and has been assigned a value of 3.55×10^{-8} cm for reaction (1) (evaluated from the sum of the Van der Waals radii for oxygen (0.140 nm) and iodine (0.215 nm)). Hence a collision cross section (πD_{AB}^2) = 3.4×10^{-15} cm^2 has been used to evaluate the standard collision number (Z^o_{AB}) = 2.6×10^{-10} cm^3 s^{-1}. Combination of the collision number (and setting P=1) with the lower limit of the measured rate of reaction (1) yields a maximum

activation energy $(E^{o})^{\dagger}$ = 9 kJ mol^{-1}. When this is combined with the bond strength of CF_3I, $D(CF_3-I)$ = 221±5 kJ mol^{-1} [11], we obtain a lower limit for the bond strength of IO as $D(I-O) \geqslant 208$ kJ mol^{-1}, which is consistent with the work of Phillips et al and Radlein et al.

The difference in rates between $O(^3P_J)$ reaction with CF_3I and iso C_3F_7I may reflect the presence of a small activation energy in the former reaction, since the bond strength of the C-I bond (206 kJ mol^{-1}) [11] in iso C_3F_7I is weaker than that in CF_3I. Alternatively it may reflect variations in the pre-exponential factors.

B) $S(^3P_J)$ + PERFLUOROALKYLIODIDES

The system was again checked by measurement of a well documented reaction rate, in this case, the reaction of $S(^3P_J)$ atoms with O_2. Following the usual kinetic analysis (sec. 6.3) yielded a rate constant for reaction, of $k = 2.2 \pm 0.4 \times 10^{-11}$ cm^3 $molecule^{-1}$ s^{-1}. This is in excellent agreement with numerous other studies[12-14]. Rate data for the reactions of $S(^3P_J)$ with the perfluoroalkyliodides were obtained in similar manner to those of the analogous $O(^3P_J)$ reactions.

† There is some difficulty in equating the E^{o} used in simple collision theory (SCT) to the activation energy of the Arrhenius equation (E_{ACT}) due to the temperature dependence of the pre-exponential factor in SCT but not in the Arrhenius expression. If E_{ACT} is defined as d(lnk)/d(1/T) then it is evident that

$$E_{ACT} = E^{o} + \tfrac{1}{2}RT \qquad 6.7$$

In the above and subsequent calculations involving SCT, E^{o} has been used directly.

$$k_{S(^3P_J)+CF_3I} = 4.7\pm1.0\times10^{-12} \text{ cm}^3 \text{ molecule}^{-1} \text{ s}^{-1}$$

$$k_{S(^3P_J)+\text{iso } C_3F_7I} = 1.5\pm0.3\times10^{-11} \text{ cm}^3 \text{ molecule}^{-1} \text{ s}^{-1}$$

Variation of $S(^3P_J)$ concentration (or rather transmitted light intensity) with time is shown in FIG 6.3 and second order plots are illustrated in FIG 6.4. The γ coefficient was determined in the conventional manner (see FIG 6.5) and was found to equal 0.67.

Reference to the rate constants illustrates reaction to be relatively rapid and again it seems likely that the reaction will proceed via halogen abstraction to yield IS. Attempts were made to observe product formation, directly, using the flash spectroscopy technique. Various pressures of CF_3I (0.67-2.66 Nm^{-2}) and $S(^3P_J)$ sources (P_{OCS} = 133 Nm^{-2}, P_{CS_2} = 76-106 Nm^{-2}) were used. All attempts to produce a strong conclusive spectrum have however failed. This may well be due to the poor resolution of our equipment coupled to disadvantageous spectroscopic characteristics ca for example, lack of predissociation (resulting in narrow lines) or low absorption coefficients. (The production of the analogous IO from reaction of $O(^3P_J)$ with CF_3I was easily monitored using this technique through the $A^2\Pi—X^2\Pi$ banded absorption spectrum of the IO product). The thermochemistry of the S-X radicals (X = halogen) is essentially unknown. Adopting exactly the same procedure as that just described for the evaluation of the IO bond strength

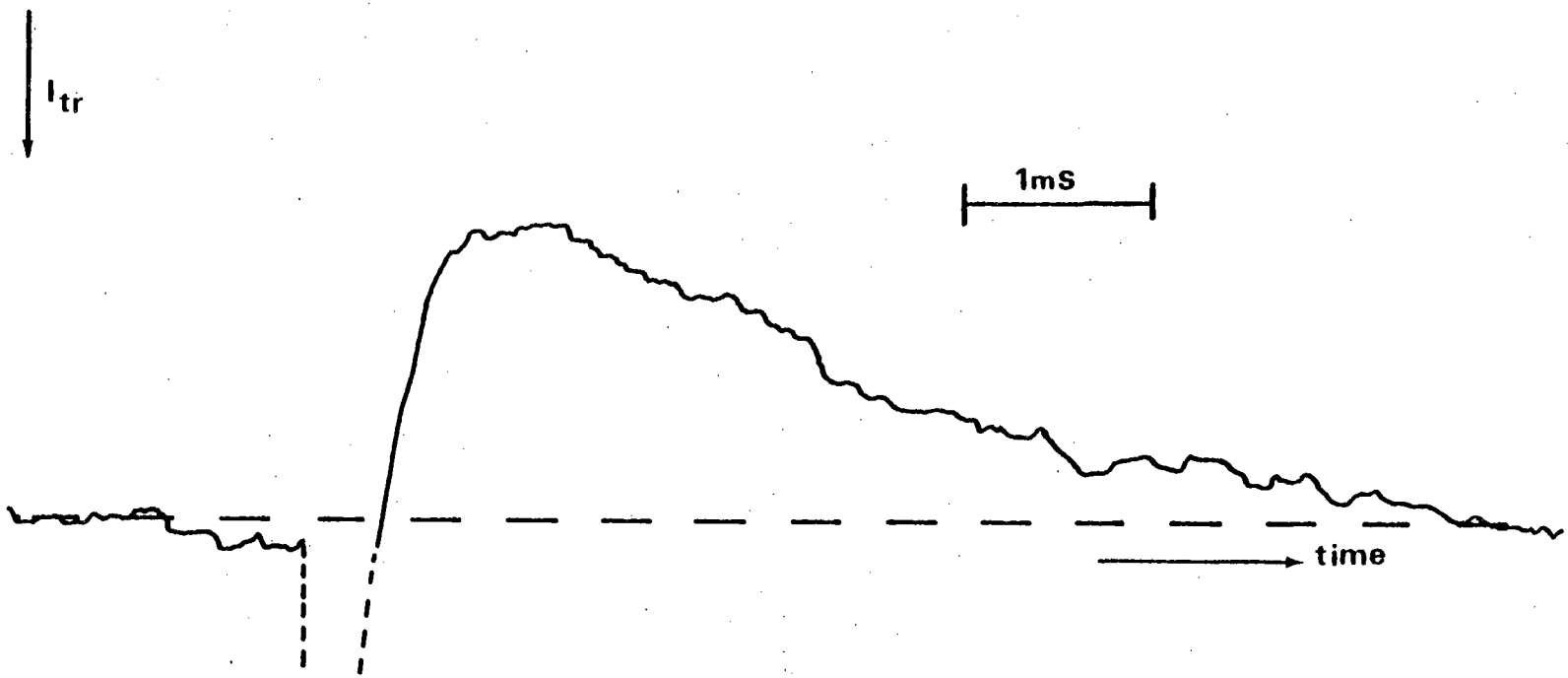

FIG 6.3: Typical $S(^3P_J)$ Decay

Conditions; [OCS] = 22 Nm^{-2}, $[C_3F_7I]$ = 0.17 Nm^{-2}, $[N_2]$ = 1.3 kNm^{-2}

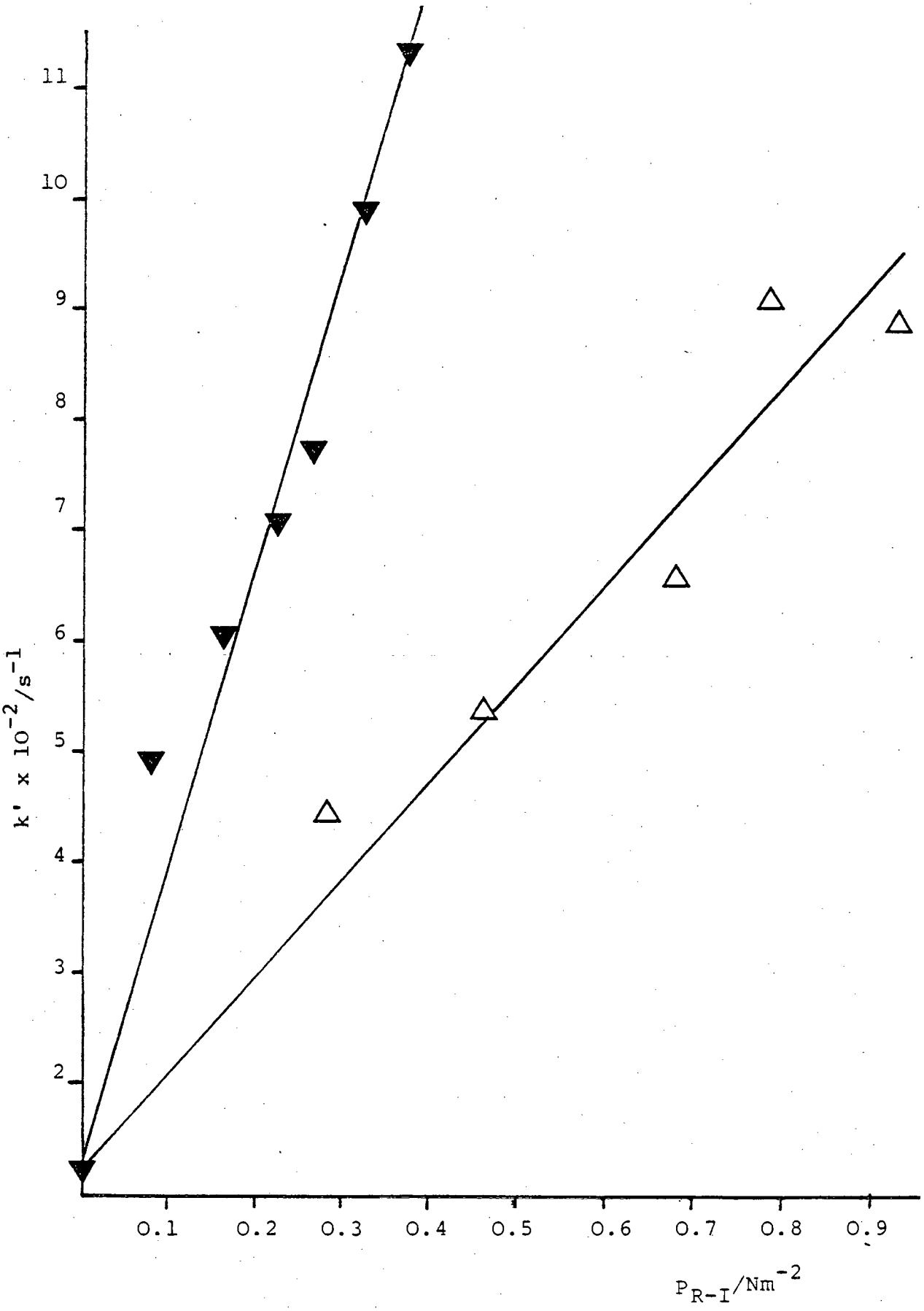

FIG 6.4: Pseudo First Order Rate Constants vs Pressure of Perfluoroalkyl Iodide (▼ = iso C_3F_7I △ = CF_3I).

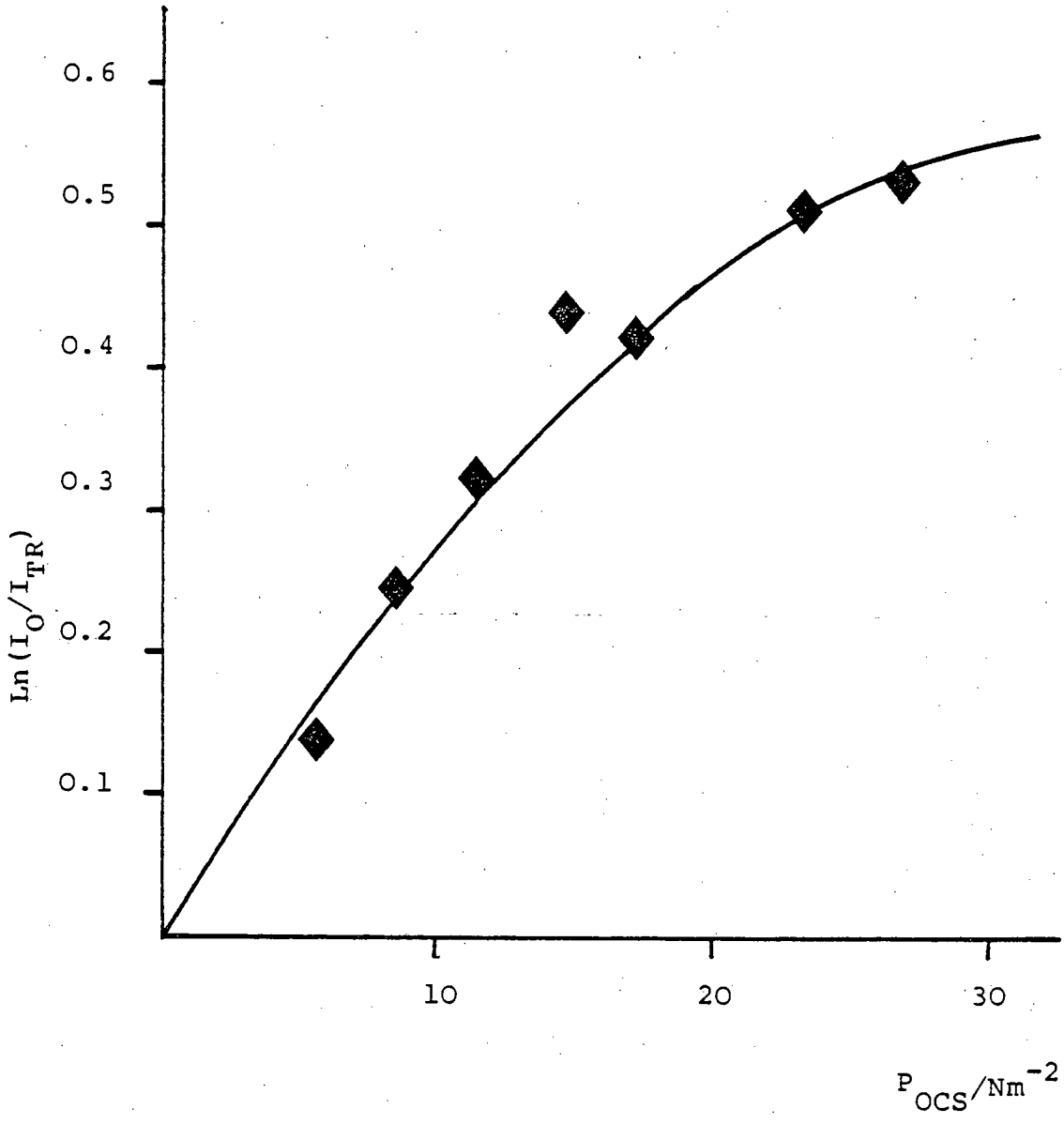

FIG 6.5 Curve of Growth for $S(^3P_0)$:- $Ln(I_0/I_{TR})$ vs Pressure (OCS).

allows a lower limit to the IS bond strength to be calculated. Using a standard collision number (Z^{o}_{AB}) = 2.57×10^{-10} cm^3 s^{-1} and the lower limit of the rate constant yields a maximum activation energy E^{o}_{max} = 11 kJ mol^{-1} for the $S(^3P_J)$ + CF_3I reaction. Using the bond dissociation energy of CF_3-I previously stated necessitates that D(S-I) $\geqslant$ 205 kJ mol^{-1}.

The reactions of the ground state oxygen and sulphur atoms with halogen containing molecules are surprisingly slow when compared with the analogous reactions for the first excited ($^1D_2$) states e.g. $k_{S(^1D_2)+CF_3I} = 2.1 \pm 0.4 \times 10^{-10}$ cm^3 $molecule^{-1}$ s^{-1}. The reaction of $O(^3P_J)$ with CF_3Br is endothermic, however temperature dependent kinetic studies have shown that the pre-exponential factor ($1.5 \pm 0.5 \times 10^{-11}$ cm^3 $molecule^{-1}$ s^{-1})[15] is very similar to the rate of reaction of $O(^3P_J)$ with CF_3I. This suggests that the lowered rate of reaction is due to steric as opposed to thermodynamic constraints. Detailed information, from molecular beam studies, of the reactions of $O(^3P_J)$ with the halogens, interhalogens[16-20] and CF_3I [4] suggest the involvement of collision complexes of the form X-Y-O. The formation of such a complex involves the near collinear collision of reactants. It is further noted that the structure of the collision complex which results has been consistent with an 'electronegativity ordering rule' which states that the preferred geometry of an OXY triatomic complex has the least electronegative atom in the centre[16,17,21-23]. Application of transition state theory to a collinear

complex of the OXY type yields a pre-exponential factor of the order observed in the fore-mentioned studies and has hence received wide acceptance as the explanation of the $O(^3P_J)$ reactivity with halogen containing molecules. However there exists a number of anomalies in connection with such an explanation. The reaction of $O(^3P_J)+F_2$ is slow due to a sizeable activation energy (43 kJ mol^{-1})[24]. One explanation of this large barrier to reaction involves the change in electronegativity ordering, which results in the participation of an FOF collision intermediate[17]. However the reaction of $S(^3P_J)$ with Cl_2 and Br_2 are rapid[1] $k = 1.1\pm0.1\times10^{-11}$ and $9.5\pm1.7\times10^{-11}$ cm^3 $molecule^{-1}$ s^{-1}, respectively. Yet reaction of $S(^3P_J)$ with these molecules reflects similar electronegativity ordering.

TABLE 6.1 ELECTRONEGATIVITIES (PAULING) OF SELECTED GROUP VI AND VII ELEMENTS

O (3.5)	F (4.0)
S (2.5)	Cl (3.0)
	Br (2.8)
	I (2.5)

An alternative explanation to the low steric factors for the ground state reactions compared to those observed for the analogous reactions of the first excited state draws on information obtained in the study of $O(^1D_2)$ with the halogenomethanes (see Chapter 3). We would suggest involvement of potential energy surfaces of the type illustrated in FIG 6.6.

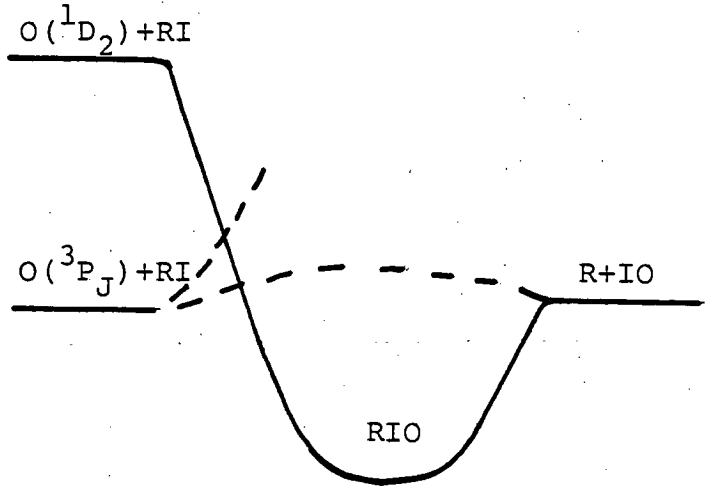

FIG 6.6 Section through the proposed potential surfaces for $O(2^3P_J)$ and $O(^1D_2)$ interacting with an iodide. The lowest singlet surface is shown by the continuous line and the triplet surfaces by dashed lines.

The most facile route from reactants to products is through a complex of the form CF_3IO on the singlet surface. Thus the low reaction cross-section could result from a 'low' triplet-singlet transition probability when one begins with reactants on the triplet surface. Clearly the rate of reaction will depend on the accessibility of the crossing region and the probability of crossing on passage through the potential surface intersection. As such it would be

of great interest to compare the pre-exponential factors for the reactions of $O(^3P_J)$ and $S(^3P_J)$, with CF_3I. The slower nature of the sulphur reaction may reflect an activation energy not experienced in the $O(^3P_J)$ reaction. Clearly work is needed on the characterisation of the spin states and energies of the intermediates involved in order to test the general applicability of the above hypothesis.

6.5 REFERENCES

1. M.A.A. Clyne and L.W. Townsend, Int. J. Chem. Kin., (1975), Symposium 1, 75.
2. M. Trainer, M.Phil. Thesis, University of Edinburgh (1980).
3. M. Kaufman and C.E. Kolb, Chem. Instrumentation 3, (1971), 175.
4. P.A. Gorry, C.V. Nowikow and R. Grice, Chem. Phys. Lett. 55, (1978), 24.
5. J.T. Herron and R.E. Huie, J. Phys. Chem. 73, (1969), 1326.
6. R.H. Strain, Ph.D. Thesis, University of Edinburgh (1977).
7. D.D. Davis, J.T. Herron and R.E. Huie, J. Chem. Phys. 58, (1973), 530.
8. R.A. Durrie and D.A. Ramsay, Can. J. Phys. 36, (1958), 35.
9. L.F. Phillips and T.M. Sugden, Trans. Faraday Soc. 57, (1961), 914.
10. D. St. A.G. Radlein, J.C. Whitehead and R. Grice, Nature 253, (1975), 37.
11. E.N. Okafo and E. Whittle, Int. J. Chem. Kinetics 7, (1975), 273.
12. R.W. Fair, A. Van Roadselaar and O.P. Strausz, Can. J. Chem. 49, (1971), 1659.
13. R.J. Donovan and D.J. Little, Chem. Phys. Lett. 13, (1972), 488.
14. D.D. Davis, R.B. Klemm and M. Pilling, Int. J. Chem. Kinetics 4, (1972), 367.
15. T.C. Frankiewicz, F.W. Williams and R.G. Gann, J. Chem. Phys. 61, (1974), 402.
16. D.D. Parrish and D.R. Herschbach, J. Am. Chem. Soc. 95, (1973), 6133.

17. D.A. Dixon, D.D. Parrish and D.R. Herschbach, Faraday Disc. Chem. Soc. 55, (1973), 385.

18. C.F. Carter, M.R. Levy, K.B. Woodall and R. Grice, Faraday Disc. Chem. Soc. 55, (1973), 381.

19. P.A. Gorry, C.V. Nowikow and R. Grice, Chem. Phys. Lett. 55, (1978), 19.

20. P.N. Clough, G.M. O'Neill and J. Geddes, J. Chem. Phys. 69, (1978), 3128.

21. J.D. McDonald, P.R. Lebreton, Y.T. Lee and D.R. Herschbach, J. Chem. Phys. 56, (1972), 769.

22. Y.T. Lee, P.R. Lebreton, J.D. McDonald and D.R. Herschbach, J. Chem. Phys. 51, (1969), 455.

23. S. Peyerimhoff and R.J. Buenker, J. Chem. Phys. 49, (1968), 2473.

24. R.H. Krech, G.J. Diebold and D.L. McFadden, J. Amer. Chem. Soc. 99, (1977), 4605.

CHAPTER VII

KINETIC STUDIES OF THE REACTIONS OF $S(3^1D_2)$

7.1 INTRODUCTION

The most extensive work on sulphur atom chemistry (^3P_J and $^1D_2$ states) was carried out in the early 1960's[1]. Since then the first excited state of sulphur ($^1D_2$) in particular has been little studied, certainly in comparison with the analogous state of oxygen. The attention given to the chemistry of excited oxygen atoms in comparison to that received by sulphur is easily understood. Firstly $O(^1D_2)$ atoms are readily produced from photolysis of ozone. The most convenient source of $S(^1D_2)$ atoms was the much more weakly absorbing carbonyl sulphide. In the latter case the necessary use of higher pressures, compared to ozone, results in more rapid removal of the excited state and hence increases the observational problems. End products in the oxygen systems are volatile and easily removed. In the sulphur system production of polymeric sulphur compounds necessitates the frequent cleaning of glassware. Secondly and more importantly, the demand for kinetic data on oxygen atom chemistry was more pertinent. The problems associated with atmospheric chemistry presented an incentive for the necessary experimental developments. In recent years, however, an increasing interest in sulphur compounds has placed more emphasis on sulphur atom chemistry. Recent work has considered the input strengths of carbon disulphide and carbonyl sulphide[2,3]

into the atmosphere and the subsequent transport of these molecules into the stratosphere. At these altitudes primary photolytic processes will yield $S(^1D_2)$ and $S(^3P_J)$ atoms. Rapid reaction with oxygen and the eventual further oxidation to form the sulphate layer is almost certain to be the major removal mechanism of these species. Consideration of alternative removal pathways is obviously of interest. Alternative removal mechanisms of sulphur atoms are of even more importance when discussing the behaviour of sulphur compounds in the prebiotic atmosphere. The atmosphere of these times was similar to that of the present with the major exception that oxygen concentrations were negligible. The fate of sulphur compounds in such an environment is of great importance in considering the sedimentary rock record[4] and is likely to involve sulphur atom intermediates.

This chapter presents absolute rate data for a large number of $S(^1D_2)$ reactions. Throughout, these reactions will be discussed together with the data available on the analogous oxygen atom reactions.

7.2 EXPERIMENTAL

$S(^1D_2)$ atoms were monitored through time resolved atomic absorption photometry using the apparatus illustrated in FIG 2.2. This work represents the first use of a direct observational technique for $S(^1D_2)$ atoms and follows a similar approach to that used by Heidner and Husain for direct observation of the $O(^1D_2)$ state[5].

The principle features of the experimental arrangement were: the use of an extreme solar blind photomultiplier (EMR 542) which totally eliminated scattered light detection at 166.67 nm (the monitoring wavelength) hence allowing kinetic information to be recorded from essentially t=0; the use of a flow lamp for generation of the atomic line. The flow lamp was operated from a H_2S/He supply (P = 400-500 Nm^{-2}) at an incident power of 50 W. The gas composition varied from ≈2% H_2S to pure helium. In the latter case the deposit of sulphur on the lamp walls, resulting from operation with a 2% H_2S in He flow, when licked by the helium plasma produced the atomic line with sufficient intensity. Reagents were handled with a conventional high vacuum system and pressures measured with MKS Baratron pressure gauges. Due to the reactivity of $S(^1D_2)$ atoms great care was taken to ensure the high purity of the reactions used.

7.3 DATA ACQUISITION AND ANALYSIS

In order to monitor the absolute rate of removal of $S(^1D_2)$ atoms by various reactants CS_2 (4×10^{-2} Nm^{-2}) was used exclusively as the photolytic (E = 180 J) source of the excited sulphur atoms. The reactant gas was added to a pressure such that the first order decays lay in the easily measurable range from $0.5-3.0 \times 10^4$ s^{-1}. Helium buffer gas was added to a total pressure of 800 Nm^{-2}. The analysis of the data followed that described in the previous chapter (6.3).

First order decays were obtained from single shot recording with a Datalab 905 transient recorder (see FIG 7.1) and were analysed by eye. The digital data was then processed by computer to give pseudo first order rate constants which were subsequently plotted against reactant pressures to yield a straight line plot, the gradient of which gives the second order rate constant. It is well known in atomic absorption photometry experiments that deviations from simple Beer Lambert behaviour are frequently observed and as such the gradient of the second order plot must be divided by the γ coefficient to yield the true second order rate constant (see section 2.6). Determination of the γ coefficient is normally achieved from a plot of (log log $I_O/I_{TR})_{t=0}$ vs. log pressure of the sulphur source molecule (CS_2). In this study, however, the rapid decay kinetics made it difficult to accurately extrapolate the curves back to t=0. The resultant plot† (FIG 7.2) illustrates the error involved. The gradient of the graph shown is 0.92. Further evidence that the γ coefficient is very close to unity is provided by the lamp performance. Changing H_2S pressure in the flow lamp and/or movement of the microwave cavity back along the flow lamp produced little change in absorption signal. This may be contrasted with the behaviour of a heavily reversed source (FIG 2.10).

† This plot was the best achieved from a number of studies. Note the large error in individual points.

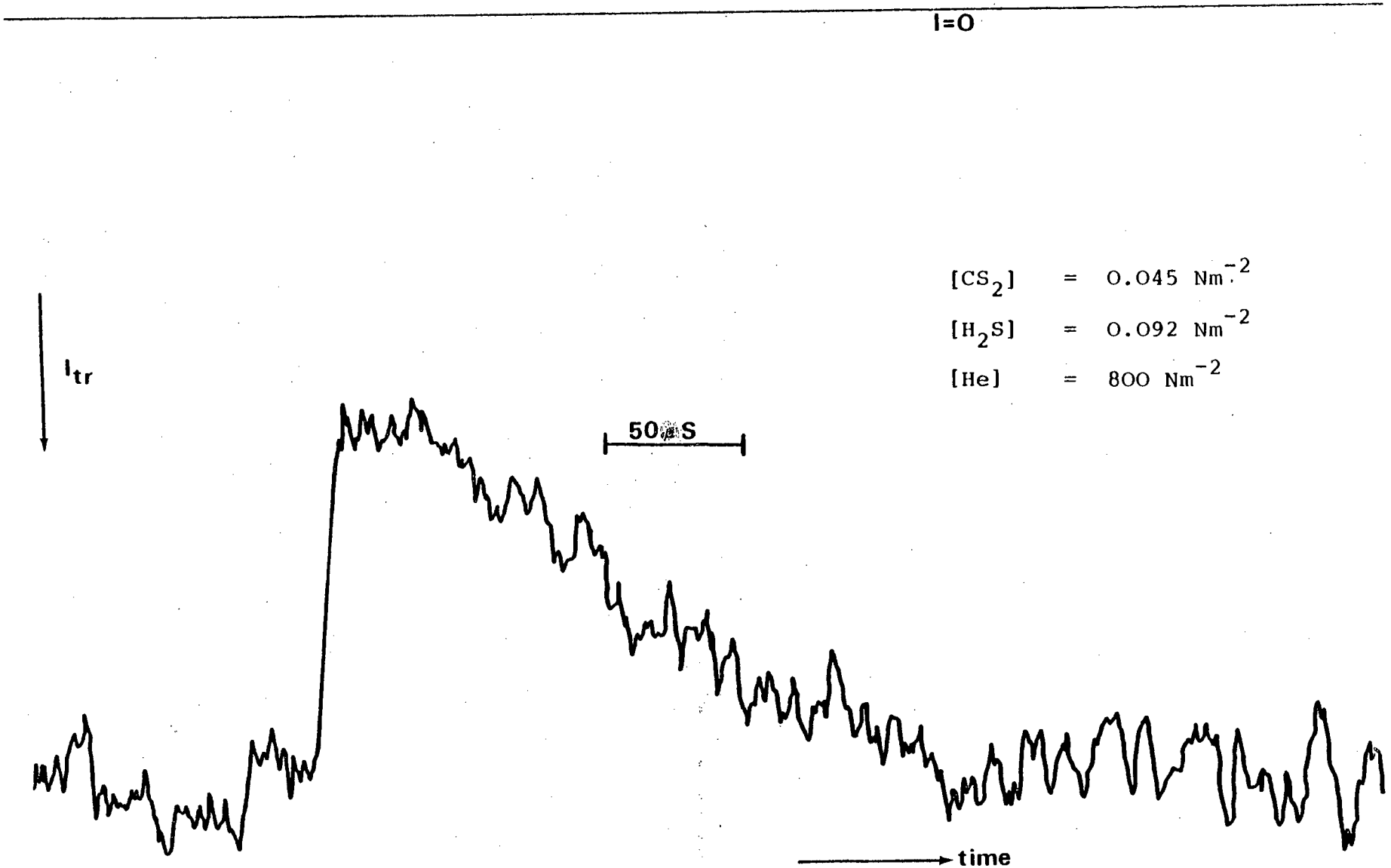

FIG 7.1: Typical $S(^1D_2)$ Decay

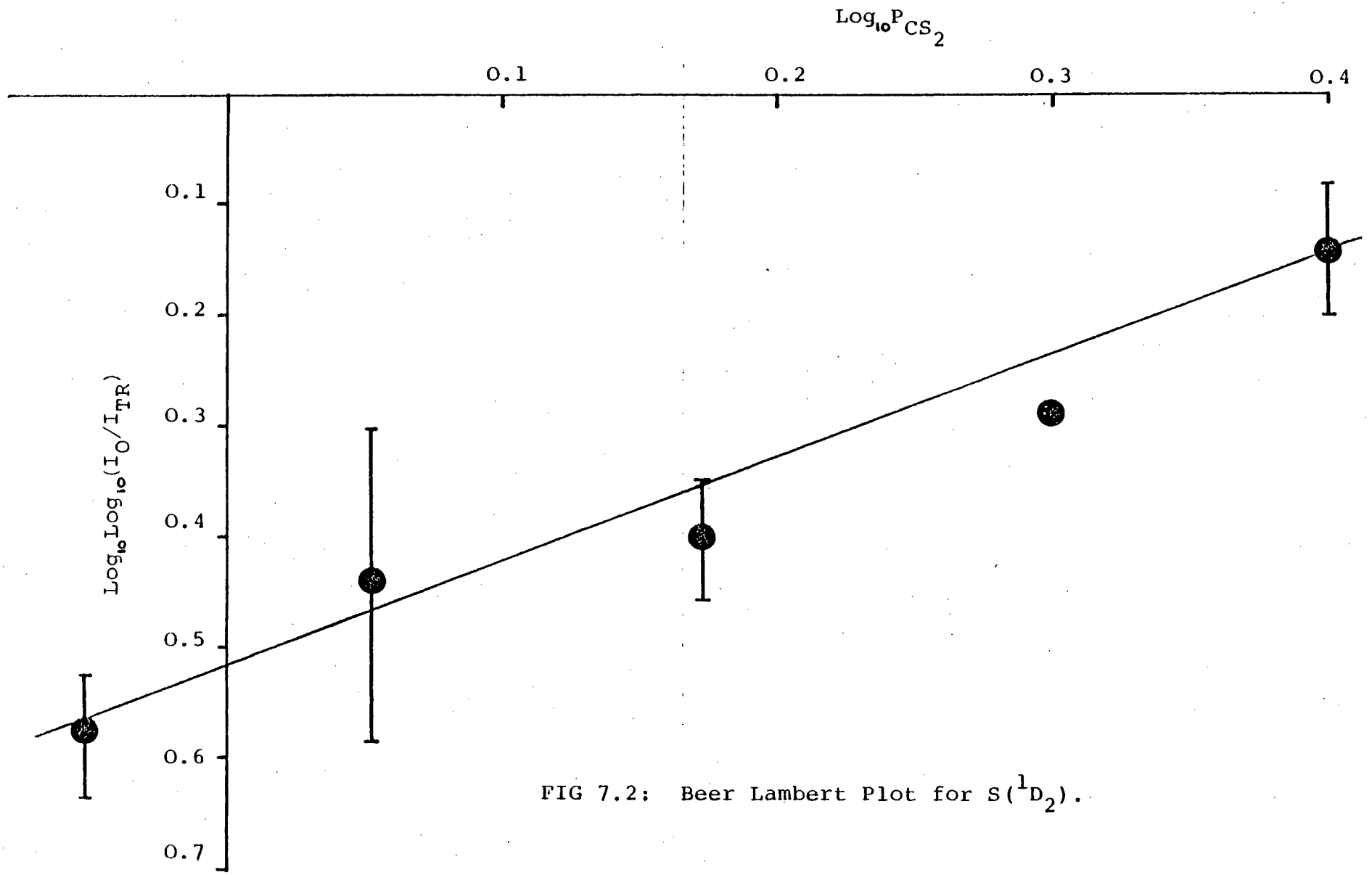

FIG 7.2: Beer Lambert Plot for $S(^1D_2)$.

7.4 RESULTS AND DISCUSSION

A) $S(3^1D_2)$ PRODUCTION

i) Flash photolysis of OCS ($\lambda \geqslant 200$ nm) has been shown, by various chemical methods, to yield $S(^1D_2)$. At $\lambda = 228.8$ nm Gunning and Strausz[1] have demonstrated quantum yields of 0.67 and 0.24 for production of $S(^1D_2)$ and $S(^3P_J)$ respectively, using alkyl mercaptan formation to monitor $S(^1D_2)$ concentrations. Sidhu et al[6] have shown the total quantum yield for sulphur atom production on photolysis at $\lambda = 253.7$ and 228.8 nm to equal 0.9. This work confirmed OCS to be a source of $S(^1D_2)$ by direct observation of the atomic species through attenuation of 166.67 nm radiation. The rate of removal of $S(^1D_2)$ was measured and found to be rapid:

$$S(^1D_2) + OCS \rightarrow \text{PRODUCTS} \qquad 1$$

$$k_1 = 1.2 \pm 0.3 \times 10^{-10} \text{ cm}^3 \text{ molecule}^{-1} \text{ s}^{-1}$$

The yield of $S(^3P_J)$ from the primary photolysis step (3) and the quenching process (5) was established by observation of $S(^3P)$ at 182.6 nm using the atomic absorption spectrometer described in section 7.2. Due to the low signal to noise ratio a 1000 pF capacitor was used in parallel to smooth the signal. $S(^3P_J)$ yields were compared in the presence of excess nitrogen and helium (FIG 7.3). In the nitrogen system all $S(^1D_2)$ is quenched to $S(^3P_J)$. With helium the time at which observations were made (5-10 ms) ensured reaction (1) to be complete. Comparison of the helium and nitrogen results from FIG 7.3 yields

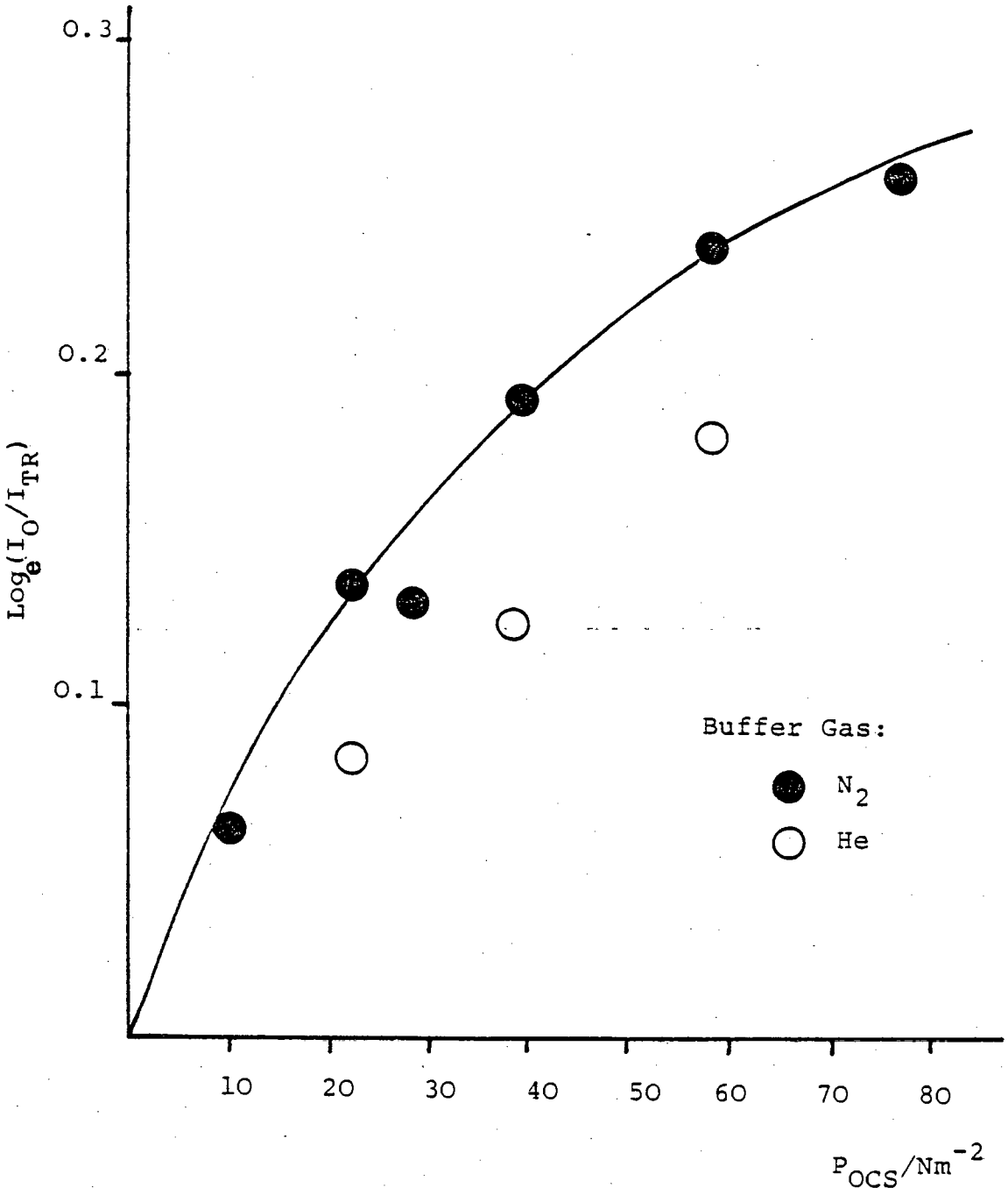

FIG 7.3: Curve of Growth of $S(^3P_J)$ from Similar Pressures of OCS in the Presence of He and N_2 Buffer Gases.

$$\frac{S(^3P) \text{ FROM } (3) + (5)}{\text{TOTAL SULPHUR ATOM PRODUCTION}} = 0.55 \pm 0.1$$

Remembering the results of Gunning and Strausz for the primary photolytic production yields from (2) and (3) suggests the quenching reaction (5) to be sizeable but a minor channel for removal of $S(^1D_2)$ atoms. The above result is in good agreement with Breckenridge et al[7] who found that 50% of the sulphur atoms, formed by reactions (3) and (5) react as $S(^3P_J)$

$OCS + h\nu$	→	$S(^1D_2) + CO$	2
	→	$S(^3P_J) + CO$	3
$S(^1D_2) + OCS$	→	$S_2(^1\Delta) + CO$	4
	→	$S(^3P_J) + OCS$	5
	→	OTHER PRODUCTS	6
$S(^1D_2) + N_2$	→	$S(^3P_J) + N_2$	7

ii) The absorption spectrum of CS_2 in the near u.v. consists of two distinct regions of absorption, one from 290-380 nm and a much stronger absorption extending from 185-230 nm. In the flash photolysis of CS_2 in the region 190-210 nm, Callear observed the production of vibrationally excited $CS(X^1\Sigma)$ and $S(^3P)$ but not $S(^1D_2)$[8]. This was thought to be due to predissociation from the $^1B_2$ state in violation of the spin conservation rules, aided by the presence of heavy sulphur atoms. Production of $S(^1D_2)$ atoms from this system becomes energetically feasible at 221 nm. This work monitored $S(^1D_2)$ atom production following photolysis of

CS_2 ($\lambda \geqslant 200$ nm) hence strongly suggesting the work of Callear to be in error.

$$CS_2 + h\nu \rightarrow CS + S(^1D_2) \quad 8$$

$$\rightarrow CS + S(^3P_J) \quad 9$$

The approximate yields into channels (8) and (9) were measured by comparison of $S(^1D_2)$ (10x greater) and the total S atom (80x greater) yields from CS_2 with OCS. Assuming the yields into channels (2) and (3) to be 0.7 and 0.3 respectively and that channels (8) and (9) account for the total loss of CS_2 results in branching ratios into (8) and (9) of 11% and 89% respectively.

Reaction of $S(^1D_2)$ with the source CS_2 molecule was again found to be rapid.

iii) Flash photolysis of H_2S/He mixtures produced no observable $S(^1D_2)$ under similar conditions as the OCS experiments. It seems likely that above 200 nm light absorption leads predominantly to H atom production.

$$H_2S + h\nu \ (\lambda < 317 \text{ nm}) \rightarrow HS + H \quad 10$$

Sulphur atoms have been noted in flash photolysis studies below 200 nm[9].

B) <u>$S(3^1D_2)$ KINETICS</u>

i) <u>CO_2, OCS, CS_2</u>

Reaction of $S(^1D_2)$ with OCS and CS_2 has been mentioned in the previous section. The detailed reaction

paths are listed below (11-15) for reaction with OCS.

		ΔH/kJ mol^{-1}	
$S(^1D) + OCS \rightarrow$	$S_2(^3\Sigma^-) + CO$	-229.5	11
$\rightarrow$	$S_2(^1\Delta_g) + CO$	-173.5	12
$\rightarrow$	$S_2(^1\Sigma) + CO$	-120.8	13
$\rightarrow$	$S(^3P_J) + OCS$	-111.2	14
$\rightarrow$	$SO(^3\Sigma^-) + CS$	+31.8	15

Reactions (11), (14) and (15) are spin forbidden and in the case of (11) and (14) have been shown to account for a minor fraction of the total cross section compared to reaction (12)[10]. Reaction of $O(^1D_2)$ with OCS has been the subject of a number of studies. The bulk rate constant is very similar to that of the $S(^1D_2)$ reaction, see TABLE 7.1.[11]

TABLE 7.1 RATE DATA FOR $S(^1D_2)/O(^1D_2)$ REACTION WITH CX_2 (X = O and/or S)

Reactant	k/cm^3 molecule^{-1} s^{-1}	
	$S(^1D_2)$	$O(^1D_2)$
	(see FIG 7.4)	
CO_2	$1.1\pm0.2\times10^{-10}$	$1.0\pm0.2\times10^{-10}$
OCS	$1.2\pm0.3\times10^{-10}$	$1.5\pm0.2\times10^{-10}$
CS_2	$1.5\pm0.3\times10^{-10}$	-

Reaction of $O(^1D_2)$ with OCS has been studied in low temperature matrices[12] and has been shown to yield the products CO and SO and CO_2 and S. No CO_2S intermediate

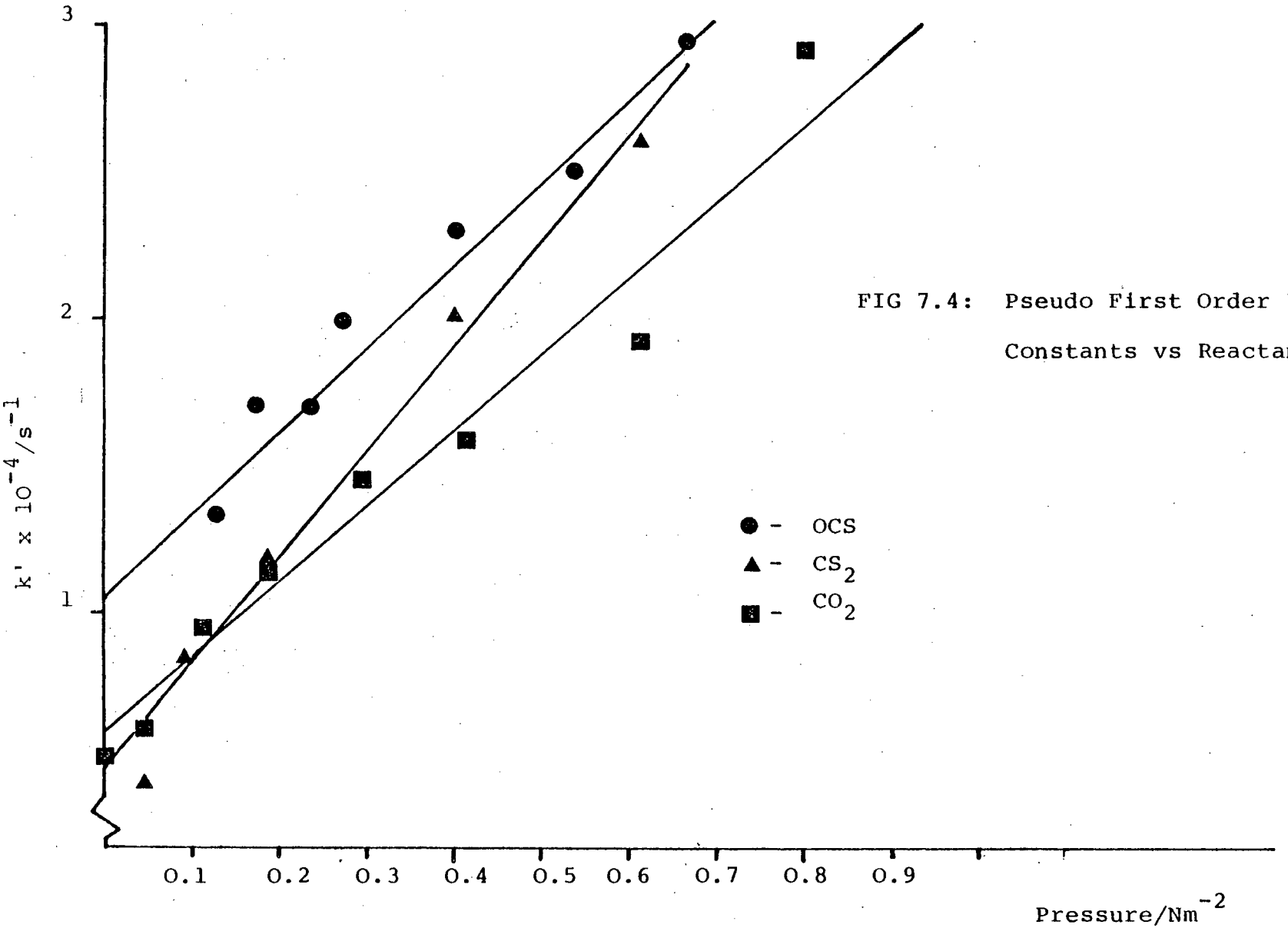

FIG 7.4: Pseudo First Order Rate Constants vs Reactant Gas Pressure

was detected using an I.R. absorption technique. The vibrational energy distribution of CO ($v \leqslant 9$) corresponds to 4 or 5% of the reaction exoergicity[13]. This value is lower than the energy partitioned into CO vibration (~9%) on reaction of ground state oxygen atoms with OCS[13]. Reaction of $S(^1D_2)$ with CS_2 and CO_2 yields similar bulk rate constants to that obtained for reaction with OCS. The analogous reaction channels are illustrated below.

		ΔH/kJ mol^{-1}	
$S(^1D) + CS_2$	$\rightarrow S_2(^3\Sigma) + CS$	-144.6	16
	$\rightarrow S_2(^1\Delta_g) + CS$	-45.6	17
	$\rightarrow S_2(^1\Sigma) + CS$	+7.1	18
	$\rightarrow S(^3P) + CS_2$	-111.2	19
	$\rightarrow SO(^3\Sigma) + CO$	+97.4	20
	$\rightarrow SO(^1\Delta) + CO$	-41.0	21
	$\rightarrow SO(^1\Sigma) + CO$	+28.4	22
	$\rightarrow S(^3P) + CO_2$	-111.2	23

Early work suggested reaction of $S(^1D_2)$ with CO_2 resulted in quenching (23) only[1]. As yet no evidence for participation of any of the reactive channels (20-22) has been presented. Preliminary evidence suggests $S(^1D_2)$ reacts with CS_2 in an analogous manner to that of CO_2 i.e. leading predominantly to quenching. We studied these reactions using the technique of flash spectroscopy with photographic recording (FIG 2.1) but failed to monitor any absorption spectrum due to $S_2(^1\Delta)$ or SO ($^1\Delta$ or $^3\Sigma$) product formation. Under similar conditions reaction of $S(^1D_2)$ with OCS produced a short lived spectrum of $S_2(^1\Delta)$. The $S_2(^1\Delta)$

undergoes rapid collisional quenching to $S_2(^3\Sigma)$ which was also observed.

For the $O(^1D_2)$ + CO_2 reaction, theoretical calculations suggest that physical quenching is the most important removal process[14]. In the same study reaction analogous to (21) was found to become more important on moving to higher temperature. The ratio of quenching to reaction at 300 K was determined by Shortridge and Lin to highly favour the former[13]. Results of isotopic labelling experiments are consistent with a CO_3 complex[15,16]. Reaction of $O(^1D_2)$ with CS_2 has not been studied.

To summarise it appears that for the reaction of $S(^1D_2)/O(^1D_2)$ with CX_2 where X = S and/or O reaction with the symmetric molecules leads predominantly to quenching while reaction with the unsymmetric OCS yields in the main products from chemical reaction. With the limited theoretical and experimental knowledge available discussions of the reaction schemes must be highly speculative. Two general reaction mechanisms have been identified from molecular dynamics, namely; direct reaction and complex reaction. There is little doubt that physical quenching of an excited atomic state to its ground state is facilitated by complex formation. The longer the lifetime of the complex the greater the opportunity to curve cross from the singlet to triplet surfaces. Analogous to the CO_3 complex we may postulate the involvement of I to produce the desired well in the singlet potential surface.

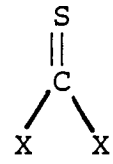

I

The relative contributions from quenching and reaction in such a system will be critically dependent on a number of, as yet, unknown factors:

a) The position of the crossing points of the singlet and triplet surfaces.

b) The geometry of the intermediate and how it varies for X=S and/or O. Certain bond angles may favour the elimination of a S-X fragment.

Further the dissociation of a complex depends on the density of states available in each product channel, which is in turn related to the energy available. Carbonyl sulphide is the only molecule of the three in which reaction to form spin allowed products is more exoergic than the quenching process.

The difference in the branching ratios, alternatively, may reflect a preference, in the OCS case, to react via a direct abstraction mechanism. This has been shown, from recent molecular beam studies, to be the reaction mechanism for $O(^3P_J)$ reaction with OCS and CS_2.[17]

ii) $\underline{N_2, O_2, CO, N_2O}$

Reaction of $S(^1D_2)$ with N_2 must proceed entirely by quenching to the ground state - no reactive channels being thermodynamically accessible. Quenching of $S(^1D_2)$ with N_2 is found to be approximately twice as fast as the analogous quenching of $O(^1D_2)$ (TABLE 7.2). This

variation in rate constant may reflect an increase in spin orbit coupling in the sulphur reaction facilitating easier singlet/triplet surface crossing. In reaction of $O(^1D_2)$ with N_2 a deep well, corresponding to N_2O, on the singlet surface facilitated curve crossing[18,19]. In reaction of $S(^1D_2)$ we would predict the involvement of an analogous N_2S intermediate.

TABLE 7.2 RATE DATA FOR REACTION OF $S(^1D_2)/O(^1D_2)$ WITH N_2, O_2, CO, N_2O

REACTANT	k/cm^3 molecule^{-1} s^{-1}		
	$S(^1D_2)$	$O(^1D_2)$	
	(see FIG 7.5)		
N_2	$5.0\pm1.0\times10^{-11}$	2.8×10^{-11}	30
O_2	$3.5\pm0.8\times10^{-11}$	3.7×10^{-11}	30
CO	$9.2\pm1.0\times10^{-11}$	3×10^{-11}	20
N_2O	$1.4\pm0.3\times10^{-10}$	1.1×10^{-10}	21

For the reaction of $S(^1D_2)$ with O_2 the following channels are available (24-28)

			ΔH/kJ mol^{-1}	
$S(^1D) + O_2(^3\Sigma_g)$	→	$SO(^3\Sigma) + O(^3P)$	-132.9	24
	→	$SO(^1\Delta) + O(^3P)$	-59.4	25
	→	$SO(^1\Sigma) + O(^3P)$	-7.1	26
	→	$S(^3P) + O_2(^3\Sigma)$	-111.2	27
	→	$S(^3P) + O_2(^1\Delta)$	-8.8	28

FIG 7.5: Pseudo First Order Rate Constants vs Reactant Pressure

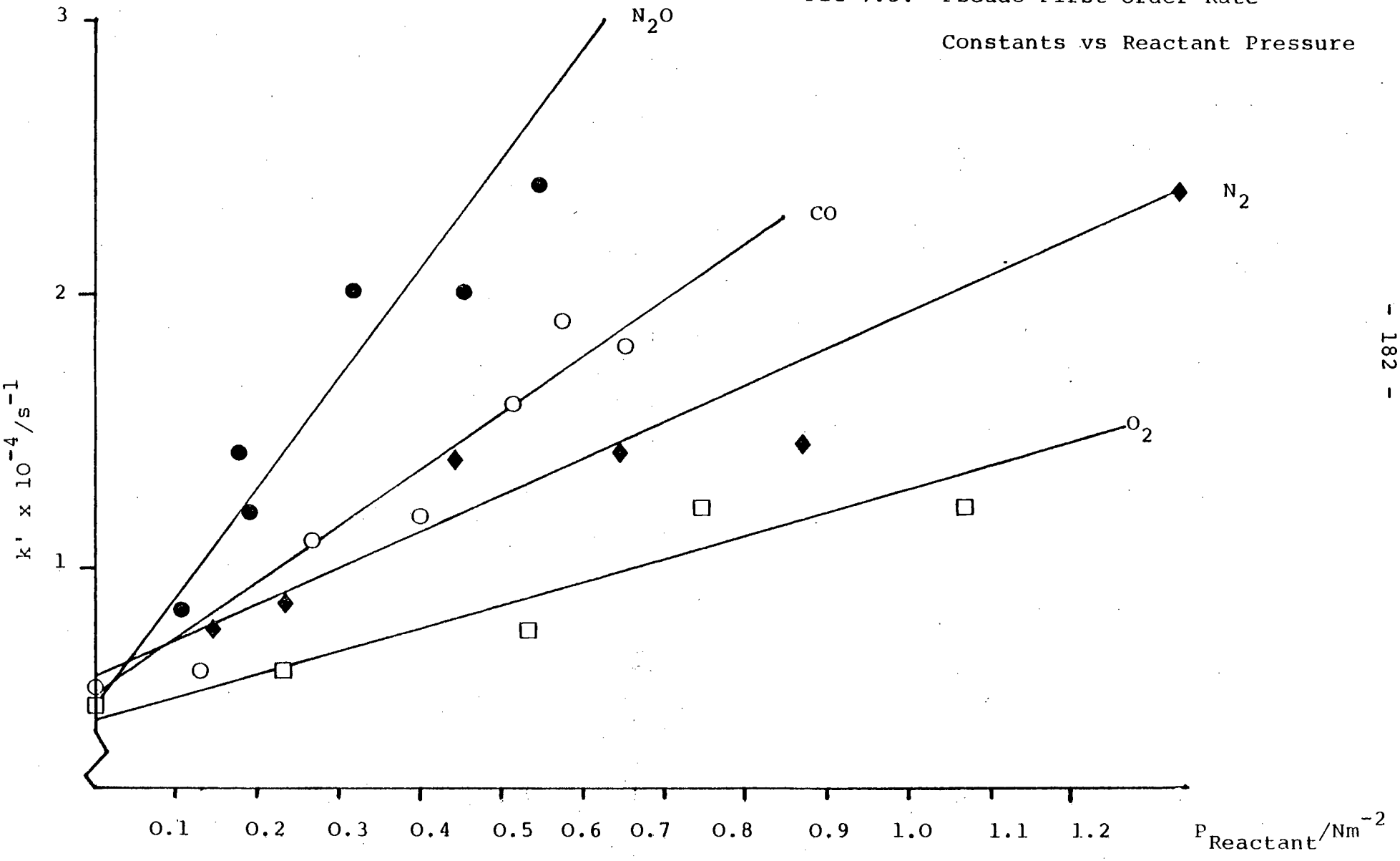

Reaction of $O(^1D)$ with oxygen is well documented. Controversy still exists however on the branching ratio into $O_2(b^1\Sigma_g^+)$ - analogous to (26). Recent work by Lee and Slanger[22] suggests it to be the major pathway with a branching ratio of 0.77 ± 0.2. The production of $O_2(^1\Delta_g)$ - analogous to (25) - appears to be a minor channel for $O(^1D_2)$ removal[23]. Reaction of $S(^1D_2)$ may proceed by two distinct pathways i.e. chemical reaction or physical quenching. Consideration of correlation diagrams (FIG 7.6) suggests channel (26) to be the only adiabatic correlation thermodynamically accessible. Various intermediates are available for the reaction of sulphur atoms with oxygen. On the singlet surface there is a deep minimum corresponding to SO_2 (ΔHf = 678 kJ mol^{-1}) above this lies a known triplet state of $SO_2(^3B_1)$ (ΔHf = 372 kJ mol^{-1}). One may also speculate on the possibility of an SOO transition state, distinct in the case of $S+O_2$, from the insertion mechanism. The correlation diagram suggests involvement of one of the SO_2 intermediates mentioned above to be unimportant. Further a consideration of inertial effects involved in the accommodation of sulphur between two oxygen atoms would tend to favour an 'end-on' approach. Clearly more work is needed to determine branching ratios and energy partitioning into the products before firm conclusions may be drawn.

The reaction of $O(^1D_2)$ with CO has received such attention[24,25]. Strong evidence suggests a CO_2 intermediate complex to be involved and hence provides a mechanism for efficient crossing from singlet to triplet

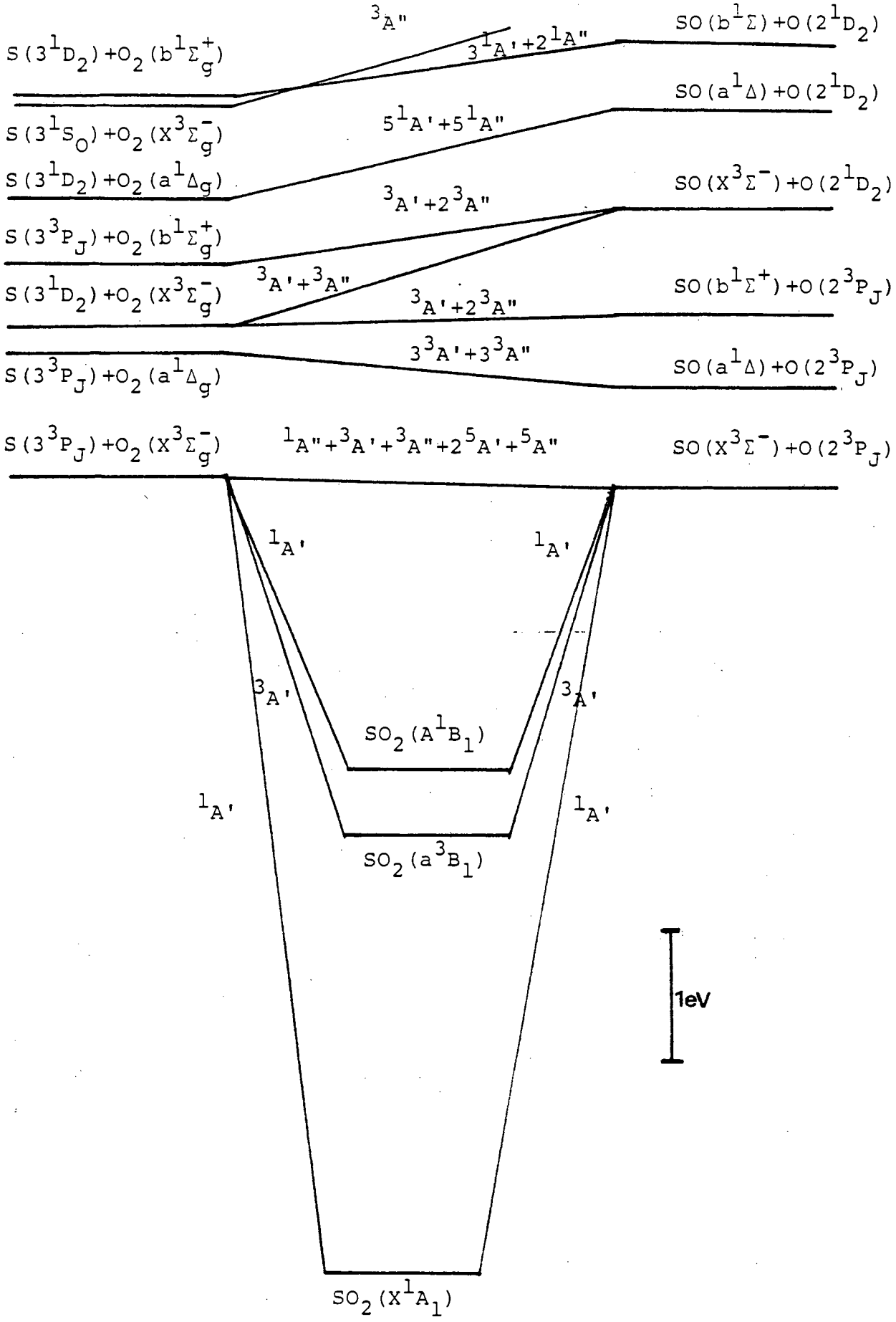

FIG 7.6 Correlation diagram connecting the states of $S+O_2$ and $SO+O$.

surfaces. The analogous reaction of $S(^1D)$ is expected to involve the OCS molecule as the reaction intermediate. Dissociation of the complex to yield oxygen atoms is endothermic and the rapid rate constant must represent efficient quenching of the $S(^1D_2)$ atoms to their ground state. The increased rate compared to the oxygen reaction may reflect an increase in spin orbit coupling due to participation of the heavier sulphur atom.

Reaction of $S(^1D_2)$ with N_2O may proceed by the following channels:

			ΔH/kJ mol^{-1}	
$S(^1D) + N_2O$	→	$N_2 + SO(^1\Delta)$	-224.0	29
	→	$N_2 + SO(^1\Sigma)$	-171.8	30
	→	$NS(^2\Pi) + NO(^2\Pi)$	+49.7±104.5	31
	→	$S(^3P) + N_2O$	-111.2	32

Donovan and Breckenridge have shown (32) to be the major removal channel following formation of an SN_2O intermediate[26]. $NS(^2\Pi)$ radicals were observed directly in the forementioned work but the branching ratio into channel (31) was adjudged to be low (<15%). Reactions (29 and 30) were also of minor importance (15±10%). The predominance of the quenching channel is in marked contrast to the results obtained for reaction of $O(^1D_2)$ with N_2O which was found to proceed in 1:1 ratio into channels (33) and (34)[27].

			ΔH/kJ mol^{-1}	
$O(^1D) + N_2O$	→	$N_2 + O_2$	-156.0	33
	→	NO + NO	-334.0	34

Boxall et al[28] have observed the NO fragments produced through channel (34) and found most of the energy released as translation with the small fraction in vibration being equally distributed in each NO fragment (as determined by isotopic labelling of the N_2O). Spectroscopic studies have established the existence of a stable dimer with a dissociation enthalpy of approximately 10 kJ mol^{-1}. From SCF calculations Boxall concluded that 'it was probable that only the lowest and possibly first excited singlet state of the dimer lay near or below the level corresponding to the $O(^1D_2)$ and N_2O reactants. The adoption of a recoil mechanism requires that the intermediate complex lies at a level much nearer the reactants than the products otherwise much of the potential energy would already have been released prior to the fragment separation'.

The similarity of the rate data for $S(^1D_2)$ and $O(^1D_2)$ leads one to expect similar mechanisms. This is clearly not the case. The explanation for the disparity between the reaction paths followed, may result from the relative positions of singlet and triplet surfaces correlating with varying ONNO and ONNS intermediates and also the lifetimes of the intermediates involved.

iii) <u>The Noble Gases</u>

Quenching of $S(^1D)$ by the rare gases has been studied. The results of this work are shown in TABLE 7.3 together with the analogous data for $O(^1D_2)$ and $Se(^1D_2)$.

TABLE 7.3: RATE DATA FOR THE QUENCHING OF $S(^1D_2)$ BY THE NOBLE GASES

Reactant	$k/cm^3 \cdot molecule^{-1} \cdot s^{-1}$		
	$O(^1D_2)$ [29,40]	$S(^1D_2)$	$Se(^1D_2)$ [31]
Xe	$7.2\pm1.4\times10^{-11}$	$1.2\pm0.2\times10^{-11}$	$6.7\pm3.0\times10^{-11}$
Kr	$6.6\pm1.0\times10^{-12}$	$1.9\pm0.4\times10^{-11}$	$2.3\pm1.2\times10^{-11}$
Ar	$3\pm2\times10^{-13}$	$1.5\pm0.3\times10^{-11}$	$7.0\pm4.9\times10^{-12}$
Ne	$5\pm2\times10^{-14}$	$1.3\pm0.3\times10^{-13}$	$\approx4\times10^{-13}$
He	$\leq7\times10^{-16}$	$\leq1.5\times10^{-14}$	$\approx3\times10^{-14}$

Explanation of the $O(^1D)$ quenching results were first proposed by Donovan and Husain as early as 1970[18]. However it was not until 1977 that calculations by Dunning and Hay[30] using ab initio C.I. techniques provided quantitative evidence as to the shapes of the potential energy surfaces, proposed to be of importance by Donovan and Husain. More recently the explanations invoked for $O(^1D)$ have been extended to cover the quenching of $Se(^1D)$ by the rare gases[31].

The form of the calculated surfaces, for the $O(^1D)$ reaction with Xe, are shown in FIG 7.7. With reference to FIG 7.7 all the potential curves with the exception of the $^1\Sigma^+$ curve in XeO and KrO are found to be repulsive. The binding in the $^1\Sigma^+$ state has in part been assigned to the incorporation of $Rg^+ + O^-$ character in the RgO intermediate and increases in the series:

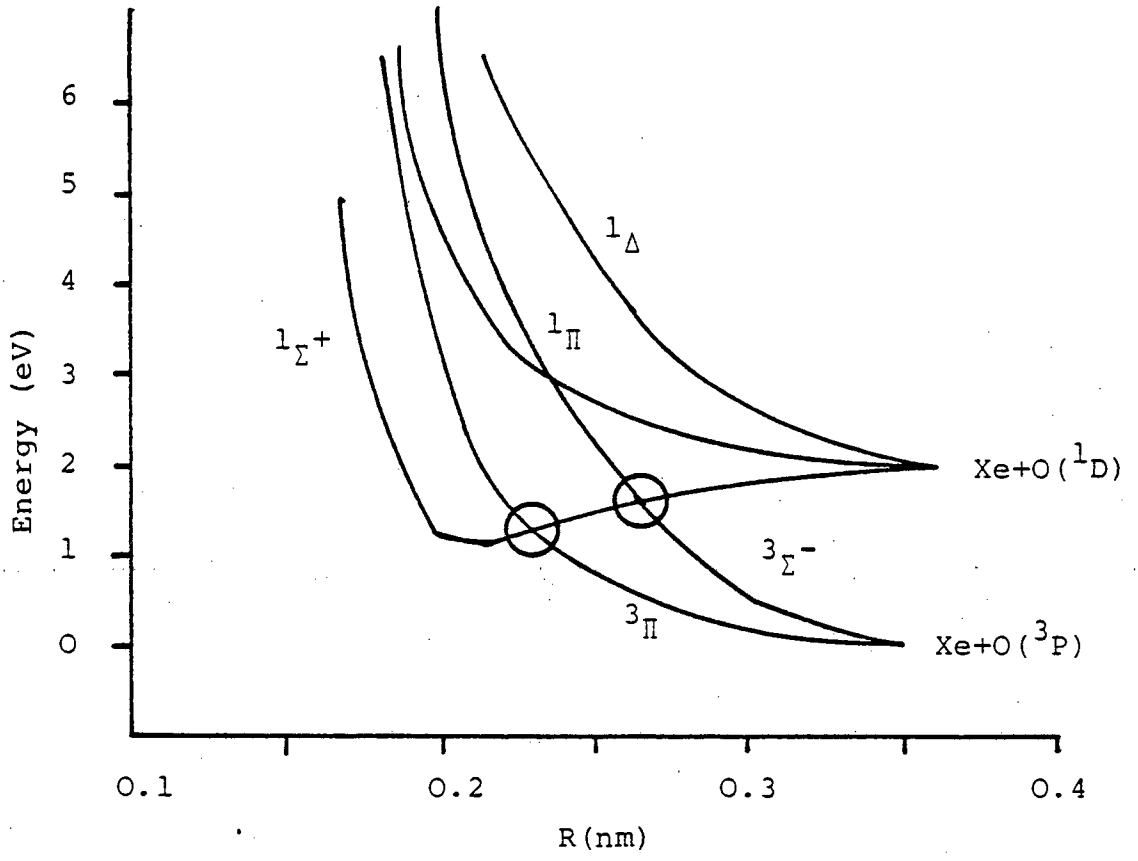

FIG 7.7: Potential Energy Curves for XeO, Following Dunning & Hay. The Two Crossing Points of Interest for Thermal Collisions (300 K) With Xe are Circled.

NeO(unbound) < ArO(flat) < KrO(De = 0.25 eV) < XeO(De = 0.70 eV

It follows from this data that quenching of the Group VI ($^1D_2$) state by the rare gases is dependent on two important factors:

i) The accessibility, at thermal temperatures, of crossings between the triplet and singlet surfaces.

ii) The probability of crossing onto the triplet surface on passage through the crossing region of the potential surface.

The first of these criteria is dealt with in the work of Dunning and Hay. From their calculations it was concluded that the accessibility of the crossing regions was directly related to the amount of charge transfer (Rg^+O^-) character in the transition RgO state. The stability of Rg^+O^- will increase with increasing electron affinity and decreasing ionisation energy. With reference to TABLE 7.4 it is observed that movement from oxygen to sulphur results in an increase in electron affinity which may facilitate for Ar^+S^- a slight well not observable in the Ar^+O^- example. In the case of Ne^+S^- the large variation in ionisation energy in moving from argon to neon is unlikely to be overcome by the increased electron affinity of the sulphur.

The probability of crossing may be represented by the Landau-Zener model. The thermal cross section for such a non-adiabatic process is given by equation 7.1, although more involved formulations also exist.

TABLE 7.4

A) FIRST IONISATION ENERGIES OF THE NOBLE GASES

Element	I.E./kJ mol^{-1}
Helium	2370
Neon	2080
Argon	1520
Krypton	1350
Xenon	1170

B) ELECTRON AFFINITY

Element	E.A./kJ mol^{-1}
Oxygen	-142
Sulphur	-200

$$\sigma = \pi R_o^2 \langle P_o \rangle \exp \frac{-\Delta E_o}{kT} \qquad 7.1$$

k = Boltzmann constant

ΔE_o = Energy barrier due to repulsion of the colliding species at R_o

$\langle P_o \rangle$ = Mean transition probability between the potential surfaces at R_o, calculated from P_o on the basis of the transition state method.

In the case of a two atom system, the intersection point must be crossed twice and P_o, the net transition probability, is related to the probability for non-adiabatic transitions P_{12} by the expression (7.2).

$$P_o = 2P_{12}(1-P_{12}) \qquad 7.2$$

For non-adiabatic transitions between potential surfaces of different symmetry we may express P_{12} in the form (7.3).

$$P_{12} = \frac{2\pi\omega^2 C_{12}^2}{h\nu|F_1-F_2|} \qquad 7.3$$

ν = relative velocity due to the radial motion

F_1, F_2 are the slopes of the two surfaces at R_o

ω = angular velocity

C_{12} = coupling matrix element, between surfaces 1 and 2.

From equation 7.2 it can be seen that P_o maximises when $P_{12} = 0.5$, hence maximising the thermal cross section ($\bar{\sigma}$). From equation 7.3 it may be qualitatively observed that P_{12} shall be increased due to an increase in C_{12} on moving from He to Xe and O to S (due to the increase in spin orbit coupling). The power dependence of this term would suggest it to outweigh any counter effect from an increase in the $|F_1-F_2|$ term due to the increase in the attractive nature of the $1\Sigma^+$ state. However the exact size of these numbers is not known at the present and an evaluation of a trend in σ due to variations in P, bearing in mind the parabolic nature of the relationship between

P_{12} and P_o is very speculative.

From the experimental data for $S(^1D_2)$ we would suggest the difference in rate between Ar and Ne to reflect the inaccessibility of the crossing points in the latter case. The similarity in rates between Xe, Kr and Ar could either be attributed to a maximisation of P_o (rejected on the basis of the $O(^1D_2)$ + Xe result) or rather a fine balance between the conflicting factors affecting P_{12}. These results appear to be consistent with those found for $Se(^1D_2)$ quenching by the noble gases.

iv) H_2S and H_2O

The comparative rates of removal of $S(^1D_2)$ by the molecules H_2O and H_2S provide a subtle insight into the competition between various exit channels to reaction and their relationship to the overall bulk rate constant. The electronic nature of the potential surface for the $S(^1D_2)$ + H_2S system should be very similar to that describing $S(^1D_2)$ + H_2O. As can be seen from the thermochemistry shown in FIG 7.8 the reactive path leading to SH formation in the latter system is thermodynamically forbidden. Comparison of the rate data for the above reaction with the analogous reaction of $O(^1D_2)$ reflects the variation in available product channels.

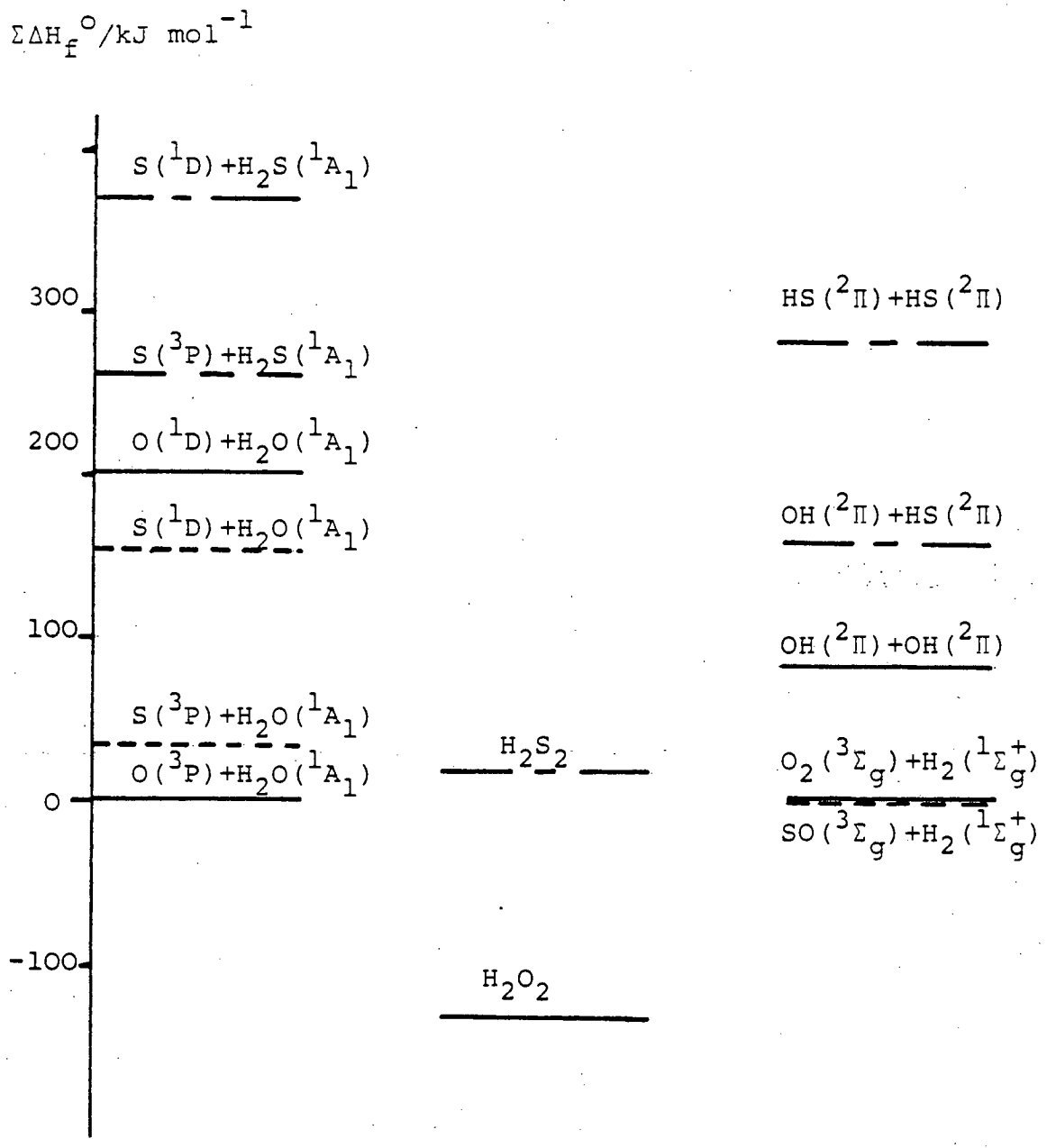

FIG 7.8: Energy Level Diagram of Reactants, Intermediates and Products for the Reaction of $O(^1D)$ and $S(^1D)$ with H_2O and H_2S.

$$k_{O(^1D)+H_2O} = 2.3\times10^{-10} \text{ cm}^3 \text{ molecule}^{-1} \text{ s}^{-1}$$ 30

$$k_{S(^1D)+H_2O} = 3.4\pm0.8\times10^{-11} \text{ cm}^3 \text{ molecule}^{-1} \text{ s}^{-1}$$

$$k_{S(^1D)+D_2O} = 2.0\pm1.5\times10^{-11} \text{ cm}^3 \text{ molecule}^{-1} \text{ s}^{-1}$$

$$k_{S(^1D)+H_2S} = 3.3\pm0.6\times10^{-10} \text{ cm}^3 \text{ molecule}^{-1} \text{ s}^{-1}.$$

Reaction of $O(^1D_2)$ with H_2O has been shown by Engleman[33] to produce one vibrationally hot OH leaving the remaining hydroxyl radical relatively cold. Such energy partitioning is indicative of an abstraction reaction. Simonaitis and Heicklen[34] have found that <4% of collisions at 373 K result in quenching to $O(^3P_J)$ in reaction of $O(^1D_2)$ with H_2O. The rate of reaction of $S(^1D_2)$ with H_2S is very similar to that of $O(^1D_2)$ with H_2O and seems likely to reflect the involvement of similar reactive channels.

In the reaction of $S(^1D_2)$ with H_2O H-atom abstraction is forbidden by thermodynamic constraints. It would be expected that the collision process would sample a well on the potential energy surface corresponding to H_2SO formation. The only spin allowed exit channel leads to formation of H_2 and $SO(^1\Delta)$. Spin forbidden exit channels lead to physical quenching or production of the ground state molecular products, H_2 and SO. It seems likely that the reactive channels will possess sizeable activation energies, considering the molecular rearrangement involved. We, therefore, postulate

that the rate constant reflects the probability of $S(^1D_2)$ being quenched, by H_2O, to its ground state. This channel we believe to be facilitated by the involvement of a H_2SO complex.

v. The Halogens and Halomethanes

Reaction of $S(^1D)$ with both the halogens and fluorocarbons are rapid and increase with the size of the halogen atom (TABLE 7.5).

TABLE 7.5: RATE DATA FOR REACTION OF $S(^1D_2)+CF_3X/X_2$

X	k/cm^3 molecule^{-1} s^{-1}	
	CF_3X (see FIG 7.9)	X_2
F	$9.0\pm1.0\times10^{-13}$	-
Cl	$8.4\pm1.0\times10^{-11}$	$1.4\pm0.3\times10^{-10}$
Br	$1.2\pm0.3\times10^{-10}$	$1.4\pm0.3\times10^{-10}$
I	$2.1\pm0.4\times10^{-10}$	$2.1\pm0.4\times10^{-10}$

The thermochemistry is sufficiently similar (although data on SX is very limited) to suggest similar reaction mechanisms to operate in each class of compounds (with the exception of CF_4). As such the gradation in rate constants likely arises due to:

a) the increase in the collision number on moving to larger molecules and/or

b) an increase in attractive dispersion forces the magnitudes of which are proportional to polarizability.

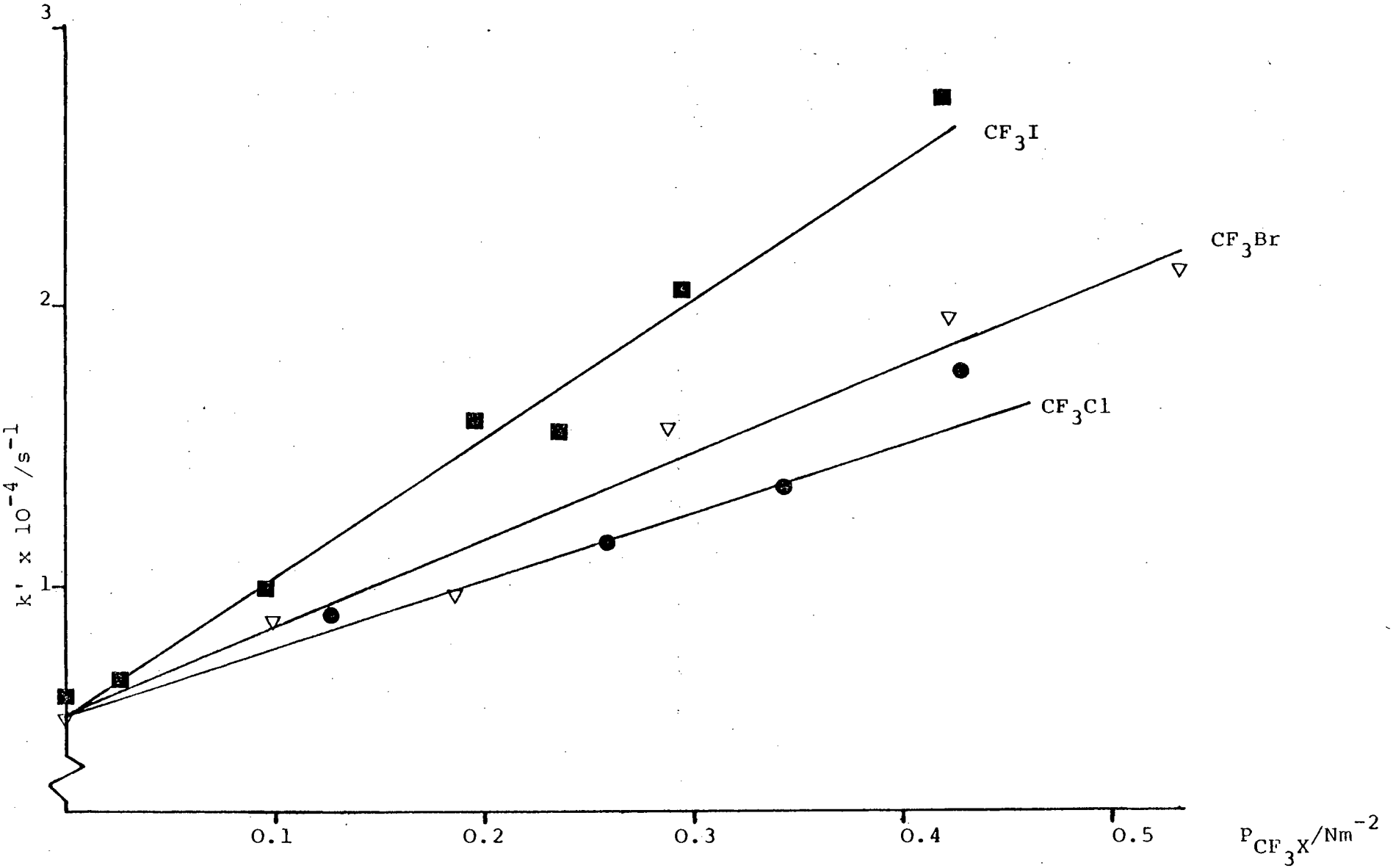

FIG 7.9: Pseudo First Order Rate Constants vs Pressure of Perfluoroalkyl Halide.

Reaction of $O(^1D_2)$ with both the halocarbons and halogens are also rapid. Reaction of $O(^1D_2)$ with CF_3Cl has been shown to proceed in the main through chlorine atom abstraction[35]. Similarly in a different study,[36] reaction of $O(^1D)$ with chlorine, ClO ($v"<9$) has been observed as the primary product in 90±10% of all reactive collisions.

The rate constant for reaction of $S(^1D_2)$ with CF_4, where no obvious reactive channel is available, is two orders of magnitude lower than the other halocarbons and halogens studied. This quenching reaction is however one order of magnitude slower than the analogous $O(^1D_2)$ reaction.

$$k_{O(^1D_2)+CF_4} = 1.7\pm0.3\times10^{-11} \text{ cm}^3 \text{ molecule}^{-1} \text{ s}^{-1}$$ [37]

This, if true, would be highly surprising and deserves a reappraisal of the $O(^1D_2)$ data.

vi <u>The Organic Molecules:- CH_4, C_2H_6, C_6H_6, C_6F_6</u>

For the alkanes, alkenes and arenes reaction with $S(^1D_2)$ is very rapid.

For reaction of $S(^1D_2)$ with ethane and higher homologues of the alkane series the only experimental products observed are the alkyl mercaptans[1]. Where more than one product is possible, product formation is purely statistical in the number of hydrogen atoms available. The role of collisional deactivation of $S(^1D_2)$ to the ground state is also of some importance in these systems. In the case of $S(^1D_2)$ reaction with methane,

established in this work to have a rate constant

$$k_{S(^1D)+CH_4} = 1.2\pm0.3\times10^{-10}\ cm^3\ molecule^{-1}\ s^{-1},$$

product analysis indicates that the hot mercaptan initially produced is not collisionally stabilised and falls apart to give a variety of products[1]. Product formation appears most consistent with RS-H bond scission as opposed to the more thermodynamically favourable R-SH bond scission. The behaviour of $S(^1D_2)$ with the alkanes is analogous to that of $O(^1D_2)$ and singlet methylene, both in rate and mechanism of reaction.

Reaction of $S(^1D_2)$ with olefins has a number of reactive channels available (35-39)[1]:

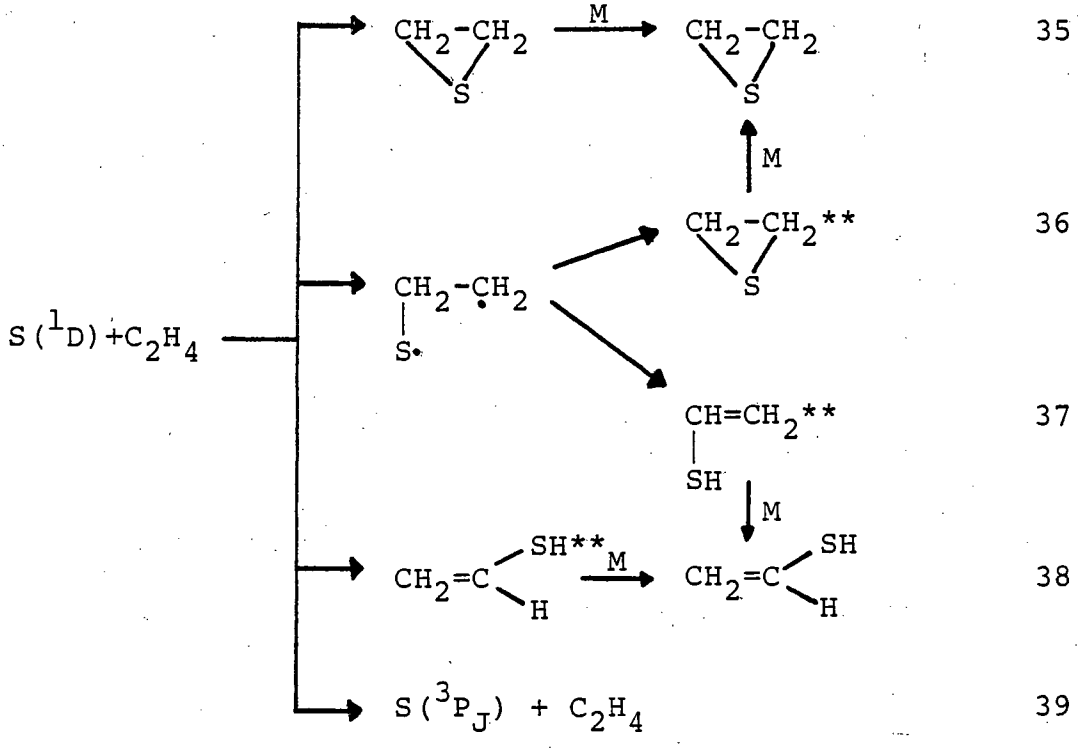

The overall rate constant for removal of $S(^1D_2)$ atoms by ethylene was established to be very rapid.

$$k_{S(^1D)+C_2H_4} = 3.2\pm0.6\times10^{-10} \text{ cm}^3 \text{ molecule}^{-1} \text{ s}^{-1}$$

Early work[1] involving end product analysis in systems at high pressure ($\geq$13 kNm^{-2}) has yielded the following information. Reaction of ground state sulphur atoms leads to episulphide formation but not to vinylic mercaptans. Reaction of $S(^1D_2)$ yields both mercaptan and the episulphide products - although the latter product may arise from secondary reaction of $S(^3P)$ atoms. The majority of experimental evidence[1] suggests vinylic mercaptan formation involves a singlet biradical intermediate. Rapid isomerisation through a hydrogen atom shift then yielding the final product. It was noted that methyl and fluoro substituents on the carbon suppressed vinylic mercaptan formation.

Reaction of $S(^1D_2)$ with benzene is also very fast (see FIG 7.10)

$$k_{S(^1D)+C_6H_6} = 3.5\pm0.6\times10^{-10} \text{ cm}^3 \text{ molecule}^{-1} \text{ s}^{-1}$$

Four possible reaction pathways may be envisaged (40-43).

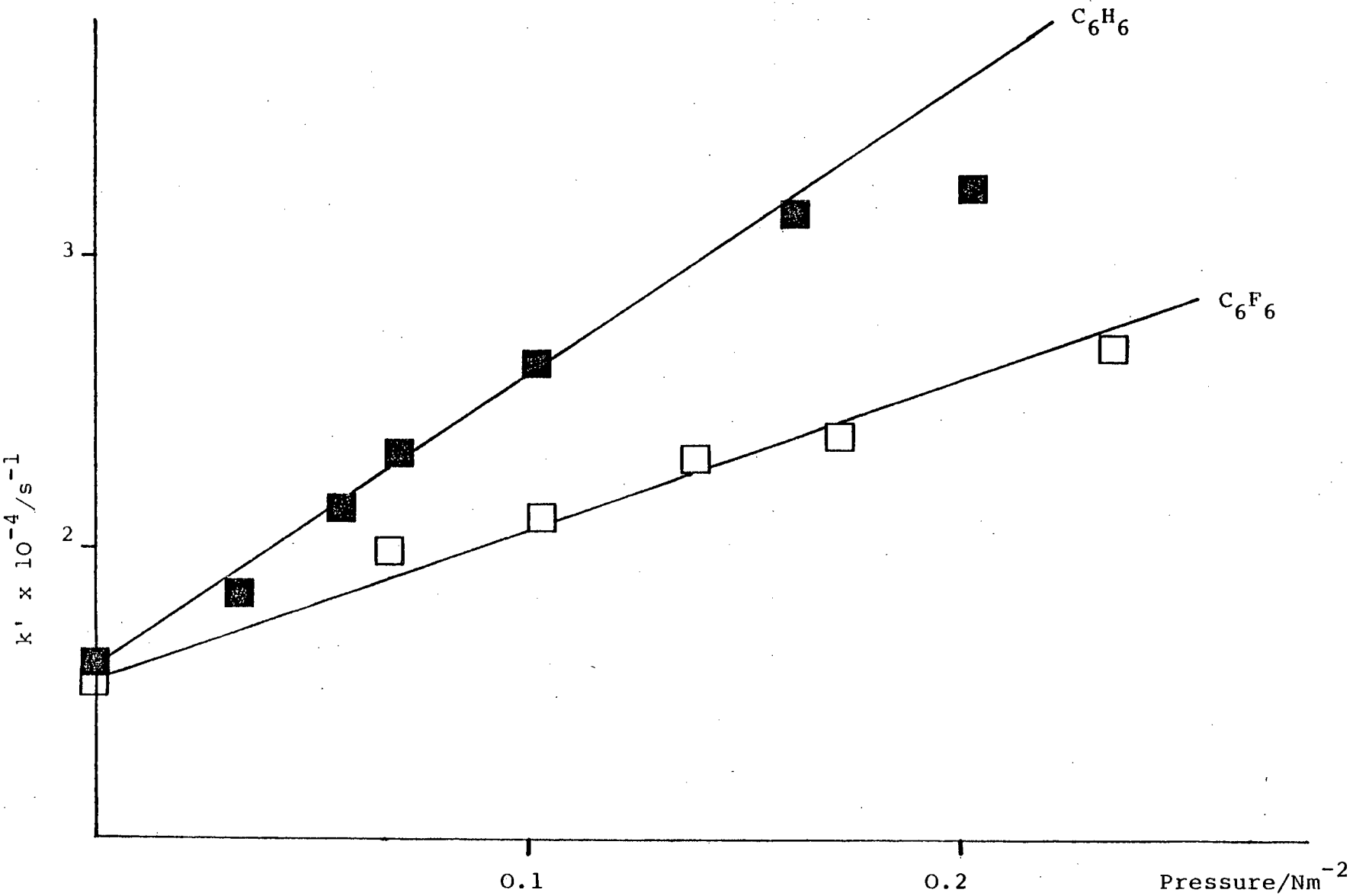

FIG 7.10: Pseudo First Order Rate Constants vs Reactant Pressure

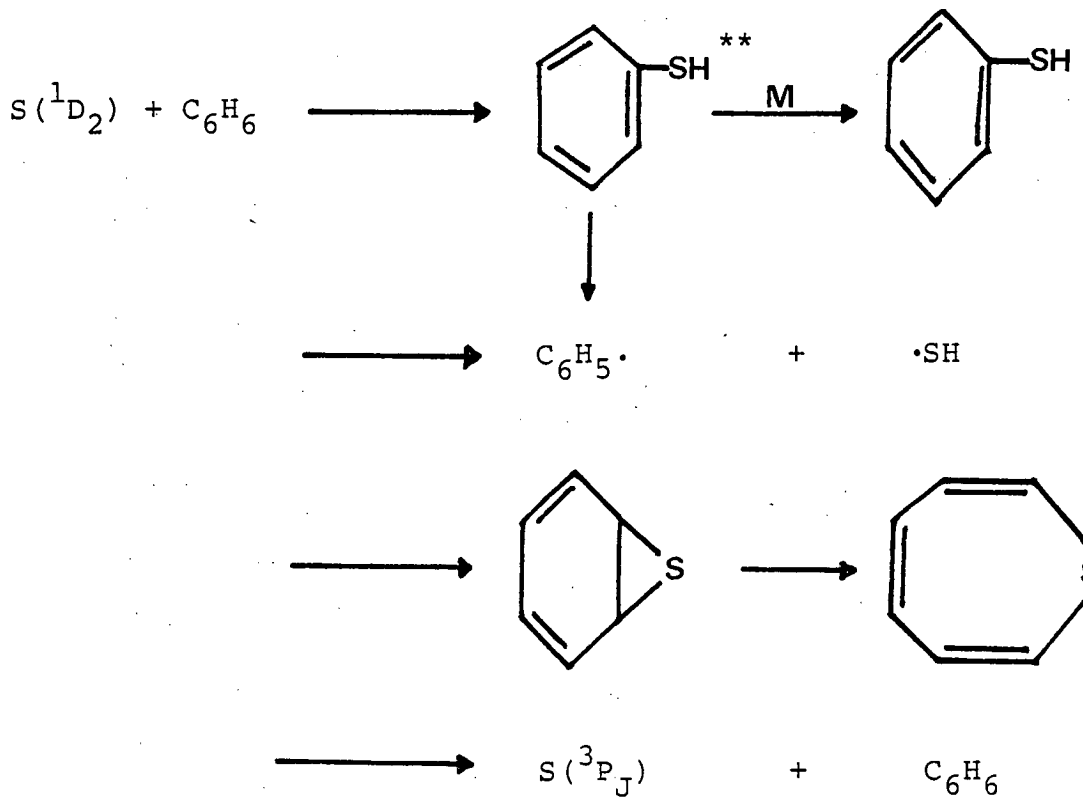

The formation of the thiophenol molecule (40) may involve direct insertion of the sulphur atom into the C-H bond or alternatively it may result from a biradical intermediate of the type postulated in the reaction of $S(^1D_2)$ atoms with C_2H_4 (reactions 36 and 37). The alternative product from the biradical would be that illustrated in reaction (42) (cf. episulphide formation in the ethylene reaction). The enhanced nature of the ethylene and benzene reactions compared with the alkane reaction suggests participation of the π orbitals in the transition state, hence we speculate channel (41) to be minor. Similarly due to the very rapid nature of $S(^1D_2)$ removal it would seem unlikely that channel (42) would play a major role.

In comparison to the reaction with benzene the rate of removal of $S(^1D_2)$ with fluorobenzene was measured

$$k_{S(^1D)+C_6F_6} = 1.9\pm0.3\times10^{-10} \text{ cm}^3 \text{ molecule}^{-1} \text{ s}^{-1}$$

This decrease in rate, compared to the benzene reaction, may be attributable to two factors:

a) the decrease in rate constant may reflect the relative importance of channel (40) to the overall rate constant or

b) if reaction (41) were the dominant reactive channel in each case i.e. C_6H_6 and C_6F_6, then the electron withdrawing effect of the fluorines would lower the reactivity of the benzene ring.

In a study of the reaction of methylene radicals with benzene[38] products analogous to channels (40) and (42) were obtained both in the liquid and gaseous phases. Whether either product was specifically the result of singlet or triplet attack was unclear.

7.5 CONCLUSIONS

This work presents the first absolute rate data for a large series of $S(^1D_2)$ reactions. The results of the study should be considered more accurate than previously monitored relative rate data[39]. In general, unless thermodynamically unfavourable channels exist (e.g. H_2O), the rate of reaction of $S(^1D_2)$ closely parallels the analogous $O(^1D_2)$ removal rates. Whether this analogy follows in product ratios is largely a matter of conjecture deserving more detailed experimental study.

7.6 REFERENCES

1. H.E. Gunning and O.P. Strausz, Advances in Photochemistry 4, (1966), 143.
2. V.P. Aneja, T.H. Overton, L.T. Cupitt, J.L. Durham and W.E. Wilson, Nature 283, (1980), 55.
3. R.P. Turco, R.C. Whitten, O.B. Toon, J.B. Pollack, P. Hamill, Nature 283, (1980), 283.
4. J.C.G. Walker, 14th Informal Conf. on Photochemistry, Newport Beach, California, March/April, 1980.
5. R.F. Heidner III and D. Husain, Int. J. Chem. Kinet. 5, (1973), 819.
6. K.S. Sidhu, I.G. Csizmadia, O.P. Strausz and H.E. Gunning, J. Am. Chem. Soc. 88, (1966), 2412.
7. W.H. Breckenridge and H. Taude, J. Chem. Phys. 53, (1970), 1750.
8. A.B. Callear, Proc. Roy. Soc. (Lond.) A276, (1963), 401.
9. M.J. Kurylo, N.C. Peterson and W. Braun, J. Chem. Phys. 54, (1971), 943.
10. R.J. Donovan, L.J. Kirsch and D. Husain, Nature 222, (1969), 1165.
11. K. Schofield, J. Photochem. 9, (1978), 55.
12. P.R. Jones and H. Taube, J. Phys. Chem. 77, (1973), 1007.
13. R.G. Shortridge and M.C. Lin, Chem. Phys. Lett., 35, (1975), 146.
14. J.G. Tully, J. Chem. Phys., 62, (1975), 1893.
15. H. Yamazaki and R.J. Cvetanovic, J. Chem. Phys. 40, (1964), 582.

16. D.L. Baulch and W.H. Breckenridge, Trans. Faraday Soc. 62, (1966), 2768.

17. D.S.Y. Hsu, W.M. Shaub, T.L. Burks and M.C. Lin, Chem. Phys. 44, (1979), 143.

18. R.J. Donovan and D. Husain, Chem. Rev. 70, (1970), 489.

19. J.C. Tully, J. Chem. Phys. 61, (1974), 61.

20. Reaction Rate and Photochemical Data for Atmospheric Chemistry (1977), NBS Publication 513, Edited by R.F. Hampson Jr. and D. Garvin.

21. J.A. Davidson, H.I. Schiff, G.E. Streit, J.R. McAfee, A.L. Schmeltekopf and C.J. Howard, J. Chem. Phys. 67, (1977), 5021.

22. L.C. Lee and T.G. Slanger, J. Chem. Phys. 69, (1978), 4053.

23. M. Gauthier and D.R. Snelling, J. Chem. Phys. 54, (1971), 4317.

24. R.G. Shortridge and M.C. Lin, J. Phys. Chem. 78, (1974), 1451.

25. R.G. Shortridge and M.C. Lin, J. Chem. Phys. 64, (1976), 4076.

26. R.J. Donovan and W.H. Breckenridge, Chem. Phys. Lett. 11, (1971), 520.

27. P.M. Scott, K.F. Preston, R.J. Andersen and L.M. Quick, Can. J. Chem. 49, (1971), 1808.

28. C.R. Boxall, J.P. Simmon and P.W. Tasker, Faraday Disc. Chem. Soc., 53, (1972), 216.

29. J.A. Davidson, H.I. Schiff, T.J. Brown, G.E. Streit and C.J. Howard, J. Chem. Phys. 69, (1978), 1213.

30. T.H. Dunning Jnr. and P.J. Hay, J. Chem. Phys. 66, (1977), 3767.

31. R.J. Donovan and D.J. Little, Chem. Phys. Lett. 53, (1978), 394.

32. G.E. Streit, C.J. Howard, A.L. Schmeltekopf, J.A. Davidson and H.I. Schiff, J. Chem. Phys. 65, (1976), 4761.

33. R. Engleman Jr., J. Am. Chem. Soc. 87, (1965), 4193.

34. R. Simonaitis and J. Heicklen, J. Phys. Chem. 77, (1973), 1096.

35. H.M. Gillespie, J. Garraway and R.J. Donovan, J. of Photochem. 7, (1977), 29.

36. K. Freudenstein and D. Biedenkapp, Berichte Der Bunsen-Gersellschaft 80, (1976), 42.

37. I.S. Fletcher and D. Husain, J. Phys. Chem. 80, (1976), 1837.

38. W. Von E. Doering and L.H. Knox, J. Am. Chem. Soc. 75, (1953), 297.

39. D.J. Little, A. Dalgleish and R.J. Donovan, Faraday Disc. of the Chem. Soc. 53, (1972), 211.

40. S.R. Kinnersly, J.N. Murrell and W.R. Rodwell, J.C.S Faraday Trans. 2, 74, (1978), 600.

CHAPTER VIII

RESONANCE FLUORESCENCE STUDY OF $S(3^1D_2)$ ATOM KINETICS

8.1 INTRODUCTION

The advantages of the resonance fluorescence detection system are widely recognised[1] and were discussed briefly in Chapter 2. In exploiting these advantages much work has been undertaken on ground state atomic reactions[2,3] using the time resolved resonance fluorescence technique. The study of excited states, using this technique, has however been limited to the study of the first excited state of the iodine atom $[I(5^2P_{1/2})]$[1,4]. The reticent use of resonance fluorescence for detection of excited electronic states is easily understood. In order to maximise light intensity incident on the photomultiplier monochromators are not generally used for wavelength selection. In the study of the ground state this is unimportant since upper state species may be removed from the system by ensuring rapid quenching with a buffer gas. In attempting to observe an excited state one must ensure that the ground state fluorescence is either not excited or not detected, in general the more reactive nature of the upper state prevents preferential removal of the ground state from the system. Work in this laboratory on $I(5^2P_{1/2})$ used a cut-off filter to eliminate ground state excitation.

An air gap between the resonance cell and atomic lamp allowed transmission of the 206.2 nm atomic line exciting the $I(6s(^2P_{3/2}) \leftarrow 5p(^2P_{1/2}))$ transition but blocked the corresponding ground state transition $I(5p^4 6s(^2P_{3/2}) \leftarrow 5p^5(^2P_{3/2}))$ at 178.3 nm. This study extends the work on excited states by application of resonance fluorescence to the detection of $S(3^1D_2)$ atoms. The success of this technique where the absorption by and emission to the upper $^1D_2$ state lies at shorter wavelengths than the ground state depends on two principles for suppression of the ground state fluorescence: (1) the strong reversal associated with the ground state atomic lines generated by a microwave discharge flow lamp and (ii) the use of an extreme solar blind photomultiplier which possesses a sharp fall off in photocathode sensitivity between the wavelengths associated with the upper and lower states (see FIG 8.1). Preliminary work in which a gas filter was used to supplement this effect will also be mentioned.

8.2 EXPERIMENTAL

The apparatus was described in detail in Chapter 2 and is shown schematically in FIG 2.5. $S(3^1D_2)$ atoms were generated by laser photolysis of CS_2 at 193 nm. The laser output is compared to the CS_2 absorption profile in FIG 8.2. For all kinetic experiments the laser energy ranged from 0.8-1.8 mJ while the CS_2 was kept constant at 0.1 Nm^{-2} (for the

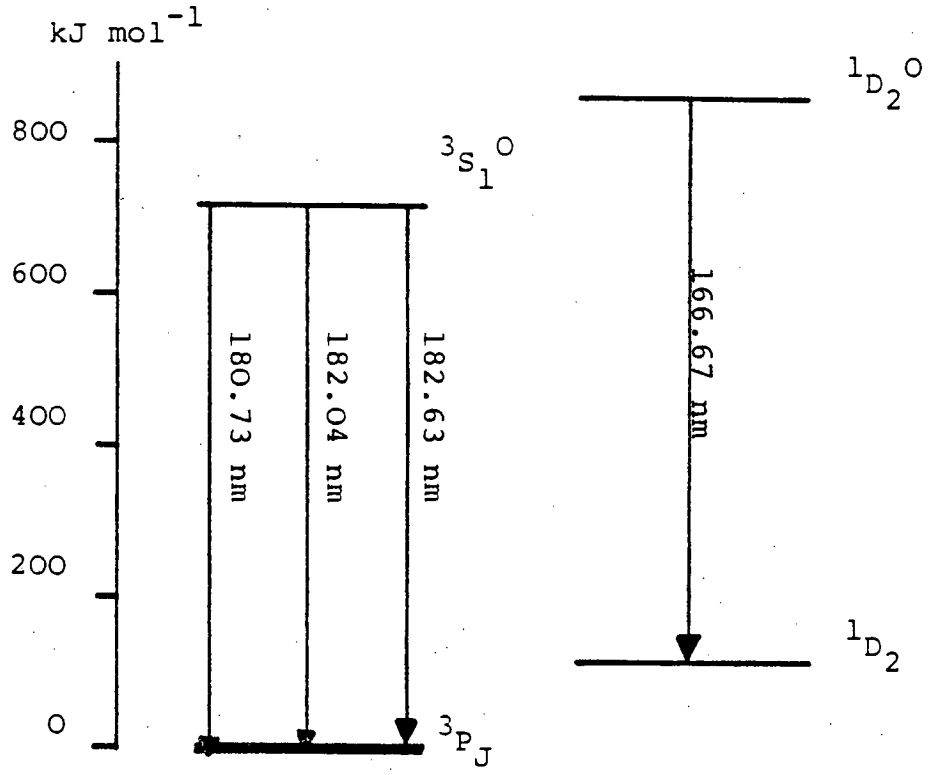

FIG 8.1 Energy level diagram for sulphur atomic states.

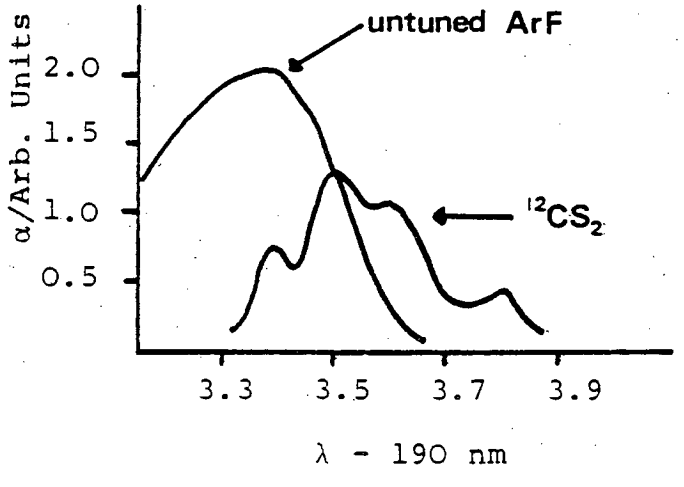

FIG 8.2 ArF laser output compared to $^{12}CS_2$ absorption structure

$S(^1D)+CS_2$ kinetic study CS_2 pressures ranged from 0.07-0.4 Nm^{-2}). The total pressure in the reaction vessel was maintained at 0.67 kNm^{-2} by the addition of research grade helium, as a buffer gas. The atomic radiation used to excite fluorescence was generated by flowing a mixture of H_2S (2%) in He (P $\sim$ 266 Nm^{-2}) through a microwave powered discharge operating at an incident power of 50 W.

Ideally the microwave discharge should be optimised such that the absolute rate of absorption of radiation by $S(3^1D_2)$ atoms is maximised while that of the $S(3^3P_J)$ atoms is minimised. In practise time did not permit the thorough determination of lamp conditions needed to maximise the ratio $I_f(S(^1D_2))/I_f(S(^3P_J))$. Rather information gained from the absorption work was used. Reference to FIG 2.10 illustrates the effect of varying H_2S concentration in the flow mixture on output intensity and absorption. As the pressure of H_2S increases it is observed that due to self reversal the percentage absorption decreases hence we may expect the rate of absorption to decrease. It should be noted that the rate of absorption is a function of the intensity at the line centre not the emission wings (see FIG 2.8A) which is the predominant cause of the increase in intensity in FIG 2.10A. Hence the 2% H_2S flow mixture should greatly reduce sensitivity to $S(3^3P_J)$ atom concentration. These principles extrapolated from absorption data have been observed experimentally with $O(^3P_J)$ resonance fluorescence (pp 129 Chapter 5). Due

to the rapid reaction with H_2S and wall removal of $S(^1D_2)$ it is expected that transitions terminating on the first excited $S(^1D_2)$ state will be essentially unreversed. In such a case the intensity at the line centre and hence the rate of absorption should mirror the trend observed in FIG 2.10A. It is therefore believed that the lamp conditions used strongly favour observation of $S(^1D_2)$ fluorescence over ground state fluorescence.

The extreme solar blind photomultiplier used was the EMR 542 model, reference to FIG 2.12 indicates that it discriminates strongly ($\sim$5x) in favour of the 166.7 nm line associated with fluorescence from $S(^1D_2)$, relative to that from $S(^3P_J)$ at 180.7-182.6 nm. The output from the photomultiplier was recorded by a transient recorder/signal averager combination. All kinetic traces recorded were averaged over sixteen shots.

Some work has been carried out employing an H_2S gas filter (5 cm path length) in front of the photomultiplier to further discriminate against the $S(^3P_J)$ transitions. Work with the vacuum monochromator system (FIG 2.2) established 29% attenuation of the $S(^1D_2)$ transition at 166.7 nm as compared with 75% attenuation of the $S(^3P_J)$ transition at 180.7 nm (P_{H_2S} = 66 Nm^{-2}, path length $\approx$60 cm).

8.3 RESULTS AND DISCUSSION

FIG 8.3 illustrates the decay of $S(3^1D_2)$ observed by resonance fluorescence at 166.7 nm. CS_2 photolysed at 193 nm was found to be an ideal source of $S(^1D_2)$.

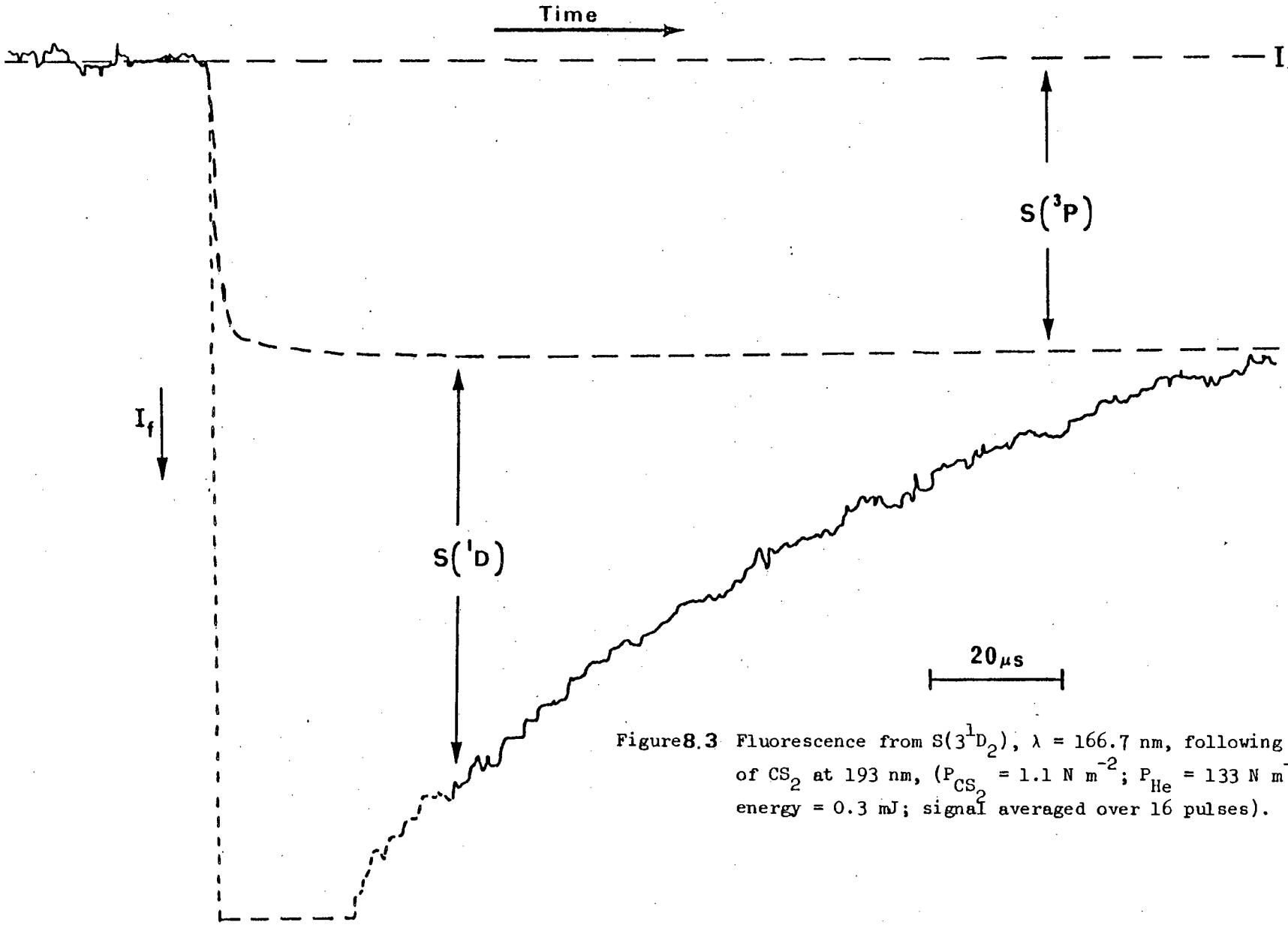

Figure 8.3 Fluorescence from $S(3^1D_2)$, λ = 166.7 nm, following photolysis of CS_2 at 193 nm, (P_{CS_2} = 1.1 N m^{-2}; P_{He} = 133 N m^{-2}; laser energy = 0.3 mJ; signal averaged over 16 pulses).

The residual fluorescence monitored after the decay of the $S(^1D_2)$ atom concentration is due to the $S(^3P_J)$ atom concentration in the system which remains essentially constant within the time scale of the experiment. Observation at longer times shows its decay kinetics to be consistent with those expected for $S(^3P_J)$ in such an environment and the baseline eventually ($\approx$50 ms) returns to its pre-trigger level. The large (S^3P_J) signal is indicative of a large primary yield of $S(^3P_J)$ from the photolysis of CS_2 at 193 nm. In order to obtain an indication of the quantitative yield of $S(^1D)$ relative to $S(^3P_J)$ the following experiments were performed:

(1) $S(^3P_J)$ yields were qualitatively compared after reaction of $S(^1D)$ with CS_2 and CH_4. The former is thought to predominantly quench $S(^1D_2)$ to its ground state[5] whereas in the latter the major reaction is insertion into the C-H bond resulting in a loss of sulphur atoms from the system[6]. In the experiments carried out very little variation in $S(^3P_J)$ yields were observed.

(2) As N_2 is a very efficient quencher of $S(^1D_2)$ comparison of the yields of $S(^3P_J)$ in the presence and absence of excess N_2 ($\approx$133 Nm^{-2}) should yield, directly, the ratio of $S(^3P_J)$ to total sulphur atom production on photolysis of CS_2. This experiment proved difficult to perform due to the strong dependence of sulphur atom yield to laser intensity. When laser energies were reproducible, results indicated that the addition of N_2 resulted in less $S(^3P_J)$ fluorescence.

This is the opposite to what would be expected if the quantum yield for $S(^1D_2)$ atom production from CS_2 was sizeable. This observation may be understood if the N_2 was quenching the upper fluorescing level (analogous to the quenching of $S(^1D_2)$). Time did not permit a study to be made using smaller N_2 pressures although this would undoubtedly have been of value.

(3) Flow lamp conditions were altered in an attempt to optimise $S(^3P_J)$ fluorescence over $S(^1D_2)$ fluorescence. Limited success was observed in these experiments: a pure helium flow (1.4 kNm^{-2}) over a sulphur deposit on the lamp walls produced a forty fold decrease in $S(3^1D_2)$ signal as compared to a factor of five decrease in $S(3^3P_J)$ signal. This experiment again pointed to a large quantum yield of $S(3^3P_J)$ from CS_2 photolysis at 193 nm. [The use of an alternative photomultiplier possessing greater sensitivity in the 180 nm region resulted in scattered light increasing the dead time to greater than 1 ms].

Consideration of the magnitude of the effects demonstrated in these experiments leads to the assertion that the quantum yield of $S(3^1D_2)$ production from CS_2 photolysis at 193 nm has an upper limit of 30% i.e.

$$CS_2 + h\nu \ (193 \text{ nm}) \rightarrow CS + S(^1D_2) \qquad \lesssim 0.3$$

This figure contrasts sharply with a less direct measurement published recently by Yang et al[7] in which a quantum yield of 80% is suggested.

Excitation of CS_2 at 193 nm populates the $A(^1B_2)$ state which is known to be predissociated by at least two repulsive states, one correlating with $S(3^3P_J)$ and the other with $S(3^1D_2)$. The fluorescence yield is low ($\Phi_f \sim 10^{-3}$) and the $A(^1B_2)$ state lifetime is very short (τ = 1.3 ps), strongly suggesting predissociation is the dominant decay channel[8]. Yang et al on photolysing CS_2 with an ArF laser monitored both the CS photofragment recoil energies and the CS vibrational distributions by use of the laser induced fluorescence technique (L.I.F.). The evidence for a large yield of $S(^1D_2)$ came from both sets of data. Firstly the translational energy distribution alters slope at an energy where $S(^1D_2)$ production first becomes feasible. Secondly, and lending considerable support to the conclusions drawn from the first set of data, the vibrational distribution of the CS radical maximises at v = 5. In rationalising the low $S(^1D_2)$ result obtained in this work with the experimental observations of Yang et al emphasis must be placed on the incomplete nature of their study, through experimental limitations. L.I.F. measurements could not be made on the $v \geqslant 7$ states, yet $S(^3P_J)$ is thermodynamically favoured to a threshold of v = 13 in the CS fragment. The 80% figure quoted essentially refers to the yield of $S(^1D_2)$ as correlated to CS fragments of vibrational excitation of $\leqslant$6 quanta. If CS fragment ($7 \leqslant v \leqslant 13$) production were high, no experimental data exists on this distribution, then the total $S(^3P_J)$ quantum yield

at λ = 193 nm would also be large. The authors acknowledge this fact and from suprisal plots to monitor the CS vibrational distribution at higher levels of excitation than those measured conclude that the total quantum yield for $S(^1D_2)$ production may indeed be as low as 50%. We conclude that the upper limit to the quantum yield expressed in this work is the more reliable.

The decay of $S(^1D_2)$ was monitored in the presence of CS_2, OCS and CH_4 and second order rate constants were obtained. $I_f(S(^1D_2))$ and $I_f(S(^3P_J))$ were shown to be proportional to $S(^1D)$ and $S(^3P_J)$ concentrations respectfully over the concentration range used. See FIGS 8.4A and B. The slow rate of removal of $S(^3P_J)$ atoms from the system coupled to its high initial yield and low detection sensitivity when compared to $S(^1D_2)$ results in the baseline off-set being essentially constant throughout the $S(^1D_2)$ decay time, hence providing no complications to the kinetic analysis. Under the conditions used approximately 10% photolysis of CS_2 occurs and reactant concentrations were such to ensure pseudo first order kinetics dominated. For a pseudo first order reaction:

$$\ln \frac{[S(^1D_2)]_{t=0}}{[S(^1D_2)]_t} = k't \qquad 8.1$$

where

$$k' = k[X] + C \qquad 8.2$$

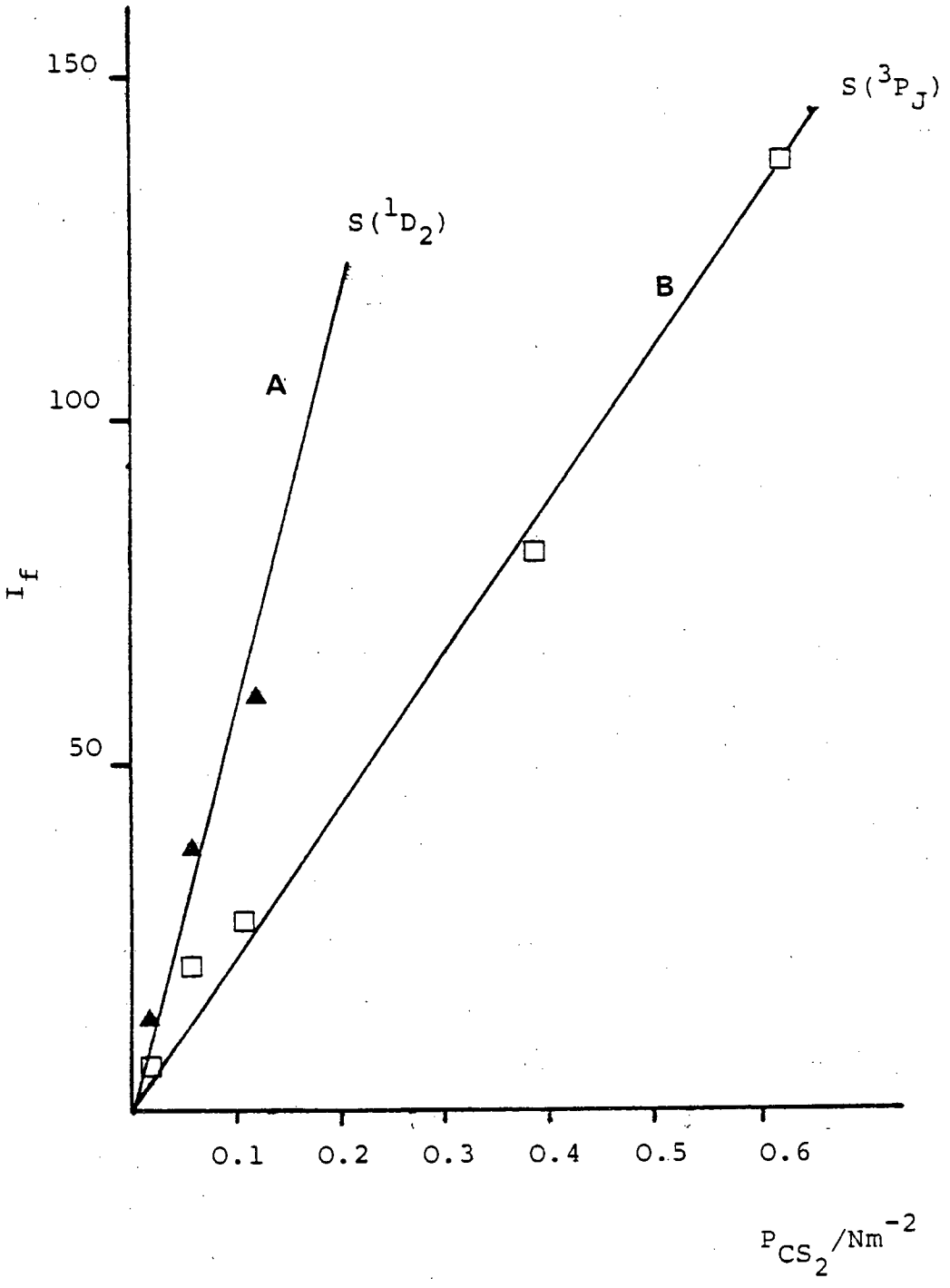

FIG 8.4 Fluorescence intensity (t=0) vs pressure of CS_2 (laser energy = 1.2 mJ).

k' = Pseudo first order rate constant

k = Bimolecular rate constant

$[X]$ = Reactant concentration

C = Constant (see sec 6.3)

Since $I_f(S(^1D_2)) \propto [S(^1D_2)]$ a plot of $\ln I_f(S(^1D_2))$ against time yields a straight line of gradient - k' (see FIG 8.5). Repeating the experiment for various values of [X] allows the bimolecular rate constant to be evaluated from a k' against [X] plot (FIG 8.6). The rate constants obtained are presented together with the relevant absorption data in TABLE 8.1.

TABLE 8.1 COMPARISON OF SECOND ORDER RATE CONSTANTS FOR REACTIONS OF $S(3^1D_2)$ OBTAINED AT 295 K USING TIME RESOLVED RESONANCE FLUORESCENCE AND ABSORPTION

Reactant/Quenching Gas	Absorption* k/cm^3 molecule^{-1} s^{-1}	Fluorescence k/cm^3 molecule^{-1} s^{-1}
CH_4	$(1.2\pm0.3)\times10^{-10}$	$(1.8\pm0.5)\times10^{-10}$
CS_2	$(1.5\pm0.3)\times10^{-10}$	$(3.5\pm1.0)\times10^{-10}$
OCS	$(1.2\pm0.3)\times10^{-10}$	$(3.0\pm1.0)\times10^{-10}$

*Quoted rate constants are based on a γ value of unity.

Errors are quoted as one standard deviation for both absorption and fluorescence data.

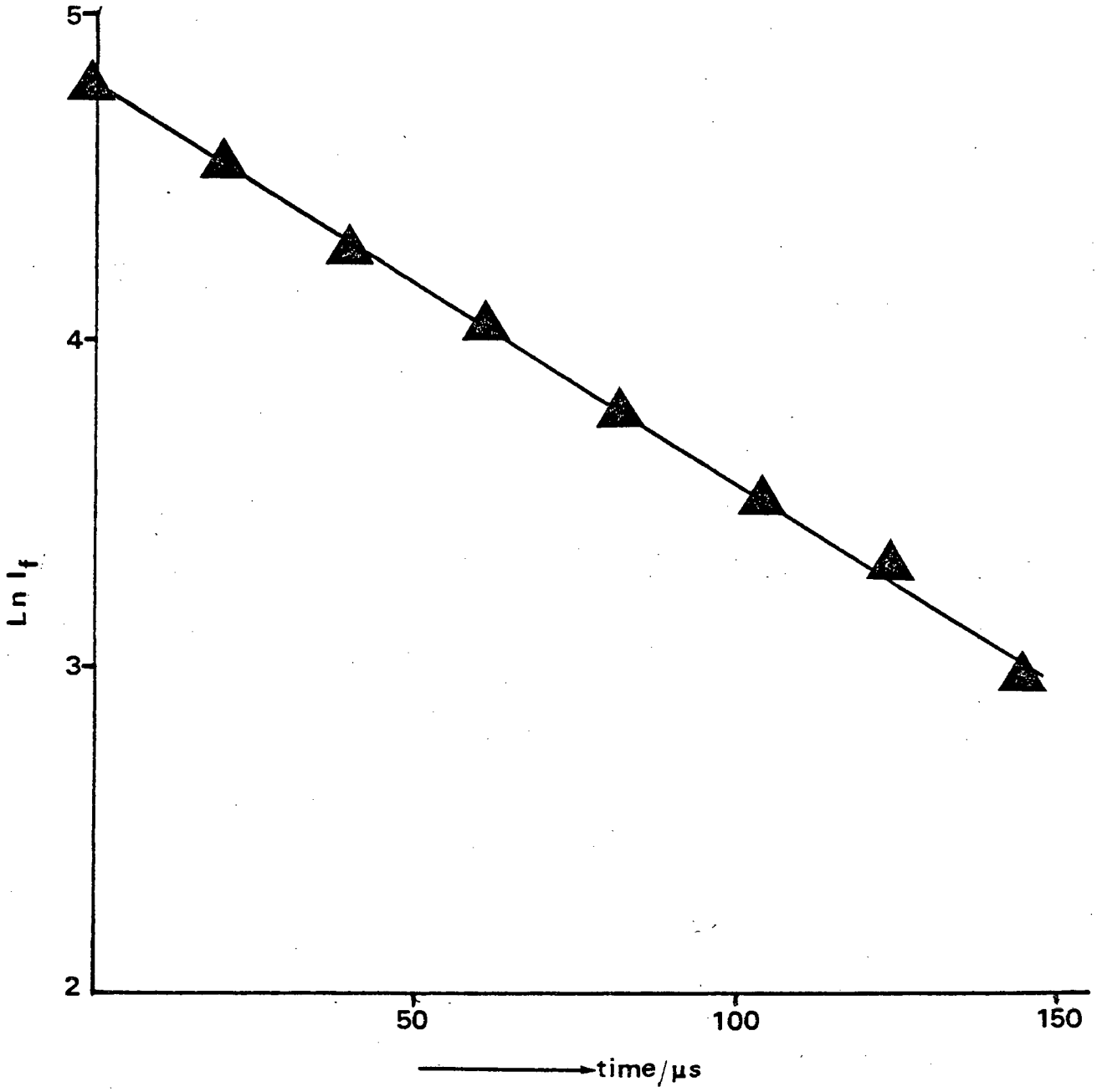

FIG 8.5 First order plot of $S(3^1D_2)$ decay (P_{CS_2} = 0.1 Nm^{-2}; P_{He} = 0.67 kNm^{-2}; laser energy = 1.2 mJ).

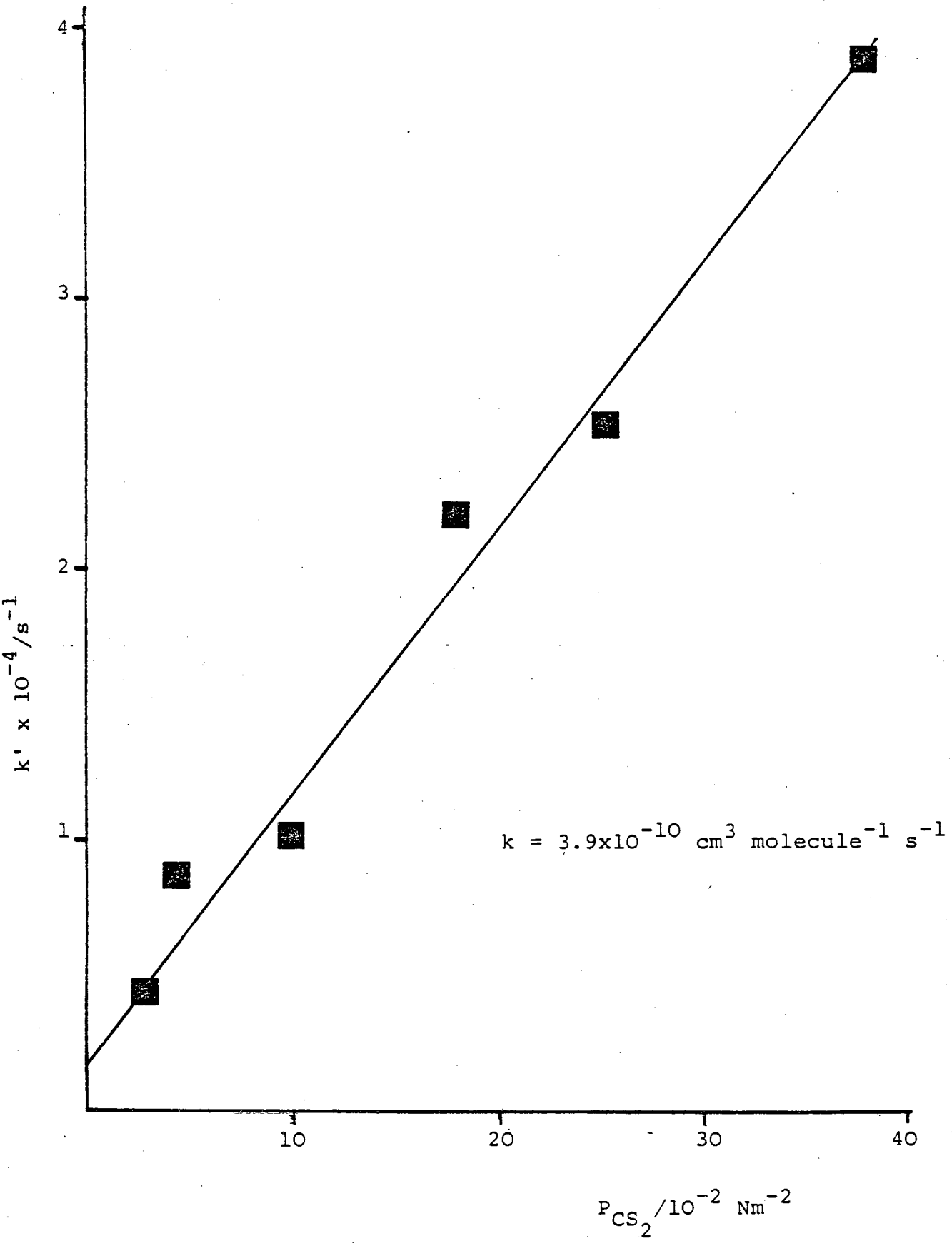

FIG 8.6 Pseudo first order rate constants vs CS_2 Pressure

The proposed mechanisms of these reactions have been covered previously in Chapter 7. In each case rate data obtained from fluorescence measurements indicates more rapid reaction/quenching than the corresponding absorption data. On careful examination, however, it is noted that the ratio of the two sets of rate data are not constant (OCS and CS_2 are in relatively good agreement being approximately 2-3 times faster from the fluorescence experiment whereas the CH_4 suggests that little variation between fluorescence and absorption data exists). Due to the very rapid nature of these reactions it is extremely unlikely that the effect observed is due to impurity or radical product interference. The most plausible explanation resides in the applicability of the Beer Lambert law to absorption experiments. The γ coefficient used in calculating the absorption rate data was unity - the evidence for this being essentially empirical due to the large uncertainty in the graphical approach normally adopted for the γ value determination (see GRAPH 7.2). If one assumes all rate measurements to be inherently free from error then the variation observed between CH_4 and OCS/CS_2 would indicate a value close to 1 in the former case and approximately 0.4 in the latter. A variation in γ over such a range is not unreasonable. Work on highly reversed emission lamps (easily diagnosed such by relative multiplet intensity measurements) already described, have illustrated large variation in absorption characteristics with flow lamp gas composition.

In carrying out absorption work utilising a $S(^1D_2)$ transition there is no easy diagnostic test of reversal. It was thought that due to the high sensitivity of $S(^1D_2)$ detection over a wide range of flow gas composition γ could be assumed to have a value of unity. This assumption now appears suspect. Indeed even for an unreversed light source it should be remembered that a linear relationship between absorbance and concentration can be expected only if the band width is narrow with respect to the absorption peak. Where the atomic lines are generated in a microwave powered flow lamp the emission line is Doppler broadened compared to the absorption line. Under such conditions deviations from the Beer Lambert law are expected. Certainly the rate data presented in this chapter as measured with time resolved resonance fluorescence should be considered the more reliable.

8.4 CONCLUSIONS

A relatively simple time resolved resonance fluorescence system utilising laser photolysis has been developed enabling kinetic measurements on $S(^1D_2)$ atom reactions to be made. The principles of operation suggest that $O(2^1D_2)$ and other excited atomic states could be monitored similarly, using a suitable photomultiplier and convenient photolysis source molecule.

The application of the technique to $O(^1D_2)$ atom kinetics would be of considerable interest.

Controversy exists between two sets of data obtained by two different techniques. The data presented by Fletcher and Husain[9] using atomic absorption spectroscopy was obtained using a γ coefficient of 0.42. Davidson et al's[10-12] data obtained using the time resolved decay of the $O(^1D \rightarrow ^3P)$ emission at 630 nm is only in agreement with Husain's work (with the exception of the rate of removal with ozone) if a γ coefficient of unity is adopted by Husain et al. The present results comparing the absorption and fluorescence detection of $S(^1D_2)$ atoms adds support to Husain's assertion that a small γ coefficient is needed to obtain an applicable relationship between absorbance and concentration of absorbing species even although one might expect that the lamp would be little reversed on these excited state transitions. Clearly much work remains to be done on the functional relationship between light absorption and concentration of absorbing species, in different systems - development of fluorescence techniques in tandem with absorption work offers one approach to a thorough investigation of the problem.

Broad band photolysis (λ>200 nm) - chapter 7 - illustrated that production of $S(^1D_2)$ was a minor photolysis pathway. In the present work photolysis at 193 nm gave a similar result ($\Phi(S^1D_2) \leqslant 30\%$). This latter result, however, is in disagreement with recently published work employing less direct measurements of the $S(^1D_2)$ produced.

It should be stressed that in many respects time did not permit thorough optimisation of the technique. The success already accorded to the system at such an early stage of development promises much for the future of excited state, time resolved resonance fluorescence detection.

8.5 REFERENCES

1. R.J. Donovan, H.M. Gillespie and R.H. Strain, J.C.S. Faraday II 72, (1977), 1553.
2. M.J. Kurylo and W. Braun, Chem. Phys. Letters 37, (1976), 232 and references therein.
3. L.J. Stief, W.A. Payne and R.B. Klemm, J. Chem. Phys. 62, (1975), 4000.
4. I. Arnold, F.J. Comes and S. Pointeck, Chem. Phys. 9, (1975), 237.
5. M. De Sorgo, A.J. Yarwood, O.P. Strausz and H.E. Gunning, Can. J. Chem. 43,
6. O.P. Strausz and H.E. Gunning, Advan. Photochem. 4, (1966), 143.
7. S.C. Yang, A. Freedman, M. Kawasaki and R. Bersohn, J. Chem. Phys. 72, (1980), 4058.
8. K. Hara and D. Phillips, J.C.S. Faraday II 74, (1978), 1441.
9. I.S. Fletcher and D. Husain, J. Phys. Chem. 80, 1837, (1976).
10. J.A. Davidson, H.I. Schiff, G.E. Streit, J.R. McAfee, A.L. Schmeltekopf and C.J. Howard, J. Chem. Phys. 67, (1977), 5021.
11. J.A. Davidson, C.M. Sadowski, H.I. Schiff, G.E. Streit, C.J. Howard, D.A. Jennings and A.L. Schmeltekopf, J. Chem. Phys. 64, (1976), 57.
12. G.E. Streit, C.J. Howard, A.L. Schmeltekopf, J.A. Davidson and H.I. Schiff, J. Chem. Phys. 65, (1976), 4761.
13. J.A. Davidson, H.I. Schiff, T.J. Brown and C.J. Howard, J. Chem. Phys. 69, (1978), 4277.

APPENDIX 1(A)

MATERIALS

CF_3Cl	I.C.I. 'Arcton' liquified gas-thoroughly degassed by repeated trap to trap distillation at 77 K with continuous pumping on the sample.
CF_3Br	Cylinder grade (Matheson gas product) - degassed by repeated freeze-pump-thaw cycles.
CCl_4	Fisons analar grade: fractionally distilled and thoroughly degassed prior to use.
CH_3Cl	B.O.C. cylinder grade.
CF_3I	Fluorochem Ltd., fractionally distilled under vacuum using appropriate slush baths and thoroughly degassed at 77 K.
iso C_3F_7I	Supplied by Pierce Chemical Company and treated similarly to CF_3I.
C_2H_4	B.O.C. cylinder grade.
C_2H_6	Cylinder grade (Matheson Co.).
C_6H_6	Fisons analar grade.
C_6F_6	Fluorochem lab reagent.
Cl_2	B.O.C. cylinder grade.
Br_2	Fisons (purity > 99%).
I_2	Fisons (purity > 99.5%).
OCS	Cylinder grade (Matheson Co.) gas, thoroughly degassed by repeated freeze-pump-thaw cycles at 77 K.

CS_2	'Analar grade' (Fisons) was fractionally distilled and subjected to numerous freeze-pump-thaw cycles at 77 K.
CO	B.O.C. cylinder (Research Grade).
O_2, CO_2, CH_4	'Grade X' used directly from break seal container
Xe, Kr, Ne	
Ar	B.O.C. 'white spot' grade.
N_2O	B.O.C. 'medical grade' (99%) was thoroughly degassed and was used directly.
H_2S	B.O.C. cylinder grade.
NO_2	Was prepared by the addition of a large excess of O_2 to NO. After several hours the NO_2 was purified by several freeze-pump-thaw cycles.
O_3	See appendix 1(B).
He (buffer gas)	'Grade X' (B.O.C. Ltd.) was used directly from a cylinder. Purity given as He - 99.9995%.
He (flow lamp)	Ordinary cylinder grade (B.O.C. Ltd.).
N_2 (buffer gas)	B.O.C. 'white spot' grade (99.9%).
N_2 (reagent)	'Grade X' (B.O.C. Ltd.) was used directly from a break-seal container.

APPENDIX 1(B)

OZONE PREPARATION

Ozone was prepared by a method similar to that described by Clough and Thrush. The ozone trap (volume ≈ 270 cm^3) was half filled with 4-6 mesh silica gel. When the gel had been exposed to the atmosphere for any length of time it was necessary to bake out the trap. This was achieved by heating the trap (300°C) while under vacuum until no further outgassing occurred (≈8 hrs).

In order to fill the trap with ozone it was first cooled using a solid CO_2/isopropanol slush bath (195 K) and then connected with PVC tubing to a Towers Ozone apparatus. Ozone was produced in the ozoniser by an electric discharge through a flowing oxygen supply (dried by passage through a conc. H_2SO_4 bubbler). When the trap was fully laden with ozone (indicated by the extent of the blue colouration of the gel) it was disconnected from the ozoniser and connected to the vacuum line (NB. silicone grease was used for all connections likely to be in contact with ozone). The silica gel was then slowly pumped, while at 195 K, to remove oxygen impurities. Any ozone pumped off at this stage was destroyed prior to reaching the pumps by passage of the gas stream through a hot glass tube containing a nickel catalyst. Ozone was then transferred to a previously aged, blackened bulb by allowing the gel to warm up and the O_3 to desorb. The pressure was

monitored continuously using the spiral gauge and a safe upper limit of 4 kNm^{-2} was not exceeded. A large backing pressure of helium was then added and the gases allowed to mix. In general ozone purities were $\leq 70\%$, however with careful pumping a purity of $\geq 95\%$ should be attainable.

APPENDIX II

FLASH LAMP PARAMETERS

The theory behind the design of discharge flash lamps is excellently covered by Porter and West. The main results from considering the flash lamp/charging circuit as an LCR network are summarised briefly. For optimum operation the circuit must be critically damped i.e. equation (1) must hold:

$$R = 2\sqrt{L/C} \qquad 1$$

where R = resistance, L = inductance and C = capacitance.

The maximum energy dissipated is given by equation (2) and the half period is proportional to $\sqrt{LC}$

$$E = \tfrac{1}{2}CV_o^2 \qquad 2$$

where V_o = voltage.

Therefore if the pulse duration is to be kept short V_o should be maximised and C kept low. Under these circumstances maintaining the critically damped specification is generally difficult although some alteration in flash lamp diameter may facilitate solution of equation (1) since R is proportional to length/diameter of the flashlamp.

APPENDIX III

PRINCIPLES OF LASER OPERATION

The concept of the laser is dependent on two basic principles: that of stimulated emission and the optical resonator. Any medium with atoms, molecules or ions in an inverted population when placed in an optical resonator or cavity can lase.

Consider the absorption of light by a two level system, ground state (N_0), upper state (N_1), then the absorption and emission processes may be represented by rate equations such that

$$\text{Stimulated absorption rate} = N_0 \frac{I\nu}{4\Pi c} B_{01} \qquad 1$$

$$\text{Stimulated emission rate} = N_1 \frac{I\nu}{4\Pi c} B_{10} \qquad 2$$

If conditions of thermal equilibrium are assumed, the coefficients of stimulated absorption (B_{01}) and stimulated emission (B_{10}) can be shown to be equal

$$B_{01} = B_{10} \qquad 3$$

and the coefficient of spontaneous emission can be shown to be related to the coefficient of stimulated emission by the formula

$$A_{10} = \frac{8\Pi h\nu_{10}^{3}}{c^3} B_{10} \qquad 4$$

$I\nu/4\Pi c$ is equal to $\rho\nu$ - the spectral density of radiation energy (Js/m^3) at the transition frequency ν_{01}.

Consider now the intensity of a monochromatic collimated beam on passage through a sample in which

the light beam does not effect the level populations in the sample, then Beers law may be applied:

$$I(x) = I_o e^{-\alpha x} \qquad 5$$

α = absorption coefficient.

Alternatively we may represent the number of photons lost from the beam on passage through a volume element of thickness Δx by

$$\frac{-dn_{ij}}{dt} = \frac{N_i I(x) B_{ij}}{4\Pi c} - \frac{N_j (I(x)) B_{ji}}{4\Pi c} \qquad 6$$

It is easily shown that:

$$\alpha = B_{ij} (N_i - N_j) \frac{h\nu_{ij}}{4\Pi c} \qquad 7$$

If $N_j > N_i$ i.e. a population inversion is created and $\alpha < 0$ leading to a 'signal gain' component and $\beta = -\alpha$ is defined as the 'small-signal gain coefficient'. Hence for laser action it is necessary to achieve a population inversion in the sample. It is not sufficient, however, to require simply that the population of the upper state be greater than that of the lower state. Various losses, including the loss of power in the form of laser output, must be accounted for. To overcome these losses, a minimum gain coefficient, the threshold gain, (β_{TH}) is required to initiate and sustain laser oscillations. If it is assumed that the active medium completely fills the region between the mirrors and that the pumping excitation is uniform. In travelling from mirror M_1

to mirror M_2 the beam irradiance increases from its initial value, I_o, to a value I given by

$$I = I_o \exp(\beta - \alpha_L)L \qquad 8$$

L = separation of the mirrors

α_L = distributed loss per unit distance due to scattering and possible absorption in nonactive constituents of the laser medium.

For a round trip involving reflection from M_1 and M_2 with reflectivities R_1 and R_2 respectively, the net round-trip power gain (G) is supplied by

$$G = R_1 R_2 \exp[2(\beta - \alpha_L)L] \qquad 9$$

The threshold condition for oscillation is G = 1 and therefore

$$\beta_{TH} = \alpha_L + \frac{1}{2L} \ln \frac{1}{R_1 R_2} = \alpha_L + \alpha_o \qquad 10$$

Only when G = 1 for a period of time does the cavity energy (and therefore the laser output power) settle down to a steady-state value. Therefore, the steady-state value of the small-signal gain must equal the threshold value, β_{TH}. This confinement of the steady-state gain at the threshold value is referred to as the gain saturation and obviously from equation (10) depends both on the constituents of the laser medium (through α_L) and on the laser construction (through R_1, R_2 and L).

APPENDIX IV

ABSORPTION COEFFICIENTS - NOMENCLATURE

The absorption coefficient (a) is defined by the equation

$$I_{TR} = I_O \, e^{(-acl)} \qquad 1$$

or

$$I_{TR} = I_O \, 10^{(-acl)} \qquad 2$$

where I_{TR} and I_O are the transmitted and incident light intensities, c denotes either pressure or concentration and l is the pathlength in centimetres. Depending on whether c is given in pressure units (torr or atm) or in concentration units (mol dm^{-3}), a is designated as k or ε. If k (pressure^{-1} cm^{-1}) is used it is necessary to specify the temperature to which the pressure is referred. At 25°C, k is 9% less than at 0°C. Sometimes the absorption cross section σ, defined as

$$\sigma = k \text{ (atm}^{-1} \text{ cm}^{-1} \text{ at } 0^{\circ}\text{C)}/n_O \qquad 3$$

where n_O = Loshmidt no. ($=2.687 \times 10^{19}$) is used instead of k or ε. The absorption cross section is sometimes expressed in megabarns (1 Mb = 10^{-18} cm^2).

The absorption cross section is nearly temperature independent between 0°C and room temperature, but may change at much higher and lower temperatures.

LECTURES ATTENDED

In accordance with the regulations of the University of Edinburgh, Department of Chemistry, the post-graduate lecture courses etc. attended during the period of study are listed below:

1) The Gaseous Environment
2) The Planetary Boundary Layer and Air Pollution
3) Quantum Optics
4) Molecular Structure and Spectra
5) Chemistry At Its Most Colourful (I.C.I. Industrial Lecture)
6) Biosynthesis
7) Computer Programming
8) Numerical Methods
9) Scientific German

In addition many of the regular departmental seminars and all gas kinetics group meetings were attended.

CONFERENCES ATTENDED

1) Nato Advanced Study Institute 'Theoretical Aspects of the Electronic Structure and Properties of the Excited States of Atoms, Molecules and Solids'; Is. of Kos, Greece; June (1978).
2) IXth International Conference on Photochemistry; University of Cambridge; August (1978).

3) Faraday Discussion No. 67, 'Kinetics of State Selected Species'; University of Birmingham; April (1979).

4) British Association for the Advancement of Science, Annual Meeting; Heriot-Watt University, Edinburgh; September (1979).

5) Faraday Division, Gas Kinetics Group Meeting; Keele University; September (1979).

6) 'Atomic Reactions', University of London; January (1980).

PUBLICATIONS

Papers published during the course of the Ph.D. are as follows:

Reaction of $CN(X^2\Sigma+)$ with OCS and Formation of SCN; M.C. Addison, A.J. Leitch, C. Fotakis and R.J. Donovan; J. of Photochemistry, 10, 273, (1979).

Reactions of $O(2^1D_2)$ and $O(^3P_J)$ with Halogenomethanes; M.C. Addison, R.J. Donovan and J. Garraway; Faraday Disc. 67, (1979), 286.

Direct Observation of $S(3^1D_2)$ and Determination of the Absolute Rate of Reaction with OCS; M.C. Addison, C.D. Byrne and R.J. Donovan; Chem. Physics Lett. 64, 57, (1979).

Kinetic Studies of Atmospheric Free Radicals; J.P. Burrows, R.A. Cox and M.C. Addison; Ozone Conf. (Nato), 1979, in press.

Absorption Spectrum and Kinetics of the Acetylperoxy Radical; R.A. Cox, M.C. Addison, J.P. Burrows and R. Patrick; Chem. Phys. Lett. 73, (1980), 283.

Resonance Fluorescence Study of Electronically Excited Sulphur Atoms: Reactions of $S(3^1D_2)$; M.C. Addison, R.J. Donovan and C. Fotakis; in press.

Journal of Photochemistry, 10 (1979) 273 - 276

Short Communication

Reaction of $CN(X^2\Sigma^+)$ with OCS and formation of SCN

MICHAEL C. ADDISON, ALAN J. LEITCH, CONSTANTINE FOTAKIS and ROBERT J. DONOVAN

Department of Chemistry, University of Edinburgh, West Mains Road, Edinburgh EH9 3JJ (Gt. Britain)

(Received June 13, 1978)

The reaction between $CN(X^2\Sigma^+)$ and OCS has been investigated using both time-resolved spectrophotometry and flash spectroscopy. The reaction is shown to be fast ($k \geq 3 \times 10^{-11}$ cm^3 molecule^{-1} s^{-1}) and to lead to the formation of SCN.

1. Introduction

Reactions involving CN radicals are of considerable importance in combustion and flame chemistry. However, by comparison with radicals such as OH, relatively little systematic effort has been made to study either their chemistry or their kinetics under controlled laboratory conditions. The most recent studies are those by Schacke *et al.* [1], Bullock and Cooper [2] and Boden and Thrush [3].

We report here direct observations on the reaction between CN and OCS which is shown to yield the SCN radical.

2. Experimental

Two independent pieces of equipment were employed for this work. Firstly a conventional apparatus for flash photolysis with flash spectroscopy in the visible and ultraviolet regions ($\lambda > 200$ nm) was used to study the formation of SCN; this equipment has been described elsewhere [4]. Secondly an apparatus for time-resolved spectrophotometry of CN radicals was employed to make detailed kinetic studies [5]; only a brief description will be given here. CN ($B^2\Sigma^+ \rightarrow X^2\Sigma^+$) emission was excited using a microwave discharge through a flowing mixture of 1% CH_4 in N_2 (P = 266 N m^{-2}), in a manner similar to that described by Boden and Thrush [3]. This emission was focused through the reaction vessel (l = 40 cm), which was surrounded by a coaxial flash lamp, and onto the entrance slit of a monochromator (Hilger Monospek 1000). The variation in light intensity as a function of time at the exit slit of the monochromator (λ = 388 nm) was monitored with an EMI 9781B photomultiplier.

The latter was wired so that only the first six dynodes were utilized, the seventh and subsequent dynodes acting as the anode; this allowed high incident light levels to be used and thus optimized the signal to noise ratio. The output from the photomultiplier was fed to a fast analogue to digital converter with an integral memory (Datalab DL905) and then (optionally) to a signal averager (Datalab DL4000). Data could be inspected on a visual display and transferred to an *X-Y* plotter for analysis. A typical single shot recording of the CN radical formation and decay is shown in Fig. 1. Flash energies of 125 J were found to be adequate for the present studies.

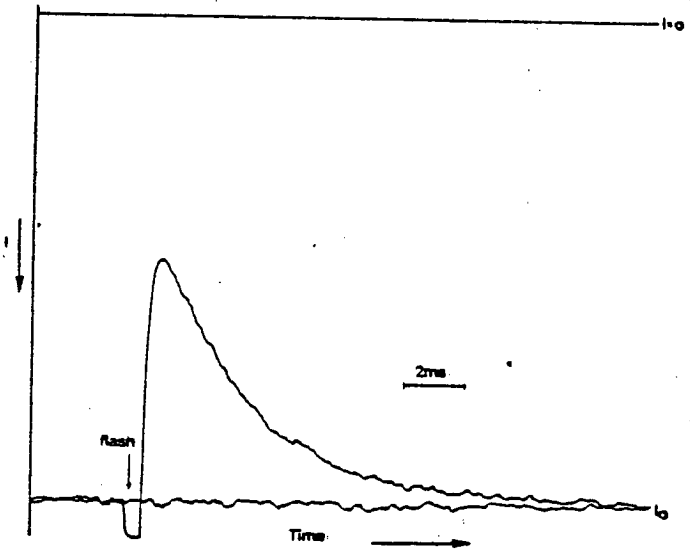

Fig. 1. Formation and decay of CN($X^2\Sigma^+$) following the photolysis of $(CN)_2$: $P_{(CN)_2}$ = 23.7 N m^{-2}, P_{N_2} = 1.24 kN m^{-2}; λ = 388 nm; flash energy = 125 J.

Boden and Thrush [3] have discussed the problems associated with using an emission source for which the rotational temperature does not match that of the absorbing species. In the present work we adopted an empirical approach and determined a curve of growth for the CN radical under our experimental conditions. The reaction vessel was divided into sections of known length so that the path length of the absorbing layer could be changed in a systematic manner. Our results show that absorption by CN can be treated in terms of a modified Beer–Lambert expression, $OD = \ln(I_0/I) = \alpha(cl)^\gamma$, where γ was found to equal 0.6.

3. Results and discussion

An intense spectrum of the SCN radical [6] was observed in absorption (λ = 346 - 382 nm) when either $(CN)_2$ or ClCN was photolysed in the presence of OCS; typical conditions were $P_{(CN)_2}$ = 1.3 kN m^{-2}, P_{OCS} = 0.23 kN m^{-2} and a flash energy of 10^3 J. The decay of SCN was rapid ($\tau \approx$ 50 μs) and led to the prompt formation of S_2. Possible reactions which could

lead to SCN formation in this system are CN reacting with OCS or $S(^1D)$ reacting with $(CN)_2$. The latter was ruled out by repeating the experiments in the presence of a large excess of N_2 which is known to quench $S(^1D)$ efficiently [7]; no significant change in the SCN yield was observed in the presence of excess N_2. Reaction of $S(^3P)$ with $(CN)_2$ is very unlikely on thermochemical grounds, however. We also eliminated this possibility by adding various pressures of C_2H_6 to the system. It was found that addition of C_2H_6 gave a marked reduction in the yield of SCN. This would be expected if CN is the precursor of SCN, as CN is known to react rapidly with C_2H_6 ($k = 2.4 \times 10^{-11}$ cm^3 molecule^{-1} s^{-1}) [2]. Removal of $S(^3P)$ by C_2H_6 would be negligible and it cannot therefore be the precursor of SCN.

By using the SCN spectrum as a "spectroscopic marker" [7], a rate constant for CN + OCS relative to that for CN + C_2H_6 was obtained as $k_{OCS} \approx 4k_{C_2H_6}$. This agrees with the lower limit for k_{OCS} (presented later) when compared with the known value [2] for $k_{C_2H_6}$.

Detailed kinetic studies of CN using time-resolved spectrophotometry proved to be more difficult than expected with OCS. From Fig. 1 it can be seen that the time scale for removal of CN in a $(CN)_2 + N_2$ mixture is relatively long and thus the "dead time" associated with the firing of the flash lamp is of little consequence under these conditions. Addition of a reagent which removes CN increases the rate of decay and a rate coefficient at a given partial pressure of reagent can be obtained, provided pseudo first order kinetics are maintained. For pseudo first order decay kinetics the reagent should be in a tenfold (or greater) excess over the CN radical concentration. We have estimated the [CN] produced in our system as about 8×10^{12} cm^{-3}; this necessitates reagent concentrations of not less than 10^{14} cm^{-3}. However, for fast reactions the amount of reagent which can be added is limited by the dead time of the detector.

The use of this technique is therefore constrained by the dead time of the detector, on the one hand, and by the need to maintain pseudo first order kinetics on the other. It is well suited to measuring rate constants in the range $1 \times 10^{-11} \cdot 10^{-16}$ cm^3 molecule^{-1} s^{-1}. The reaction of CN with OCS is one of the fastest reactions that we have attempted to study and thus only a limited range of OCS partial pressures could be used. The signal to noise ratio is lower and hence the kinetic data are subject to larger uncertainties when such fast reactions are studied. To help alleviate this problem signal averaging was employed. The first order rate coefficients determined for various pressures of OCS are presented in Table 1: the second order rate constant derived from these data and corrected for γ was found to be $(3.8 \pm 0.8) \times 10^{-11}$ cm^3 molecule^{-1} s^{-1}. The stated error is for 2σ but is based only on an analysis of random errors in the rate measurements; it does not allow for systematic errors associated with departure from pseudo first order kinetics. In view of the limitations discussed above we prefer to quote a lower limit for the rate constant as $k_{OCS} \geqslant 3 \times 10^{-11}$ cm^3 molecule^{-1} s^{-1}.

The reaction of CN with OCS has thus been shown to be rapid, leading to the formation of SCN:

TABLE 1

Rate data for the removal of CN by OCS (295 K)

P_{OCS} (N m^{-2})	First order rate coefficient (s^{-1})
0	660 ± 120
6.7×10^{-2}	1070 ± 260
0.133	1350 ± 360

$$CN + OCS \rightarrow SCN + CO$$

A lower limit for the C–S bond strength in SCN can be derived as not less than 306.4 kJ mol^{-1}, based on the known bond energy [8] of OCS.

Acknowledgments

We are indebted to Professor C. Kemball for his encouragement and laboratory facilities and to the S.R.C. for equipment grants and support for M.C.A. and A. J. L. We also thank Dr. C. Morley for helpful discussions and Shell Research Limited for partial support of A.J.L. under the S.R.C./C.A.S.E. scheme.

1 H. Schacke, H. Gg. Wagner and J. Wolfrum, Ber. Bunsenges. Phys. Chem., 81 (1977) 670.
2 G. E. Bullock and R. Cooper, J. Chem. Soc. Faraday Trans. 1, 68 (1972) 2185.
3 J. C. Boden and B. A. Thrush, Proc. R. Soc. London, Ser. A, 305 (1968) 107.
4 H. M. Gillespie and R. J. Donovan, Chem. Phys. Lett., 37 (1976) 468.
5 A. J. Leitch, Ph.D. Thesis, University of Edinburgh, to be published (1978).
6 R. Holland, D. W. G. Style, R. N. Dixon and D. A. Ramsay, Nature (London), 182 (1958) 336.
7 D. J. Little, A. Dalgleish and R. J. Donovan, Faraday Discuss. Chem. Soc., 53 (1972) 211.
8 S. W. Benson, Chem. Rev., 78 (1978) 23.

Reactions of $O(2^1D_2)$ and $O(2^3P_J)$ with Halogenomethanes

By Michael C. Addison, Robert J. Donovan and John Garraway

Department of Chemistry, University of Edinburgh, West Mains Road, Edinburgh EH9 3JJ

Reprinted from

FARADAY DISCUSSIONS
OF
THE CHEMICAL SOCIETY

No. 67
FARADAY SYMPOSIUM 67

1979

Reactions of $O(2^1D_2)$ and $O(2^3P_J)$ with Halogenomethanes

By Michael C. Addison, Robert J. Donovan and John Garraway

Department of Chemistry, University of Edinburgh, West Mains Road, Edinburgh EH9 3JJ

Received 20th December, 1978

Product branching ratios for the reaction of $O(2^1D_2)$ with the halogenomethanes CF_3Cl, CF_3Br, CF_3I and CF_2HCl are presented. The dominant channel is shown to be abstraction yielding a halogen oxide. This contrasts with the behaviour observed with hydrocarbons, where insertion into C–H bonds dominates. Quenching of $O(2^1D_2)$ to the ground state is also observed with the halogenomethanes and accounts for $\approx 30\,\%$ of the total removal cross-section.

Reaction of $O(2^1D_2)$ with CF_2HCl leads to the formation of ClO (55 %) and to the elimination of HCl (40 %). The latter process is accompanied by the formation of CF_2 and $O(2^3P_J)$.

The reactions of $O(2^1D_2)$ are compared with those for $O(2^3P_J)$, where these are known, and the absolute rate for reaction of $O(2^3P_J)$ with CF_3I is determined as $(1.1 \pm 0.3) \cdot 10^{-11}$ cm^3 molecule^{-1} s^{-1} at 300 K.

The results are discussed in terms of the main topological features on the potential surfaces involved.

Reactions of $O(2^1D_2)$ with hydrocarbons have been studied extensively.[1–3] The reaction cross-sections are large and the main reaction channel involves insertion into C–H bonds. Insertion has been shown to proceed indiscriminately and the total reaction cross-section found to be proportional to the number of C–H bonds in the molecule.[3] A number of other reaction channels have also been recognised and may be summarised as follows,

$$O(2^1D_2) + RH \rightarrow ROH^{\ddagger} \xrightarrow{+M} ROH\ (65\ \%) \quad (1)$$

$$\rightarrow R + OH\ (20\text{–}30\ \%) \quad (2)$$

$$\rightarrow R'O + H_2 (\leqslant 10\ \%) \quad (3)$$

$$\rightarrow RH + O(2^3P_J) (< 3\ \%). \quad (4)$$

It is clear that quenching is negligible and that a *direct* abstraction reaction, leading to OH formation, plays an appreciable role.

By comparison the reactions of $O(2^1D_2)$ with halogen-containing molecules have been little studied, although it is known that the reaction cross-sections are again large.[4,5] The formation of halogen oxide products has been observed and lower limits for branching into this channel presented.[6,7]

In the present work we have made a detailed study of the branching ratios into different reaction channels for a number of halogen-containing molecules. The dominant channel is shown to be *abstraction* of a halogen atom. Quenching to the ground state is also an important process.

We also present data for the reaction of $O(2^3P_J)$ with CF_3I and compare these, together with data for the other halogenomethanes, with those for the analogous reactions involving $O(2^1D_2)$.

EXPERIMENTAL

Three separate experimental arrangements were employed for this work, all of them based on the flash photolysis technique.

(i) FLASH SPECTROSCOPY

A conventional arrangement, suitable for photographing transient spectra in the visible and ultraviolet regions, was used to obtain kinetic data on the halogen oxides and CF_2. Spectra were dispersed on a Hilger–Watts medium quartz spectrograph and recorded on Kodak Panchro-Royal film. A more detailed description of this technique and the data processing has been given in ref. (6) and (7).

(ii) TIME-RESOLVED PHOTOMETRY IN THE VACUUM ULTRAVIOLET

This apparatus employed a conventional flash photolysis unit coupled to a vacuum ultraviolet monochromator and fast photometric recording system. It was used to monitor the formation and decay of $O(2^3P_J)$ (*via* the resonance lines at $\lambda \simeq 130$ nm), following quenching of $O(2^1D_2)$ by the halogenomethanes, and also to obtain absolute rate data for reaction of $O(2^3P_J)$ with CF_3I. The experimental arrangement was similar to one described previously [8] for work on $S(3^3P_J)$; however, for the present work an EMR542 solar blind photomultiplier was used. The use of this photomultiplier eliminated the effect of scattered light from the flash lamp and allowed kinetic measurements to commence during the flash. A flow system was used for the atomic lamp and the best results were obtained when very low (<0.1 %) oxygen/helium ratios were passed through the microwave discharge. An extensive series of experiments was carried out to establish that this new arrangement gave a linear photometric response with stable molecules such as O_3. Curves of growth for $O(2^3P_J)$ were then determined by photolysing O_3 under optically thin conditions [in the presence of excess N_2 to quench $O(2^1D_2)$ to $O(2^3P_J)$] over a range of pressures (fig. 1). As a final check the rate of the reaction between $O(2^3P_J)$ and NO_2 was determined* as $k = (1.1 \pm 0.3) \times 10^{-11}$ cm^3 molecule^{-1} s^{-1}, in excellent agreement with the accepted result obtained by resonance fluorescence [9] [$k = (9.12 \pm 0.44) \times 10^{-12}$ cm^3 molecule^{-1} s^{-1} at 295 K].

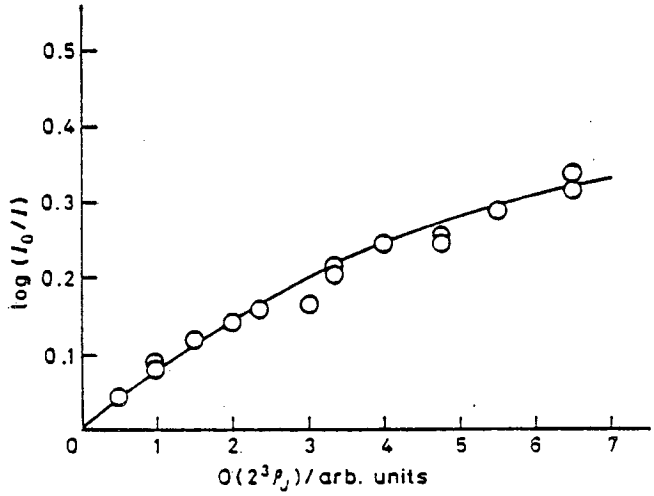

FIG. 1.—Curve of growth for $O(2^3P_J)$ using the three resonance lines at 130.2, 130.5, 130.6 nm. The $O(2^3P_J)$ concentration was taken to be proportional to that of O_3, which was varied over the range 0.4-6.1 N m^{-2}.

* In these experiments $O(2^3P_J)$ was formed by photolysis of NO_2 (≈ 1 %) in the visible and near u.v. regions.

In all of these experiments the output from the photomultiplier was fed to a fast analogue-to-digital converter (Datalab DL905) and data were processed in the standard way.

(iii) TIME-RESOLVED PHOTOMETRY IN THE NEAR-ULTRAVIOLET

The yield of OH from reaction of $O(2^1D_2)$ with CF_2HCl was determined using an arrangement similar to that described by Morley and Smith.[10] The intense OH emission produced by a microwave discharge through a flowing mixture of water vapour in argon carrier gas was focused through the reaction vessel and onto the slit of a McKee-Pederson (MP1018B) monochromator which selected[10] the $Q_1 3$ line at 308.15 nm. A chlorine gas filter surrounded the reaction vessel and reduced scattered light from the flash to a negligible level. The output from the photomultiplier was fed to a transient recorder (Datalab DL905) and data were processed as in section (ii) above.

For all experiments $O(2^1D_2)$ was produced by the ultraviolet photolysis of $O_3(\lambda = 200$-300 nm) and, where required, $O(2^3P_J)$ was formed by adding an excess of N_2 to quench $O(2^1D_2)$ to $O(2^3P_J)$. The experimental conditions used with the three different techniques varied significantly and will be described in the appropriate section dealing with results.

RESULTS

ABSOLUTE CONCENTRATIONS OF $O(2^1D_2)$ PRODUCED BY THE FLASH

Photolysis of O_3 in the ultraviolet (200-300 nm) is known to produce almost exclusively $O(2^1D_2)$ and thus the absolute yield of this atomic state can be determined by observing the amount of O_3 removed by the flash. In pure O_3 (or $O_3 + SF_6$ and $O_3 + He$ mixtures) $O(2^1D_2)$ reacts rapidly with a second O_3 molecule, and under our conditions the amount of O_3 removed immediately after the flash will in fact be twice the amount photolysed in the primary photochemical step. However, by adding excess CO_2 to the ozone, the effect of the secondary reaction can be eliminated, as $O(2^1D_2)$ is quenched to the ground state. We therefore carried out experiments to determine the amount of O_3 removed after the flash (30 μs) both in the presence and absence of CO_2. The depletion in the presence of CO_2 was found to be 12 ± 1 % ($P_{O_3} = 26.6$ N m^{-2}) and in the absence of CO_2 24 ± 2 %, this gives a yield of $O(2^1D_2)$ of 8×10^{14} atoms cm^{-3} per flash. These results confirm that the yield of $O(2^3P_J)$ in the ultraviolet photolysis of O_3 is negligible (< 10 %) and that $O(2^1D_2)$ is removed entirely by reaction with O_3, physical quenching being unimportant. The decay of O_3 at times > 30 μs was observed to be very slow, as expected from the known slow rates for reactions involving $O(2^3P_J)$ and $O_2(a^1\Delta_g)$ with O_3.

REACTION OF $O(2^1D_2)$ WITH CF_3Cl

When O_3 is photolysed in the presence of excess CF_3Cl ($P_{CF_3Cl} = 2.7$ kN m^{-2}) a strong spectrum of ClO is observed *via* the ($A^2\Pi \leftarrow X^2\Pi$) system, and its rate of formation closely follows the integrated form of the flash. No ClO is observed when CO_2 or N_2 is added to quench $O(2^1D_2)$ and it is clear from these, as well as earlier experiments,[6,7] that ClO results from a fast reaction between $O(2^1D_2)$ and CF_3Cl. There are, however, three possible mechanisms for ClO formation. The first and most obvious is the direct formation of ClO in a primary abstraction step

$$O(2^1D_2) + CF_3Cl \rightarrow ClO + CF_3. \quad (5)$$

A second possibility is insertion into the C-Cl bond followed by fragmentation to yield ClO

$$O(2^1D_2) + CF_3Cl \rightarrow CF_3OCl^{\ddagger} \rightarrow CF_3 + ClO. \quad (6)$$

The third possibility is that Cl atoms are produced by a displacement reaction, followed by the fast reaction of Cl with O_3, *i.e.*,

$$O(2^1D_2) + CF_3Cl \rightarrow CF_3O + Cl \quad (7)$$

$$Cl + O_3 \rightarrow ClO + O_2. \quad (8)$$

Under the conditions of our experiment it would be difficult to distinguish between these three mechanisms simply by observing the rate of formation of ClO as they are all very rapid. We can, however, use a chemical method to distinguish between the first two and the third mechanisms. By adding a small amount of ethane to mixtures of O_3 and CF_3Cl ($P_{C_2H_6} = 67$ N m^{-2}), any Cl atoms formed in the primary step can be removed before reacting with O_3; the yield of ClO will then be reduced by an amount which depends on the yield of free chlorine atoms in the primary step. As the pressure of C_2H_6 used is very much lower than that of CF_3Cl it will not interfere by reacting with $O(2^1D_2)$ (~ 95 % of the excited oxygen atoms react with CF_3Cl). Our results show that the yield of ClO is only slightly reduced by addition of C_2H_6 and Cl atom formation accounts for $\leqslant 20$ % of the total $O(2^1D_2)$ removal by CF_3Cl.

Quantitative yields of ClO were determined *via* the (5, 0) band of the $A^2\Pi \leftarrow X^2\Pi$ system[11] [see ref. (7) for a detailed discussion], and when these are compared with the amount of $O(2^1D_2)$ produced by the flash we find that 65 % of the excited oxygen gives rise to ClO formation in a primary step.

Measuring the yield of $O(2^3P_J)$ by time resolved photometry in the vacuum ultraviolet proved more difficult than first envisaged. Absorption by CF_3Cl reduced the intensity of the oxygen resonance line reaching the photomultiplier (the 130.6 nm line was used), as expected; however, we also observed a change in the sensitivity with which $O(2^3P_J)$ could be detected: as the extent of absorption by CF_3Cl increased, the sensitivity for detecting $O(2^3P_J)$ decreased. Thus in order to measure the yield of $O(2^3P_J)$ quantitatively, new curves of growth were determined over a range of conditions under which the oxygen resonance lines were attenuated by an absorbing gas such as CF_3Cl.

For the present work relative $O(2^3P_J)$ concentrations were read directly from the appropriate curve of growth and the yield of $O(2^3P_J)$ formed by the quenching of $O(2^1D_2)$ by CF_3Cl was determined by comparing the concentrations produced in the absence and presence of excess N_2 [the N_2 quenches a large and calculable fraction of the $O(2^1D_2)$ directly to the ground state]. By this means the branching ratio for $O(2^3P_J)$ formation was determined as $30 \pm^{10}_{15}$ %. Typical conditions in these experiments were $P_{O_3} \sim 0.5$ N m^{-2}, $P_{CF_3Cl} \sim 4.0$ N m^{-2}, with a flash energy of 180 J.

The branching ratios for all the channels determined in this work are summarised in table 1. We also include a recent estimate[12a] for the elimination channel[12b]

$$O(2^1D_2) + CF_3Cl \rightarrow CF_3O + FCl \quad (9)$$

which is seen to have a small branching ratio.

REACTION OF $O(2^1D_2)$ WITH CF_3Br AND CF_3I

Reaction of $O(2^1D_2)$ with CF_3Br results in the rapid formation of BrO; however the decay is also rapid and this makes the absolute determination of the BrO yield extremely difficult.[7] Nevertheless we can obtain a useful lower limit for the yield of BrO and using the extinction coefficient given by Clyne *et al.*[13] for the (4, 0) band of the $A^2\Pi$–$X^2\Pi$ system we find a branching ratio for BrO formation of >25 %. It should be noted that reaction between Br and O_3 is much slower than the corre-

sponding reaction for Cl atoms, and that we can therefore distinguish between BrO formed in a primary step and that formed by secondary reaction of Br with O_3.

Experiments to determine the yield of IO from reaction of $O(2^1D_2)$ with CF_3I are considerably more difficult than the corresponding experiments with CF_3Cl and CF_3Br. A strong spectrum of IO is observed; however, some photolysis of CF_3I occurs, (it absorbs in the same region as O_3) and it is known that iodine atoms react rapidly with O_3 to yield IO. Preliminary results from our laboratory show that spin–orbit excited

TABLE 1.—BRANCHING RATIOS FOR PRODUCT CHANNELS IN THE REMOVAL OF $O(2^1D_2)$ BY HALOGENOMETHANES

reactant	products/%			
	quenching to $O(2^3P_J)$	halogen oxide	halogen atom	other products
CF_3Cl	$30 \pm {}^{19}_{15}$ %	65 ± 10 %	$\leqslant 20$ %	FCl(≈ 10 %)
CF_2HCl	$28 \pm {}^{19}_{13}$ %*	55 ± 10 %	$\leqslant 10$ %	OH(5 %)
CF_3Br		>25 %		

* Yield of $O(2^3P_J)$ based on CF_2 formation (*i.e.*, *via* the dissociative excitation channel yielding $CF_2 + HCl + O$) is 45 ± 10 %.

iodine atoms, $I(5^2P_{1/2})$, react more rapidly with O_3 than ground state $I(5^2P_{3/2})$ atoms; the rate constant for the ground state iodine atom reaction has been determined[14] as $k = 0.8 \times 10^{-12}$ cm^3 molecule^{-1} s^{-1}. Thus IO can be formed by more than one reaction and detailed experiments are required to distinguish between the various possibilities. Our present results indicate that the yield of IO from reaction of $O(2^1D_2)$ with CF_3I is substantial and we hope to report a quantitative measure for the branching ratio into this channel at the Discussion.

REACTION OF $O(2^1D_2)$ WITH CF_2HCl

Strong transient spectra of ClO and CF_2 were observed following the photolysis of O_3 or N_2O in the presence of CF_2HCl ($P_{O_3} = 13.3$ N m^{-2}; $P_{CF_2HCl} = 2.7$ kN m^{-2}). Both spectra were completely suppressed by addition of excess N_2, showing that they resulted from reaction of $O(2^1D_2)$ with CF_2HCl. Photolysis of CF_2HCl in the far-ultraviolet is known to produce CF_2; however, this region is not transmitted by our equipment and CF_2 was not observed when CF_2HCl ($P_{CF_2HCl} = 2.7$ kN m^{-2}) alone was flashed in the reaction vessel. The yield of ClO was measured as described for CF_3Cl and found to be 55 ± 10 % of the initial $O(2^1D_2)$ yield. Addition of small amounts of ethane to the system had no significant effect on the ClO yield, showing that Cl atom formation is of little importance ($\leqslant 10$ %) in the removal of $O(2^1D_2)$ by CF_2HCl.

The yield of CF_2 was determined using the known extinction coefficient for the $v_2' = 6$ band (249 nm) of the $A^1B_1 \leftarrow X^1A_1$ system, given by Tyerman.[15] The branching ratio into this channel was determined as 45 ± 10 %.

The branching ratio for $O(2^3P_J)$ formation was measured using the method described above for CF_3Cl and found to be $28 \pm {}^{10}_{13}$ %, which suggests that both CF_2 and $O(2^3P_J)$ must be formed in the same process.

The formation of OH radicals was not observed using plate photometry, however we would expect OH to react rapidly with CF_2HCl under the conditions employed. Using the more sensitive technique of time resolved spectrophotometry at 308 nm

(P_{CF_2HCl} = 2.0 kN m^{-2}, P_{O_2} = 40 N m^{-2}) formation of OH was detected but in very low yield. A careful calibration of the system was achieved using the reactions of $O(2^1D_2)$ with H_2O and CH_4. Assuming that H_2O gives two OH radicals for each $O(2^1D_2)$ atom reacting, the yield of OH from CH_4 was found to be 80 %, in good agreement with previous work.[16] The yield of OH from CF_2HCl, based on the same method, was found to be only 5 %.

REACTION OF $O(2^3P_J)$ WITH CF_3I

The kinetics of $O(2^3P_J)$ removal by CF_3I were investigated using time-resolved spectrophotometry at 130 nm (the slit width used was 800 μm and thus the three atomic lines at 130.2, 130.5 and 130.6 nm were transmitted by the monochromator). By photolysing O_3(P_{O_2} = 1.33 N m^{-2}) in the presence of excess N_2(P_{N_2} = 800 N m^{-2}), suitable concentrations of $O(2^3P_J)$ could be generated ($\approx$3 % photolysis of O_3 occurred). The decay of the ground state oxygen atom under these conditions was found to be very slow, as expected. Addition of small partial pressures of CF_3I (0.13-0.6 N m^{-2}) resulted in a marked increase in the rate of decay and by measuring the pseudo first-order rate coefficients for removal of $O(2^3P_J)$ over a range of CF_3I pressures (data are shown in fig. 2) the second-order rate constant was determined as,

$$k_{O(2^3P_J)\,+\,CF_3I} = (1.1 \pm 0.3) \times 10^{-11}\ \text{cm}^3\ \text{molecule}^{-1}\ \text{s}^{-1}.$$

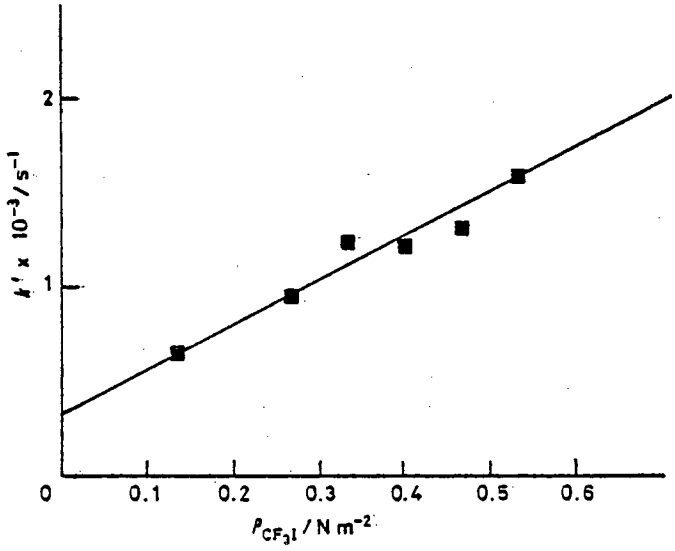

FIG. 2.—Plot of the first-order rate coefficients for removal of $O(2^3P_J)$ against partial pressure of CF_3I. (P_{O_2} = 1.3 N m^{-2}; P_{N_2} = 800 N m^{-2}).

A small correction[17] was made for departure from Beer–Lambert behaviour and the slope of fig. 2 should be multiplied by 1.3 (γ = 0.76 based on the data in fig. 1) to obtain the rate constant given above.

Some photolysis of CF_3I will inevitably occur under the conditions used; however, the percentage photolysis will be much less than that for O_3 (*i.e.*, $\ll$3%), due to the lower extinction coefficient for CF_3I, and should have no effect on the kinetics of the oxygen atom decay. As a check, further experiments were carried out over a range of flash energies (180-320 J). No significant difference in the decay rate for $O(2^3P_J)$

could be detected and we conclude that radical–radical reactions do not influence the observed kinetics and that photolysis of CF_3I is unimportant.

Some slow regeneration of $O(2^3P_J)$ will occur *via* the reaction of $O_2(a^1\Delta_g)$ with O_3, but this is entirely negligible on the time scale used here.

DISCUSSION

REACTION OF $O(2^1D_2)$ WITH CF_3Cl, CF_3Br AND CF_3I

A major channel in the reactions of $O(2^1D_2)$ with halogenomethanes (excepting attack on C–F bonds),* is clearly the formation of a halogen oxide molecule. We shall concentrate our discussion on the reaction with CF_3Cl, as the data for this molecule are most complete, but we expect the same general points to apply for CF_3Br and CF_3I.

Formation of ClO from CF_3Cl can in principle occur by two mechanisms, the more direct being abstraction of a chlorine atom. The second possible mechanism involves insertion of $O(2^1D_2)$ into the C–Cl bond, to form a vibrationally excited hypochlorite CF_3OCl^*, followed by fragmentation. CF_3OCl is a stable molecular species and its thermal and photochemical reactions have been examined. The results suggest that the favoured primary dissociation channel is formation of CF_3O and Cl (thermochemically this is the most favourable dissociation process). Thus if insertion of $O(2^1D_2)$ into C–Cl bonds was important, we would expect a high yield of Cl and not ClO, contrary to observations. Our results therefore suggest that ClO formation occurs by a direct abstraction mechanism. Similar behaviour has been reported previously for reactions of singlet methylene (CH_2), which is isoelectronic with $O(2^1D_2)$, with halogenomethanes.[19–22] Thus, while both singlet methylene and $O(2^1D_2)$ undergo fast insertion reactions into C–H bonds, the main reaction channel with halogenomethanes involves direct abstraction.[19–22]

The above behaviour can be understood when we consider the strong interaction that will occur between the vacant *p*-orbital of $O(2^1D_2)$ (or CH_2) and the lone pairs on the halogen atom. Thus the potential surface contains an attractive basin which surrounds the halogen atom and facilitates attack at this point in the molecule. A further attractive region must exist on the potential surface, corresponding to insertion of $O(2^1D_2)$ into the C–Cl bond (the minimum corresponding to the ground state configuration for CF_3OCl): however, it appears that this region is less accessible, possibly due to inertial effects: both Cl and CF_3 are relatively heavy and need to move a substantial distance for insertion to occur (contrast this with the situation for C–H insertion where the much lighter H atom can move rapidly to accommodate the insertion process).

Our data also provide information on another aspect of the singlet potential surface discussed above. Thus the singlet surface must be sufficiently attractive to be crossed by one or more triplet surfaces correlating with $O(2^3P_J) + CF_3Cl$ and non-adiabatic transitions at these crossings must be favourable, as evidenced by the relatively high branching ratio for $O(2^3P_J)$ formation.

For $O(2^1D_2)$ interacting with CF_3I the singlet surface may pass below the asymptote for $O(2^3P_J) + CF_3I$ (fig. 3) and could therefore influence the dynamics of the reaction between $O(2^3P_J)$ with CF_3I (see below). Stable compounds with the structure RIO can be prepared (*e.g.*, iodosobenzene, C_6H_5IO) showing that the singlet surface has a very deep minimum in the region occupied by the lone pair electrons of iodine.

* Removal of $O(2^1D_2)$ is much slower by CF_x groups[4,5] and appears to proceed entirely by quenching.[18]

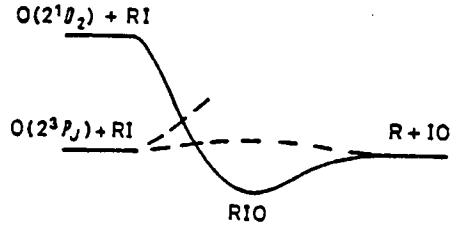

FIG. 3.—Section through the proposed potential surfaces for $O(2^3P_J)$ and $O(2^1D_2)$ interacting with an iodide. The lowest singlet surface is shown by the continuous line and the triplet surfaces by dashed lines.

REACTION OF $O(2^1D_2)$ WITH CF_2HCl

Lin[23] has studied the photolysis of O_3 in the presence of a number of hydrogen containing halogenomethanes, including CF_2HCl, and observed stimulated emission from vibrationally excited hydrogen halide molecules formed in these systems. He proposed that this resulted from the insertion of $O(2^1D_2)$ into C–H bonds followed by the elimination of a vibrationally excited hydrogen halide molecule from the hot intermediate, *e.g.*,

$$O(2^1D_2) + CF_2HCl \rightarrow CF_2ClOH^{\ddagger} \rightarrow CFClO + HF^{\ddagger}. \quad (10)$$

With CF_2HCl, only HF emission was observed, although the formation of HCl is more exothermic. The present results clearly show that HF elimination cannot account for more than 10-20 %* of the total reaction cross-section and that elimination of ground state HCl is a more important process.

It seems unlikely that chemical laser emission would result from a minor reaction channel and an alternative explanation for Lin's result is that excited HF is produced by secondary radical reactions. In a separate series of studies, Lin[24] has suggested that the reaction,

$$O(2^3P_J) + CF_2H \rightarrow CFO + HF \quad (\Delta H = -433 \text{ kJ mol}^{-1}) \quad (11)$$

can give rise to HF laser emission. Our results show that both $O(2^3P_J)$ and CF_2H are major products of the interaction of $O(2^1D_2)$ with CF_2HCl and we therefore suggest that reaction (11) could account for Lin's observations in the $O_3 + CF_3HCl$ photochemical laser system.[23]

The dominant channel in the interaction of $O(2^1D_2)$ with CF_2HCl is clearly that leading to the formation of ClO(55 %) and, as the branching ratio is similar to that for CF_3Cl, we infer that the mechanism is the same.

The second most important channel involves dissociative excitation *viz.*,

$$O(2^1D_2) + CF_2HCl \rightarrow CF_2 + HCl + O(2^3P_J). \quad (12)$$

This channel is thermoneutral within the bounds of current thermodynamic data ($\Delta H = 17 \pm 19$ kJ mol^{-1}) and it is surprising that it competes so effectively with the other highly exothermic channels. However, the observed rapid formation of CF_2 and $O(2^3P_J)$ cannot be accounted for by any other process. We have shown that Cl atom formation is unimportant ($\leqslant 10$ % of the total cross-section) which rules out reactions such as

$$O(2^1D_2) + CF_2HCl \rightarrow CF_2 + OH + Cl. \quad (13)$$

* This is an upper limit based on the error bounds for the products which are directly observed.

This is further confirmed by the very low yield of OH(5 %) observed. CF_2 is known to be formed by the disproportionation reaction

$$2CF_2H \rightarrow CF_2 + CF_2H_2 \qquad (14)$$

however, this could only account at most for 10 % of the CF_2 observed as the dominant removal channel for two CF_2H radicals is dimerisation. We, therefore, conclude that dissociative excitation [reaction (12)] accounts for $\approx$40 % of the total cross-section. It is interesting to note that both the thermal and infrared multiphoton dissociation[25] of CF_2HCl lead to the formation of CF_2 and HCl. The other surprising feature is that $O(2^3P_J)$ escapes from the force field of CF_2, as CF_2O is a very strongly bound molecule. This can, however, be understood when it is realised that $CF_2(X^1A_1)$ and $O(2^3P_J)$ do *not* correlate directly with the ground state of CF_2O, but with an excited triplet state which may not allow efficient combination.

The branching ratio for OH formation (5 %) is surprisingly low. From the bond additivity relationships suggested by Cvetanovic *et al.*[3] and by Davidson *et al.*,[5] we would expect OH formation to account for $\approx$30 % of the total cross-section. This is clearly not the case and it appears that the distribution in the product channels does not follow the simple additivity relationship suggested for the total removal rates. The low yield of OH is in fact similar to the situation previously encountered with singlet methylene reactions, where it was found that attack at C–H bonds was reduced to a very low level when a chlorine atom is present on the same, or adjacent, carbon atom.[26]

REACTION OF $O(2^3P_J)$ WITH CF_3Br AND CF_3I

Reaction of $O(2^3P_J)$ with CF_3Br, to yield BrO, is strongly endothermic ($\Delta H = +65 \pm 5$ kJ mol^{-1}) and negligibly slow at 300 K. However, the reaction has been studied at elevated temperatures (800-1200 K) and Arrhenius parameters determined[27] as $A = (1.5 \pm 0.5) \times 10^{-11}$ cm^3 molecule^{-1} s^{-1} and $E_a = 57 \pm 4$ kJ mol^{-1}. The activation energy for reaction is thus close to the endothermicity and the pre-exponential factor (A) is low when compared with reactions involving $O(2^1D_2)$. We shall return to the latter point after discussing the corresponding reaction with CF_3I.

The reaction of $O(2^3P_J)$ with CF_3I has been studied in some detail by Gorry *et al.*[28] using the molecular beam technique and has been shown to involve the formation of a weakly bound collision complex. The product scattering (IO) changes from a mainly backward, to a near isotropic distribution as the kinetic energy of the incident $O(2^3P_J)$ is increased. It was suggested[28] that at low collision energies the lifetime of the complex is shorter than its rotational period (as it is probably formed in low impact parameter collisions with low angular momentum). At higher collision energies the rotational period is reduced (higher angular momentum) and this leads to an increase in the forward scattering.

The total cross-section for reaction was not determined in the molecular beam work but a thermally averaged (300 K) cross-section can be obtained from the present data as $\sigma \simeq 2$ Å^2. It is clear that the reaction must be close to thermoneutral and our results provide an upper limit for the activation energy of $E_a \leqslant 6$ kJ mol^{-1}. When this is combined with the bond strength of CF_3I,[29] $D(CF_3\text{–}I) = 221 \pm 5$ kJ mol^{-1}, we obtain a lower limit for the bond strength of IO as, $D_0(IO) \geqslant 210$ kJ mol^{-1}, which is consistent with the value given earlier by Radlein *et al.*[30]

We might expect the Arrhenius pre-exponential factor for reaction of $O(2^3P_J)$ with CF_3I to be similar to that for the analogous reaction with CF_3Br, and the fact that the rate constant (at 300 K) for $O(2^3P_J) + CF_3I$ is close to the pre-exponential factor for

$O(2^3P_J) + CF_3Br$, suggests that this is probably the case. These values are surprisingly low when compared with the analogous reactions for $O(2^1D_2)$ (where any kinematic constraints should be the same), but appear to be characteristic of reactions involving $O(2^3P_J)$ with halogen, or halogen-containing molecules. As these reactions involve attractive potential surfaces and a bound collision complex we would normally expect a substantial reaction cross-section or large pre-exponential factor. It has been suggested that the low values observed result from a very restrictive reaction geometry and that a near collinear collision is required before reaction can occur.[28,31] This was rationalised in terms of the molecular orbital structure for the collision intermediate which favours a linear O–X–Y structure for lowest energy on the triplet potential surface. However, the above discussion on the quenching of $O(2^1D_2)$ by halogenomethanes leads us to suggest an alternative explanation. We have seen that crossings between triplet and singlet surfaces must occur and that for iodoso compounds one of these may be close to the dissociation asymptote for $O(2^3P_J) + RI$ (fig. 3). Thus the low reaction cross-section could result from a "low" triplet–singlet transition probability, while the scattering dynamics would be determined by the potential minimum in the singlet surface.

CONCLUSIONS

Reactions of $O(2^1D_2)$ with halogenomethanes proceed with a large total cross-section, the dominant channel being abstraction to yield a halogen oxide. The singlet potential surface, on which these reactions occur, is strongly attractive and is crossed by lower lying triplet surfaces correlating to $O(2^3P_J)$. This provides an efficient mechanism by which $O(2^1D_2)$ is quenched to the ground state.

The reactions of $O(2^1D_2)$ closely parallel those of singlet methylene.

Reactions of $O(2^3P_J)$ with halogenomethanes have relatively low total cross-sections (and Arrhenius pre-exponential factors) and may involve a triplet–singlet surface crossing.

We thank Drs H. Gillespie and G. Black for help in initiating this work and I.C.I. Ltd for the gift of samples of CF_2HCl.

[1] H. Yamazaki and R. J. Cvetanovic, *J. Chem. Phys.*, 1964, **41**, 3703.
[2] A. J. Colussi and R. J. Cvetanovic, *J. Phys. Chem.*, 1975, **79**, 1891.
[3] P. Michaud, G. Paraskevopoulos and R. J. Cvetanovic, *J. Phys. Chem.*, 1974, **78**, 1457.
[4] I. S. Fletcher and D. Husain, *J. Phys. Chem.*, 1976, **80**, 1837.
[5] J. A. Davidson and H. I. Schiff, *J. Chem. Phys.*, 1978, **69**, 4277.
[6] H. M. Gillespie and R. J. Donovan, *Chem. Phys. Letters*, 1976, **37**, 468.
[7] H. M. Gillespie, J. Garraway and R. J. Donovan, *J. Photochem.*, 1977, **7**, 29.
[8] R. J. Donovan and D. J. Little, *Chem. Phys. Letters*, 1972, **13**, 488.
[9] D. D. Davis, J. T. Herron and R. E. Huie, *J. Chem. Phys.*, 1973, **58**, 530.
[10] C. Morley and I. W. M. Smith, *J.C.S. Faraday II*, 1972, **68**, 1016.
[11] M. A. A. Clyne and J. A. Coxon, *Proc. Roy. Soc. A*, 1968, **303**, 207.
[12] (*a*) J. Wolfrum and K. Kaufmann, personal communication; (*b*) R. J. Donovan, K. Kaufmann and J. Wolfrum, *Nature*, 1976, **262**, 204.
[13] M. A. A. Clyne and H. W. Cruse, *Trans. Faraday Soc.*, 1970, **66**, 2214.
[14] M. A. A. Clyne and H. W. Cruse, *Trans. Faraday Soc.*, 1970, **66**, 2227.
[15] W. J. R. Tyerman, *Trans. Faraday Soc.*, 1969, **65**, 1188.
[16] C-L Lin and W. B. DeMore, *J. Phys. Chem.*, 1973, **77**, 863.
[17] R. J. Donovan and H. M. Gillespie, *Reaction Kinetics* (Specialist Periodical Report, Chemical Society, London, 1975), vol. **1**, p. 14.
[18] R. G. Green and R. P. Wayne, *J. Photochem.*, 1977, **6**, 371.
[19] D. W. Setser, R. Littrell and J. C. Hassler, *J. Amer. Chem. Soc.*, 1965, **87**, 2062.
[20] C. H. Bamford, J. E. Casson and R. P. Wayne, *Proc. Roy. Soc. A*, 1966, **289**, 287.
[21] C. H. Bamford, J. E. Casson and A. N. Hughes, *Proc. Roy. Soc. A*, 1968, **306**, 135.

[22] R. L. Johnson and D. W. Setser, *J. Phys. Chem.*, 1967, **71**, 4366.
[23] M. C. Lin, *J. Phys. Chem.*, 1972, **76**, 1425.
[24] M. C. Lin, *Int. J. Chem. Kinetics*, 1973, **5**, 173.
[25] J. C. Stephenson and D. S. King, *J. Chem. Phys.*, 1978, **69**, 1485.
[26] C. H. Bamford and J. E. Casson, *Proc. Roy. Soc. A*, 1969, **312**, 163.
[27] T. C. Frankiewicz, F. W. Williams and R. G. Gann, *J. Chem. Phys.*, 1974, **61**, 402.
[28] P. A. Gorry, C. V. Nowikow and R. Grice, *Chem. Phys. Letters*, 1978, **55**, 19.
[29] E. N. Okafo and E. Whittle, *Int. J. Chem. Kinetics*, 1975, **7**, 273.
[30] D. St. A. G. Radlein, J. C. Whitehead and R. Grice, *Nature*, 1975, **253**, 37.
[31] D. D. Parrish and D. R. Herschbach, *J. Amer. Chem. Soc.*, 1973, **95**, 6133.

DIRECT OBSERVATION OF S(3 $^1D_2$) AND DETERMINATION OF THE ABSOLUTE RATE OF REACTION WITH OCS

M.C. ADDISON, C.D. BYRNE and R.J. DONOVAN
Department of Chemistry, University of Edinburgh, Edinburgh EH9 3JJ, UK

Received 26 February 1979

We report the first direct kinetic study of electronically excited sulphur atoms in the 3 $^1D_2$ state. The formation and decay of S(3 $^1D_2$), following ultraviolet photolysis of OCS ($\lambda \approx 200-260$ nm), were monitored using time-resolved atomic absorption photometry in the vacuum ultraviolet ($\lambda = 167$ nm). The absolute rate of reaction with OCS was determined at 290 K as $k = (1.2 \pm 0.3) \times 10^{-10}$ cm^3 molecule^{-1} s^{-1}, close to unit collision efficiency.

1. Introduction

The discovery by Strausz and Gunning et al. [1,2] that the first electronically excited state of the sulphur atom, S(3 $^1D_2$), undergoes insertion reactions into C–H bonds,

$$S(3\,^1D_2) + RH \rightarrow RSH^{\ddagger} \xrightarrow{+M} RSH \qquad (1)$$

did much to stimulate interest in excited-state chemistry. The analogous reactions of O(2 $^1D_2$) were discovered [3] shortly after those of S(3 $^1D_2$), and these studies have since been extended to encompass a wide range of physical and chemical processes, some of which are of central importance to our understanding of atmospheric chemistry [4]. However, whilst a number of direct spectroscopic studies of O(2 $^1D_2$) have been reported [5,6], no such direct studies of S(3 $^1D_2$) have been made. This has been due to a combination of factors, the two most important being the highly reactive nature of S(3 $^1D_2$) and the lack of a favourable photochemical source. Thus, whilst photolysis of OCS in the ultraviolet ($\lambda = 200-260$ nm) yields S(3 $^1D_2$), absorption in this region is very weak and necessitates the use of relatively high partial pressures to produce detectable quantities of S(3 $^1D_2$). Unfortunately however the excited atoms react rapidly with OCS, leading to the formation of electronically excited sulphur molecules [7],

$$S(3\,^1D_2) + OCS \rightarrow S_2(a\,^1\Delta_g) + CO\,, \qquad (2)$$

which compels the use of low partial pressures of OCS.

Despite these conflicting constraints, we have (after numerous attempts over several years) finally succeeded in making direct kinetic observations on S(3 $^1D_2$), using time-resolved atomic absorption photometry in the vacuum ultraviolet. We here present the results of our first study in which the absolute rate for removal of S(3 $^1D_2$) by OCS is determined.

2. Experimental

The experimental arrangement for time-resolved atomic absorption photometry in the vacuum ultraviolet has been described previously [8]; however, the success of the present experiments resulted from a number of refinements which will be outlined briefly below.

The principal modification for the present work involved the use of an extreme solar-blind photomultiplier (EMR 542; $\lambda = 190-105$ nm). With this photomultiplier the effects of scattered light from the photolysis flash were completely suppressed and even the *formation* of S(3 $^1D_2$) could be observed as it followed the integrated form of the flashlamp output. The output from the photomultiplier was fed to a fast transient recorder (Datalab DL905) and the data processed by standard methods. Rate coefficients as fast as $\approx 3 \times$

10^4 s^{-1} can be measured with this arrangement.

Another important feature of the present experimental arrangement was the use of a flow system for the atomic emission lamp. In previous attempts we had employed a sealed atomic lamp, which is adequate for studies involving ground-state atoms [9], but proved to be too weak and insensitive for the detection of $S(3\,^1D_2)$. A mixture of H_2S and He (≈1% H_2S) was flowed through the lamp, at a pressure of 500 N m^{-2}, and the discharge powered by an EMI T1001 (2450 MHz) microwave generator (≈50 W incident power). The atomic line at 166.67 nm ($3p^3 4s\,^1D_2 \rightarrow 3p^4\,^1D_2$) was isolated with a vacuum monochromator (Hilger and Watts E766, slit width 0.5 mm; grating ruled area 54 × 54 mm, 1221 lines mm^{-1}, blazed for 121.6 nm).

The flash lamp and reaction vessel were 50 cm in length and constructed of quartz; the flash lamp dissipated ≈250 J of electrical energy per flash.

Reagents were handled with a conventional high-vacuum system and pressures measured with MKS Baratron pressure gauges (type 221; ranges 0.1–10^3 N m^{-2} and 10–10^5 N m^{-2}). High purity helium (>99.99%, B.O.C. grade X) was used for all experiments.

3. Results

$S(3\,^1D_2)$ atoms were produced by flash photolysis of low partial pressures of OCS (typically 0.2 N m^{-2}) in dilute mixture with helium (P_{He} = 800 N m^{-2}).

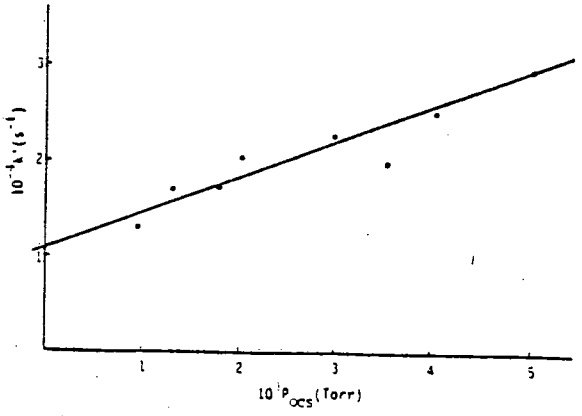

Fig. 1. Plot of first-order rate coefficients against partial pressure of OCS (1 Torr = 133 N m^{-2}).

The rate of decay of $S(3\,^1D_2)$ was found to depend linearly on the partial pressure of OCS, as shown in fig. 1. The same rate was observed when a given mixture was subjected to a second flash (or even up to eight flashes, this being the maximum number actually tried). Thus the degree of photolysis must be extremely low and there are no kinetic problems resulting from photolysis products. By analogy with similar experiments using O_3, for which 4% photolysis was observed, we estimate that ≪1% photolysis of OCS occurs, per flash, in our system. Thus, for the typical partial pressures of OCS used, this corresponds to atomic concentrations of $S(3\,^1D_2)$ of ≈10^{11} cm^{-3}. The signal-to-noise ratio achieved with single-shot recording is shown in fig. 2. The technique described here therefore provides a highly sensitive means of detecting $S(3\,^1D_2)$, and this feature, combined with the lack of disturbance from the photolysis flash, allowed us to make the present measurements.

The slope of the line in fig. 1 should yield the absolute second-order rate constant for removal of $S(3\,^1D_2)$ by OCS (all channels). However, in atomic absorption photometry, deviations from simple Beer–Lambert behaviour are frequently observed and the rate constant derived from second-order plots, such as fig. 1, needs to be corrected. In the present study we followed the standard practice of determining the correction coefficient, γ, and found this to be equal to unity, within the experimental uncertainty. Thus the rate constant determined from fig. 1, k_2 = (1.2 ± 0.3) × 10^{-10} cm^3 $molecule^{-1}$ s^{-1}, is correct as it stands.

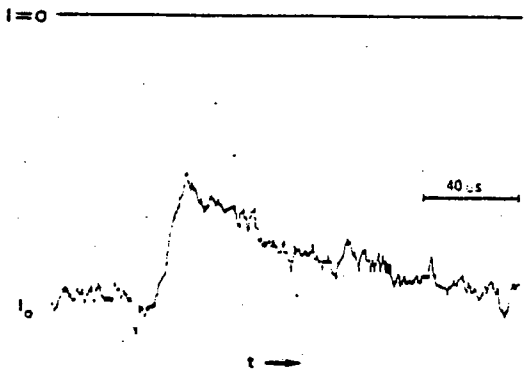

Fig. 2. Absorption signal at 167 nm due to formation and decay of $S(3\,^1D_2)$. P_{OCS} = 0.4 N m^{-2}; P_{He} = 800 N m^{-2}; E = 250 J.

Finally we mention briefly some preliminary results on the photolysis of CS_2 ($\lambda \approx 200$ nm) which show that substantial yields of $S(3\,^1D_2)$ are formed from this molecule also.

4. Discussion

Although the kinetics of $S(3\,^1D_2)$ have not previously been observed directly, it was known [7,10] that this excited state reacts rapidly with OCS to yield $S_2(a\,^1\Delta_g)$. Furthermore, spectroscopic observations in the vacuum ultraviolet [7] have shown that the quenching of $S(3\,^1D_2)$, to yield ground state $S(3\,^3P_J)$, and reaction to form $S_2(X\,^3\Sigma_g^-)$, are both minor channels, compared with formation of $S_2(a\,^1\Delta_g)$ via reaction (2). We have therefore a reasonably complete knowledge of the electronic state-to-state kinetics in this system. Information on the vibrational, rotational and translational energy distribution in the reaction products is however still required for a full understanding of the reaction dynamics.

The rapid rate of reaction of $S(3\,^1D_2)$ with OCS is in marked contrast to that for the more highly excited but less reactive $S(3\,^1S_0)$ state ($k_{OCS} = (4 \pm 2) \times 10^{-13}$ cm^3 molecule^{-1} s^{-1}) [11]. This behaviour has been discussed previously, but on the basis of less detailed data, in terms of the adiabatic potential surfaces available for these two excited singlet states [7]. For reaction of $S(3\,^1D_2)$ with OCS there are two electronic surfaces ($^1A'$ and $^1A''$) correlating with the product $S_2(a\,^1\Delta_g)$ and one surface ($^1A'$) correlating with $S_2(b\,^1\Sigma_g^+)$. Only one electronic surface ($^1A'$) is available for reaction of $S(3\,^1S_0)$ with OCS and provided that OCS remains linear, or the collision complex remains planar, there are no low-lying (exothermic) adiabatic surfaces leading to singlet product molecules. The kinetic data therefore suggest that during the collision of $S(3\,^1S_0)$ with OCS the four atoms retain an approximately co-planar geometry (this is necessarily the case if OCS remains linear).

In conclusion, we have developed a sensitive method for direct kinetic studies of $S(3\,^1D_2)$ and have determined the absolute rate constant for its reaction with OCS, which is close to unit collision efficiency ($k_2 = (1.2 \pm 0.3) \times 10^{-10}$ cm^3 molecule^{-1} s^{-1}).

Acknowledgement

We thank Professor C. Kemball for his encouragement and laboratory facilities and the Royal Society for an equipment grant.

References

[1] A.R. Knight, O.P. Strausz and H.E. Gunning, J. Am. Chem. Soc. 85 (1963) 1207, 2349.
[2] O.P. Strausz and H.E. Gunning, Advan. Photochem. 4 (1966) 143.
[3] H. Yamazaki and R.J. Cvetanović, J. Chem. Phys. 41 (1964) 3703.
[4] R.J. Cvetanović, Can. J. Chem. 52 (1974) 1452.
[5] R.F. Heidner III, D. Husain and J.R. Wiesenfeld, J. Chem. Soc. Faraday II 69 (1973) 927;
I.S. Fletcher and D. Husain, J. Phys. Chem. 80 (1976) 1837.
[6] J.A. Davidson, C.M. Sadowski, H.I. Schiff, G.E. Streit, C.J. Howard, D.A. Jennings and A.L. Schmeltekopf, J. Chem. Phys. 64 (1976) 57.
[7] R.J. Donovan, L.J. Kirsch and D. Husain, Nature 222 (1969) 1165.
[8] R.J. Donovan and D.J. Little, J. Chem. Soc. Faraday II 69 (1973) 952.
[9] R.J. Donovan and D.J. Little, Chem. Phys. Letters 13 (1972) 488.
[10] O.P. Strausz, R.J. Donovan and M. de Sorgo, Ber. Bunsenges. Physik. Chem. 72 (1968) 253.
[11] O.J. Dunn, S.V. Filseth and R.A. Young, J. Chem. Phys. 59 (1973) 2892.

ABSORPTION SPECTRUM AND KINETICS OF THE ACETYLPEROXY RADICAL

M.C. ADDISON ‡, J.P. BURROWS, R.A. COX and R. PATRICK ‡
Environmental and Medical Sciences Division, A.E.R.E., Harwell, Oxfordshire, UK

Received 10 April 1980; in final form 29 April 1980

The UV absorption spectrum of acetylperoxy radicals, produced in several photochemical systems, has been investigated using the molecular modulation technique. Rate coefficients were determined at 28 and 715 Torr for the reaction $CH_3COO_2 + NO_2(+M) \rightarrow CH_3COO_2NO_2(+M)$, which exhibits a pressure dependence.

1. Introduction

Organic peroxy radicals play a central role in the low-temperature oxidation of organic compounds. The reactions of peroxy radicals with NO and NO_2 in the gas phase are particularly important in atmospheric photo-oxidation processes [1]. The acetyl peroxy radical CH_3COO_2 has been identified as a precursor to peroxyacetylnitrate (PAN), a well-known constituent of photochemical smog, by its combination with NO_2 [2,3]:

$$CH_3COO_2 + NO_2 (+M) \rightarrow CH_3COO_2NO_2 (+M). \quad (1)$$

There appear to be no measurements of the rate coefficient k_1 although an estimate based on the decomposition rate of PAN, k_{-1}, and the equilibrium constant K_1^* indicate $k_1 \approx 10^{-12}$ cm^3 molecule^{-1} s^{-1} (± a factor of 10) [4].

We have recently reported kinetic measurements of reactions of HO_2 [5] and CH_3O_2 [6] with NO_2 using the molecular modulation technique. The radicals were monitored in absorption by their characteristic spectral feature in the UV. The same method was used in this work to investigate the UV spectrum and kinetics of the CH_3COO_2 radical.

‡ Present address: Department of Chemistry, University of Edinburgh, Edinburgh, UK.
* Present address: Physical Chemistry Laboratory, University of Oxford, Oxford, UK.

2. Experimental

CH_3COO_2 was produced by the modulated photolysis at 350 (±50) nm of Cl_2 in the presence of CH_3CHO and O_2:

$$Cl_2 + h\nu \rightarrow 2Cl, \quad (2)$$

$$Cl + CH_3CHO \rightarrow CH_3CO + HCl, \quad (3)$$

$$CH_3CO + O_2 (+M) \rightarrow CH_3COO_2 (+M). \quad (4)$$

Observation of the modulated absorption in this system as a function of wavelength (280–205 nm) enabled characterisation of the absorption spectrum of CH_3COO_2. Kinetic measurements were made using a fixed wavelength by varying the photolysis period τ in the range 40 ms to 10 s.

The apparatus used for this study has been described in detail [7]. Gaseous mixtures flowed through the 120 cm × 2.5 cm diameter silica reaction cell, illuminated by up to 6 square-wave-modulated fluorescent lamps. The photolytic intensity was determined from the rate of decay of Cl_2. Absorption was monitored on a collimated beam from a well-stabilised D_2 lamp, which passed along the long axis of the cell before dispersion on a double monochromator (Spex Doublemate). The digital lock-in detector provided separate in-phase and in-quadrature components of modulated absorption. All experiments were conducted at 302 ± 1 K.

3. Results

3.1. Absorption spectrum of CH_3COO_2

To investigate the spectrum, CH_3COO_2 was generated in the photolysis of $Cl_2 + CH_3CHO + O_2 + NO_2$ mixtures. In this system PAN is formed in 95% yield [8] showing that reactions (1)–(4) adequately describe the chemical changes. $[NO_2]$ was kept low so that reaction of CH_3COO_2 with NO, produced in photolysis of NO_2, accounted for ≈2% of the overall removal of CH_3COO_2

$$CH_3COO_2 + NO \rightarrow CH_3CO_2 + NO_2, \quad (5)$$

based on a published value of $k_1/k_5 = 0.54$ [4]. The modulated absorption components measured at 1 Hz photolysis were corrected for the contributions due to the product PAN in the previously described manner [9], using absorption cross sections determined in our laboratory, which substantially confirmed previously reported values [10]. The resultant radical spectrum is illustrated by the filled points in fig. 1 (lower section). The upper section of fig. 1 shows the ratio of the in-quadrature (Q) and in-phase (P) absorption components, which is a measure of the phase shift of the modulated absorption. There is no systematic change in this quantity over the wavelength range, providing evidence that the absorption feature is attributable to a single radical species.

The absorptions in the presence of NO_2 were relatively small which resulted in appreciable statistical scatter as indicated by the error bars. In the absence of NO_2, absorption was greater and more precisely measured. Under these conditions radical absorption exhibited a $k_2[Cl_2]^{1/2}$ dependence indicating that CH_3COO_2 decays by radical + radical pathways. CH_3COO_2 recombination gives mainly CH_3CO_2 which decomposes to $CH_3 + CO_2$ [11,12].

$$2CH_3COO_2 \rightarrow 2CH_3 + 2CO_2 + O_2, \quad (6)$$

$$CH_3 + O_2\,(+M) \rightarrow CH_3O_2\,(+M). \quad (7)$$

Methyl peroxy radicals, which possess an absorption feature maximising at 240 nm [13,14], are therefore expected to be present in the absence of NO_2. Assuming that CH_3COO_2 (A) and CH_3O_2 (B) are the only absorbing species, the observed in-phase absorption components at a pair of wavelengths, λ_1, λ_2, are given

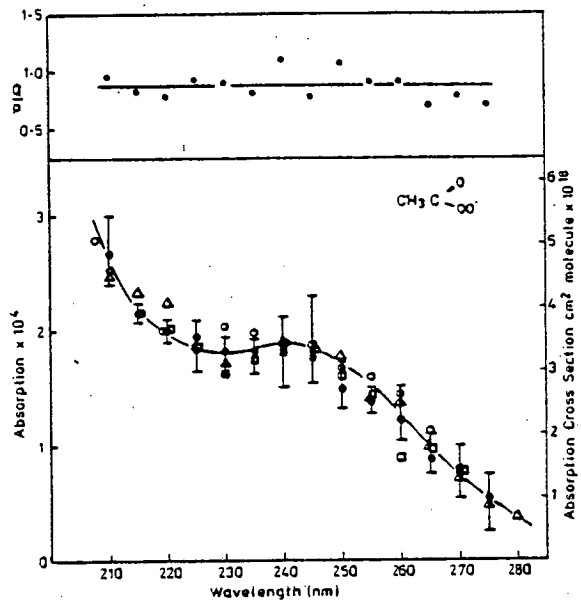

Fig. 1. Absorption spectrum of the acetylperoxy radical. Lower section: Filled points: spectrum from photolysis of $Cl_2 + CH_3CHO + O_2 + NO_2$ mixtures; error bars show spread of measurements. Open points: residual spectrum from $Cl_2 + CH_3CHO + O_2$ (△), $CH_3COCH_3 + O_2$ (○), and $(CH_3CO)_2 + O_2$ (□) photolysis with absorption due to CH_3O_2 subtracted out. Absorption cross sections based on mean from kinetic measurements. Upper section shows ratio of in-quadrature to in-phase absorption in $Cl_2 + CH_3CHO + O_2 + NO_2$ system. The spectrum was recorded at low resolution using a spectral width of 3 nm.

by:

$$P_1 = (\sigma_{\lambda_1})_A l p_A + (\sigma_{\lambda_1})_B l p_B, \quad (8)$$

$$P_2 = (\sigma_{\lambda_2})_A l p_A + (\sigma_{\lambda_2})_B l p_B, \quad (9)$$

where p_A and p_B are the in-phase components of the concentration modulation and l is the length of the vessel. These equations can be solved to give the individual absorption components if the relative absorption cross sections $\sigma_{\lambda_1}/\sigma_{\lambda_2}$ for the two components are known. Using averaged spectral data for CH_3O_2 from the literature and the relative absorption cross section of CH_3COO_2 at 210 and 240 nm from the observations in the presence of NO_2, the components due to CH_3O_2 were subtracted from the observed radical spectra in the following systems where CH_3COO_2 and CH_3O_2 are likely to be present: $Cl_2 + CH_3CHO + O_2 + h\nu$ (350 ± 50 nm); $CH_3COCH_3 + h\nu$ (315 ± 35 nm) + O_2;

best estimate from our data. This result confirms the previous conclusion [4] that association of CH_3COO_2 with NO_2 is fast and that this reaction, together with reaction (5) will dominate the chemistry of CH_3COO_2 in the lower atmosphere. Clearly there is a pressure dependence of k_1 indicating that the association of CH_3COO_2 with NO_2 is in its fall-off region in the pressure range investigated.

3.3. The reaction $CH_3COO_2 + CH_3COO_2 \rightarrow$ products

Absorption was measured as a function of τ in the $Cl_2 + CH_3CHO + O_2$ system at two wavelengths, 210 and 240 nm. The components at each τ due to CH_3O_2 were subtracted out by solution of eqs. (8) and (9), and the analogous pair of equations for in-quadrature absorption. The reduced residual absorptions (i.e. $\propto B^{1/2}$) at 210 nm, attributed to CH_3COO_2, are plotted against $\tau B^{1/2}$ in fig. 3. The broken curves were generated using the weighted least-mean-squares procedure, assuming that CH_3COO_2 decay followed the second-order rate law:

$$d[CH_3COO_2]/dt = 2B - 2k_0[CH_3COO_2]^2,$$

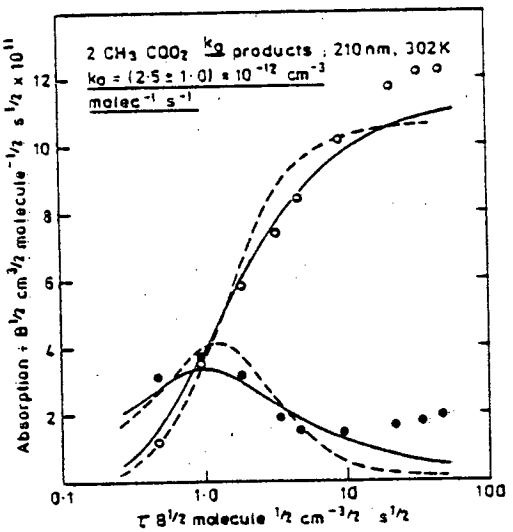

Fig. 3. Reduced acetyl peroxy radical absorption in-phase (open points) and in-quadrature (closed points) versus $\tau B^{1/2}$ in the $Cl_2 + CH_3CHO + O_2$ system. Solid curve shows weighted least-squares fit assuming a simple second-order rate law. Broken curve generated by computer simulation with CH_3COO_2 decay via reaction with CH_3O_2 and HO_2 in addition to reaction (6).

where k_0 is the overall second-order decay constant. This fit yielded the following values:

$$k_0 = (6.5 \pm 3.0) \times 10^{-12} \text{ cm}^3 \text{ molecule}^{-1} \text{ s}^{-1},$$

$$\sigma(210) = (4.9 \pm 2.5) \times 10^{-18} \text{ cm}^2 \text{ molecule}^{-1}.$$

The data were also fitted by computer simulation of the system, using a more complete reaction mechanism in which radical plus radical reactions involving CH_3COO_2, CH_3O_2 and HO_2 were included:

$$CH_3COO_2 + CH_3COO_2 \xrightarrow{O_2} 2CH_3O_2 + 2CO_2 + O_2, \quad (6)$$

$$CH_3O_2 + CH_3O_2 \rightarrow HCHO + CH_3OH + O_2, \quad (10a)$$

$$\rightarrow 2CH_3O + O_2, \quad (10b)$$

$$CH_3COO_2 + CH_3O_2 \rightarrow CH_3 + CH_3O + O_2 + CO_2, \quad (11)$$

$$CH_3 + O_2 + M \rightarrow CH_3O_2 + M, \quad (7)$$

$$CH_3O + O_2 \rightarrow HCHO + HO_2, \quad (12)$$

$$HO_2 + CH_3COO_2 \rightarrow CH_3COO_2H + O_2, \quad (13)$$

$$HO_2 + CH_3O_2 \rightarrow CH_3O_2H + O_2, \quad (14)$$

$$HO_2 + HO_2 \rightarrow H_2O_2 + O_2. \quad (15)$$

k_6 and k_{11} were varied and k_{13} was assumed to be the same value as k_{14} (i.e. 6.5×10^{-12} cm^3 molecule^{-1} s^{-1} [6]). The values of k_7, k_{10}, k_{12} and k_{15} used in the simulation were taken from the CODATA evaluation [17]. The broken curves in fig. 3 were generated using

$$k_6 = 2.5 \times 10^{-12} \text{ cm}^3 \text{ molecule}^{-1} \text{ s}^{-1},$$

$$\sigma(210) = 4.4 \times 10^{-18} \text{ cm}^2 \text{ molecule}^{-1},$$

$$k_{11} = 3 \times 10^{-12} \text{ cm}^3 \text{ molecule}^{-1} \text{ s}^{-1}.$$

These curves give a reasonable description of the data and the estimated overall uncertainty on k_6 is a factor of 2.

The absorption cross sections determined from the kinetic studies of reactions (1) and (6) give a mean value of $\sigma(CH_3COO_2)$, normalised at 210 nm, of $(4.7 \pm 1.0) \times 10^{-18}$ cm^2 molecule^{-1}. This allows the data in fig. 1 to be put on an absolute basis; the absorption

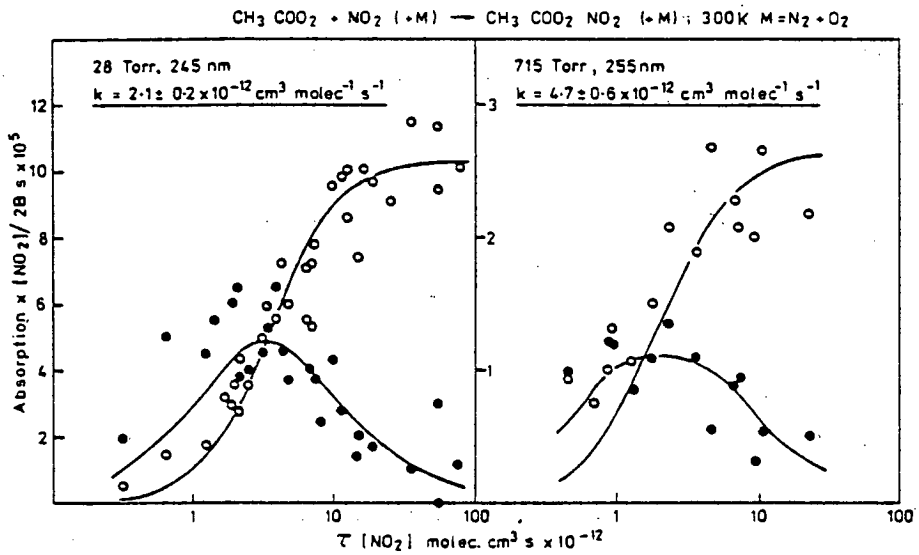

Fig. 2. Reduced acetyl peroxy radical absorption in-phase (open points) and in-quadrature (closed points) versus $\tau[NO_2]$ in the $Cl_2 + CH_3CHO + O_2 + NO_2$ system at total pressures of 28 and 715 Torr. Curves show weighted least-squares fit using indicated values of k_1 and the values of σ given in the text.

$CH_3COCOCH_3 + h\nu$ (315 ± 35 nm) + O_2. The resultant spectra are shown as open points in fig. 1, and provide additional evidence for the assignment of the absorption feature to CH_3COO_2. Another possible assignment of the observed spectrum is the CH_3CO radical. However, the spectrum obtained in the flash photolysis of acetone, methyl ethyl ketone and biacetyl in the absence of O_2 [15], which is attributed to CH_3CO, exhibits two maxima at 215 nm and 207 nm and no "flattening" in the 220–240 nm region as observed here.

3.2. Kinetics of the reaction of $CH_3COO_2 + NO_2$

The variation of absorption with τ was investigated in the $Cl_2 + CH_3CHO + O_2 + NO_2$ system at total pressures of 715 and 28 Torr. $[NO_2]$ was in the range $(0.5–1.85) \times 10^{13}$ molecules cm^{-3} and the photolysis rate $k_2[Cl_2]$ $(= B)$ was $(0.62–4.91) \times 10^{12}$ molecules $cm^{-3}\ s^{-1}$. In order to represent all of the data on a single plot, the absorption components and photolysis period were reduced in the following manner [16]. $P_{red} = P[NO_2]/2B$, $Q_{red} = Q[NO_2]/2B$, $\tau_{red} = \tau[NO_2]$. The reduced data are shown in fig. 2.

A weighted least-squares fitting procedure was used to generate the curves shown, which are unique for the pairs of values of k_1 and σ given below. The expressions used for calculation of absorption [16] assumed pseudo-first-order removal of CH_3COO_2 by reaction (1) and took account of the concentration gradient along the cell, due to consumption of NO_2.

At 715 Torr:

$k_1 = (4.7 \pm 0.3) \times 10^{-12}$ cm^3 molecule^{-1} s^{-1};

$\sigma(255\ \text{nm}) = (2.0 \pm 0.2) \times 10^{-18}$ cm^2.

At 28 Torr:

$k_1 = (2.1 \pm 0.1) \times 10^{-12}$ cm^3 molecule^{-1} s^{-1},

$\sigma(245\ \text{nm}) = (3.9 \pm 0.1) \times 10^{-18}$ cm^2.

The error limits are 2 standard deviations from the least-squares fit. The overall experimental error is estimated to be ±20% at 28 Torr and ±30% at 760 Torr. Because the fitting procedure placed undue weight on the data near the curve-crossing region, which in the 715 Torr experiments was near the limit of our experimentally accessible range, the above value of k_1 at this pressure is considered a lower limit. The observed in-phase absorption at low frequency combined with an averaged value of σ (q.v.) gives $k_1 = (6.0 \pm 2.0) \times 10^{-12}$ cm^3 molecule^{-1} s^{-1}, which we consider the

is of similar intensity to that of other peroxy radicals in this region.

A detailed study of the reaction products in the disproportionation of CH_3COO_2 was not undertaken. However it was found that ozone was formed with an intensity independent quantum yield of ≈0.05 in the photolysis of $Cl_2 + CH_3CHO + O_2$ and $CH_3COCOCH_3 + O_2$. Ozone was identified by its characteristic absorption maximising at 255 nm and also by chemiluminescence detection. It is probably formed in reaction (6) as a minor channel. The formation of ozone in the photolysis of α-diketone + oxygen mixtures was also reported by Haagen-Smit et al. [18] in their early work on photochemical smog.

Acknowledgement

This work was supported by the UK Department of the Environment. RP thanks the Science Research Council for the award of a CASE studentship.

References

[1] K.R. Demerjian, J.A. Kerr and J.G. Calvert, Advan. Environ. Sci. Technol. 4 (1974) 1.
[2] R. Louw, J. van Ham and H. Nieboer, J. Air Pollut. Contr. Assoc. 23 (1973) 716.
[3] R.A. Cox, R.G. Derwent, P.M. Holt and J.A. Kerr, J. Chem. Soc. Faraday I 72 (1976) 2061.
[4] R.A. Cox and M. Roffey, Environ. Sci. Technol. 11 (1977) 900.
[5] R.A. Cox and K.F. Patrick, Intern. J. Chem. Kinetics 11 (1979) 635.
[6] R.A. Cox and G.S. Tyndall, Chem. Phys. Letters 65 (1979) 357.
[7] R.A. Cox, R.G. Derwent, A.E.J. Eggleton and H.J. Reid, J. Chem. Soc. Faraday I 75 (1979) 1648.
[8] B.W. Gay, R.C. Noon, J.J. Bufalini and P.L. Hanst, Environ. Sci. Technol. 10 (1976) 82.
[9] R.A. Cox and G.S. Tyndall, J. Chem. Soc. Faraday II 76 (1980) 153.
[10] E.R. Stephens, Advan. Environ. Sci. Technol. 1 (1969) 119.
[11] J. Weaver, J. Meagher, R. Shortridge and J. Heicklen, J. Photochem. 4 (1975) 341.
[12] R.A. Kenley and T.G. Traylor, J. Am. Chem. Soc. 97 (1975) 4700.
[13] D.A. Parkes, D.M. Paul, C.P. Quinn and R.C. Robson, Chem. Phys. Letters 23 (1973) 425.
[14] C.J. Hochanadel, J.A. Ghormley, J.W. Boyle and P.L. Ogren, J. Phys. Chem. 81 (1977) 3.
[15] H. Adachi, N. Basco and D.G.L. James, Chem. Phys. Letters 59 (1978) 502.
[16] R.A. Cox and R. Lewis, J. Chem. Soc. Faraday I 75 (1979) 2649.
[17] CODATA Bulletin 33, Evaluated Kinetic and Photochemical Data for Atmospheric Chemistry, ICSU CODATA, Paris (August 1979).
[18] A.J. Haagen-Smit, C.E. Bradley and M.M. Fox, Ind. Eng. Chem. 45 (1953) 2086.